

**Fast Cycle Low Pressure Drop Systems for the
Separation of CO₂**

By

Anna J Rouse

February 2004

**A thesis submitted for the Degree of Doctor of Philosophy of
the University of London**

**Department of Chemical Engineering
University College London
Torrington Place
London, WC1E 7JE, United Kingdom**

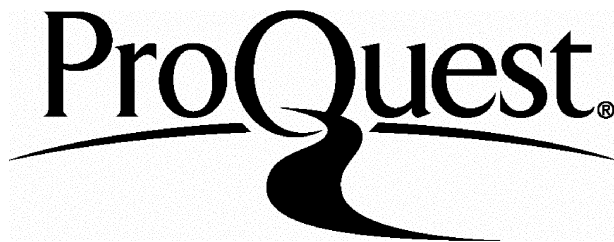
ProQuest Number: 10014845

All rights reserved

INFORMATION TO ALL USERS

The quality of this reproduction is dependent upon the quality of the copy submitted.

In the unlikely event that the author did not send a complete manuscript and there are missing pages, these will be noted. Also, if material had to be removed, a note will indicate the deletion.



ProQuest 10014845

Published by ProQuest LLC(2016). Copyright of the Dissertation is held by the Author.

All rights reserved.

This work is protected against unauthorized copying under Title 17, United States Code.
Microform Edition © ProQuest LLC.

ProQuest LLC
789 East Eisenhower Parkway
P.O. Box 1346
Ann Arbor, MI 48106-1346

Abstract

In the effort to reduce CO₂ emissions, industry is increasingly looking at sequestering CO₂. Estimates currently suggest that 50% of the total capture and storage costs lies in the CO₂ separation stage. In this thesis one specific CO₂ separation technology, Dual Piston Driven Pressure Swing Adsorption (DP-D PSA), has been evaluated, using both an experimental study and mathematical modelling. It was hoped that the process, which encounters very low pressure drops and could be operated at fast cycles, could be efficiently utilised for this low value separation.

The initial mathematical studies undertaken centred on the validity of one of the modelling assumptions made for adsorption processes; the linear driving force (LDF) approximation used to describe mass transfer. Using both numerical simulations and analysis of analytical expressions a new approach to the LDF model for fast cycles was developed, and was verified for various cyclic adsorptions systems.

Preliminary experiments began with characterisation of two monolithic adsorption columns, using chromatography and ZLC techniques. Experiments, which incorporated the activated carbon columns, were then conducted using a DP-D PSA test rig, operated both at total reflux and under production conditions. Runs were undertaken to analyse the behaviour of the rig under adsorbing and non adsorbing conditions, while the effect of rig parameters such as cycle speed and stroke length were also investigated.

Mathematical models were then developed to simulate the system, incorporating both of the columns. Comparing the simulated and experimental results showed that the models represented system behaviour well under both adsorbing and non adsorbing conditions at total reflux. Results were reasonable but not as good when feed and product streams were considered and further work was suggested to improve agreement.

Final comments were made with regard to the industrial feasibility of the process and possible improvements which could make the system more attractive.

Acknowledgements

I would like to thank my supervisor, Prof. Stefano Brandani, for his guidance and patience throughout the course of this work. I would also like to acknowledge the invaluable academic and personal support of Dr. Ruthven in Maine. At BP I would like to thank Michael Wilkinson and Mark Simmonds for their advice and assistance.

I could not have completed this work without the help and encouragement of numerous colleagues. Within the CO₂ Centre I would especially like to recognise Massimilano, Gianluca, Prim and Giovanna, and within the CAPE group I would like to thank Rob, Darren, Dave, Sharon and Dimitrious for their assistance and good company. In Maine I was very grateful for the assistance of Federico Brandani, who undertook the ZLC experimental work reported within Chapter 3 of this work, and the friendship of Bob Rioux and his family.

On a personal level I would like to thank my friends and family, especially my parents, for their immeasurable help and support, and Nicholas, for his belief and love.

I would like to gratefully acknowledge the financial support I have received from the EPSRC and BP.

"The supreme reality of our time is ...the vulnerability of our planet.. "

- John F. Kennedy

" As we deepen our imprint on the natural world, we increase our responsibility for it. "

- Dr. E.O. Wilson

"Science can amuse and fascinate us all, but it is engineering that changes the world."

- Isaac Asimov

Table of Contents

Abstract	2
Acknowledgements	3
Table of Contents	4
List of Figures	10
List of Tables	16
Nomenclature	17

1. INTRODUCTION

1.1 Separation of CO ₂	20
1.2 CO ₂ sequestration	21
1.3 Aims of the thesis	23
1.4 Organisation of the thesis	23
<i>Tables</i>	26

2. THE LINEAR DRIVING FORCE MODEL FOR FAST CYCLIC PROCESSES

2.1 Introduction	27
2.2 Literature Review of Linear Driving Force (LDF) model	28
2.2.1 Early LDF model development	28
2.2.2 Relevance of the LDF model to cyclic adsorption processes	29
2.2.3 The historical analogy with heat transfer	30
2.2.4 Extending the single particle approach	32
2.2.5 Mathematical approaches developed for the cyclic LDF problem	32
2.3 Mathematical approaches to the cyclic LDF problem	34
2.3.1 Approach 1 – Numerical simulation	34
2.3.1.1 The single particle model	34
2.3.1.2 The CSTR model	35
2.3.1.3 Numerical solution methods	37
2.3.2 Approach 2 – Frequency response techniques	37

2.3.2.1	The relevance of frequency response	37
2.3.2.2	The single particle model	38
2.3.2.3	The CSTR model	41
2.3.2.4	Frequency response for the CTR model	44
2.3.3	Approach 3 – Full analytical solutions	47
2.3.3.1	Analytical solutions assuming the LDF model	48
2.3.3.2	Analytical solutions assuming the Diffusion model	50
2.3.4	The PSA model	51
2.3.4.1	The PSA cycle	52
2.3.4.2	Mathematical modelling of the simple PSA cycle	52
2.4	Analysis of the results assuming the different problem approaches	57
2.4.1	Approach 1 – Numerical solutions	57
2.4.1.1	Comparison between numerical simulations of the CSTR	57
2.4.1.2	Direct steady state solutions	58
2.4.2	Approach 2 – Frequency response	59
2.4.2.1	Comparison between numerical simulations of the CSTR assuming the new 2 parameter LDF model	59
2.4.3	Approach 3 – Full analytical solutions	60
2.4.3.1	Determining the time to cyclic steady state	60
2.4.4	The PSA model	61
2.4.4.1	The PSA model of Raghavan et al. (1986)	61
2.4.4.2	The PSA model and the two parameter LDF approach	62
2.5	Concluding Remarks	65
	<i>Figures</i>	67
	<i>Tables</i>	78

3. ADSORBENT CHARACTERISATION

3.1	Introduction	81
3.2	Literature review of structured adsorbent columns and characterisation techniques	82
3.2.1	Structured adsorbent columns	82
3.2.1.1	Manufacture	82

3.2.1.2	Suitability of structured columns for PSA applications	83
3.2.2	Characterisation techniques	85
3.2.2.1	Gravimetric method	85
3.2.2.2	Pulse or step chromatography	86
3.2.2.3	Zero Length Column (ZLC) technique	89
3.3	Characterisation experiments	92
3.3.1	The columns	92
3.3.2	Chromatography experimental procedure	93
3.3.3	Zero Length Column (ZLC) experimental procedure	95
3.4	Results from characterisation experiments	96
3.4.1	Graphical results from chromatography experiments	96
3.4.1.1	Conformation of linear adsorption behaviour	96
3.4.1.2	Analysis of chromatography curves	97
3.4.2	Comparing chromatography and ZLC results	98
3.4.2.1	Equilibrium adsorption coefficients for CO ₂	98
3.4.2.2	Equilibrium adsorption coefficients for N ₂	99
3.4.2.3	Diffusional time constants	99
3.5	Concluding Remarks	100
	<i>Figures</i>	102
	<i>Tables</i>	125

4. AN EXPERIMENTAL STUDY OF A DUAL PISTON DRIVEN PSA RIG

4.1	Introduction	127
4.2	Literature review of pressure swing related technologies	128
4.2.1	Pressure Swing Adsorption	128
4.2.2	Parametric pumping	130
4.2.3	Rapid PSA	131
4.2.4	The origins of dual piston driven PSA	133
4.2.5	More recent experimental piston driven PSA studies	135
4.3	The description of the experimental rig	137
4.3.1	The rig	138

4.3.2	The columns	138
4.3.3	The pistons	139
4.3.4	Phase angle adjustments	139
4.3.5	Stroke length arrangement	140
4.3.6	Feed-product relay system	140
4.3.7	TCD sampling loop	140
4.3.7.1	TCD calibration	141
4.3.7.2	Sampling technique	141
4.3.8	Data acquisition	142
4.4	Experimental procedure	142
4.4.1	Non adsorbing total reflux runs	143
4.4.2	Adsorbing total reflux runs	143
4.4.3	Adsorbing feed-product runs	144
4.5	Experimental results	145
4.5.1	Results for total reflux non adsorbing runs	145
4.5.1.1	Empty system runs	145
4.5.1.2	Helium runs including columns	146
4.5.2	Results for total reflux adsorbing runs	147
4.5.2.1	Temperature, pressure and concentration profiles	147
4.5.2.2	The effect of parametric variation	149
4.5.3	Feed-product runs	149
4.6	Concluding Remarks	151
	<i>Figures</i>	153
	<i>Tables</i>	168

5. A MATHEMATICAL MODEL OF A DUAL PISTON DRIVEN PSA SYSTEM

5.1	Introduction	172
5.2	Literature review of mathematical techniques and mathematical modelling of PSA processes	173
5.2.1	Mathematical approaches to cyclic adsorption processes	173
5.2.1.1	Finite difference methods	173

5.2.1.2	Orthogonal collocation	174
5.2.1.3	Orthogonal collocation on finite elements	174
5.2.1.4	Cells in series	174
5.2.2	Development of PSA modelling	175
5.2.3	Mathematical modelling of rapid PSA	177
5.2.4	Mathematical modelling of piston driven PSA	179
5.3	Model Development	182
5.3.1	Model assumptions	182
5.3.2	Modelling of the adsorption column	183
5.3.2.1	Mass Balances	183
5.3.2.2	Equilibrium isotherm	184
5.3.2.3	Mass transfer resistance	184
5.3.2.4	Boundary conditions	185
5.3.3	Modelling of the pistons	185
5.3.3.1	Overall mass balances for the pistons	185
5.3.3.2	Component mass balances for the pistons	186
5.3.3.3	Piston volume changes	186
5.3.4	Overall mass balance	187
5.3.5	Initial conditions	187
5.3.6	Direct steady state model	188
5.3.7	Initial experimental observations and model refinement	189
5.3.8	Equilibrium, kinetic and system parameters	191
5.3.9	Numerical simulation	191
5.4	Concluding remarks	192
	<i>Figures</i>	194
	<i>Tables</i>	196

6. A COMPARISON BETWEEN THE MATHEMATICAL AND EXPERIMENTAL STUDIES OF THE DUAL PISTON DRIVEN PSA

6.1	Introduction	200
6.2	Comparison of results	201
6.2.1	Total reflux helium runs	201

6.2.1.1	Empty system runs	201
6.2.1.2	Small column non adsorbing runs	202
6.2.1.3	Large column non adsorbing runs	202
6.2.2	Total reflux adsorbing runs	203
6.2.2.1	Small column total reflux adsorbing runs	203
6.2.2.2	Large column total reflux adsorbing runs	204
6.2.3	Small column total reflux parametric study	205
6.2.3.1	Effect of column choice	205
6.2.3.2	Effect of cycle time	206
6.2.3.3	Effect of stroke length	206
6.2.3.4	Effect of phase angle difference and column temperature	207
6.2.4	Small column feed-product runs	208
6.2.5	Modelling efficiency	210
6.3	Practical considerations	211
6.3.1	Flue gas pre-treatment	211
6.3.2	Power	212
6.3.3	Design and manufacture	212
6.3.4	Use and storage of CO ₂	212
6.4	Concluding remarks	213
	<i>Figures</i>	215
	<i>Tables</i>	222

7. CONCLUSIONS AND RECOMMENDATIONS FOR FURTHER WORK

7.1	Conclusions and contributions of the thesis	223
7.1.1	LDF approximation for cyclic adsorption processes	223
7.1.2	Adsorbent characteristics	224
7.1.3	Experimental study of a Dual Piston Driven PSA system	225
7.1.4	Mathematical modelling	226
7.1.5	Validating the model using the experimental results	227
7.2	Direction for further work	227
	References	231

List of figures

CHAPTER 2

Fig. 2.1	Average and full concentration profiles in a single particle	67
Fig. 2.2	Cyclic concentration profiles in a single particle	67
Fig. 2.3	Comparison between the lumped mass transfer coefficient correlations and Hausen lumped heat transfer coefficient correction factor applied to mass transfer for a range of dimensionless cycle times	67
Fig. 2.4	Dependency of particle mass transfer coefficient upon cycle time - one particle and column model results (Raghavan et al., 1986)	68
Fig. 2.5	Simple CSTR model and assumptions	68
Fig. 2.6	Steady state cyclic concentration profiles and the relevance of the frequency response technique	68
Fig. 2.7	Graphical solutions for all cycle times for a) η and b) η'	69
Fig. 2.8	Correction factor divergence	70
Fig. 2.9	A schematic diagram of a simple PSA cycle	70
Fig. 2.10	Comparison between diffusion & LDF models for cycle time 0.01	71
Fig. 2.11	Comparison between adsorbed and bulk concentration profiles using diffusion and Suzuki-corrected LDF models a) $a=0.05$ b) $a=0.005$ c) $a=0.0005$	72
Fig. 2.12	Revised relationship between a and η (based on CSTR simulations)	73
Fig. 2.13	Comparisons for adsorbed and bulk concentrations using diffusion and corrected LDF models for $a = 0.005$ ($\eta = 628.32$, $\eta' = 5.91$)	73
Fig. 2.14	Comparison between the transient and steady state response for the external gas phase a) $\gamma = 0.1$, $\sigma = 1$, b) $\gamma = 0.2$, $\sigma = 5$	74
Fig. 2.15	Product concentration profiles from column 2 ($a = 0.00076$) for 55 half cycles	75
Fig. 2.16	Product concentration profiles from column 2 ($a = 0.00076$) for 500 complete cycles	75
Fig. 2.17	Concentration profiles using the diffusion model over 28 cycles for $a = 0.00076$ and $a = 0.00567$	76
Fig. 2.18	The effect of changing the parameter W on the concentration profile	76
Fig. 2.19	Concentration profiles across the column at the end of the adsorption step for the full and steady state models	77

CHAPTER 3

Fig. 3.1	Honeycomb adsorber structure (Silica gel on ceramic fibre)	102
Fig. 3.2	Details of the parallel passage adsorber (a) Outside view of the cell (b) Top view of the open cell (c) Side view of the open cell (d) Cross section view of the parallel sided duct coated with two or more layers of activated carbon fiber	102
Fig. 3.3	Graph showing contribution to HETP for HETP vs superficial velocity (Yang,1988)	103
Fig. 3.4	Top and bottom view of larger column assembly a) Top viewed from above b) bottom viewed from below c) bottom viewed from above (no columns in place)	104
Fig. 3.5	Side and cross sectional views of the larger column structure and monolith a) Side view without columns b) Side view with columns c) Individual column from side and cross section view	105
Fig. 3.6	Smaller column structure	106
Fig. 3.7	Small Monolith Cross Section (x24)	106
Fig. 3.8	Large Monolith Cross Section (x 2)	106
Fig. 3.9	Chromatography Experimental Set Up	107
Fig. 3.10	ZLC experimental set up	107
Fig. 3.11	Adsorption And Desorption Plots for 1% CO ₂ in N ₂	108
Fig. 3.12	Adsorption And Desorption Plots For 15% CO ₂ in He	108
Fig. 3.13	Alternative adsorption, desorption and average plots for 1% CO ₂ in N ₂	109
Fig. 3.14	Alternative adsorption, desorption and average plots for 15% CO ₂ in He	109
Fig. 3.15	Adsorption/Desorption/Average Plot Conditions: Small column, Flowrate=190cc/min, 1%CO ₂ in He	110
Fig. 3.16	Adsorption/Desorption/Average Plot Conditions: Small column, Flowrate=242cc/min, 1%CO ₂ in He	110
Fig. 3.17	Adsorption/Desorption/Average Plot Conditions: Small column, Flowrate=294cc/min, 1%CO ₂ in He	111
Fig. 3.18	Adsorption/Desorption/Average Plot Conditions: Small column, Flowrate=346cc/min, 1%CO ₂ in He	111
Fig. 3.19	Adsorption/Desorption/Average Plot Conditions: Small column, Flowrate=398cc/min, 1%CO ₂ in He	112
Fig. 3.20	Adsorption/Desorption/Average Plot Conditions: Small column, Flowrate=350cc/min, 1%CO ₂ in N ₂	112
Fig. 3.21	Adsorption/Desorption/Average Plot Conditions: Small column, Flowrate=410cc/min, 1%CO ₂ in N ₂	113

Fig. 3.22	Adsorption/Desorption/Average Plot Conditions: Small column, Flowrate=470cc/min, 1%CO ₂ in N ₂	113
Fig. 3.23	Adsorption/Desorption/Average Plot Conditions: Small column, Flowrate=530cc/min, 1%CO ₂ in N ₂	114
Fig. 3.24	Adsorption/Desorption/Average Plot Conditions: Small column, Flowrate=590cc/min, 1%CO ₂ in N ₂	114
Fig. 3.25	Adsorption/Desorption/Average Plot Conditions: Large column, Flowrate=300cc/min, 1%CO ₂ in He	115
Fig. 3.26	Adsorption/Desorption/Average Plot Conditions: Large column, Flowrate=400cc/min, 1%CO ₂ in He	115
Fig. 3.27	Adsorption/Desorption/Average Plot Conditions: Large column, Flowrate=500cc/min, 1%CO ₂ in He	116
Fig. 3.28	Adsorption/Desorption/Average Plot Conditions: Large column, Flowrate=600cc/min, 1%CO ₂ in He	116
Fig. 3.29	Adsorption/Desorption/Average Plot Conditions: Large column, Flowrate=700cc/min, 1%CO ₂ in He	117
Fig. 3.30	Adsorption/Desorption/Average Plot Conditions: Large column, Flowrate=800cc/min, 1%CO ₂ in He	117
Fig. 3.31	Adsorption/Desorption/Average Plot Conditions: Large column, Flowrate=400cc/min, 1%CO ₂ in He	118
Fig. 3.32	Adsorption/Desorption/Average Plot Conditions: Large column, Flowrate=500cc/min, 1%CO ₂ in He	118
Fig. 3.33	Adsorption/Desorption/Average Plot Conditions: Large column, Flowrate=600cc/min, 1%CO ₂ in He	119
Fig. 3.34	Adsorption/Desorption/Average Plot Conditions: Large column, Flowrate=650cc/min, 1%CO ₂ in He	119
Fig. 3.35	Adsorption/Desorption/Average Plot Conditions: Large column, Flowrate=700cc/min, 1%CO ₂ in He	120
Fig. 3.36	Adsorption/Desorption/Average Plot Conditions: Large column, Flowrate=750cc/min, 1%CO ₂ in He	120
Fig. 3.37	Adsorption/Desorption/Average Plot Conditions: Large column, Flowrate=25cc/min, 1%N ₂ in He	121
Fig. 3.38	Adsorption/Desorption/Average Plot Conditions: Large column, Flowrate=30cc/min, 1%N ₂ in He	121
Fig. 3.39	Adsorption/Desorption/Average Plot Conditions: Large column, Flowrate=37cc/min, 1%N ₂ in He	122
Fig. 3.40	1 st moment plots for the larger column using 1% CO ₂ in both He and N ₂ carriers	122
Fig. 3.41	1 st moment plots for the smaller column using 1% CO ₂ in both He and N ₂ carriers	123
Fig. 3.42	1 st moment plots for the larger column using 1% N ₂ in He	123
Fig. 3.43	HETP plots for the larger column using 1% CO ₂ in He and N ₂	124

Fig. 3.44	HETP plots for the smaller column using 1% CO ₂ in He and N ₂	124
-----------	---	-----

CHAPTER 4

Fig. 4.1	Steps of a typical Skarstrom cycle (Ruthven, 1994)	153
Fig. 4.2	Batch-recuperative thermal mode of parametric pumping (reproduced from Sweed, 1988)	154
Fig. 4.3	Direct mode of parametric pumping (reproduced from Sweed, 1988)	154
Fig. 4.4	Movement of a chosen variable in a batch mode parametric pump, where upflow and heating are in phase (Pigford et al, 1969)	155
Fig. 4.5	Rapid RPSA a) One-bed “PSA-parametric pumping” system (Keller, 1983) b) Typical axial pressure profiles at cyclic steady state during steps 1 and 2 (Alpay et al, 1994)	156
Fig. 4.6	Single piston PSA apparatus of Ericksson (1979)	157
Fig. 4.7	Dual-Piston Driven PSA unit (adapted from Keller and Kuo, 1982)	158
Fig. 4.8	Pillow block arrangement from side	158
Fig. 4.9	View of dual piston driven rig from above showing pillow block arrangement	159
Fig. 4.10	Dual Piston Driven PSA test rig instrumentation	159
Fig. 4.11	Phase angle arrangement for hubs 1 and 2.	160
Fig. 4.12	TCD calibration curve	160
Fig. 4.13	Dimensionless pressure profiles when no column is present (Helium total reflux runs at 10rpm and 20rpm $\phi_1=0$ $\phi_2=\pi/2$ S1=15.24cm S2=4.34cm)	161
Fig. 4.14	Dimensionless temperature profiles when no column is present (Helium total reflux runs at 10rpm and 20rpm $\phi_1=0$ $\phi_2=\pi/2$ S1=15.24cm S2=4.34cm)	161
Fig. 4.15	Dimensionless average temperature profiles when no column is present (Helium total reflux runs at 20rpm $\phi_1=0$ $\phi_2=\pi/2$ S1=15.24cm S2=4.34cm)	162
Fig. 4.16	Dimensionless pressure profiles when large and small columns are present (Helium total reflux runs at 10rpm $\phi_1=0$ $\phi_2=\pi/2$ S1=15.24cm S2=4.34cm)	162
Fig. 4.17	Dimensionless temperature profiles when large and small columns are present (Helium total reflux runs at 10rpm $\phi_1=0$ $\phi_2=\pi/2$ S1=15.24cm S2=4.34cm)	163
Fig. 4.18	Dimensionless pressure profiles when large and small columns are present (Total reflux runs 10%CO ₂ /90%10rpm N ₂ $\phi_1=0$ $\phi_2=\pi/2$ S1=15.24cm S2=4.34cm)	163
Fig. 4.19	Dimensionless temperature profiles when large and small columns are present (Total reflux runs 10%CO ₂ /90%10rpm N ₂ $\phi_1=0$ $\phi_2=\pi/2$ S1=15.24cm S2=4.34cm)	164

Fig. 4.20	Dimensionless pressure profiles when large column is present (Total reflux runs 10%CO ₂ /90%N ₂ 10rpm and 20rpm $\phi_1=0$ $\phi_2=\pi/2$ S1=15.24cm S2=4.34cm)	164
Fig. 4.21	Mole % of CO ₂ measured at piston 1 as steady state is approached using both large and small columns (Total reflux runs 10%CO ₂ /90%N ₂ 5,10 and 20rpm $\phi_1=0$ $\phi_2=\pi/2$ S1=15.24cm S2=4.34cm)	165
Fig. 4.22	Variation in the mole % of CO ₂ at piston 1 at steady state with changes in phase angle 2 (Total reflux runs 10%CO ₂ /90%N ₂ $\phi_1=0$ S1=15.24cm S2=4.34cm)	165
Fig. 4.23	Variation in the mole % of CO ₂ at piston 1 at steady state with changes in stroke length 2 (Total reflux runs 10%CO ₂ /90%N ₂ $\phi_1=0$ $\phi_2=\pi/2$ S1=15.24cm)	166
Fig. 4.24	Dimensionless pressure profiles when small column is present (Feed-Product runs 10%CO ₂ /90%N ₂ 10rpm $\phi_1=0$ $\phi_2=\pi/2$ S1=15.24cm S2=4.34cm $\phi_F=\pi/2$, $\phi_{P1}=\pi$, $\phi_{P2}=3\pi/2$ t _{valve} =0.05secs for all)	166
Fig. 4.25	Dimensionless pressure profiles when small column is present (Feed-Product runs 10%CO ₂ /90%N ₂ 10rpm $\phi_1=0$ $\phi_2=\pi/2$ S1=15.24cm S2=4.34cm $\phi_F=0$, $\phi_{P1}=\pi$, $\phi_{P2}=3\pi/2$ t _{valve} (feed and product 2)=0.1secs, t _{valve} (product 1)=0.05secs)	167
Fig. 4.26	Mole % of CO ₂ measured at piston 1 and in product 1 tank as steady state is approached using small column (Feed-Product runs 10%CO ₂ /90%N ₂ 10rpm $\phi_1=0$ $\phi_2=\pi/2$ S1=15.24cm S2=4.34cm $\phi_F=\pi/2$, $\phi_{P1}=\pi$, $\phi_{P2}=3\pi/2$ t _{valve} =0.05secs for all)	167

CHAPTER 5

Fig. 5.1	Finite element grid for z domain	194
Fig. 5.2	Orthogonal collocation grid for z domain	194
Fig. 5.3	Orthogonal collocation on finite elements grid for z domain	194
Fig. 5.4	Conventions used for Dual Piston Driven PSA Modelling	195
Fig. 5.5	Representation of Large Column Model	195

CHAPTER 6

Fig. 6.1	Comparison between experimental observations, calculated and simulated dim. pressure profiles for the empty system (10rpm)	215
Fig. 6.2	Comparison between experimental observations, calculated and simulated dim. pressure profiles for the empty system (20rpm)	215
Fig. 6.3	Comparison between experimental observations and simulated dimensionless pressure profiles for the small column (Helium total reflux run at 10rpm $\phi_1=0$ $\phi_2=\pi/2$ S1=15.24cm S2=4.34cm)	216

Fig. 6.4	Dimensionless pressure profiles comparing experimental and simulated dimensionless pressure profiles using the original and new model approaches for the large column (Helium total reflux run at 10rpm, $\phi_1=0$ $\phi_2=\pi/2$ S1=15.24cm S2=4.34cm)	216
Fig. 6.5	Comparison between experimental and simulated dimensionless pressure profiles when adsorbing (Small column, CO ₂ /N ₂ total reflux runs at 10rpm $\phi_1=0$ $\phi_2=\pi/2$ S1=15.24cm S2=4.34cm)	217
Fig. 6.6	Experimental and simulated composition profiles for CO ₂ at end 1 for the small column (CO ₂ /N ₂ total reflux runs $\phi_1=0$ $\phi_2=\pi/2$ S1=15.24cm S2=4.34cm)	217
Fig. 6.7	Experimental and simulated dimensionless pressure profiles for the large column when adsorbing (CO ₂ /N ₂ total reflux runs $\phi_1=0$ $\phi_2=\pi/2$ S1=15.24cm S2=4.34cm)	218
Fig. 6.8	Experimental and simulated composition profiles for CO ₂ at end 1 for the large column (CO ₂ /N ₂ total reflux runs $\phi_1=0$ $\phi_2=\pi/2$ S1=15.24cm S2=4.34cm)	218
Fig. 6.9	Comparison between experimental and simulated concentration profiles for CO ₂ at end 1 for runs undertaken at 5, 10 and 20rpm (Small column CO ₂ /N ₂ total reflux runs $\phi_1=0$ $\phi_2=\pi/2$ S1=15.24cm S2=4.34cm)	219
Fig. 6.10	Effect of changing stroke length ratio on the concentration of CO ₂ at end 1, shown experimentally for the large column. Simulated results for the small column, along with one experimental result, is shown. (CO ₂ /N ₂ total reflux runs $\phi_1=0$ $\phi_2=\pi/2$ S2=4.34cm)	219
Fig. 6.11	Effect of changing ϕ_2 on the concentration of CO ₂ at end 1, shown experimentally for the large column and the large column in an ice bath. Simulated results for the small column along with one experimental result are shown. A simulated large column point is also shown (CO ₂ /N ₂ total reflux runs $\phi_1=0$ S1=15.24cm S2=4.34cm)	220
Fig. 6.12	Comparison between experimental and simulated dimensionless pressure profiles for the small column (Ideal feed-product operating procedure used CO ₂ /N ₂ feed-product runs $\phi_1=0$ $\phi_2=\pi/2$ S1=15.24cm S2=4.34cm)	220
Fig. 6.13	Comparison between experimental and simulated concentration profiles for CO ₂ at end 1 for the small column (Ideal feed-product operating procedure used CO ₂ /N ₂ feed-product runs $\phi_1=0$ $\phi_2=\pi/2$ S1=15.24 S2=4.34cm)	221
Fig. 6.14	General layout of CO ₂ separation system	221

List of tables

CHAPTER 1

Table 1.1	CO ₂ separation options	26
-----------	------------------------------------	----

CHAPTER 2

Table 2.1	Dimensionless CSTR equations	78
Table 2.2	Dimensionless PSA equations	79
Table 2.3	Physical parameters used in PSA simulation (Raghavan et al(1986))	80
Table 2.4	Comparison between LDF and diffusion simulations	80

CHAPTER 3

Table 3.1	Column Dimensions	125
Table 3.2	Experimental Chromatography Runs	125
Table 3.3	Summary of parameters derived from Chromatography and ZLC experiments for the larger and smaller monoliths	126

CHAPTER 4

Table 4.1	System parameters for dual piston driven PSA experiments (Keller and Kuo, 1982)	168
Table 4.2	Monitoring and controlling devices for dual piston driven PSA rig	168
Table 4.3	Summary of experimental procedures	169
Table 4.4	List of experimental runs a) Helium and total reflux experiments b) Feed-product experiments	170
Table 4.5	Best System Set Up	171

CHAPTER 5

Table 5.1	Modelling assumptions for a selection of Pressure Swing Adsorption studies	196
Table 5.2	Key features and assumptions of published piston driven PSA work	197
Table 5.3	Dimensionless DP- PSA models	198
Table 5.4	Parameters used for simulations	199

CHAPTER 6

Table 6.1	Comparison between computing times for all simulations	222
-----------	--	-----

Nomenclature

a	Dimensionless cycle time
A_c	Column cross sectional area
A_p	Piston cross sectional area
a_p	Dimensionless cycle time of PSA steps 2 and 4
$\text{aps}1, \text{aps}2$	Dimensionless parameters
a_s	External surface area per unit volume
A_s	External surface area
$A1, A2$	Input/Output amplitude
c, c_1, c_2, c_i	Bulk/external concentration
\tilde{c}	Bulk concentration (in Laplace domain)
$c_{i,1,2}$	Pore concentrations
c^*	Equilibrium (external) concentration
c_0	Initial/reference concentration
c_{in}	Inlet concentration
C_{in}	Dimensionless inlet concentration
C_{eq}	Dimensionless equilibrium concentration
$C_{i,1,2}$	Dimensionless pore concentrations
$C_{1,2}$	Dimensionless bulk concentrations
\tilde{C}	Dimensionless bulk concentration (in Laplace domain)
\tilde{C}_{in}	Dimensionless inlet concentration (in Laplace domain)
$\tilde{C}_{ldf}, \tilde{C}_{diff}$	Dimensionless bulk concentration (in Laplace domain)
C_{ldf}, C_{diff}	LDF/ Diffusion
$C_{ldf,ss}, C_{diff,ss}$	Dimensionless bulk concentration LDF/ Diffusion
	Dimensionless bulk concentration (at steady state)
	LDF/ Diffusion
$C_{p,m}$	Heat capacity of solid
$C_{p,f}$	Heat capacity of fluid
C_T	Total concentration
d	Channel width
d_c	Hydraulic diameter of channel
D	Diffusivity
D	Monolith diameter
D_{ax}	Axial diffusion coefficient
D_c	Intracrystalline diffusivity
D_e, D_{eff}	Effective diffusivity
D_p	Pore diffusivity
D_{p1}	Piston 1 displacement
D_{p2}	Piston 2 displacement
D_L, D_{L1}, D_{L2}	Axial dispersion coefficients
D_m	Molecular diffusivity
D_v	Self diffusion coefficient
f	Friction factor
F	Flowrate
f_{f1}, f_{f2}	Feed flowrate to piston 1/piston 2
f_{p1}, f_{p2}	Product flowrate from piston 1/piston2
$Ff1, Ff2$	Dimensionless feed flowrate to piston 1/piston 2
$Fp1, Fp2$	Dimensionless product flowrate from piston 1/piston2
G	Ratio of fluid velocities
\bar{h}	Lumped heat transfer coefficient
h_1, h_2, h_3	Internal/external resistances
K, K^*, K_i	Dimensionless equilibrium constant
$k, k_1, k_2, k_i, k'_i, k'$	Effective mass transfer coefficient
k_f	External film mass transfer coefficient
k'_f	Dimensionless film mass transfer coefficient
k_g	Mass transfer coefficient across surface
k_m	Thermal conductivity

l	Wall thickness
L	Laplace operator
L	Dimensionless group
L	Length
L_c	Channel length
L_1, L_2	PSA bed length
M_m	Mass of solid
M_f	Mass of fluid
mtc_i	Dimensionless mass transfer coefficient
n_{p1}, n_{p2}	Total number of moles in piston 1/piston 2
P', P''	Hot, cold cycle time
P	Pressure
P_o	Initial pressure
P_c	Column Pressure
P_p	Pressure after pressure drop
PL	Phase lag
P_H, P_L	High/low PSA bed pressure
p_1, p_2	Column pressure in bed 1,2
P_1, P_2	Dimensionless column pressure in bed 1,2
\hat{P}_H, \hat{P}_L	Dimensionless high/low PSA bed pressure
Pe, Pe_H, Pe_L	Peclet number
psi	Dimensionless parameter
$q, q_i; q_1, q_2,$	Adsorbed phase concentration
$\bar{q}, \bar{q}_1, \bar{q}_2$	Average adsorbed phase concentration
q^*, q^{eq}, q_i^{eq}	Equilibrium adsorbed phase concentration
q_0, q_{oi}	Initial adsorbed phase concentration
Q, Q_i	Dimensionless adsorbed phase concentration
\bar{Q}	Dimensionless average adsorbed phase concentration
Q_i^{eq}	Dimensionless equilibrium adsorbed phase concentration
Q_{ldf}, Q_{diff}	Dimensionless adsorbed phase concentration, LDF/Diffusion
$\bar{Q}_{ldf}, \bar{Q}_{diff}$	Dimensionless average adsorbed phase concentration, LDF/Diffusion
$\tilde{\bar{Q}}_{ldf}, \tilde{\bar{Q}}_{diff}$	Dimensionless average adsorbed phase concentration, LDF/Diffusion (Laplace)
$\tilde{Q}_{ldf}, \tilde{Q}_{diff}$	Dimensionless adsorbed phase concentration, LDF/Diffusion (Laplace)
$\bar{Q}_{ldf,ss}, \bar{Q}_{diff,ss}$	Dimensionless average adsorbed phase concentration, LDF/Diffusion at steady state
r	Radial direction
r_c	Crystal radius
R_p, R	Particle radius
R	Gas constant
Re	Reynolds number
s	Laplace variable
$S1, S2$	Piston stroke lengths
Sc	Schmidt number
Sh	Sherwood number
t, t'	Time domain , discretised time domain
\bar{t}	Mean retention time
t_c	Cycle time
t_{cyc}	Cycle time, DP-D PSA/PSA
t_{valve}	Length of time valve opens for
T, T_o	Temperature, initial temperature
T_m, T_f	Temperature of solid, fluid
u_i	Interstitial velocity
u_1, u_2	Fluid velocities (PSA – step 1,3)
u_1', u_2'	Fluid velocities (PSA – step 2,4)
U_1, U_2	Dimensionless velocities
v, v_1, v_2, v_p	Superficial velocities
v_w	Wave velocity
$V, Velo1, Velo2$	Dimensionless velocity

V_{ads}	Adsorbent volume
V_c	Column volume
V_D	Dead volume
VD	Dimensionless dead volume
V_f	Fluid volume
V_g	Gas volume
$Volp_1, Volp_2$	Dimensionless piston volumes
V_{p1}, V_{p2}	Piston volumes
w	Slab thickness
W	Dimensionless parameter
x	Slab spatial domain
y_i, y_{io}	Mole fraction of component i in column
y_{i_p1}, y_{i_p2}	Mole fraction of component i in product 1,2
y_{i_f1}, y_{i_f2}	Mole fraction of component i in feed1,2
y_{1D}, y_{2D}	Dummy variable for PSA
Y	Dimensionless parameter
z, z_1, z_2	Axial direction
Z, Z_1, Z_2	Dimensionless axial direction

Greek letters

α	Dimensionless parameter
α_m	Thermal diffusivity
β	Dimensionless parameter
β_n	Residue integration pole
δ	Penetration thickness
δ	Wall thickness
ϵ	Void fraction
ϵ_p	Particle porosity
ϕ	Correction factor (heat transfer)
ϕ_1, ϕ_2	Piston phase angles
$\phi_{P1}, \phi_{P2}, \phi_F$	Angles at which solenoid valves open
γ	Dimensionless parameter
η	Nakao and Suzuki correction factor
η'	Additional correction factor
η_{AR}	Correction factor found using amplitude ratio
η_{PS}	Correction factor found using phase shift
λ	Dimensionless parameter
μ	First moment
Π	Dimensionless Pressure
σ	Dimensionless parameter
σ^2	Second moment
τ	Dimensionless time
τ_b	Dimensionless blowdown time
ω	Frequency
ξ	Dimensionless radial direction
ψ	Dimensionless parameter

Chapter 1

Introduction

1.1 Separation of CO₂

Separation of CO₂ is of interest for a variety of applications. These include the removal of CO₂ from natural gas to improve its heating value (Green Chemistry Lab, 2002) and make it a more energy efficient fuel, removal of CO₂ from the local environment in space craft (LeVan et. al, 2000) and separation of CO₂ from power station flue gas (IEA-Carbon Dioxide Capture from Power Stations, 2003). Due to rising levels of CO₂ in the atmosphere thought to be responsible for the greenhouse effect, this latter application has received much attention over the last ten years. Pre-industrial revolution the temperature of the Earth was well regulated by the presence of various greenhouse gases, such as carbon dioxide and methane, in the atmosphere. Radiation from the Sun hit the Earth and the level of gases present were able to adsorb the correct amount of heat to keep the Earth at one temperature. However, over the last 250 years temperatures have been slowly increasing, over the last 100 years the average temperature has increased by 0.6°C (Defra, 2002). The majority of the blame has been placed on the vast volumes of CO₂ that have been released in the need to generate power, in the main, from burning fossil fuels. If the current trend is continued the fear is that catastrophic climatic changes could occur across the planet, with sea levels rising in some areas leading to widespread flooding, and drought and food shortages elsewhere (IEA-Common Questions about Climate Change, 2003). Since CO₂ is the most abundant greenhouse gas and the one that human activity contributes to the most, the challenge is therefore to limit the amount released. In the UK the government has accepted the aim of reducing the amount of CO₂ in the atmosphere by 60% based on current levels over the next 50 years (Dti, 2003). Several options exist for doing this under the headings of reduction and prevention. Strategies such as using renewable energy options or hydrogen-fuelled processes are in development but are viewed as a long-term solutions. So, in the short to medium term at least, reduction is far more achievable. This can be attempted by either making efficiency improvements or by

capturing and storing CO₂ or both. Efficiency improvements are usually reasonably easy to implement, since, up to a certain degree, they are usually accompanied by cost benefits. However capture and storage, or sequestration, is far more difficult since it can be costly and the economic motivation is not present. In the longer term it will clearly become important to sequester, since, to continue burning fossil fuels for energy generation, which will undoubtedly happen even if reduced, then large amounts of CO₂ cannot be allowed to escape into the atmosphere. Therefore the stress lies on trying to improve sequester technology.

1.2 CO₂ Sequestration

The US Department of Energy defines CO₂ sequestration as the capture, separation, storage or reuse of CO₂, and of these elements, it estimates that three quarters of the related cost is made up of capture costs alone (US DoE, 2003). This clearly indicates that the main challenge lies in improving the economics of capture, which can be achieved by addressing and exploring the technology options available. The four main categories of interest are:

- Absorption – CO₂ is removed by chemical or physical absorption using amines, typically MEA, DEA or MDEA when the concentration is low, or a physical solvent, such as Selexol, when the concentration is high. Absorption is the most common method used at present for CO₂ separation. However stripping the solvents of the CO₂ is highly energy intensive and, without inhibitors, the contaminants (SO_x, NO_x etc.) greatly degrade the solvent, therefore the process is costly (US DoE, 1999).
- Membranes – In this technology a gas stream flows at high pressure across a membrane, made of, for example, palladium or a polymer. Separation is achieved as one component permeates faster through the highly porous material than the other components, thus creating an enriched and depleted stream. Clearly the quality of this separation relies on the selectivity of the membrane, which is generally low, hence recycling of the permeate occurs which increases recompression costs. At

present a suitable membrane for CO₂ separation that makes the process economically feasible has not been found (David, 2000).

- Cryogenic separation – Low temperature distillation is only feasible when a high concentration of CO₂ is present, greater than that present in the majority of flue gas streams. However, it may be applicable in a few cases (David, 2000).
- Adsorption – This process relies on physical adsorption of CO₂ on to a highly porous, high area adsorbent selective towards CO₂. Varying the pressure or temperature, as is done in a Pressure Swing Adsorption or Temperature Swing Adsorption process, causes the CO₂ to adsorb and desorb in a cyclic manner. In a Pressure Swing Adsorption process at the highest pressure a CO₂ depleted stream can be removed and at the lowest pressure a CO₂ rich stream is produced. Both PSA and TSA processes are energy intensive, PSA two-three times less so, but both are effective for CO₂ separation and are used commercially for other applications (US DoE, 1999).

A comparison between the different technologies can be found in table 1.1. Much work is being carried out in the area of absorption, with the emphasis on introducing better inhibitors to stop costly solvent degradation and better mass transfer equipment design to reduce stripping costs. This can be linked to some advances being made in the membrane field, where gas adsorption membrane technology, which combines a membrane, used simply as a high mass transfer area contacting device, with an MEA stream is proving promising, although the membrane is expensive and the problem with contaminants and MEA remains. Pressure swing adsorption has largely been discounted and work has focused on improving adsorbents for alternative applications. However, if significant improvements can be made to reduce energy costs and increase throughput then it may provide a feasible alternative for CO₂ removal.

1.3 The Aims of the Thesis

It is the aim of this study to consider how Pressure Swing Adsorption (PSA) can be made more attractive for CO₂ separation. To enhance performance of the technology two improvements can be made. Firstly a dual piston driven configuration can be used which helps reduce compression and expansion costs, and, secondly, structured adsorbent beds can be used to reduce pressure drop. In a packed bed small particles lead to very good mass transfer behaviour but a large pressure drop which, in turn, for a cyclic process reduces the attainable cycle time. Therefore there must be a trade off between mass transfer and pressure drop. A direct comparison between a parallel passage contactor and a packed bed, carried out using an HETP analysis (Ruthen and Thaeron, 1996), showed that the pressure drop per theoretical stage was always lower for the contactor. For optimum behaviour i.e. to obtain the fastest possible cycle time and hence best throughput, a bed consisting of thin uniform walls and small passages would be desirable. In this study the aim is to look at the performance of a dual piston driven system for separating CO₂ and N₂ where the adsorbent beds consist of two differently sized activated carbon monoliths. Comparing an experimental study undertaken using a test rig with mathematical models it is hoped that the performance and viability of the system can be assessed. Particular attention has been paid to the assumptions used in modelling of cyclic adsorption processes, specifically to the linear driving force model, used to represent mass transfer.

1.4 Organisation of the thesis

The research undertaken is presented here in the following form:

- Chapter 2 – The linear driving force model for fast cyclic processes

In this chapter all the various observations found in the literature regarding the LDF model are reconciled and a new method to derive the equivalent lumped LDF model is proposed to correctly predict the cyclic steady state performance of an adsorption

process. To do this three approaches are investigated; a pure numerical simulation, a frequency response study to derive analytically the solution to the cyclic steady state problem and full analytical solution of the dynamic equations.

- Chapter 3 - Adsorbent Characterisation

In order to establish the kinetic and mass transfer characteristics of the adsorption columns used two experimental techniques are examined, namely pulse chromatography and zero length column methods. Values of the adsorption equilibrium constants and effective diffusivities are obtained from both methods and the results compared.

- Chapter 4 – An experimental study of a Dual Piston Driven PSA system

A complete description of the experimental test rig is given. The rig offers great flexibility and numerous physical parameters such as phase angle and stroke length can be altered to change the system performance. The experimental procedures, including runs with no adsorption, total reflux runs (no feed or product streams) and feed-product runs, are explained and the pressure and concentration profiles obtained are discussed.

- Chapter 5 – A mathematical model of a Dual Piston Driven PSA system

The derivation of representative models are outlined. Experimental observations demonstrated that, while the model was valid for the small column, some alterations were required so that the large column could be modelled. By incorporating some resistance terms into the model this was achieved and the resulting equations are shown. In addition a third direct steady state model is presented.

- Chapter 6 – A comparison between simulated and experimental results

In this chapter the experimental and simulated results are reconciled. For all class of experimental run (non adsorbing, total reflux and feed and product) and for both columns concentration and pressure profiles are compared. By analysing the agreement between the two sets of results the models can be verified. In addition a short discussion of how feasible the system is for industrial scale CO₂ removal is presented.

- Chapter 7 – Conclusions and Recommendations for Future work

The final chapter draws together the conclusions of the research undertaken and suggests some directions for future work.

Chapter 1: Tables

Method	Comment	Effective?	Operating Cost	Capital Cost
<i>Absorption</i>	Proven technology - low risk	Yes	High	High
<i>Membranes</i>	Not useful alone	No	Low	High
<i>Cryogenics</i>	Only for high concentrations	No	Low	High
<i>PSA</i>	Low throughput & high energy cost	Yes	High	Low

Table 1.1 CO₂ separation technologies

Chapter 2

The Linear Driving Force Model for Fast Cyclic Processes

2.1 Introduction

In order to consider the dynamic behaviour of an adsorption system such as Pressure Swing Adsorption mathematical modelling becomes necessary. With equation sets that include mass and heat balances plus rate expressions, simulations can often become long and to increase calculating speed simplifying assumptions are sought. One of these assumptions is the linear driving force (LDF) model, originated by Glueckhauf and Coates (1947), used to represent mass transfer. This lumped model, where all the resistances e.g. macropore, micropore, film, are lumped into one parameter and an average adsorbed concentration derived, provides an alternative to using the diffusion equations. In the latter case the resistances are not lumped and the profile of the adsorbed concentration across the adsorbent particle is found, hence an extra domain must be added to any simulation, leading to increased computing time.

In this chapter the applicability of the LDF model for fast cyclic adsorption processes is examined. Initially a literature review is undertaken following the development of the model since its inception. Then, with the objective of finding an equivalent lumped LDF model capable of accurately predicting both the adsorbed and external concentration profiles obtained from the diffusion model, two different approaches are explored. These include a pure numerical simulation and a frequency response study to analytically derive the solution to the cyclic steady state problem. In addition a third approach involving the full analytical solution of the dynamic equations is used to consider transient and steady state behaviour. The systems under consideration are a single particle subjected to a cyclic concentration change at the surface, a perfectly mixed tank with a cyclic inlet concentration and finally a two-bed Skarstrom PSA system.

2.2 Literature review of LDF model

In this review the historical development of the linear driving force (LDF) model is discussed. Attention is paid in particular to the different methods that have been explored to ensure that the model remains applicable for cyclic adsorption processes. It is important to note, however, that a great many authors have worked in this area and the studies discussed below are a selection of the most important and relevant.

2.2.1 Early LDF model development

The linear driving force model was first introduced by Glueckauf and Coates (1947) to describe intraparticle mass transfer in adsorptive processes. They showed that using an effective or lumped mass transfer coefficient the average adsorbed concentration can be found from the bulk and equilibrium concentrations (assuming linear equilibrium). The LDF equation can therefore be written as:

$$\frac{\partial \bar{q}}{\partial t} = ka_s(q^* - q) \quad (2.1)$$

This is in contrast to the diffusion equation where the adsorbed concentration is dependant on particle radius or plate thickness. For example, for a spherical particle, the diffusion equation and condition at the particle surface is written as:

$$\frac{\partial q}{\partial t} = D_p \left(\frac{\partial^2 q}{\partial r^2} + \frac{2}{r} \frac{\partial q}{\partial r} \right) \text{ and } \left. \frac{\partial \bar{q}}{\partial t} \right|_{r=R_p} = -D_p a_s \frac{\partial q}{\partial t} \quad (2.2)$$

Fig 2.1 demonstrates the adsorbed phase concentration profiles obtained using the two different approaches for a single adsorbent particle.

Due to the emergence of adsorption processes with non uniform bulk concentrations Glueckauf (1955) later expanded the LDF theory by considering how the intraparticle diffusion rate changed with varying adsorbed concentration at the surface. He obtained the following series:

$$\frac{dq}{dt} = \frac{\pi^2 D_p}{R_p^2} (q^* - q) + \left(1 - \frac{\pi^2}{15}\right) \frac{dq^*}{dt} \quad (2.3)$$

and when $\frac{dq}{dt} \approx \frac{dq^*}{dt}$ then

$$\frac{dq}{dt} = \frac{15D_p}{R_p^2} (q^* - q) \text{ i.e. } ka_s = \frac{15D_p}{R_p^2} \quad (2.4)$$

For slow surface concentration changes then:

$$\frac{dq}{dt} = \frac{\pi^2 D_p}{R_p^2} (q^* - q) \text{ i.e. } ka_s = \frac{\pi^2 D_p}{R_p^2} \quad (2.5)$$

The result above can be found from the full series expansion solution of the diffusion equation, considering the first term only.

2.2.2 Relevance of the LDF model to cyclic adsorption processes

With the advent of cyclic adsorption/desorption processes and the rising popularity and scope of Pressure Swing Adsorption (PSA) applications, the effect of cycle time (t_c) on mass transfer was investigated in detail. Nakao and Suzuki (1983) were the first to identify a clear link between cycle time and ka_s . They found that for a dimensionless cycle time, $a > 0.1$ where

$a = \frac{D_p t_c}{R_p^2}$, then Glueckauf's (1955) finding still applied and hence:-

$$\text{For } a = 1 \text{ then } ka_s = \frac{\pi^2 D_p}{R_p^2} \quad (2.6)$$

$$\text{For } a = 0.1 \text{ then } ka_s = \frac{15D_p}{R_p^2} \quad (2.7)$$

However, for shorter cycle times, they were able to derive an empirical correlation, obtained by matching diffusion and LDF solutions for a single spherical particle. This showed

$$ka_s \propto \frac{1}{\sqrt{a}} \text{ for } a < 0.1.$$

Representative cyclic concentration profiles across a particle are shown in fig.2.2.

Alpay and Scott (1992) also looked into the adsorption behaviour of a single particle at short cycle times, and using superposition of the penetration theory onto the series expansion of the diffusion equation, were able to derive the following for short cycle times:

$$ka_s = \frac{5.14}{\sqrt{a}} \quad (2.8)$$

The results, using this correlation, agree closely with Nakao and Suzuki's (1983) for moderate to fast cycle times but not for long or very fast cycle times. Agreement for long cycle times is not expected since the particle would be fully penetrated and hence the superposition is redundant; the series expansion alone can approximate the solution.

At very fast cycle times, such as those anticipated for a dual piston driven PSA system, it is essential that mass transfer is accurately represented across the small region of the particle that is penetrated during adsorption/desorption cycles. When subdividing the entire particle radius, as would be required for solving the computational diffusion model, a great many elements would be required to ensure enough are present within the active region. Using an LDF model, which assumes that the concentration across the particle can be treated independently of the particle radius, removes the radial domain from the problem and hence substantially reduces computing time.

2.2.3 The historical analogy with heat transfer

As the isothermal mass transfer problem has its analogy in heat transfer when modelling heat regenerators (Hausen, 1942) it is interesting to note that an approximate analytical expression for cycle time dependency had been evaluated by Hausen (1942) over 40 years before Nakao and Suzuki (1983). Interestingly this work also predates that of Glueckauf (1955) by 13 years.

Hausen looked specifically at heat transfer in a thermal regenerator, which can be represented mathematically by the commonly used two dimensional model for a flat plate:

$$\bar{h}a_s(T_m - T_f) = M_f C_{p,f} \frac{\partial T_f}{\partial x} + M_f C_{p,f} \frac{\partial T_f}{\partial t} \text{ and} \quad (2.9)$$

$$\bar{h}a_s(T_f - T_m) = M_m C_{p,m} \frac{\partial T_m}{\partial t} \quad (2.10)$$

He identified the need to combine all the various internal and external resistances into one lumped parameter, \bar{h} , and his approach was to make a comparison to electrical resistance using the inverse sum equation i.e.

$$\frac{1}{\bar{h}} = \frac{1}{h_1} + \frac{1}{h_2} + \frac{1}{h_3} + \dots \quad (2.11)$$

where h_1, h_2 etc. are internal/external resistances

Hausen proposed an equation for the correction factor ϕ used in defining the equivalent lumped heat transfer coefficient:-

$$\frac{1}{\bar{h}} = \frac{wC_{p,m}}{3\alpha_m} \phi \quad (2.12)$$

where α_m is the thermal diffusivity.

In his case the correction factor was used to average out distortions in the parabolic temperature profile across the slab which were the result of reversing the heat flow at the end of a half cycle. For a flat plate, he found that the correction factor was dependant on the cyclic operation of the regenerator and derived the following:

$$\text{For } \frac{w^2}{\alpha_m} \left(\frac{2}{t_c} \right) \leq 5 \quad \text{then} \quad \phi = 1 - \frac{w^2}{15\alpha_m} \left(\frac{2}{t_c} \right) \quad (2.13)$$

$$\text{and for } \frac{w^2}{\alpha_m} \left(\frac{2}{t_c} \right) > 5 \quad \text{then} \quad \phi = \frac{2.142}{\sqrt{0.3 + 4w^2 \left(\frac{2}{t_c} \right) / 2\alpha_m}} \quad (2.14)$$

Hausen's equation can be modified to represent Nakao and Suzuki's results by substituting the appropriate transport constants, corrected for the system geometry.

The agreement between Hausen's results and those found by Nakao and Suzuki (1983) and

Alpay and Scott (1992) is shown in fig.2.3, where the dependence of the parameters on cycle time is demonstrated. Again this method is only for a single particle and ignores full column effects. It is clear that agreement is good and that Hausen and Suzuki's approaches are analogous.

2.2.4 Extending the single particle approach

All the studies discussed so far are concerned with single particles and adsorbed concentration profiles. Raghavan et al. (1986) argued that these findings have only limited use, as in a real system, such as adsorption columns subject to periodic flows, other mass transfer mechanisms will be present therefore giving rise to a different value for the lumped mass transfer coefficient, again associated with cycle time. Also in real systems the external concentration profiles are of great importance. Raghavan and his colleagues investigated, numerically, the effect of isotherm non linearity, Knudsen and molecular diffusion, and were able to show that, contrary to previous findings, the value of the effective mass transfer coefficient for a PSA system follows the Suzuki one particle behaviour only up to around a dimensionless cycle time, α , of 0.01. After this time the coefficient remains constant and is therefore independent of cycle time. The results obtained can be seen reproduced in fig. 2.4.

2.2.5 Mathematical approaches developed for the cyclic LDF problem

A common approach to considering the cyclic LDF problem has been to look at matching the diffusion and LDF results using Laplace transforms often leading to frequency response techniques. When the problem is written in the Laplace domain the amplitude ratio and phase lag can be found relatively easily. By looking at limiting cases and using simple equivalence a value for an appropriate mass transfer constant can be found. Carta (1993) used Laplace transforms to develop a periodic solution for the diffusion equation and showed that for short cycle times his solution approached the results of Nakao and Suzuki (1983) as did those of Alpay and Scott (1992). For long cycles the results matched the series solution of Alpay and Scott, confirmed by Buzanowski and Yang (1991). The latter study considered a third

separate approach, which was concerned with extending the LDF using a third order cyclic steady state function. Many studies (e.g. Liaw et al., 1979, Kim, 1989) have looked, with some moderate success, at various series extensions based on a parabolic concentration profile assumption. More recently Kim (1996) has considered using a linear approximation to estimate cyclic mass transfer in a particle.

Rodrigues and Dias (1998) used the frequency response technique to find equivalencies between various models, namely the homogenous diffusion equation, the pore diffusion model and the intraparticle diffusion and convection model. Using these solutions they were then able to analyse a continuous tank adsorber (or CSTR) and a plug flow adsorber to check the accuracy of the equivalence approach. Using Bode diagrams they showed that the amplitude ratio and phase lag give different values for ka_s , concluding that, using a single parameter value, the LDF will not match the cyclic steady state solution of the diffusion model.

Additional issues addressed in literature include the effect of particle/slab geometry, non linearity of the isotherm and the importance of the process under consideration; a single particle or entire PSA system for example. The nature of the concentration change has also been considered. Both Sheng and Costa (1997) and Kim (1996) found that different perturbations gave rise to slightly different mass transfer behaviour, generally sinusoidal input or square or triangular wave gave similar but shifted results. In addition Kim et al. (Kim, 1997, Lee and Kim, 1998) have completed studies concerned with developing linear approximations for the LDF equation for both cyclic and non cyclic approximations.

It is clear that there is some disagreement about the best method of finding an equivalent lumped LDF model capable of accurately representing the cyclic steady state external concentration solution of the diffusion model. Since it is this concentration that is of the utmost importance when optimising a cyclic adsorption system then accurate prediction of this profile is crucial.

2.3 Mathematical approaches to the cyclic LDF problem

Clearly there have been many approaches taken to obtaining accurate LDF concentration profiles for cyclic adsorption, some reporting greater success than others, and it is the intention of this study to reconcile these techniques. Using case studies involving a single particle, CSTR and simple PSA model, the derived adsorbed and bulk concentration profiles assuming the LDF and diffusion equations are compared using a numerical simulation and a frequency response study. In addition by examining the pure analytical solution the important issue of how to predict the number of cycles needed to reach cyclic steady state can also be addressed.

2.3.1 Approach 1 - Numerical simulation

2.3.1.1 The single particle model

The approach used by Nakao and Suzuki (1983) to match the LDF and the diffusion model at cyclic steady state is based on the numerical simulation of the solution for both models of the average adsorbed concentration in a single particle, subject to instantaneous equilibration at the surface. The constant, η , needed to evaluate the LDF coefficient,

$$ka_s = \frac{\eta D}{R_p^2} \quad (2.15)$$

is determined in order to approximate correctly the solution from the diffusion equation and was evaluated as a function of the dimensionless half-cycle time, a , and plotted by Nakao and Suzuki (1983). The system used to derive this result can be represented as follows.

LDF model:-

$$\frac{\partial \bar{q}}{\partial t} = ka_s (q_{eq} - \bar{q}) \quad (2.16)$$

Diffusion model:-

$$\frac{\partial \bar{q}}{\partial t} = -D_p a_s \left. \frac{\partial q}{\partial r} \right|_{r=R_p}$$

where

$$q_{eq} = Kc_{in}(t) \quad (2.17)$$

with

$$\frac{\partial q}{\partial t} = D_p \left(\frac{\partial^2 q}{\partial r^2} + \frac{2}{r} \frac{\partial q}{\partial r} \right) \quad (2.2)$$

subject to

$$\left. \frac{\partial q}{\partial r} \right|_{r=0} = 0 \text{ and } q|_{r=R_p} = Kc_{in}(t) \quad (2.18)$$

The assumption that the external bulk concentration changed only as function of time and was not affected by the adsorption process was made. To find the equilibrium values of the adsorbed concentration in the cyclic process a series, which was based on equating the value at the end of an adsorption step with the value at the start of the next desorption step until equilibrium is reached, was used. This present work simply uses a sinusoidal function namely:-

$$c_{in}(t) = \frac{c_0}{2} \left(1 + \sin \frac{\pi t}{t_c} \right) \quad (2.19)$$

Since this study is concerned with matching the changing external concentration as well as the adsorbed concentrations for the LDF and diffusion models an extension to the single particle approach is required.

2.3.1.2 The CSTR model

Raghavan et al. (1986) showed that the correction factor for the mass transfer coefficient relied not only on cycle time but also on the system configuration as discussed in section 2.2.4. In their study they examined a PSA system, considering particularly diffusional column effects on the mass transfer coefficient. In this study the model chosen to look into equivalency problems was a CSTR or perfectly mixed adsorber. There are several reasons for this choice, which are:-

- the model is simple, leading to results that are not complicated by non linear or complex relationships that often occur in distributed systems,
- the modelling equations can be solved analytically, which is of importance when later applying the frequency response technique,
- a perfectly mixed cell represents the limiting behaviour of a full column dispersed plug flow model and hence, in some respects, a real system is being approximated. The real

represented system is a short column where perfect mixing can be assumed due to the very small value of the Peclet number,

- there is the opportunity to look at equivalence in terms of both the external and adsorbed concentration profiles as a function of flowrate. This is not the case for Suzuki's one particle model.

Fig.2.5 shows a diagram of the CSTR along with the assumptions made.

In order to obtain the bulk and adsorbed phase concentration profiles it was necessary to derive mathematical models including both the LDF and the diffusion equations. In both cases the fluid phase mass balance was given by,

$$V_f \frac{dc}{dt} + V_s \frac{d\bar{q}}{dt} = F(c_{in} - c) \quad (2.20)$$

with cyclic inlet concentration defined as,

$$c_{in}(t) = \frac{c_0}{2} (1 + \sin \frac{\pi t}{t_c}) \quad (2.21)$$

In the case of the LDF model the average adsorbed concentration was given by,

$$V_s \frac{d\bar{q}}{dt} = A_s k (q_{eq} - \bar{q}) \quad (2.22)$$

where $q_{eq} = Kc$,

and for the diffusion model by,

$$\frac{d\bar{q}}{dt} = \frac{3D_p}{R_p} \left. \frac{\partial q}{\partial r} \right|_{r=R_p} \quad \text{and} \quad \bar{q} = \frac{3}{R_p^3} \int_0^{R_p} qr^2 dr \quad (2.23)$$

where the adsorbed phase concentration is obtained from a mass balance in the solid,

$$\frac{\partial q}{\partial t} = D_p \left(\frac{\partial^2 q}{\partial r^2} + \frac{2}{r} \frac{\partial q}{\partial r} \right) \quad (2.24)$$

with boundary conditions

$$\left. \frac{\partial q}{\partial r} \right|_{r=0} = 0, \quad q|_{r=R_p} = Kc \quad (2.25)$$

To generalise the results dimensionless equation sets were derived then coded in gPROMS (Process System Enterprises Ltd., 1999) and an appropriate discretisation method used to

allow the adsorbed and bulk concentration profiles to be found.

The dimensionless CSTR model equations for both the LDF and diffusion approaches are given in table 2.1.

Additionally a technique was employed by which direct calculation of cyclic steady state cycle could be obtained. This involved removing the automatic time domain and distributing equations and variables over a dummy time domain, defined by the dimensionless cycle time. To obtain one cycle of steady state behaviour periodicity conditions were set (by definition, this implies the value of the parameters were the same at the end and beginning of the cycle (Nilchan and Pantelides, 1998; Schmidt and Willmott, 1981).

2.3.1.3 Numerical solution methods

Various methods, such as finite difference and orthogonal collocation methods, are available to convert partial differential equations to ordinary differential equations, allowing them to be solved. These methods are further explained in Chapter 5 section 5.2.1. To obtain solutions for the CSTR model the orthogonal collocation on finite elements was chosen to allow discretisation of the spatial domain. A third order polynomial with four finite elements was chosen for the problem, giving rise to 12 discretisation points in total. The number of discretisation points is of greatest consequence when considering diffusion in the adsorbent at short cycle times when only a small volume of the particle is active; there must be enough points within the active region to describe the behaviour, but not too many to make the computing time too long¹. Results of the simulations are given in section 2.4.1.

2.3.2 Approach 2-Frequency response techniques

2.3.2.1 The relevance of frequency response

The concept of analysing the cyclic LDF problem using frequency response methods was

¹ Section 2.3.2.4 shows how being able to accurately predict the penetration depth for any cycle time makes it possible to discretise the radial domain correctly

suggested by Rodrigues and Dias (1998).

Frequency response is defined as the analysis of the output dependency on a forced sinusoidal input, frequency ω , for a linear process. Seborg et al (1989) give the two distinct features as:-

- “- The output sine wave has the same frequency but its phase is shifted relative to the input sine wave by the angle θ (referred to as the phase shift or the phase angle): the amount of **phase shift** depends on the forcing frequency.
- The output sine wave has an **amplitude** (A_2) that also is a function of the forcing frequency”.

The concepts of phase shift and amplitude shift can be seen explained diagrammatically in fig. 2.6.

In this study the output and input waves of fig. 2.6 represent either external or adsorbed concentrations, where the output curve is given by the solution to the LDF or diffusion equation at steady state. Assuming that the amplitude ratio and phase shift can be simply expressed for both equations then by equating them the correction(s) needed for the LDF equation can be found directly. This approach was first applied to the single particle and then expanded to the CSTR model using the same equation set as previously, but ignoring accumulation in the gas phase.

2.3.2.2 The single particle model

The first step of the frequency response method is to express the problem mathematically. This is achieved using equations (2.15) – (2.19), which show the LDF and diffusion models for a single particle. As noted in the previous section dimensionless equations help to simplify the problem and allow easier analysis. The dimensionless variables and groups used in this derivation are given by:

$$\xi = \frac{r}{R_p} \quad \tau = \frac{t}{t_c} \quad C_{in} = \frac{c_{in}}{c_0} \quad Q = \xi \frac{q}{q_0} \quad \bar{Q} = \frac{\bar{q}}{q_0} \quad a = \frac{D_p t_c}{R_p^2} \quad k a_s = \frac{\eta D_p}{R_p^2} \quad (2.26)$$

This gave:-

LDF:-

$$\frac{d\bar{Q}}{d\tau} = \eta a (C_{in} - \bar{Q}) \quad (2.27)$$

Diffusion:-

$$\bar{Q}_{diff}(s) = 3 \int_0^s Q(\xi) d\xi \quad \text{with} \quad (2.28)$$

$$\frac{\partial Q}{\partial \tau} = a \frac{\partial^2 Q}{\partial \xi^2} \quad \text{subject to} \quad (2.29)$$

$$Q|_{\xi=0} = 0 \quad \text{and} \quad Q|_{\xi=1} = C_{in} \quad (2.30)$$

Frequency response requires transformation to the Laplace domain, which, assuming the particle is initially clean gives:

LDF:-

$$\bar{Q}(0) = 0$$

Diffusion:-

$$Q(0) = 0$$

$$\tilde{Q}(s) = \frac{a}{s} \frac{d^2 \tilde{Q}(s)}{d\xi^2} \quad (2.31)$$

$$\boxed{\tilde{Q}_{ldf}(s) = \frac{\eta a \tilde{C}_{in}(s)}{\eta a + s}} \quad (2.32)$$

which, with boundary conditions, gives,

$$\tilde{Q}(s) = \frac{\sinh\left(\sqrt{\frac{s}{a}}\xi\right)}{\sinh\left(\sqrt{\frac{s}{a}}\right)} \tilde{C}_{in}(s) \quad (2.33)$$

The average adsorbed concentration is found from (2.28) giving,

$$\boxed{\tilde{Q}_{diff}(s) = \frac{3\tilde{C}_{in}(s)a}{s} \left(\sqrt{\frac{s}{a}} \coth\left(\sqrt{\frac{s}{a}}\right) - 1 \right)} \quad (2.34)$$

Substituting $s=i\pi$ gives:-

$$\bar{Q}_{ldf}(i\pi) = \frac{\eta a C_{in}(i\pi)}{\eta a + i\pi} \quad \text{and} \quad \bar{Q}_{diff}(i\pi) = \frac{3a C_{in}(i\pi)}{i\pi} \left(\sqrt{\frac{i\pi}{a}} \coth\left(\sqrt{\frac{i\pi}{a}}\right) - 1 \right) \quad (2.35)$$

These functions can then be expressed in series for two limiting cases; when $a \gg 1$ and when $a \ll 1$ i.e. very slow and very fast cycle times. The graphical solution for all cycle times is shown in fig. 2.7a).

- CASE 1 - Slow cycle times ($a \gg 1$)

LDF:-

$$\bar{Q}_{ldf}(i\pi) = C_{in}(i\pi) \left(1 - \frac{\pi^2}{\eta^2 a^2} - i \frac{\pi}{\eta a} \right) \quad \text{Diffusion:-} \quad \bar{Q}_{diff}(i\pi) = C_{in}(i\pi) \left(1 - \frac{2\pi^2}{315a^2} - i \frac{\pi}{15\eta a} \right) \quad (2.36)$$

Finding the modulus (i.e. amplitude ratio) of each and equating leads to the limiting value:

$$\eta_{AR} = 15 \sqrt{\frac{7}{13}} \cong 11 \quad (2.37)$$

At the same time equating the phase shifts found from the arguments gives:

$$\eta_{PL} = 15 \quad (2.38)$$

This latter result is the same as the classic Glueckauf and Coates (1947) solution whereas the η_{AR} solution is closer to π^2 ; the long time solution of both Glueckauf (1955) and Alpay and Scott (1992). When a is very large, by definition, cycle times are long therefore this result is expected. It should, however, be noted that the amplitude ratio calculated is very close to 1 and hence the solutions obtained using $\eta = \pi^2$, 11 or 15 are all very similar. Also the value of the phase lag is very small indicating that, when comparing solutions, the value of η used would allow a match for the amplitude ratio.

- CASE 2 - Fast cycle times ($a \ll 1$)

LDF:-

$$\bar{Q}_{ldf}(i\pi) = C_{in}(i\pi) \left(\frac{\eta^2 a^2}{\pi^2} - i \frac{\eta a}{\pi} \right) \quad \text{Diffusion:-} \quad \bar{Q}_{diff}(i\pi) = \frac{3C_{in}(i\pi)}{\pi} \left(\sqrt{\frac{\pi a}{2}} + i \left(a - \sqrt{\frac{\pi a}{2}} \right) \right) \quad (2.39)$$

In this case

$$\eta_{AR} = \frac{5.32}{\sqrt{a}} \text{ and} \quad (2.40)$$

$$\eta_{PL} = \frac{\pi}{a} \quad (2.41)$$

For short cycle times Nakao and Suzuki (1983) found that the mass transfer coefficient was

proportional to $\frac{1}{\sqrt{a}}$ and hence this indicates the first of the above equations can be used to

match the amplitude ratio of adsorbed concentration profile of the diffusion equation.

In their study Rodrigues and Dias (1998) analysed the concentration profiles obtained for the LDF model using an approach similar to that derived above, and concluded that, at fast cycles, the correction obtained using the phase lag equivalence gives rise to the best match to the diffusion model. The resulting phase difference observed was then corrected for using a plot of the LDF phase lag function against the diffusion phase lag function. However, the results obtained, expressed in the form of Bode diagrams and limiting functions, did not demonstrate that matching between the profiles had been achieved.

Clearly, at fast cycle times solving for η using amplitude ratio and phase shift leads to two different values, where either the phase lag or amplitude are matched and simply adjusting the mass transfer coefficient will not lead to full matching. Indeed as demonstrated in fig. 2.8, disagreement becomes worse as the cycle time becomes smaller and the two values diverge.

It is therefore necessary, we suggest, to also adjust the other constant; the equilibrium constant. Extending the model to incorporate more than a single particle will show whether such a technique may be possible.

2.3.2.3 *The CSTR model*

As previously, the CSTR model allows both analysis of the adsorbed and external concentrations. The frequency response techniques, used for the single particle case, can be used to examine how these concentration profiles behave given a sinusoidal inlet concentration. Initially mathematical representations of the system for both the LDF and diffusion models were required. It was possible to use most of the equations derived for the computational model, but in this instance accumulation in the gas phase has been neglected, since this accumulation is likely to be small for a gas system. To obtain the CSTR models using either the LDF approximation or the full diffusion approach, equations (2.21 - 2.25) are employed with the exception of the fluid phase mass balance (2.20) which, in this case, is given by,

$$Fc_{in} = Fc + V_s \frac{d\bar{q}}{dt} \quad (2.42)$$

As previously the models are then written in a dimensionless form. Here the same parameters as for the single particle case are used, given by equation (2.26).

- Dimensionless CSTR models assuming LDF equation

Additional dimensionless parameters for the LDF case included:

$$C_{ldf} = \frac{c}{c_0} \text{ and } Q_{ldf} = \frac{q}{q_0} \quad (2.43)$$

To further simplify the equations more dimensionless groups are defined,

$$\alpha = \frac{F}{F + A_s k K}, \beta = \frac{\alpha A_s k t_c}{V_s}, \sigma = \frac{A_s k t}{V_s} \text{ and } \gamma = \frac{F t_c}{K V_s} \quad (2.44)$$

where σ can be said to represent the ratio of half cycle time to mass transfer and, γ , the ratio between half cycle time to the washout of the solid. They can also be written:-

$$\alpha = \frac{\gamma}{\gamma + \sigma} \text{ and } \beta = \alpha \sigma \quad (2.45)$$

After manipulating the fluid phase mass balance for the LDF case (2.42) the following is obtained,

$$\frac{dC_{ldf}}{d\tau} + \beta C_{ldf} - \left(\alpha \frac{dC_{in}}{d\tau} + \beta C_{in} \right) = 0 \quad (2.46)$$

Rearranging (2.46) above gives,

$$\frac{dC_{ldf}}{d\tau} + \beta C_{ldf} = \boxed{\alpha \frac{dC_{in}}{d\tau} + \beta C_{in}} = f(\tau), \text{ a known function of } \tau \text{ since } C_{in} \text{ is known.} \quad (2.47)$$

This can now be written in the Laplace domain,

$$s \tilde{C}_{ldf}(s) - C_{ldf}(0) + \beta \tilde{C}_{ldf}(s) = L[f(t)] \quad (2.48)$$

Rearranging gives

$$\tilde{C}_{ldf}(s) = \frac{(s\alpha + \beta)\tilde{C}_{in}}{s + \beta} \text{ where } C_{ldf}(0) = 0 \text{ and } C_{in}(0) = 0 \quad (2.49)$$

Substituting for α and β gives:-

$$\tilde{C}_{\text{ldf}}(s) = \frac{\gamma(s + \sigma)\tilde{C}_{\text{in}}}{\gamma(s + \sigma) + s\sigma} \quad (2.50)$$

Using the dimensionless groups detailed in table 2.1 and (2.45) above then $\sigma = a\eta$ and therefore,

$$\boxed{\tilde{C}_{\text{ldf}}(s) = \frac{\tilde{C}_{\text{in}}}{1 + \frac{a\eta}{\gamma} \frac{s}{s + a\eta}}} \quad (2.51)$$

The adsorbed phase concentration can be found from:-

$$\bar{Q}_{\text{ldf}} = \gamma \int (C_{\text{in}} - C_{\text{ldf}}) d\tau \quad (2.52)$$

which, in the Laplace domain gives:-

$$\boxed{\tilde{Q}_{\text{ldf}}(s) = \frac{a\eta}{a\eta + s \left(1 + \frac{a\eta}{\gamma} \right)} \tilde{C}_{\text{in}}} \quad (2.53)$$

- Dimensionless CSTR models assuming Diffusion model

For the **diffusion** case the dimensionless parameters are again as defined by (2.26), except that the reference concentration is here the equilibrium bulk concentration such that:-

$$C_{\text{in}} = \frac{c_{\text{in}}}{c^*} \quad Q = \xi \frac{q}{q^*} \quad \bar{Q}_{\text{diff}} = \frac{\bar{q}}{q^*} \quad C_{\text{diff}} = \frac{c}{c^*} \quad (2.54)$$

The adsorbed phase concentration can therefore be written as,

$$\frac{\partial Q_{\text{diff}}}{\partial \tau} = a \frac{\partial^2 Q_{\text{diff}}}{\partial \xi^2} \quad (2.55)$$

with

$$Q_{\text{diff}} \Big|_{\xi=0} = 0 \quad \text{and} \quad Q_{\text{diff}} \Big|_{\xi=1} = C_{\text{diff}} \quad (2.56)$$

Hence the average adsorbed phase concentration is given by,

$$\frac{\partial \bar{Q}_{\text{diff}}}{\partial t} = \frac{A_s}{V_s} \frac{D_p}{R_p} \left[K C_{\text{diff}} \left(\frac{\partial Q_{\text{diff}}}{\partial \xi} \Big|_{\xi=1} - C_{\text{diff}} \right) \right] \quad (2.57)$$

$$\text{For a sphere then } \frac{A_s}{V_s} = \frac{3}{R_p} \quad (2.58)$$

Substituting into the fluid phase mass balance gives,

$$C_{in} = C_{diff} + \frac{3V_s D_p K}{R_p^2 F} \left(\frac{\partial Q_{diff}}{\partial \xi} \Big|_{\xi=1} - C_{diff} \right) \quad (2.59)$$

Defining another useful dimensionless group,

$$Y = \frac{FR_p^2}{3V_s D_p K} \quad (2.60)$$

then (2.59) becomes:-

$$C_{in} = C_{diff} + \frac{1}{Y} \left(\frac{\partial Q_{diff}}{\partial \xi} \Big|_{\xi=1} - C_{diff} \right) \quad (2.61)$$

In both the LDF and diffusion cases the inlet concentration is given by,

$$C_{in} = \frac{1}{2} (1 + \sin \pi \tau) \quad (2.62)$$

Transforming (2.55) to the Laplace domain and applying boundary conditions (2.56) gives,

$$\tilde{Q}_{diff}(s) = \frac{\sinh\left(\sqrt{\frac{s}{a}}\xi\right)}{\sinh\left(\sqrt{\frac{s}{a}}\right)} \tilde{C}_{diff}(s) \quad (2.63)$$

Differentiating and evaluating at $\xi=1$ gives:-

$$\frac{\partial \tilde{Q}_{diff}}{\partial \xi} \Big|_{\xi=1} = \tilde{C}_{diff}(s) \sqrt{\frac{s}{a}} \coth \sqrt{\frac{s}{a}} \quad (2.64)$$

Substituting into (2.61) in the Laplace domain gives:-

$$\tilde{C}_{diff}(s) = \frac{Y \tilde{C}_{in}}{\sqrt{\frac{s}{a}} \coth \sqrt{\frac{s}{a}} + Y - 1} \quad (2.65)$$

Using $Q_{diff} = 3Ya \int (C_{in} - C_{diff}) d\tau$ then

$$\tilde{Q}_{diff}(s) = \frac{3Ya \tilde{C}_{in}}{s} \frac{\sqrt{\frac{s}{a}} \coth \sqrt{\frac{s}{a}} - 1}{\sqrt{\frac{s}{a}} \coth \sqrt{\frac{s}{a}} + Y - 1} \quad (2.66)$$

2.3.2.4 Frequency response for the CSTR model

With the LDF and diffusion models expressed in the Laplace domain, the amplitude ratios and phase lags can be found as before. Initially s is replaced by $i\omega$ giving rise to the

following:

$$\begin{aligned}\tilde{C}_{\text{lef}}(i\omega) &= \frac{\tilde{C}_{in}}{1 + \frac{a\eta}{\gamma} \frac{i\omega}{i\omega + a\eta}} \\ \tilde{Q}_{\text{lef}}(i\omega) &= \frac{a\eta}{a\eta + i\omega \left(1 + \frac{a\eta}{\gamma}\right)} \tilde{C}_{in}\end{aligned}\quad (2.67)$$

$$\begin{aligned}\tilde{C}_{\text{diff}}(i\omega) &= \frac{Y\tilde{C}_{in}}{\sqrt{\frac{i\omega}{a}} \coth \sqrt{\frac{i\omega}{a}} + Y - 1} \\ \tilde{Q}_{\text{diff}}(i\omega) &= \frac{3Ya\tilde{C}_{in}}{s} \frac{\sqrt{\frac{i\omega}{a}} \coth \sqrt{\frac{i\omega}{a}} - 1}{\sqrt{\frac{i\omega}{a}} \coth \sqrt{\frac{i\omega}{a}} + Y - 1}\end{aligned}\quad (2.68)$$

The moduli and arguments can then be found when the functions are expanded as series and, as previously, limiting solutions can be evaluated and expressions for η found.

However, the interest lies in not just matching to give a solution for η but also for an additional correction factor for the equilibrium constant. This can be defined as

$$\eta' = \frac{\gamma}{3Ya} \quad (2.69)$$

or, more generally,

$$\eta' = \frac{\bar{Q}_{\text{lef}}}{\bar{Q}_{\text{diff}}} = \frac{a\eta}{(a\eta + i\pi) \frac{3a}{i\pi} \left(\sqrt{\frac{i\pi}{a}} \coth \sqrt{\frac{i\pi}{a}} - 1 \right)} \quad (2.70)$$

Substituting into the derivations above and solving for both correction factors it was found that the η and η' parameters are simply dependant on cycle time, independent of Y and hence non system specific. Therefore since the single particle case is obtained when $Y \rightarrow \infty$ both constants can be obtained from this, the simplest model. It was found that the value obtained when the phase lags for the single particle case are matched is the correction factor η . We can therefore presume that η' can be used to correct for the amplitude.

Considering the limiting cases for $a \gg 1$ then $\eta' = 1$. Therefore, as expected, for long time cycles the equilibrium constant does not need to be adjusted and the proposed method reverts to the Glueckauf approximation.

$$\text{For } a \ll 1 \text{ then } \eta' = \frac{1}{3} \sqrt{\frac{\pi}{2a}} \quad (2.71)$$

Correspondingly, the η that must be employed, found from the phase lag, is π/a . By definition it is clear that the amplitude of the adsorbed phase solution must be adjusted by η' in order for matching to occur. The full graphical solutions for both correction factors dependant on cycle time can be found in fig. 2.7.

The physical meaning of the parameter, η' , can be interpreted in various ways. One could consider this to be the ratio of the effective equilibrium constants, but this interpretation leads to difficulties when extending the application of the equivalence relations to non-linear isotherms or multicomponent systems. Another interpretation is to consider this the ratio of the effective volumes, thus the inverse of η' gives an indication of the use of the adsorbent material. For $a \ll 1$, regardless of the geometry, the dimensionless penetration depth is

$$\delta = \sqrt{\frac{2a}{\pi}} \quad \text{and} \quad \frac{1}{\eta'} = 3\sqrt{\frac{2a}{\pi}} = \frac{4\pi R_p^2 \delta R_p}{\frac{4}{3}\pi R_p^3} = 3\delta \quad (2.72)$$

Therefore η' is simply a dimensionless volume, the multiplier (3 in this case) is due to the spherical geometry. In addition if we consider the method of solution for the computational models the ability to be able to calculate the penetration depth is extremely useful. Considering the diffusion case, it makes it possible to space the collocation points suitably through the particle; using an appropriate polynomial order and number of finite elements, such that there are enough points in the “active region” to describe the concentration changes, without making computations unnecessarily slow.

In order to verify the new LDF approach simulations were undertaken, using the previously developed numerical CSTR model but employing the new correction factors. Results are shown in section 2.4.2. To investigate general applicability a simple PSA model, detailed in section 2.3.4, was also developed and simulated using the derived correction factors. Results

are presented in section 2.4.4. Before this development, however, the issue of how steady state behaviour can be predicted was explored.

2.3.3 Approach 3 – Full Analytical Solutions

The two approaches used so far have been pursued with the aim of matching concentration profiles using the LDF and diffusion models at steady state. By considering the full analytical problem solutions the approach to steady state can be examined.

It was suggested in the section previous to this that by using two correction factors both the adsorbed and external concentrations using the LDF and diffusion models can be matched at steady state. The Alpay and Scott (1992) and Nakao and Suzuki(1983) single particle studies were only able to do this for the adsorbed phase. Predicted concentration profiles, however, could not be matched in the transient profile using the 2 parameter approach, although it was found that the LDF and diffusion models reached steady state at the same time. In terms of operational significance, especially for the dual piston system, it would be extremely useful to be able to anticipate when steady state is reached since when this point is reached it is hoped that the profiles can be correctly modelled using the LDF equation and hence the piston movement can be optimised accordingly. By considering the full analytical LDF and diffusion solutions a direct method which would show what parameters contributed to the concentration profiles temporal behaviour could be developed.

To find the solution the problem is first expressed in the Laplace domain, where it can be solved. Then transferring back to the original domain gives the required profile. The analytical solutions presented here are for a CSTR where accumulation in the gas phase has been neglected. Therefore the full analytical solutions take as their start point the expressions for the concentration profiles in the Laplace domain as derived for the frequency response analysis of section 2.3.2.3.

2.3.3.1 Analytical solution assuming the LDF model

Previously the expression for the external concentration in the Laplace domain was found as:-

$$\tilde{C}_{ldf}(s) = \frac{(s\alpha + \beta)\tilde{C}_{in}}{s + \beta} \quad (2.49)$$

In the original domain, and applying the convolution theorem, this solution gives:-

$$C_{ldf} = \int_0^{\tau} f(u) e^{-\beta(\tau-u)} du \quad (2.73)$$

After solving the integral the solution is:-

$$C_{ldf} = 0.5 \left[\frac{\pi\beta(\alpha-1)\cos\pi\tau + (\alpha\pi^2 + \beta^2)\sin\pi\tau - e^{-\beta\tau}(\pi\beta(\alpha-1))}{\pi^2 + \beta^2} - e^{-\beta\tau} + 1 \right] \quad (2.74)$$

Substituting for α and β yields:-

$$C_{ldf} = \frac{1}{2} \left[1 - \frac{\pi \cos \pi\tau \frac{\gamma\sigma}{\gamma+\sigma} - \left(\frac{\gamma\sigma}{\gamma+\sigma} \right)^2 \sin \pi\tau}{\pi^2 + \left(\frac{\gamma\sigma}{\gamma+\sigma} \right)^2} - \left(1 - \frac{\left(\frac{\pi\gamma\sigma}{\gamma+\sigma} \right)}{\pi^2 + \left(\frac{\gamma\sigma}{\gamma+\sigma} \right)^2} \right) e^{-\frac{\gamma\sigma\tau}{\gamma+\sigma}} \right] + \\ \dots \frac{1}{2} \left[\frac{\gamma}{\gamma+\sigma} \left(\frac{\left(\cos \pi\tau - e^{-\frac{\gamma\sigma\tau}{\gamma+\sigma}} \right) \frac{\pi\gamma\sigma}{\gamma+\sigma} + \pi^2 \sin \pi\tau}{\pi^2 + \left(\frac{\gamma\sigma}{\gamma+\sigma} \right)^2} + e^{-\frac{\gamma\sigma\tau}{\gamma+\sigma}} \right) \right] \quad (2.75)$$

This is the full solution using the LDF approach appropriate to the stated assumptions shown in fig. 2.5. Using this solution the cyclic steady state solution can be found since as steady

state is approached then the term $e^{-\frac{\gamma\sigma\tau}{\gamma+\sigma}} \rightarrow 0$.

Therefore:-

$$C_{ldf,ss} = \frac{1}{2} \left[1 - \left(\frac{\pi \cos \pi\tau \frac{\gamma\sigma}{\gamma + \sigma} - \left(\frac{\gamma\sigma}{\gamma + \sigma} \right)^2 \sin \pi\tau}{\pi^2 + \left(\frac{\gamma\sigma}{\gamma + \sigma} \right)^2} \right) + \frac{\gamma\pi}{\gamma + \sigma} \left(\frac{\frac{\gamma\sigma}{\gamma + \sigma} \cos \pi\tau + \pi \sin \pi\tau}{\pi^2 + \left(\frac{\gamma\sigma}{\gamma + \sigma} \right)^2} \right) \right] \quad (2.76)$$

The adsorbed phase concentration in the Laplace domain was found earlier to be:-

$$\tilde{Q}_{ldf}(s) = \frac{a\eta}{a\eta + s \left(1 + \frac{a\eta}{\gamma} \right)} \tilde{C}_{in} \quad (2.53)$$

and can be solved, remembering $\sigma = a\eta$, to give:-

$$\overline{Q}_{ldf} = \frac{\gamma}{2} \left[\frac{1 - \frac{\cos \pi\tau}{\pi} + \frac{\gamma\sigma}{\gamma + \sigma} \sin \pi\tau - \left(\frac{\gamma\sigma}{\gamma + \sigma} \right)^2 \left(\frac{1}{\pi} - \frac{\cos \pi\tau}{\pi} \right)}{\left(\frac{\gamma\sigma}{\gamma + \sigma} \right)^2 + \pi^2} - \left[1 - \frac{\frac{\gamma\sigma\pi}{\gamma + \sigma}}{\left(\frac{\gamma\sigma}{\gamma + \sigma} \right)^2 + \pi^2} \right] \exp\left(-\frac{\gamma\sigma\tau}{\gamma + \sigma}\right) - 1 \right] \\ - \frac{\gamma\pi}{\gamma + \sigma} \left[\frac{\frac{\gamma\sigma}{\gamma + \sigma} \left[\frac{\sin \pi\tau}{\pi} + \frac{\exp\left(-\frac{\gamma\sigma\tau}{\gamma + \sigma}\right) - 1}{\frac{\gamma\sigma}{\gamma + \sigma}} \right] + 1 - \cos \pi\tau}{\left(\frac{\gamma\sigma}{\gamma + \sigma} \right)^2 + \pi^2} + \frac{\exp\left(-\frac{\gamma\sigma\tau}{\gamma + \sigma}\right) - 1}{\frac{\gamma\sigma\pi}{\gamma + \sigma}} \right] \quad (2.77)$$

with the cyclic steady state solution given by:-

$$\overline{Q}_{ldf,ss} = \frac{\gamma}{2} \left[\frac{1 - \frac{\cos \pi\tau}{\pi} + \frac{\gamma\sigma}{\gamma + \sigma} \sin \pi\tau - \left(\frac{\gamma\sigma}{\gamma + \sigma} \right)^2 \left(\frac{1}{\pi} - \frac{\cos \pi\tau}{\pi} \right)}{\left(\frac{\gamma\sigma}{\gamma + \sigma} \right)^2 + \pi^2} + \left[1 - \frac{\frac{\gamma\sigma\pi}{\gamma + \sigma}}{\left(\frac{\gamma\sigma}{\gamma + \sigma} \right)^2 + \pi^2} \right] \frac{1}{\frac{\gamma\sigma}{\gamma + \sigma}} \right] \\ - \frac{\gamma\pi}{\gamma + \sigma} \left[\frac{\frac{\gamma\sigma}{\gamma + \sigma} \left[\frac{\sin \pi\tau}{\pi} - \frac{1}{\frac{\gamma\sigma}{\gamma + \sigma}} \right] + 1 - \cos \pi\tau}{\left(\frac{\gamma\sigma}{\gamma + \sigma} \right)^2 + \pi^2} - \frac{1}{\frac{\gamma\sigma\pi}{\gamma + \sigma}} \right] \quad (2.78)$$

2.3.3.2 Analytical solution assuming the Diffusion model

The solution for the external concentration in the Laplace domain using the diffusion model was found to be:-

$$\tilde{C}_{\text{diff}}(s) = \frac{Y\tilde{C}_{in}}{\sqrt{\frac{s}{a}} \coth \sqrt{\frac{s}{a}} + Y - 1} \quad (2.65)$$

This can also be written, transferring to the original domain, using the convolution theorem:-

$$C_{\text{diff}} = f(\tau) * C_{in} \quad (2.79)$$

Using a residue integration method to invert (2.65) then the following can be found:-

$$f(\tau) = \sum \frac{2Y\beta_n^2 \exp(-\beta_n^2 \tau)}{\frac{\beta_n^2}{a} + Y(Y-1)} \quad (2.80)$$

where β_n = simple poles.

Using (2.80) C_{diff} can be found. Since $\frac{2Y\beta_n^2}{\frac{\beta_n^2}{a} + Y(Y-1)}$ is constant then the convolution integral is:-

$$\int_0^\tau e^{-\beta_n^2(\tau-x)} (1 + \sin \pi x) dx \quad (2.81)$$

This leads to the solution for C_{diff} of :-

$$C_{\text{diff}} = \sum_{n=1}^N Y \frac{[\beta_n^4 + \pi^2 - \beta_n^2 \pi \cos \pi \tau + \beta_n^4 \sin \pi \tau] - [\beta_n^4 + \pi^2 - \pi \beta_n^2] \exp(-\beta_n^2 \tau)}{\left[\frac{\beta_n^2}{a} + Y(Y-1) \right] [\beta_n^4 + \pi^2]} \quad (2.82)$$

As before the steady solution can also be found:-

$$C_{\text{diff},ss} = \sum_{n=1}^N Y \frac{[\beta_n^4 + \pi^2 - \beta_n^2 \pi \cos \pi \tau + \beta_n^4 \sin \pi \tau]}{\left[\frac{\beta_n^2}{a} + Y(Y-1) \right] [\beta_n^4 + \pi^2]} \quad (2.83)$$

The adsorbed concentration in the Laplace domain was previously derived as:-

$$\tilde{Q}_{\text{diff}}(s) = \frac{3Ya\tilde{C}_{in}}{s} \frac{\sqrt{\frac{s}{a}} \coth \sqrt{\frac{s}{a}} - 1}{\sqrt{\frac{s}{a}} \coth \sqrt{\frac{s}{a}} + Y - 1} \quad (2.66)$$

As with the external concentration profiles this can be solved in the original domain to give:-

$$\bar{Q}_{\text{diff}} = \frac{\gamma}{2} \left[\frac{\pi\tau - \cos\pi\tau + 1}{\pi} - \sum_{n=1}^N Y \frac{\left[(\beta_n^4 + \pi^2)\tau + \beta_n^4 \left(\frac{1 - \cos\pi\tau}{\pi} \right) - \beta_n^2 \sin\pi\tau \right]}{\left[\frac{\beta_n^2}{a} + Y(Y-1) \right] [\beta_n^4 + \pi^2]} \right] - \frac{\left[\beta_n^4 + \pi^2 - \pi\beta_n^2 \right] \left[1 - \exp(-\beta_n^2\tau) \right]}{\left[\frac{\beta_n^2}{a} + Y(Y-1) \right] [\beta_n^4 + \pi^2]} \quad (2.84)$$

with the cyclic steady state solution being:-

$$\bar{Q}_{\text{diff,ss}} = \gamma \left[\frac{\pi\tau - \cos\pi\tau + 1}{2\pi} - \sum_{n=1}^N Y \frac{\left[(\beta_n^4 + \pi^2)\tau + \beta_n^4 \left(\frac{1 - \cos\pi\tau}{\pi} \right) - \beta_n^2 \sin\pi\tau - \frac{\beta_n^4 + \pi^2 - \pi\beta_n^2}{\beta_n^2} \right]}{\left[\frac{\beta_n^2}{a} + Y(Y-1) \right] [\beta_n^4 + \pi^2]} \right] \quad (2.85)$$

Introducing various parameter values allows comparison between the steady state concentration profiles obtained assuming the CSTR model and the results obtained by doing this are shown in section 2.4.3.

2.3.4 The PSA model

In order to validate the new LDF approach, a real cyclic adsorption processes was chosen. A simple four step pressure swing adsorption process is selected and the mathematical model derived assuming both mass transfer representations. By comparing the results obtained from the diffusion approach to those found when using the newly developed LDF approach the applicability of the approach can be validated.

2.3.4.1 The PSA cycle

In a basic Skarstrom PSA cycle, discussed in detail in Chapter 4, section 4.2.1, there are four basic steps shown in fig. 2.9. Firstly the feed gas enters at the bottom of column 2, which operates at a high pressure of P_{high} .

Preferential adsorption occurs, the effluent passes through and is partially withdrawn as product and partially makes up the purge passing through column 1, operating at a low pressure P_{low} . During step 2, column 2 is blown down to P_{low} and column 1 is pressurised, using feed gas, to P_{high} . Steps 3 and 4 are exactly the same as the first two steps except that the column are interchanged, i.e. flow is in the reverse direction.

2.3.4.2 Mathematical modelling of the simple PSA cycle

The modelling of the system is based on that of Raghavan et al (1986). The assumptions made in order to simplify the model were:-

- Fluid velocity remains constant during adsorption and desorption
- The system is isothermal
- Pressure drop is negligible
- Resistance to mass transfer occurs in the external fluid film and in the particle macropores.
- The adsorption equilibrium isotherm is linear
- During blowdown/pressurisation, concentrations within the particle are assumed to remain frozen.
- Flow in the columns can be described by the axial dispersed plug flow model including either the LDF equation or the diffusion equation

The aim, as in the previous cases presented in this study, is to match the external phase concentration using the LDF or diffusion equations to represent mass transfer. Therefore mathematical models were developed for the PSA system described, where the four steps of

the process were described by appropriate equation sets. Steps 1 and 2 are shown in full below, since steps 3 and 4 are similar.

- *The PSA model - Diffusion*

The first PSA model below assumes mass transfer described by the **Diffusion** equation.

Step1

COLUMN 2

The external fluid phase, in the diffusion case, is given by,

$$-D_{L2} \frac{\partial^2 c_2}{\partial z_2^2} + u_2 \frac{\partial c_2}{\partial z_2} + \frac{\partial c_2}{\partial t} + \left(\frac{1-\varepsilon}{\varepsilon} \right) \frac{3}{R_p} k_g (c_2 - c_{i2}|_{r=R_p}) = 0 \quad (2.86)$$

where the particle mass balance is,

$$(1-\varepsilon_p) \frac{\partial q_2}{\partial t} + \varepsilon_p \frac{\partial c_{i2}}{\partial t} = \varepsilon_p D_p \left(\frac{\partial^2 c_{i2}}{\partial r^2} + \frac{2}{r} \frac{\partial c_{i2}}{\partial r} \right) \quad (2.87)$$

Since the equilibrium isotherm is $q_2 = Kc_{i2}$ and defining,

$$D_{eff} = \frac{\varepsilon_p D_p}{K^*} \text{ where } K^* = \varepsilon_p + (1-\varepsilon_p)K \quad (2.88)$$

then we obtain:-

$$\frac{\partial c_{i2}}{\partial t} = D_{eff} \left(\frac{\partial^2 c_{i2}}{\partial r^2} + \frac{2}{r} \frac{\partial c_{i2}}{\partial r} \right) \quad (2.89)$$

Boundary conditions at the column ends are given by,

At $z_2=0$

$$D_{L2} \frac{\partial c_2}{\partial z_2} \Big|_{z_2=0} = -u_2 [c_2|_{z_2=0^-} - c_2|_{z_2=0^+}] \quad (2.90)$$

At $z_2=L2$

$$\frac{\partial c_2}{\partial z_2} \Big|_{z_2=L2} = 0 \quad (2.91)$$

Boundary conditions are also needed for the particle and are given as,

$$\left. \frac{\partial c_{i2}}{\partial r} \right|_{r=0} = 0 \quad (2.92)$$

$$\varepsilon_p D_p \left. \frac{\partial c_{i2}}{\partial r} \right|_{r=R_p} = k_g \left(c_2 - c_{i2} \Big|_{r=R_p} \right) \quad (2.93)$$

COLUMN 1

The external fluid phase, in column 1, is expressed as,

$$-D_{L1} \frac{\partial^2 c_1}{\partial z_1^2} + u_1 \frac{\partial c_1}{\partial z_1} + \frac{\partial c_1}{\partial t} + \left(\frac{1-\varepsilon}{\varepsilon} \right) \frac{3}{R_p} k_g \left(c_1 - c_{i1} \Big|_{r=R_p} \right) = 0 \quad (2.94)$$

with the particle mass balance expressed as,

$$\frac{\partial c_{i1}}{\partial t} = D_{eff} \left(\frac{\partial^2 c_{i1}}{\partial r^2} + \frac{2}{r} \frac{\partial c_{i1}}{\partial r} \right) \quad (2.95)$$

Boundary conditions for column 1 are given as,

at $z_1=0$,

$$D_{L1} \left. \frac{\partial c_1}{\partial z_1} \right|_{z_1=0} = -u_1 \left[\frac{P_L}{P_H} c_2 \Big|_{z_2=L2} - c_1 \Big|_{z_1=0^+} \right] \quad (2.96)$$

at $z_1 = L1$,

$$\left. \frac{\partial c_1}{\partial z_1} \right|_{z_1=L1} = 0 \quad (2.97)$$

and, for the particle, are given by

$$\left. \frac{\partial c_{i1}}{\partial r} \right|_{r=0} = 0 \quad (2.98)$$

$$\varepsilon_p D_p \left. \frac{\partial c_{i1}}{\partial r} \right|_{r=R_p} = k_g \left(c_1 - c_{i1} \Big|_{r=R_p} \right) \quad (2.99)$$

Step 2

Blowdown occurs in column 2, while column 1 is pressurised.

COLUMN 2

Noting that pressure and velocity are no longer constant, the external fluid phase is given by

$$-D_{L2} \frac{\partial^2 c_2}{\partial z_2^2} - u'_2 \frac{\partial c_2}{\partial z_2} - c_2 \frac{\partial u'_2}{\partial z_2} + \frac{\partial c_2}{\partial t} = 0 \quad (2.100)$$

with the continuity equation

$$\frac{\partial u'_2}{\partial z_2} = \frac{1}{p_2} \frac{dp_2}{dt}$$
(2.101)

Boundary conditions are given as,

$$\left. \frac{\partial c_2}{\partial z_2} \right|_{z_2=0} = 0 \quad \left. \frac{\partial c_2}{\partial z_2} \right|_{z_2=L2} = 0 \quad \left. u'_2 \right|_{z_2=L2} = 0 \quad (2.102)$$

COLUMN 1

Similarly the external fluid phase is expressed as,

$$-D_{L1} \frac{\partial^2 c_1}{\partial z_1^2} - u'_1 \frac{\partial c_1}{\partial z_1} - c_1 \frac{\partial u'_1}{\partial z_1} + \frac{\partial c_1}{\partial t} = 0 \quad (2.103)$$

with the continuity equation,

$$\frac{\partial u'_1}{\partial z_1} = \frac{1}{p_1} \frac{dp_1}{dt}$$
(2.104)

Boundary conditions are defined as,

$$\left. \frac{\partial c_1}{\partial z_1} \right|_{z_1=0} = 0 \quad \left. \frac{\partial c_1}{\partial z_1} \right|_{z_1=L1} = 0 \quad \left. u'_1 \right|_{z_1=L1} = 0 \quad (2.105)$$

Steps 3 and 4 are the same as Steps 1 and 2 except that the direction of flow is reversed.

- *The PSA model - LDF*

The same system is considered as previously but mass transfer is represented by the LDF equation.

Step 1

Absorption is occurring in column 2, where the pressure is high, while column 2 is desorbing at low pressure.

COLUMN 2

The external fluid phase for the LDF model may be written as,

$$-D_{L2} \frac{\partial^2 c_2}{\partial z_2^2} + u_2 \frac{\partial c_2}{\partial z_2} + \frac{\partial c_2}{\partial t} + \left(\frac{1-\varepsilon}{\varepsilon} \right) \frac{\partial \bar{q}_2}{\partial t} = 0 \quad (2.106)$$

with the average adsorbed phase concentration given by,

$$\frac{\partial \bar{q}_2}{\partial t} = k_f (c_2 - \bar{c}_{i2}) \quad (2.107)$$

Combining the resistances in the macropores and the film then k_f is defined as,

$$\frac{1}{k_f} = \frac{R_p}{3k_g} + \frac{R_p^2}{\eta \varepsilon_p D_p} \quad (2.108)$$

The boundary conditions for the column are the same as for step 1 of the diffusion case, given by (2.90) and (2.91).

COLUMN 1

Similarly the external fluid phase is given by,

$$-D_{L1} \frac{\partial^2 c_1}{\partial z_1^2} + u_1 \frac{\partial c_1}{\partial z_1} + \frac{\partial c_1}{\partial t} + \left(\frac{1-\varepsilon}{\varepsilon} \right) \frac{\partial \bar{q}_1}{\partial t} = 0 \quad (2.109)$$

with the average adsorbed concentration expressed as,

$$\frac{\partial \bar{q}_1}{\partial t} = k_f (c_1 - \bar{c}_{i1}) \quad (2.110)$$

Boundary conditions for the column are as for the diffusion case, given by (2.96) and (2.97).

Step 2

Since it is assumed that concentrations within the particle remain frozen during step 2 then all the equations are the same as those for the step 2 diffusion model (2.100 – 2.105). Also again steps 3 and 4 are the same as steps 1 and 2 except that the direction of flow is reversed.

As before the dimensionless models, detailed in table 2.2, can be written for both equation sets, using appropriate parameters and groups. Simulations using this model were used to verify the new LDF approach developed from the frequency response analysis.

2.4 Analysis of the results assuming the different LDF problem approaches.

2.4.1 Approach1 – Numerical Simulation

The initial aim of the simulation approach is to compare the results obtained when using different published values for the LDF coefficient. In order to consider both the external and adsorbed concentration profiles a CSTR model was chosen and simulations performed both from time zero to steady state and also using a direct cyclic steady state method, the results are given in sections 2.4.1.1 and 2.4.1.2 respectively.

2.4.1.1 Comparison between numerical simulations of the CSTR

Using the equation set developed for a CSTR described in section 2.3.1.2 simulations were undertaken assuming both the LDF and diffusion models. Representative dimensionless half cycle times were used and the corresponding values of the LDF coefficient as found by Nakao and Suzuki (1983) and Alpay and Scott (1992) were employed. Fig. 2.10 shows the adsorbed phase concentration profile obtained from both simulations for a dimensionless half cycle time of 0.01.

Generally agreement between the profiles assuming the full and approximated mass transfer models is good. It can be seen, however, looking at the period 0-0.5 that transient behaviour is not represented well when the LDF model, using Alpay's (1992) correlation for η , is used, and the plots show how the concentration is over estimated. This was also found to be true by Nakao and Suzuki (1983).

It is clear that a great many cycles (>700) are required for steady state to be reached. Also it should be noted that modelling transient behaviour in this way, especially for very fast cycle times, leads to long computing times and difficulties with data handling. A real system will run at steady state and therefore analysis can be carried out assuming cyclic steady state behaviour.

2.4.1.2 Direct cyclic steady state solutions

It is hoped that the system of interest; the dual piston-driven PSA process, will run at very short cycle times. Therefore it is necessary to guarantee the accuracy of the suggested approximations of Nakao and Suzuki (1983) and Alpay and Scott (1992) for this region. In order to consider cyclic steady state behaviour directly it was possible to rewrite the models in a way such that a single steady state cycle could be obtained. The technique involved removing the automatic time domain over which distributes variables and equations, and imposing a dummy time domain, defined by the dimensionless cycle time (as discussed by Nilchan and Pantelides (1998)). To obtain one cycle of steady state behaviour periodicity conditions were set (by definition, this implies the value of the parameters were the same at the end and beginning of the cycle). These replace the initial conditions of a standard model. Figs. 2.11a)-c) show the cyclic steady state profiles obtained when using half cycle times of $a=0.05, 0.005$ and 0.0005 respectively, where a is defined as,

$$a = \frac{D_p t_c}{R_p^2} \quad (2.26)$$

Both the adsorbed and external concentration profiles are shown, using both the LDF and diffusion models.

It is clear that using Nakao and Suzuki's (1983) approximation, applied in each of the LDF simulations, the adsorbed concentration can be approximated reasonably well for all cycle times. It should be noted that when the half cycle time is shorter than 0.001 the mass transfer coefficient, η , no longer obeys the Suzuki cycle time relationship. Fig. 2.12 shows that a constant value, here 51.4, can be employed for the very short cycle time region. This behaviour was also found in Raghavan's (1986) analysis using a PSA process. Most importantly it can be seen from these graphs that the external concentration is not matched when Nakao and Suzuki's (1983) correction is employed. In order to optimise any adsorption process it is necessary to predict correctly both concentration profiles and in particular the gas phase concentration. Therefore the additional correction coefficient is needed. Considering

the lag and amplitude differences observed, the relevance of the frequency response technique is clear.

2.4.2 Approach 2 – Frequency Response

As shown when using the values for the LDF coefficient suggested in literature matching of both the adsorbed and external concentration profiles using the LDF and diffusion models cannot be achieved. The analysis of section 2.3.2, in which matching of the phase lag and amplitude ratio of the concentration profiles obtained from mathematical representations using both mass transfer models was undertaken, led to the development of a two parameter LDF model. Using this new approach a numerical simulation of a CSTR model, as presented in section 2.3.1.2, was undertaken and compared to the results obtained using the diffusion model.

2.4.2.1 Comparison between numerical simulations of the CSTR assuming the new approach to the LDF model.

Using the direct steady state approach the computational CSTR model was simulated using the new derived correction factors for the LDF model and using the diffusion model Fig. 2.13 shows both the adsorbed and external concentration profiles obtained and demonstrates the excellent match obtained.

We have therefore shown that for a simple system operating at cyclic steady state the new approach is validated. The two outstanding issues of importance are how can prediction of when steady state is reached be achieved and how we can guarantee the two parameter LDF model is valid for a real cyclic system. The results of the approaches taken to answer these questions are given in sections 2.4.3 and 2.4.4 below.

2.4.3 Approach 3 – Full Analytical Solution

In order to obtain the full analytical solutions for the concentration profiles for the CSTR model assuming the LDF and diffusion models analysis began with the solutions for the adsorbed and external concentrations in the Laplace domain, as found for the frequency response technique. Transforming these equations and solving gave complex equations which could be examined further to consider the contributions to steady state and transient behaviour. The equations were clearly composed of steady state and transient terms hence as the transient terms tended to zero the steady state solution could be obtained.

2.4.3.1 Determining the time to cyclic steady state

The analytical solutions for the external and adsorbed phase concentrations at steady state assuming the LDF model are given in equations (2.76) and (2.78) respectively and those found assuming the diffusion model are given in equations (2.83) and (2.85). Figures 2.14a) and b) show both the transient and steady state external concentration profiles calculated from the complete analytical solutions using first values of $\gamma=0.1$ and $\sigma=1$, and secondly values of $\gamma=0.2$ and $\sigma=5$ where γ and σ are defined as:-

$$\gamma = \frac{Ft_c}{KV_s} \quad \text{and} \quad \sigma = \frac{A_s k t_c}{V_s} \quad (2.44)$$

The figure clearly shows how the transient solution approaches the steady state solution in fig.2.14 a) after 50 dimensionless half cycles and in fig. 2.14 b) after 25 half cycles. The effect of changing the two dimensionless parameters is clearly evident. When σ is changed the amplitude is affected and most importantly, when γ is changed then the number of cycles to steady state is altered.

From the full analytical solution it is evident that the characteristic time needed to achieve cyclic steady state will depend on $\frac{\gamma\sigma}{\gamma+\sigma}\tau$. Therefore to have a general order of magnitude

the ratio $\sigma/\gamma = A_s kK/F$ needs to be evaluated. If this ratio is large, as in the simulations shown in fig. 2.14, then only the accumulation in the solid phase relative to the inlet flowrate will determine the time needed to approach cyclic steady state. For the cases considered, a simple relationship can be developed to give the time to steady state for any cycle time :-

$$\gamma\tau = \frac{Ft}{KV_s} \approx 5 \quad (2.111)$$

This simple result indicates that if the two parameter correction is applied, the resulting model will have a different effective solid volume. Therefore, while the correct cyclic steady state behaviour is correctly predicted, the resulting dynamic simulations will underestimate the time needed to reach cyclic steady state.

In order to verify the results obtained so far; the correction coefficients and time needed to reach cyclic steady state can be generalised, a simple 4 step PSA model was derived and solved computationally.

2.4.4 The PSA model

As a representative cyclic adsorption process a Pressure Swing Adsorption model was chosen to test the applicability of the new two parameter LDF model, developed using frequency response techniques. The modelling approach taken to mathematically represent the PSA system, assuming either the LDF or Diffusion model is outlined in section 2.3.4. Both equation sets derived were coded into gPROMS and, adopting the parameter values used by Raghavan et al. (1986), the simulations were carried out.

2.4.4.1 The PSA model of Raghavan et al (1986)

As the present study is based on that of Raghavan et al (1986) then the first aim was to consider the results that we obtained and compared them to this study, based itself on a moist air-alumina heatless drier study by Chihara and Suzuki (1983). The parameters used are given in table 2.3. Unlike Raghavan and his colleagues, we made several additional

simplifying assumptions, considering only Knudsen diffusion and also assuming a linear equilibrium isotherm. Concentration profiles were generated for the diffusion model and the LDF model, where, initially, various values of η , suggested from literature, were employed to try and achieve matching. Fig. 2.15 shows product (or external) concentration profiles from the top of column 2 for various LDF and diffusion runs up to 55 half cycles.

The first point of interest can be clearly observed from this graph. Raghavan et al (1986) makes the assumption that at 55 cycles the system is nearing steady state, however it is clear that the concentrations are still rising. It would therefore be unwise to try match the LDF and diffusion models since the system is still in the transient operating zone. As previously noted, matching in this region means that matching is not achieved at steady state. Nevertheless there are some other useful observations that can be made. It is clear that using the suggested Glueckhauf value, $\eta = 15$, gives a profile nowhere near any diffusion solution. Raghavan et al (1986) found that using a value of 40 gave a good match to the diffusion profile they obtained. However the method of discretisation they used only placed 4 collocation points across the particle radius. Looking at simulation results and calculating the penetration depth, as detailed in section 2.3.2.4, shows that the particles are only penetrated up to a dimensionless depth of 0.02. Therefore using only a few points means very little of the adsorption process in the particle is actually represented. It is therefore important to ensure that an adequate number of collocation points are distributed in the radial domain of the particle. The difference between the two diffusion profiles highlight this requirement.

2.4.4.2 The PSA model and the two parameter LDF approach

The objective in this study is to use the derived correction factors to guarantee the external concentration profiles are matched at steady state for the LDF and diffusion models. η and η' can either be calculated using the correlations derived for very fast cycle times , found in

section 2.3.2.4, or can be found from graphical solutions given in fig 2.7. For a value of $a =$

$$0.00076, \text{ where } a = \frac{D_{\text{eff}} t_c}{R_p^2}, \text{ then } \eta = 4.21 \times 10^3 \text{ and, } \eta' = 15.452$$

Rewriting the dimensionless LDF model to include these corrections means simply adjusting the particle mass balance equations, presented in table 2.2, to give:

$$\frac{\partial \bar{Q}_2}{\partial \tau} = k_f' \eta' (C_2 - \bar{C}_{i2}) \quad \text{where} \quad (2.112)$$

$$\frac{1}{k_f'} = \frac{K^*}{3\lambda} + \frac{\eta'}{\eta} \quad (2.113)$$

and

$$\frac{\partial \bar{Q}_1}{\partial \tau} = k_f' \eta' (C_1 - \bar{C}_{i1}) \quad (2.114)$$

With these correction factors it can be seen in fig. 2.16 that for the product concentration profiles a good agreement can be reached at steady state. Computing difficulties due to the large number of equations meant that the diffusion model would not execute for more than 300 cycles, but it is clear that the concentration profile is levelling. By placing a polynomial approximation through the diffusion solution it is possible to estimate that steady state is reached at around 500 cycles; this is not easy to determine from the LDF solution since the approach to steady state is very gradual from 150 cycles on. We can also observe that the assumed value of Raghavan et al (1986) is not correct for steady state approximation when an increased number of collocation points are used across the particle radius.

The necessity for employing the LDF model when modelling was evident as runs progressed, as demonstrated in table 2.4. Even with a fairly conservative number of elements across the particle radius the number of variables in the diffusion case is ten times that of the LDF case. The result is that the simulation time is hugely increased.

Estimating the time to reach cyclic steady state was achieved in the CSTR case (section 2.4.3.1) by analysing the full analytical solutions. In fig. 2.16, a polynomial approximation to the full diffusion solution was used to find the necessary number of cycles. This latter method has no practical use since it is the LDF model that we want to use for PSA modelling. Analysis at another cycle time, shown in fig. 2.17, helps to show how the time to steady state may be estimated, without simulating the full diffusion model.

The similarity of the two profiles for the two cycle times supports the assumption made in section 2.4.3.1 that changing the parameter values will affect the number of cycles required for steady state. If these values remain the same then the number of cycles remains unchanged. Therefore with the values of Raghavan et al given in table 2.3 then for any cycle time steady state is reached at 500 cycles.

Fig. 2.18. gives more weight to this argument. It can be seen that by doubling W the profile obtained is a similar shape to the original graph, except that it occurs over half the number of cycles. It could thus be inferred that steady state is reached in half the time. This finding is parallel to that found in section 2.4.3.1 where a relationship was developed between the parameter γ and time to steady state. In this case considering W alone the relationship can be characterised by

$$\frac{W\tau}{50} \frac{D_{eff}}{R_p^2} = 5(a + a_p) \text{ where } a_p \text{ is the length of step 2,4} \quad (2.115)$$

Further parameter analysis however is necessary to establish whether this relationship still holds when operating conditions are varied.

As in the CSTR case it is also possible to directly obtain the steady state solution, imposing a time domain derived from the cycle time. Unfortunately it was only possible to obtain a solution with some degree of accuracy with the LDF model. The diffusion model could only be solved when the number of discretisation points across the time, axial and radial domains

were too few to give a meaningful result. However solutions found using the LDF model could be generated quickly, in around 5 minutes and it is these solutions that are of operational importance.

Looking at fig 2.19 it can be seen that the direct solution is very close to the steady state solution obtained using the full model. In terms of accuracy there is 10% error in the calculated value at $z = 1$, compared to the 5% error found when using the full solution. The increased error is due to discretisation in time domain, where it was only possible to enforce 120 points across the domain. In relative terms the discrepancy is acceptable since at $z = 1$ the Nakao and Suzuki (1983) value gives an error of 33%, whereas single lumped mass transfer values of 40 and 15 give 73% and 200% errors respectively. Therefore solutions using a steady state model are acceptable for modelling purposes, given the improvements on previous approaches.

2.5 Concluding Remarks

The work presented in this chapter has shown the clear advantages of using the two parameter corrector approach as applied to the LDF equation to model fast cycle adsorption processes. These can be summarised as follows.

- Using the LDF model and employing the two derived coefficients external concentrations at steady state can be found with a high degree of accuracy.
- Finding and applying the correctors is simple. The modeller can either use the derived correlations at the fast cycle time limit or, for increased accuracy, full graphical solutions.
- Since the correctors have proven to depend on cycle time alone, they are non-system specific and are equally valid for a single particle or a PSA system.
- The geometry of the adsorbent is also of no issue as it may be incorporated into the mathematical model and the correction factors changed respectively.

- A cyclic adsorption system may be subjected to various types of perturbation. We have been able to show that the two parameter corrector approach may be used for both sinusoidal (CSTR case) and square wave (PSA case) perturbations.
- Including more than one resistance to mass transfer across an adsorbent particle is easily achieved. Raghavan et al.(1986) suggested resistance to mass transfer occurs in the external fluid film and in the particle macropores. This premise was incorporated into a lumped coefficient for the PSA case and correction factors were applied accordingly.
- The equilibrium or volume corrector is very useful for calculating penetration depth. In terms of modelling this meant we could ensure enough collocations points were distributed across the particle to give accurate results. In a commercial sense the implication is that particles or slabs may be developed with outer coatings of costly adsorbent, the thickness of the penetration depth, with inexpensive inert centres.
- Using the LDF model gives immensely improved computational efficiency. In the PSA case the corrected model is 50 times faster than the diffusion case.

All of these benefits can be taken forward into developing a dual piston driven PSA system for CO₂ separations. We anticipate that our findings regarding the LDF model will prove an extremely powerful modelling tool in the study of the design and optimisation of PSA processes.

Chapter 2: Figures

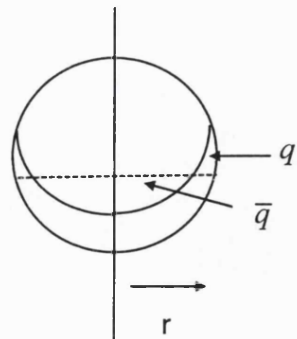


Fig.2.1 Average and full concentration profiles in a single particle

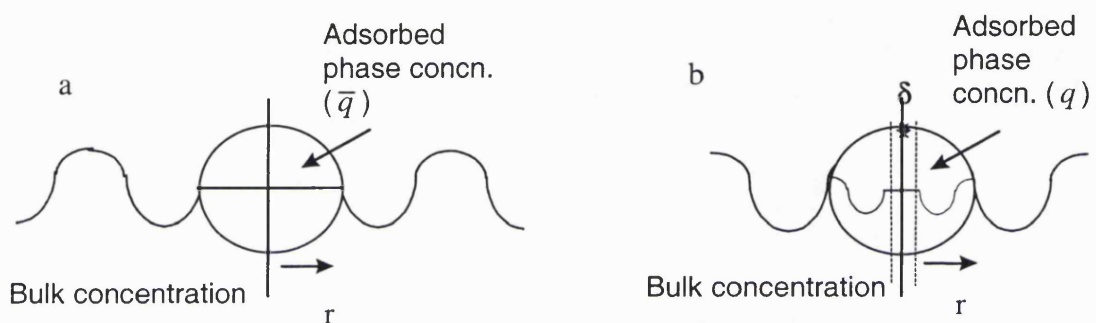


Fig.2.2 Cyclic concentration profiles at steady state a) LDF model b) Diffusion model (δ = width of unpenetrated core)

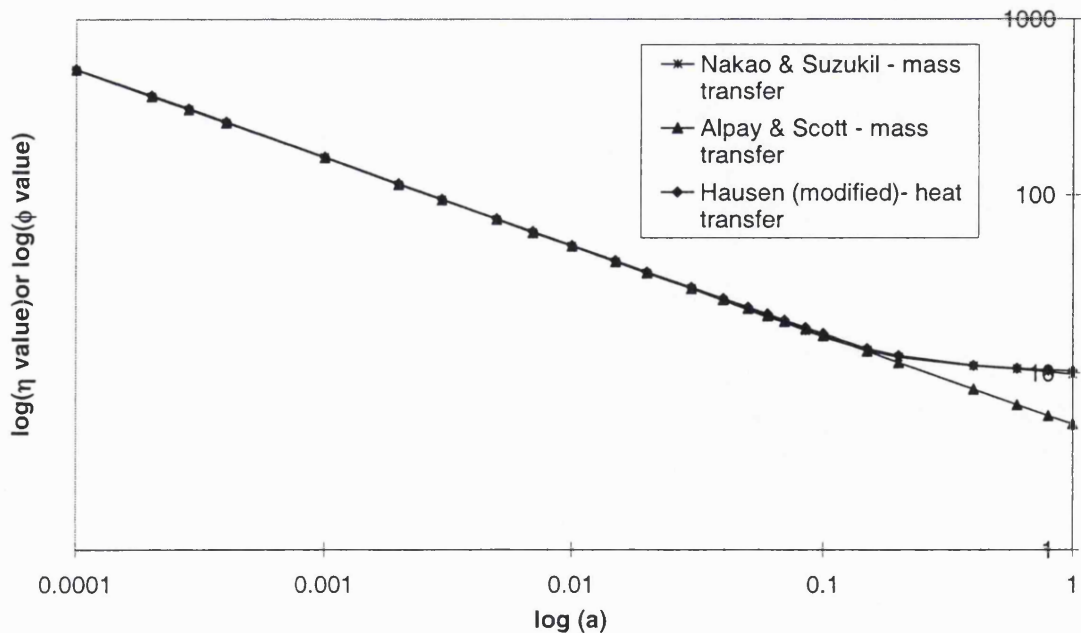


Fig.2.3 Comparison between the lumped mass transfer coefficient correlations and Hausen lumped heat transfer coefficient correction factor applied to mass transfer for a range of dimensionless cycle times.

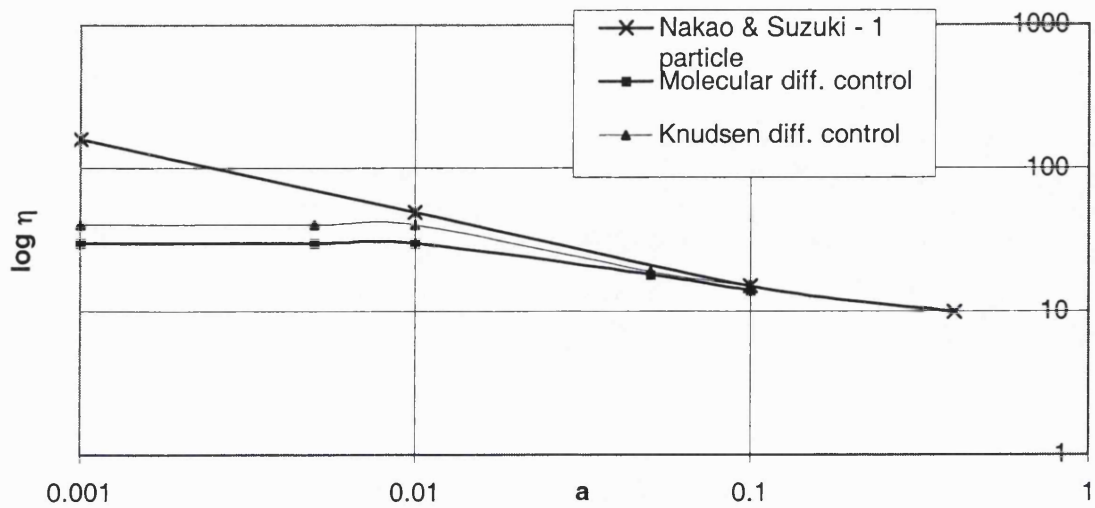


Fig.2.4 Dependency of particle mass transfer coefficient upon cycle time - one particle and column model results (Raghavan et al., 1986).

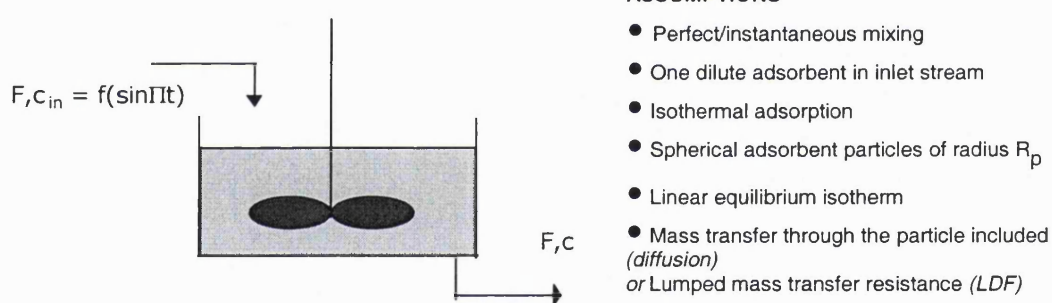


Fig.2.5 Simple CSTR model and assumptions

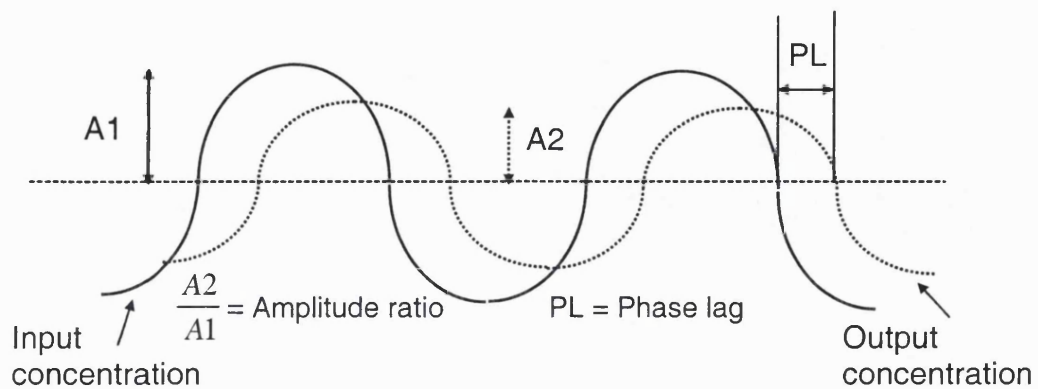


Fig.2.6 Steady state cyclic concentration profiles and the relevance of the frequency response technique.

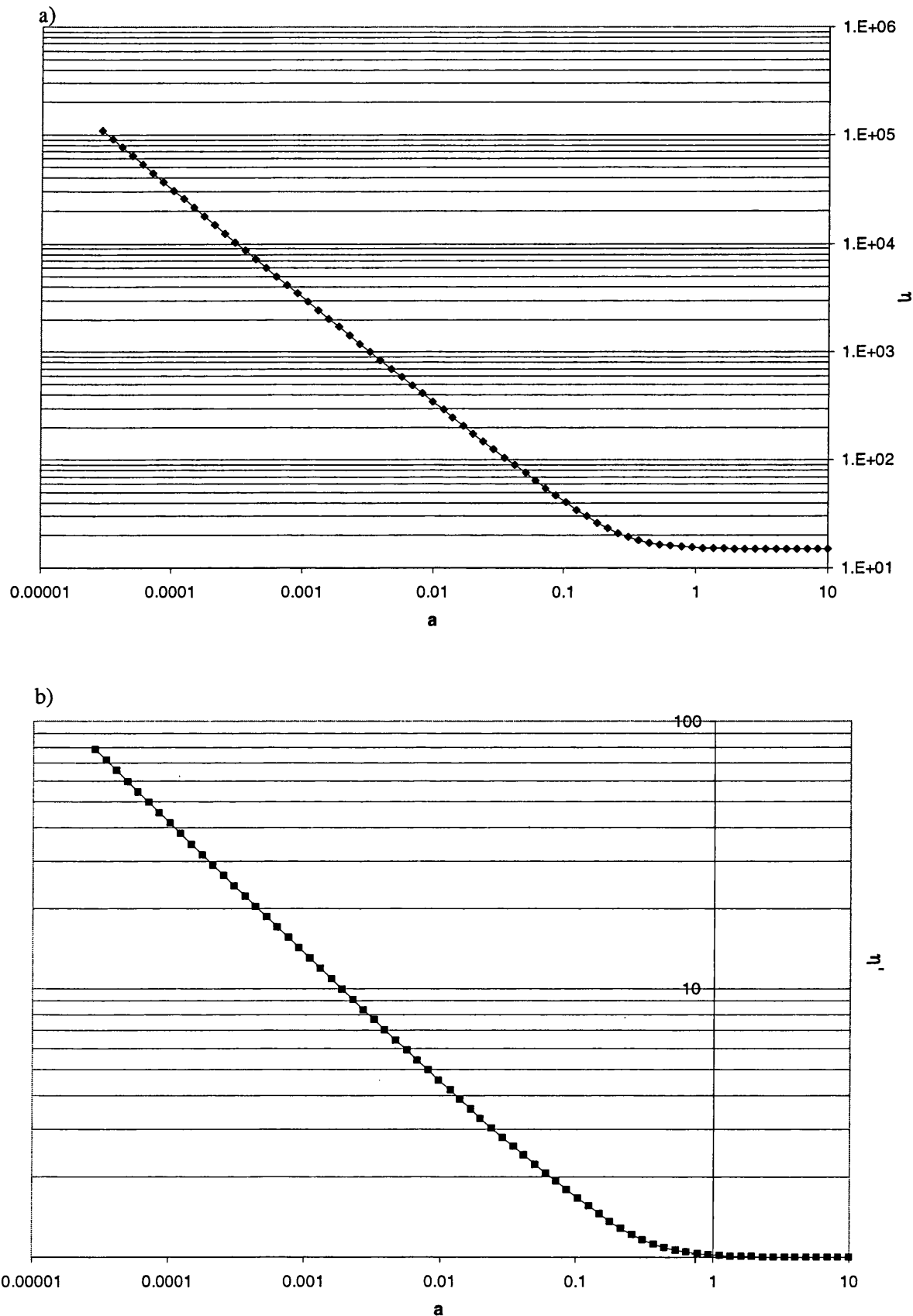


Fig.2.7 Graphical solutions for all cycle times for a) η and b) η'

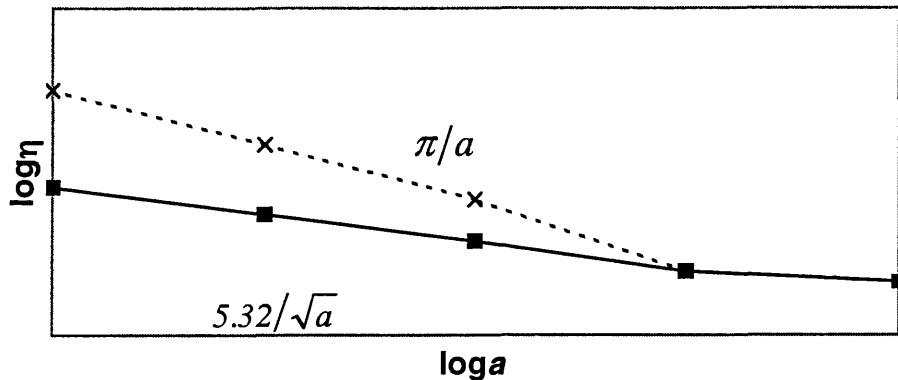


Fig.2.8 Correction factor divergence

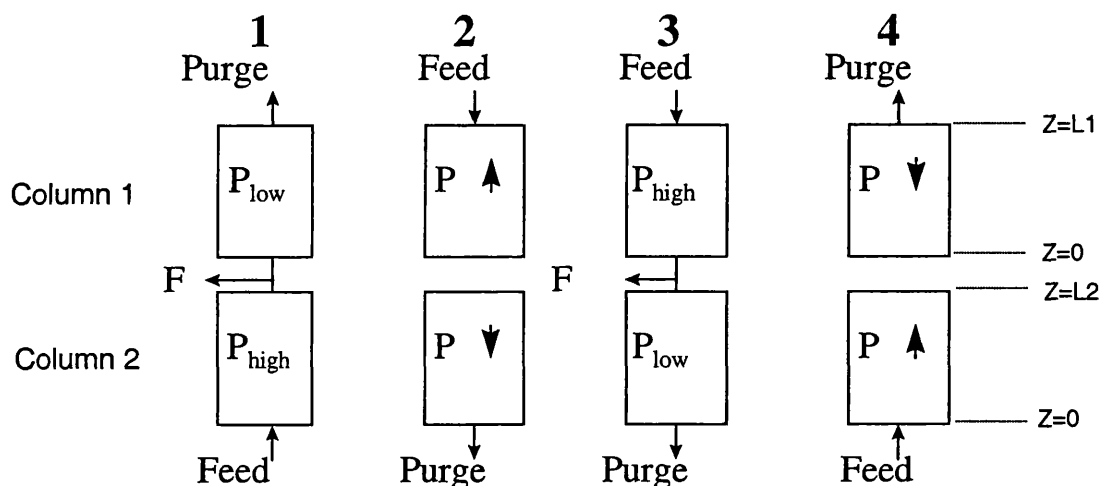


Fig.2.9 A schematic diagram of a simple PSA cycle

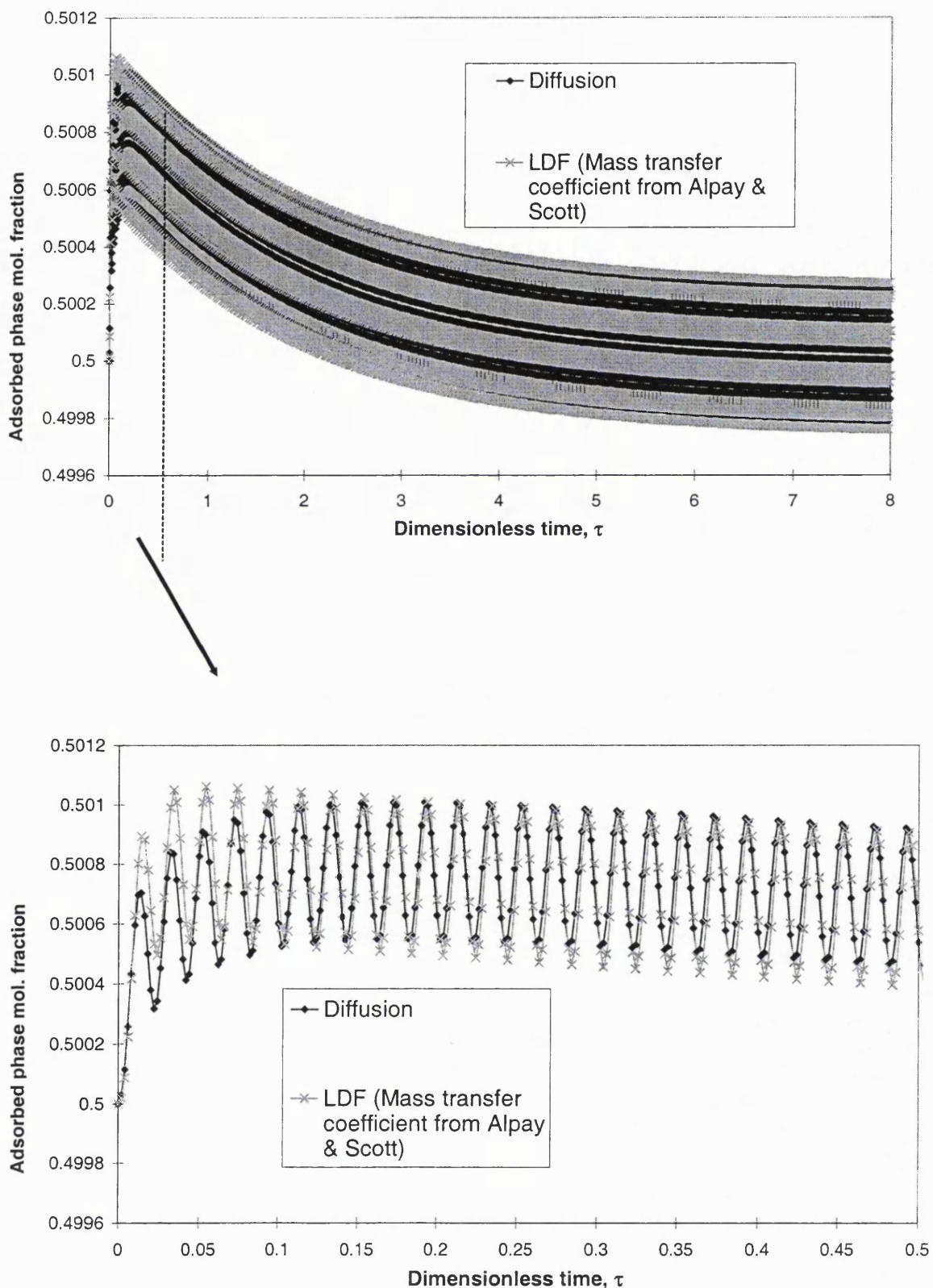


Fig.2.10. Comparison between diffusion & LDF models for cycle time 0.01

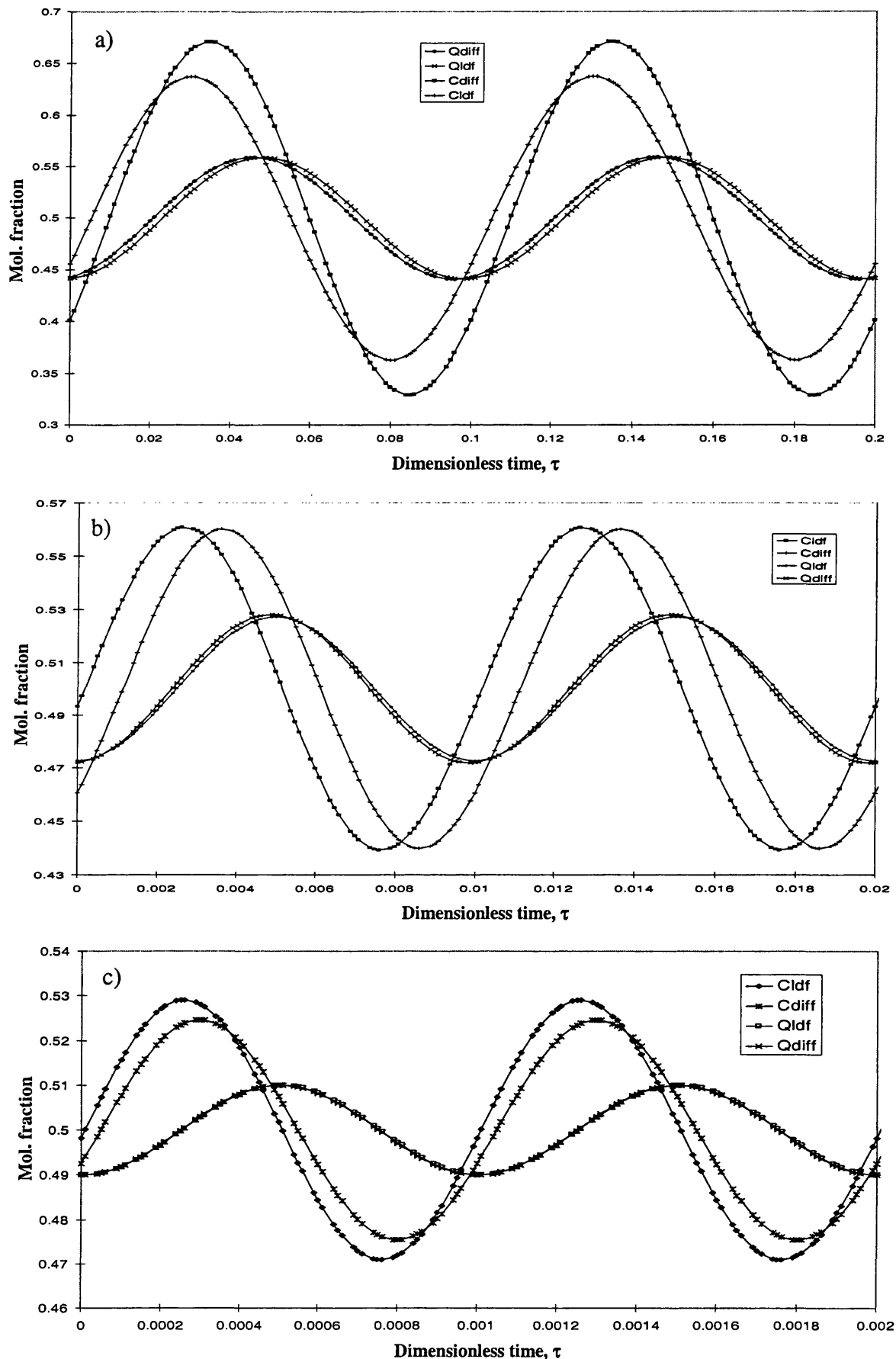


Fig.2.11 Comparison between adsorbed and bulk concentration profiles at cyclic steady state using diffusion and Suzuki-corrected LDF models a) $a=0.05$ b) $a=0.005$ c) $a=0.0005$

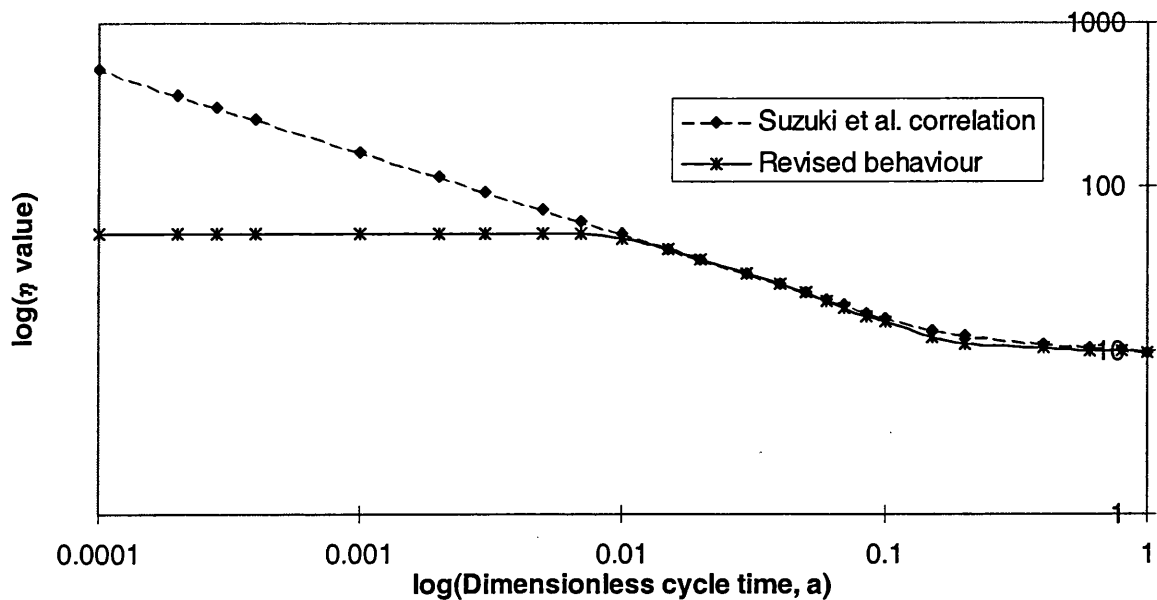


Fig.2.12. Revised relationship between a and η (based on CSTR simulations)

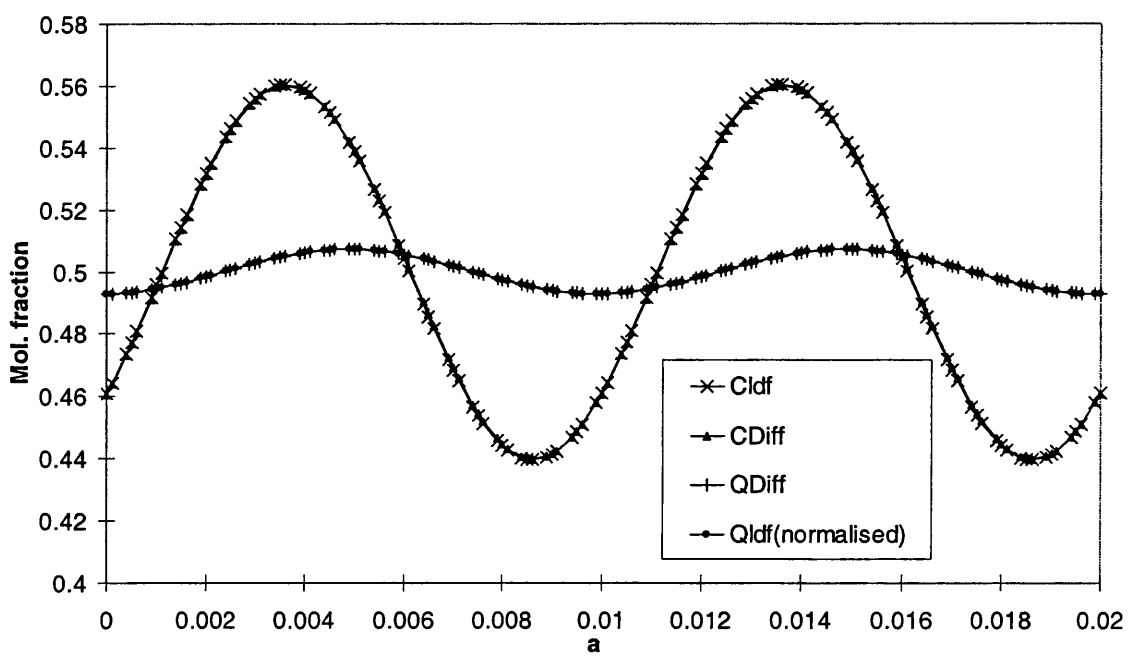
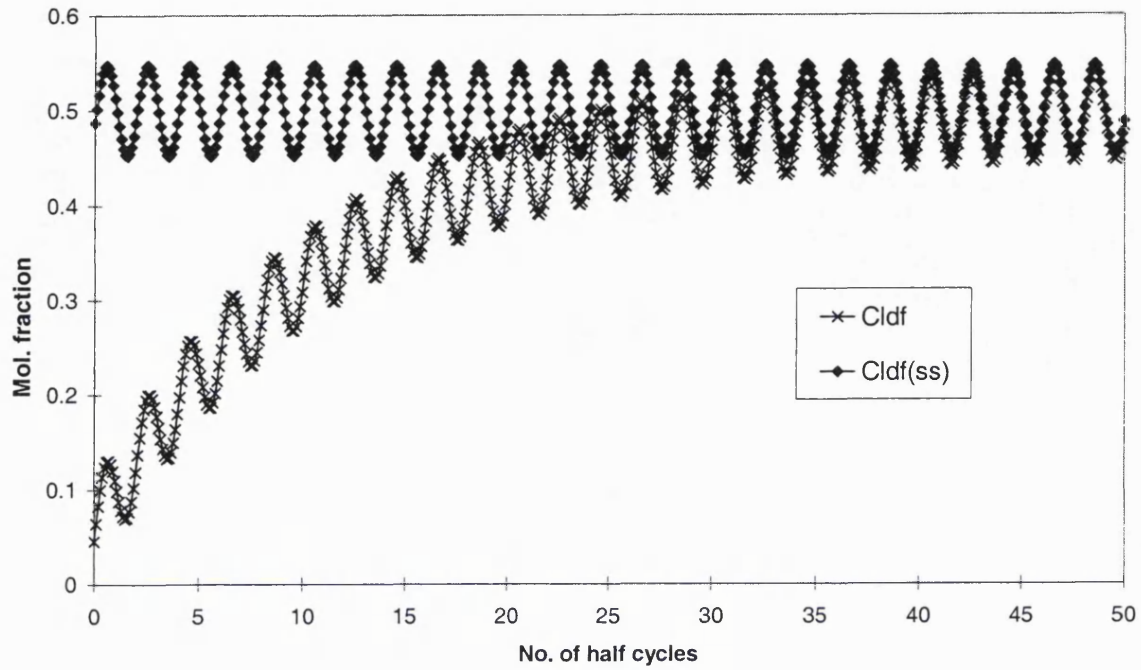


Fig.2.13. Comparisons for adsorbed and bulk concentrations using diffusion and corrected LDF models for $a = 0.005$ ($\eta = 628.32$, $\eta' = 5.91$)

a)



b)

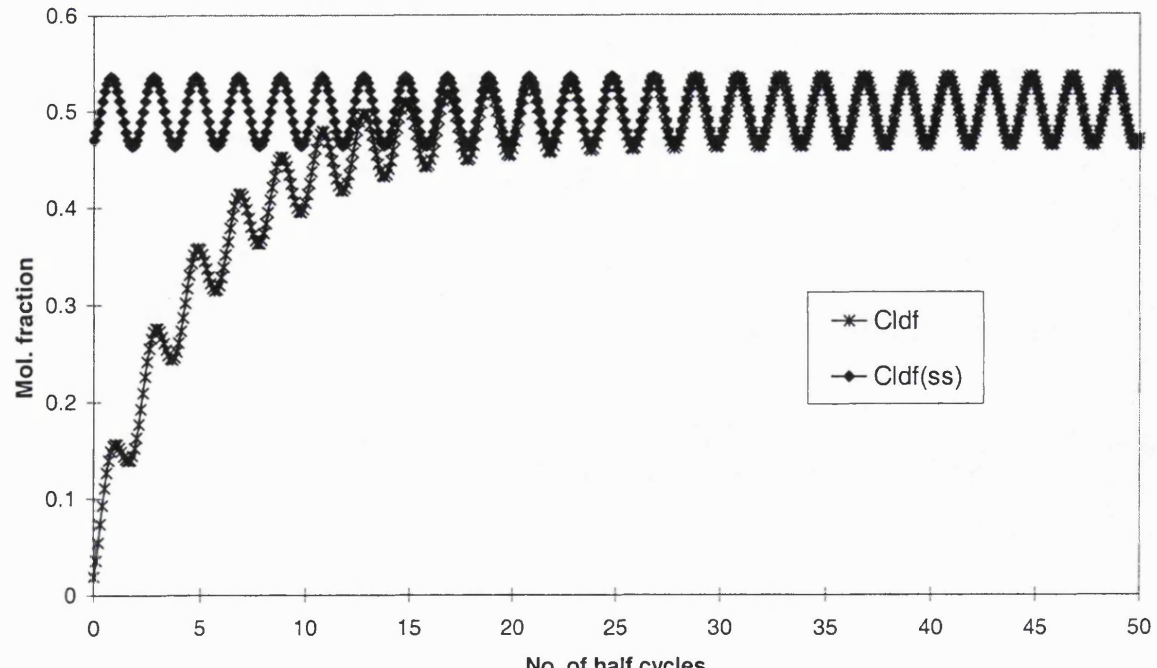


Fig.2.14 Comparison between the transient and steady state response for the external gas phase a) $\gamma = 0.1$, $\sigma = 1$, b) $\gamma = 0.2$, $\sigma = 5$

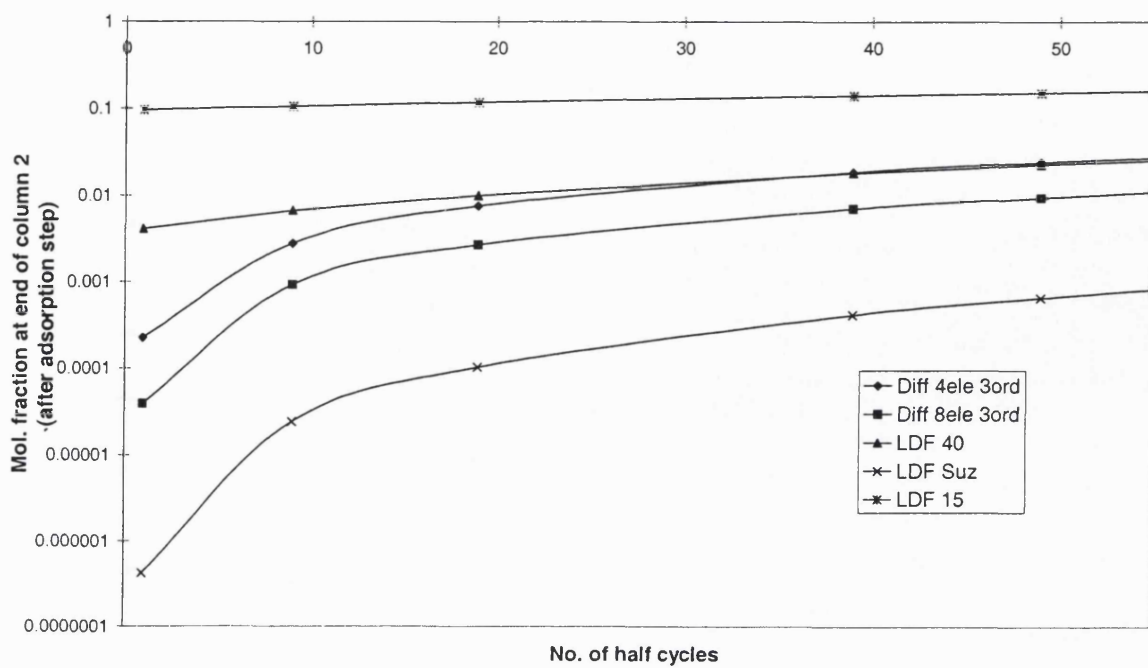


Fig.2.15 Product concentration profiles from column 2 ($a = 0.00076$) for 55 half cycles

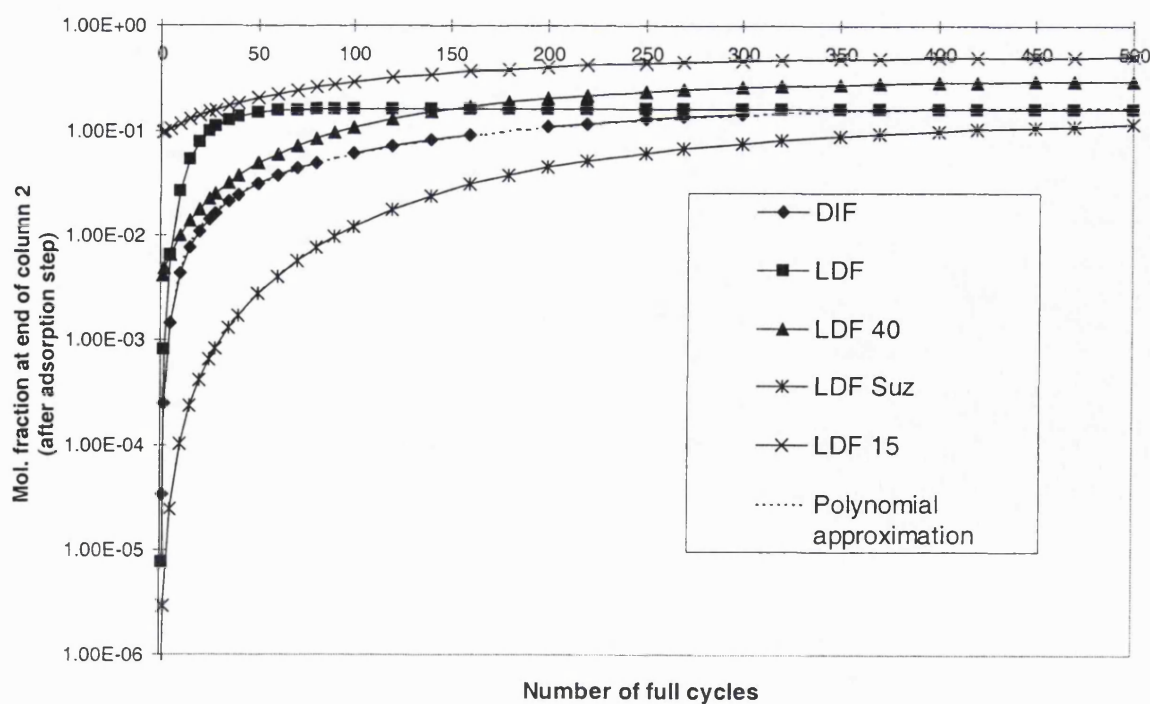


Fig.2.16 Product concentration profiles from column 2 ($a = 0.00076$) for 500 complete cycles

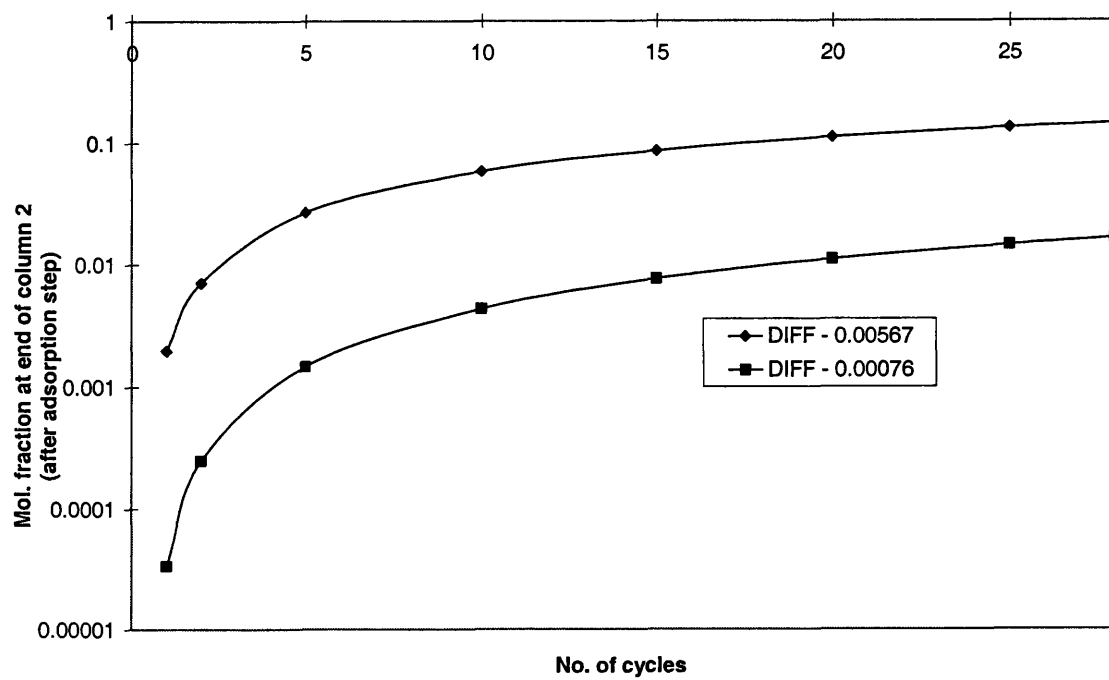


Fig.2.17. Concentration profiles using the diffusion model over 28 cycles for $a = 0.00076$ and $a = 0.00567$

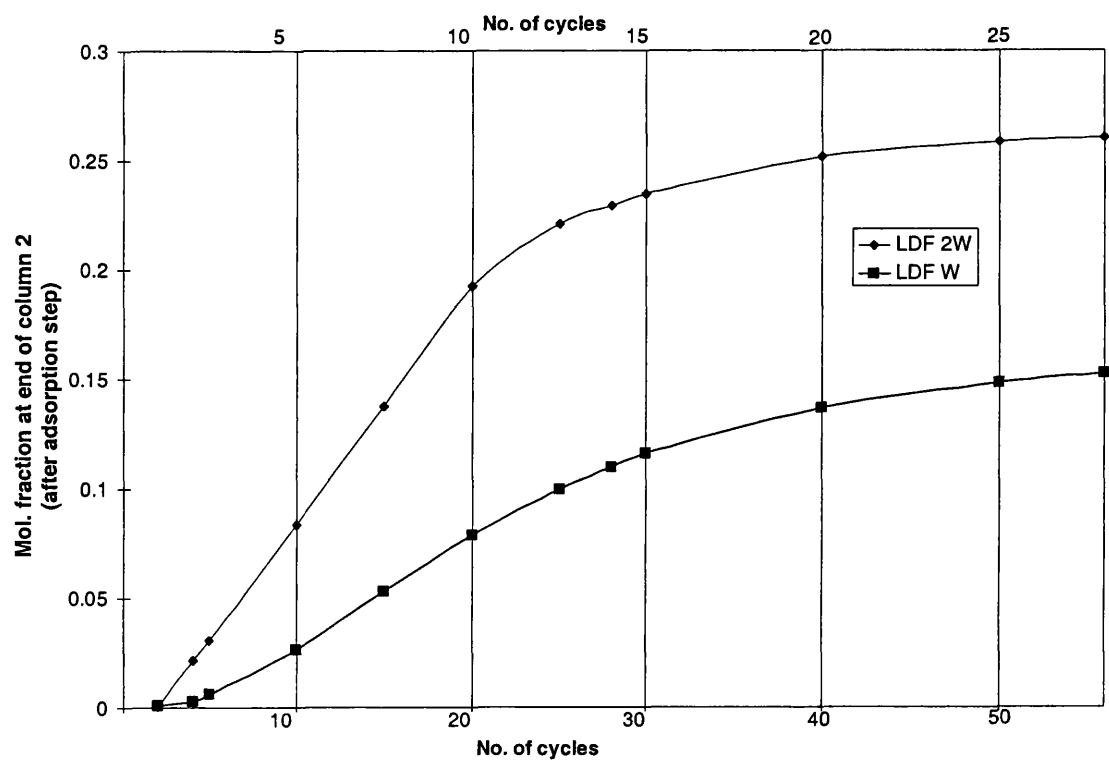


Fig.2.18 The effect of changing the parameter W on the concentration profile.

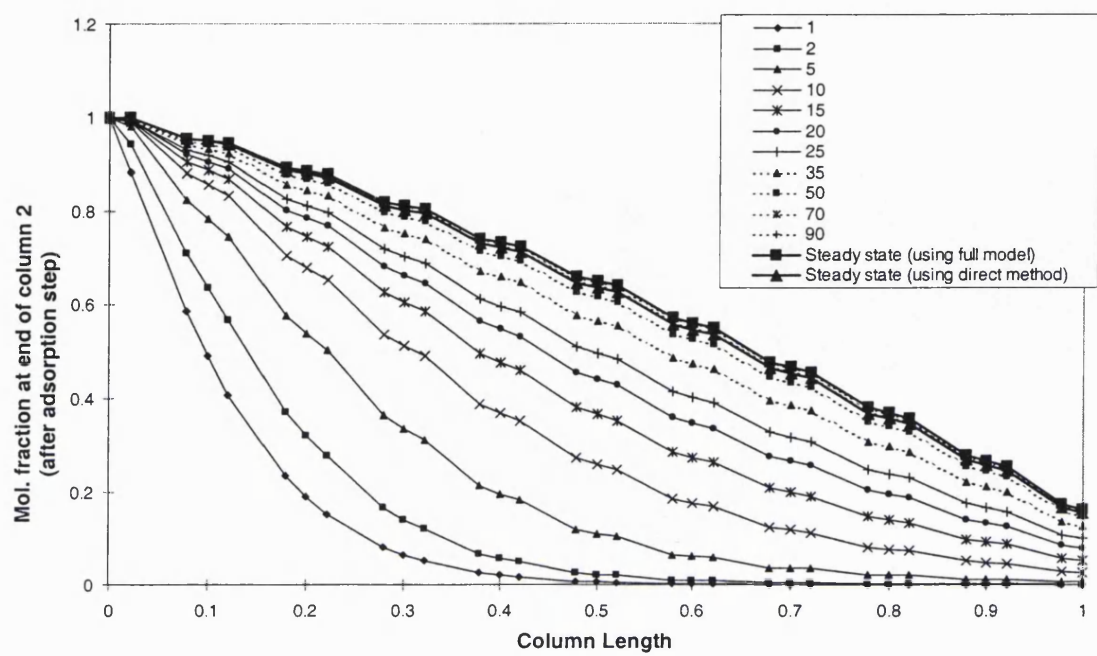


Fig.2.19. Concentration profiles across the column at the end of the adsorption step for the full and steady state models

Chapter 2: Tables

Dimensionless parameters	Dimensionless groups
$\xi = \frac{r}{R_p}$	$\tau = \frac{D_p t}{R_p^2}$
$C_{in} = \frac{c_{in}}{c_0}$	$\frac{k a_s}{V_s} = \frac{\eta D_p}{R_p^2}$
$\psi = \frac{\varepsilon}{(1-\varepsilon)K}$	$a = \frac{D_p t_c}{R_p^2}$
$Q = \frac{q}{q_0}$	$\bar{Q} = \frac{\bar{q}}{q_0}$
	$Y = \frac{F R_p^2}{3 V_s D_p K}$
Mass balance in fluid:	Cyclic inlet concentration:
$\psi \frac{dC}{d\tau} + \frac{d\bar{Q}}{d\tau} = 3Y(C_{in} - C)$	$C_{in} = \frac{1}{2}(1 + \sin \frac{\pi \tau}{a})$
Mass balance in solid - LDF:	Mass balance in solid - Diffusion:
$\frac{d\bar{Q}}{d\tau} = \eta(\bar{Q} - Q_{eq})$	$\frac{\partial Q}{\partial \tau} = \left(\frac{\partial^2 Q}{\partial \xi^2} + \frac{2}{\xi} \frac{\partial Q}{\partial \xi} \right)$ where $\frac{d\bar{Q}}{d\tau} = 3 \frac{\partial Q}{\partial \xi} \Big _{\xi=1}$
	and $\bar{Q} = 3 \int_0^1 Q \xi^2 d\xi$
	Boundary conditions:
	$\frac{\partial Q}{\partial \xi} \Big _{\xi=0} = 0$ and $Q \Big _{\xi=1} = C$

Table 2.1 Dimensionless CSTR equations

<u>STEP 1:</u>			
Dimensionless parameters		Dimensionless groups	
$C_{i,2} = \frac{C_{i,2}}{c_0}$	$\bar{Q}_{i,2} = \frac{\bar{q}_{i,2}}{q_0}$	$Q_{i,2} = \frac{q_{i,2}}{q_0}$	$\tau = \frac{D_{\text{eff}} t}{R_p^2}$ $G = \frac{u_i}{u_z}$ $\eta = \frac{k_f R_p^2}{D_{\text{eff}}}$ $\lambda = \frac{k_f R_p}{D_{\text{eff}}}$
$C_{ii,2} = \frac{C_{ii,2}}{c_0}$	$Z_{i,2} = \frac{z_{i,2}}{L}$	$\xi = \frac{r}{R_p}$	$W = \frac{u_2 R_p^2}{D_{\text{eff}} L}$ $Pe_H = \frac{u_2 L}{D_{L2}}$ $Pe_L = \frac{u_1 L}{D_{L1}}$

Dimensionless LDF PSA model:

External fluid phase mass balance:

$$-\frac{W}{Pe_H} \frac{\partial^2 C_2}{\partial Z_2^2} + W \frac{\partial C_2}{\partial Z_2} + \frac{\partial C_2}{d\tau} + 3 \left(\frac{1-\varepsilon}{\varepsilon} \right) \lambda \left(C_2 - C_{i2} \Big|_{\xi=1} \right) = 0$$

Particle mass balance:

$$\frac{\partial C_{i2}}{\partial \tau} = \left(\frac{\partial^2 C_{i2}}{\partial \xi^2} + \frac{2}{\xi} \frac{\partial C_{i2}}{\partial \xi} \right)$$

Boundary conditions - column

$$\frac{\partial C_2}{\partial Z_2} \Big|_{Z_2=0} = -Pe_H \left[1 - C_2 \Big|_{Z_2=0^+} \right] \quad \& \quad \frac{\partial C_2}{\partial Z_2} \Big|_{Z_2=J} = 0$$

Boundary conditions for the particle

$$\frac{\partial C_{i2}}{\partial \xi} \Big|_{\xi=0} = 0 \quad \frac{\partial C_{i2}}{\partial \xi} \Big|_{\xi=J} = \frac{\lambda}{K^*} \left(C_2 - C_{i2} \Big|_{\xi=J} \right)$$

<u>STEP 1:</u>			
Dimensionless groups		Dimensionless Diffusion PSA model:	
$\tau = \frac{D_{\text{eff}} t}{R_p^2}$	$G = \frac{u_i}{u_z}$	$W = \frac{u_2 R_p^2}{D_{\text{eff}} L}$	$Pe_H = \frac{u_2 L}{D_{L2}}$ $Pe_L = \frac{u_1 L}{D_{L1}}$

Dimensionless Diffusion PSA model:

$$-\frac{W}{Pe_H} \frac{\partial^2 C_2}{\partial Z_2^2} + W \frac{\partial C_2}{\partial Z_2} + \frac{\partial C_2}{d\tau} + \left(\frac{1-\varepsilon}{\varepsilon} \right) K \frac{\partial \bar{Q}_2}{\partial \tau} = 0$$

Particle mass balance:

$$\frac{\partial \bar{Q}_2}{\partial \tau} = k_f' (C_2 - \bar{C}_{i2}) \quad \text{where} \quad \frac{1}{k_f'} = \frac{K^*}{3\lambda} + \frac{1}{\eta}$$

Boundary conditions - column

$$\frac{\partial C_2}{\partial Z_2} \Big|_{Z_2=0} = -Pe_H \left[1 - C_2 \Big|_{Z_2=0^+} \right] \quad \& \quad \frac{\partial C_2}{\partial Z_2} \Big|_{Z_2=J} = 0$$

NB: The models are similar for column 1/step 3 but must be adjusted to take account of the flow direction reversal/boundary conditions.

Dimensionless parameters

$$U_{i,2} = \frac{u'_{i,2}}{u_{i,2}} \quad P_{i,2} = \frac{P_{i,2}}{P_H} \quad \hat{P}_H = \frac{P_H}{P_H} = 1 \quad \hat{P}_L = \frac{P_L}{P_H}$$

The same model may be used for both the LDF and diffusion models

External fluid phase mass balance:

$$-\frac{W}{Pe_H} \frac{\partial^2 C_2}{\partial Z_2^2} - y_{2D} (Z_2 - I) \frac{\partial C_2}{\partial Z_2} - C_2 y_{2D} + \frac{\partial C_2}{d\tau} = 0$$

Definition of y_{2D}

$$U_2 W = y_{2D} (Z_2 - I)$$

Continuity equation:

$$W \frac{\partial U_2}{\partial Z_2} = \frac{1}{P_2} \frac{\partial P_2}{d\tau}$$

Boundary conditions:

$$\frac{\partial C_2}{\partial Z_2} \Big|_{Z_2=0} = 0 \quad \frac{\partial C_2}{\partial Z_2} \Big|_{Z_2=I} = 0 \quad U_2 \Big|_{Z_2=I} = 0$$

NB: Again the models are the same for column 1/step 4 , once adjusted as before

Table 2.2 Dimensionless PSA equations

P_L/P_H	= 0.2	$\lambda\varepsilon_p/K^*$	= 20
u_2	= 50cm/s	Pe_H	= ∞
u_1	= 100cm/s	Pe_L	= ∞
L	= 100cm	D_p/R_p^2	= 0.168s^{-1}
ε	= 0.4	Length of step 1,3	= 270 secs
ε_P	= 0.34	Length of step 2,4	= $0.25 \times 270\text{secs}$

Table 2.3. Physical parameters used in PSA simulation (Raghavan et al (1986)).

	LDF PSA model	Diffusion PSA model
Discretisation across column axis	3 rd order 10 element orthogonal collocation	3 rd order 10 element orthogonal collocation
Discretisation across particle radius	-----	3 rd order 6 element orthogonal collocation
Number of variables	252	2546
Time to simulate 30 cycles*	$\sim 2^{1/2}$ hours	~ 125 hours

Table 2.4. Comparison between LDF and diffusion simulations (* the same computer was used for both runs)

Chapter 3

Adsorbent Characterisation

3.1 Introduction

One of the key areas in the development of industrial adsorption processes is the choice of the adsorbent material and design of the column. Adsorbent selection is based primarily on criteria such as selectivity, capacity and durability. In addition, depending on whether there is moisture in the process, the hydrophobicity of the material is important, as is, of course, the cost. When considering the separation of CO₂ from flue gas the adsorbents of interest are activated carbon or a hydrophobic zeolite (since moisture is present). In the interest of keeping the cost of this low value separation down then activated carbon may be the most suitable choice.

In this study the focus is on a novel PSA technology to carry out the CO₂ separation. As an energy intensive process any reduction in power requirements is useful. One method of reducing the energy required is to use a structured column. With uniform channels for the gas to pass along, this column does not experience the high pressure drops encountered with packed columns and may help to make the overall system more economically attractive.

In this chapter two activated carbon columns, of similar honeycomb design, are characterised for CO₂ separation. The manufacture and design of structured adsorbent columns is first discussed before a selection of characterisation techniques are reported. An experimental study of the columns using a chromatography method is then presented and the kinetic and mass transfer parameters obtained compared with the results from ZLC measurements.

3.2 Literature Review of Structured Adsorbent Columns and Characterisation Techniques

In this section aspects relating to structured adsorbent column manufacture and characterisation are reviewed. Three methods of experimentally determining the kinetic and mass transfer parameters of the column are outlined, namely gravimetric methods, pulse or step chromatographic techniques and the ZLC method.

3.2.1 Structured adsorbent columns

In the great majority of industrial adsorption applications, packed columns of adsorbent particles are used. Despite many problems that include high pressure drop, particle entrainment and channelling, which make them inefficient, they are an accepted technology that is cheap and commonplace. However, when considering processes of low added value such as VOC removal or removal of CO₂ from stack gas, these inefficiencies cannot be tolerated. To improve the effective utilisation of the adsorbent it must be manufactured in a structured form, in such a way as to lead to as high a surface area as possible being explored without the adsorbent compromising the passing flow. The need for affordable air and pollution control has helped to drive development, the most prominent success being the catalytic converter; a monolithic honeycomb structure fitted to vehicle exhausts to reduce harmful emissions such as carbon monoxide, VOCs and NOx (Bardhan, 1997). A honeycomb structured device is also employed in a rotary wheel air dehumidifier, shown in fig.3.1 (Ruthven, 2001). Gas passes in uniform channels through the silica gel-coated ceramic material, reducing pressure drop, the complex structure helping to ensure maximum mass transfer area.

3.2.1.1 Manufacture

To manufacture structured adsorbent contactors, typically the process begins with combining finely powdered carbon material with binders and support materials. The paste formed is then

extruded into the desired shape. Drying and firing completes the process. The main problem encountered is that the properties of the adsorbent are not retained, properties such as pore size distribution and adsorption capacity. This means the separation efficiency is greatly reduced. A technique whereby powdered activated carbon is extruded into a honeycomb structure using a polymeric resin has shown some promise and has been used in the removal of ozone in laser printers (Gadkaree, 1998). There are, however, still problems as structures made using this method suffer from poor durability because of the weak bonding between the carbon and binder. Such a column would need frequent replacement and would add a substantial cost to any application therefore an alternative is required. Trials using a highly porous carbon-ceramic composite honeycomb structure were undertaken by Gadkaree (1998). The monolithic column was manufactured using drying and curing cycles such that the carbon material formed a cross-linked structure in the ceramic. Obtaining breakthrough curves for butane, toluene, formaldehyde, acetaldehyde and isopropanol Gadkaree found that he could obtain similar adsorption properties to those found when using a packed bed. In another study by Li, Perera and Crittenden (1998a) the focus was on developing a zeolite monolith, using 5A zeolite, for air separation specifically using a pressure swing adsorption process. Once manufactured, using the steps of paste preparation, extrusion, drying and firing, the properties of the material were examined using x-ray diffraction, scanning electron microscopy, image analysis and compression and hardness testing. Results showed that the monolith compared well with commercially available 5A zeolite pellets and it was noted that the monolith had much higher macroporosity than the pellet. Separation performance, analysed by obtaining adsorption isotherms for nitrogen and oxygen, was the same for both the monolith and pellet.

3.2.1.2 Suitability of structured columns for Pressure Swing Adsorption applications

The first study using structured adsorbent beds in a pressure swing adsorption process was undertaken by Ruthven and Thaeron (1996). A parallel passage contactor, shown in fig.3.2, consisting of activated carbon fiber plates of 0.6 and 0.9mm thickness, spaced at 100 μ m apart was considered. The suitability of the column was first established using an HETP (height-

equivalent-to-a-theoretical-plate) comparison between this column and a packed column. By comparing the HETP expression derived by Golay (1958) for a packed column and comparing it to a similar expression, found from extending the Golay analysis to the parallel passage contactor, it could be shown that, under all conditions, the parallel passage contactor gave an advantage over the packed column in terms of pressure drop. It is most desirable to reduce the HETP to as low a value as possible and this can be done by decreasing the layer spacing in the contactor. As pointed out in the study the ideal layout for a column would be a monolith structure with many uniform small passages. Li et al (1998a), who manufactured a zeolite monolith for air separation adopted an experimental approach to determining its suitability for PSA processes (Li et al,1998b). They analysed two idealised steps of the PSA cycle for air separation; oxygen enrichment following vacuum purge and oxygen enrichment following oxygen purge, comparing the structured bed with a packed bed of equal weight. For both steps the packed bed out-performed the monolith, demonstrating better separation capabilities. However, in terms of pressure drop the experiments showed that the pressure drop was 3-5 times greater in the packed bed than in the structured and the pressurisation time in the packed bed was also greater by the same amount. This suggests that power required during the PSA cycle would be greatly reduced if the monolith were used. Calculation and comparison between the external film resistance and the axial dispersion coefficients for the two columns was carried out using Sherwood number correlations. For the packed bed the Wakao and Funazkri (1978) correlation was used:

$$Sh = 2.0 + 1.1 Sc^{0.33} Re^{0.60} \quad (3.1)$$

And for the monolith a correlation analogous to that derived for heat transfer in square channels was used:

$$Sh = 2..98 \left(1 + 0.095 Sc Re \frac{d_c}{L_c} \right) \text{ where } d_c = \text{diameter of channel } L_c = \text{length} \quad (3.2)$$

To derive the axial dispersion coefficients for the packed column and monolith columns the following were used respectively:

$$\frac{\varepsilon D_{ax}}{D_v} = 20.0 + 0.5 Sc Re \quad (3.3)$$

and $D_{ax} = D_v + \frac{1}{192} \frac{u_i^2 d_c^2}{D_v}$ where u_i =interstitial velocity (3.4)

Results showed that the monolith demonstrated worse external film resistance but gave a better axial dispersion coefficient. Using this approach also led to suggestions on how to improve the monolith. Since the Sherwood number was found to be almost independent of velocity it was suggested that the best way to improve the film mass transfer coefficient was to reduce the channel size. It has been found by Irandoost and Andersson (1988) that the coefficient may be increased nine fold by reducing the channel size by a factor of three. Another improvement suggested was that the wall thickness be decreased. This can be compared to decreasing the particle size in packed beds, a well known method for improving mass transfer behaviour, but it has the advantage of not introducing any additional pressure drop.

3.2.2 Characterisation techniques

There are various techniques available to ascertain the equilibrium and kinetic parameters that would characterise a particular adsorption column. Examples include gravimetric measurements, pulse and step chromatography and ZLC experiments. Of these, gravimetric analysis is the oldest, dating back to the time of Leonardo da Vinci (Robens, 1995).

3.2.2.1 Gravimetric method

The gravimetric method is simple and the main requirement is for a very accurate microbalance. In the study of Ruthven and Thaeron (1996), where they consider a parallel passage contactor, as shown in fig.3.2, they use gravimetric methods to obtain the equilibrium isotherms, to determine the rate controlling resistance to mass transfer and evaluate the diffusional time constant for CO₂, CH₄, CF₄ and N₂. From the initial slopes of the isotherms the equilibrium constants were determined. Analysis of transient uptake curves, obtained by

making a small differential step change in sorbate pressure in the microbalance system, made it possible to establish that mass transfer was controlled by macropore diffusion and from derived mathematical representations, values for the tortuosity factor and Knudsen diffusion were extracted from the experimental data. To validate these results moments analysis of pulse chromatography experiments were used for comparison.

3.2.2.2 Pulse or Step Chromatography

This is a widely used technique whereby a pulse or step of a chosen absorbable species is introduced into the inlet flow to an adsorption column. The dynamic response to this change is measured at the column outlet. By fitting a suitable theoretical curve, found from a mathematical representation of the system, to the experimental curve the kinetic and equilibrium parameters can be found. To be able to carry out such an analysis it is assumed that the system is in the linear regime and therefore in practice the step or pulse size must be sufficiently small (Ruthven, 1984). However, in general, it is extremely difficult to derive suitable analytical curves to fit the experimental data to. To address this problem moments are employed. Using van der Laan's (1958) theorem, expressions for the first and second moments can be found easily; a match between the experimental and theoretical first moment leading to the adsorption equilibrium constant and a match between the second moment gives the mass transfer limitations of the system. The moments expressions for a pulse response can be derived from the mathematical solution of the system in the Laplace domain and can be written as (Ruthven, 1984):

First moment:

$$\mu = \bar{t} = \frac{\int_0^\infty c t dt}{\int_0^\infty c dt} = - \lim_{s \rightarrow 0} \frac{\partial \tilde{c}}{\partial s} \frac{1}{c_o} \quad (3.5)$$

Second moment:

$$\sigma^2 = \frac{\int_0^\infty c(t-\mu)^2 dt}{\int_0^\infty c dt} = \lim_{s \rightarrow 0} \frac{\partial^2 \tilde{c}}{\partial s^2} \left(\frac{1}{c_o} \right) - \mu^2 \quad (3.6)$$

In every case, regardless of system, the first moment is equivalent to the mean retention time, which can be found from an overall mass balance giving:

$$\mu = \frac{L}{v} \left(1 + \frac{(1-\varepsilon)}{\varepsilon} K \right) \text{ where } v \text{ is the superficial velocity} \quad (3.7)$$

From this well known expression the equilibrium constant can be directly obtained. The second moment, however, must be derived from the mathematical equations of the system. When considering a general model of a column the dispersed plug flow model can be assumed to represent flow. Assuming the system is isothermal, there is negligible pressure drop encountered and the concentration of the adsorbable species is small then by undertaking a mass balance on a small element the following differential equation may be found:

$$-D_L \frac{\partial^2 c}{\partial z^2} + \frac{\partial(vc)}{\partial z} + \frac{\partial c}{\partial t} + \frac{(1-\varepsilon)}{\varepsilon} \frac{\partial \bar{q}}{\partial t} = 0 \quad (3.8)$$

Assuming that the mass transfer rate can be expressed using the linear driving force (LDF) model:

$$\frac{\partial \bar{q}}{\partial t} = k'(q^* - q) \quad (3.9)$$

and the concentration is small enough to allow the use of Henry's law to express the linear equilibrium:

$$q^* = Kc \quad (3.10)$$

then the second moment is derived as:

$$\frac{\sigma^2}{2\mu^2} = \frac{D_L}{vL} + \frac{\varepsilon v}{L(1-\varepsilon)} \left(\frac{1}{k'K} \right) \quad (3.11)$$

When the model is written explicitly including external film mass transfer, micropore and macropore resistances then the final term of the second moment expression includes the terms specific to these resistances and it can be shown that (Ruthven and Karger, 1992):

$$\frac{1}{k'K} = \frac{R_p}{3k_f} + \frac{R_p^2}{15\epsilon_p D_p} + \frac{r_c^2}{15KD_c} \quad (3.12)$$

where the resistances are linearly additive. A further interpretation of the derived second moment was explored by Aris (1956) and Golay (1958). By modelling the chromatography column assuming a plate model, where N mixed cells with mass transfer between fluid and the adsorbed phase in each exist, moments could again be derived. By defining $N/\ell=L$, where ℓ is the length of one cell and L the length of the column, and $N=v\ell/2D_L$ then the HETP (Height-Equivalent-to-a-Theoretical-Plate) could be related to the first and second moments derived from the approach using a mass balance over an element through (Ruthven and Karger, 1992):

$$HETP = \frac{\sigma^2}{2\mu^2} L \quad (3.13)$$

By considering the system geometry for a circular tube and parallel sided duct Golay was able to derive the following HETP expressions:

$$\text{For the circular tube: } HETP = \frac{2D_m}{v} + \frac{22}{48} \frac{vr^2}{D_m} + \frac{Wr\nu}{3KD_e} \quad (3.14)$$

$$\text{Parallel sided duct: } HETP = \frac{2D_m}{v} + \frac{51}{105} \frac{vr^2}{D_m} + \frac{2Wz\nu}{3KD_e} \quad (3.15)$$

Using the same assumptions made by Golay, Ruthven and Thaeron (1996) were able to derive an expression for the HETP of a parallel passage adsorber contactor, which was of the form:

$$HETP = \frac{2D_m}{v} + \frac{vr^2}{4.117D_m} + \frac{Wr\nu}{3KD_e} \quad (3.16)$$

Spangler (1998) also used an extension of Golay's work, applying it to miniature rectangular chromatography columns suitable for high speed chromatography. To manufacture the column a rectangular channel was first etched and then a plate of similar material placed over the channel, therefore all four sides of the gas passage are coated with adsorbent material. Using the same moments approach taken by Golay, Spangler (1998) derived an HETP expression, which was then verified against experiments. To solve the long and complex

expression required a fairly large computational effort and, mindful of the need for a simpler approach, Spangler was able to develop an HETP expression for the rectangular duct (Spangler, 2001), which was very similar to those found by Golay and had the form:

$$HETP = \frac{2D_m}{v} + \frac{70vr^2}{48D_m} + \frac{Wrv}{3KD_e} \quad (3.17)$$

All the HETP equations shown have the general form of the van Deemter equation:

$$HETP = \frac{A}{v} + B + Cv \quad (3.18)$$

where $A = 2D_m$, $B = f(vr^2/D_m)$ and $C = f(Wzv/3KD_e)$. The general dependence of HETP on the interstitial velocity is shown in fig. 3.3, along with the three contributions to the HETP value. Clearly as velocity increases the second and third terms become more dominant and the HETP can be seen to vary linearly with velocity. In the case of the parallel passage adsorber the effective diffusivity was found from the experimentally obtained HETP data using a plot in this region. Under the conditions used only the final term of the HETP expression was valid and hence the gradient of the asymptote was given by:

$$\text{Gradient} = \frac{W}{3KD_e}, \quad (3.19)$$

making evaluation of D_e very straightforward. Comparing the results obtained from the first moment and HETP data for the K and D_e values to those obtained from the gravimetric experiments showed that both methods were in agreement.

3.2.2.3 Zero length column technique

The traditional chromatographic method used to obtain mass transfer and kinetic parameters previously described is commonly used and is easy to carry out. However the major disadvantage is that the response curve obtained depends on both mass transfer and axial dispersion. The zero length column (ZLC) method, an extension to the chromatographic technique, eliminates the contribution of axial dispersion and hence permits the determination of the mass transfer resistance (Karger and Ruthven, 1992). The method was first developed

by Eic and Ruthven (1988), and has principally been used to find intracrystalline diffusivities in zeolithic adsorbents. It has shown to be versatile, being applied to both gaseous (Karger and Ruthven, 1992) and liquid systems (Ruthven and Stapleton, 1993). The basis of the technique is in matching experimentally obtained desorption curves to the solutions of the equation set describing the system.

While the experimental technique required for ZLC analysis has varied little over time the analysis of the desorption curves has been widely explored depending on the system assumptions (Ruthven and Brandani, 2000). In the most simple form, making the assumptions of a gaseous system at uniform temperature, a well mixed carrier, a linear adsorption isotherm and spherical adsorbent particles, solving the equations for Fickian diffusion and the cell mass balance leads to an expression for the effluent concentration, given by:

$$\frac{c}{c_0} = 2L \sum_{n=1}^{\infty} \frac{\exp(-\beta_n^2 \frac{Dt}{R_p^2})}{\beta_n^2 + L(L-1)} \quad (3.20)$$

where β_n are the roots of $\beta_n \cot \beta_n + L - 1 = 0$ (3.21)

$$\text{and } L = \frac{FR_p^2}{3V_sKD} \quad (3.22)$$

When L becomes large equation (3.20), in the long time region, becomes:

$$\frac{c}{c_0} = \frac{2L}{\beta_1^2 + L(L-1)} \exp\left(\frac{-\beta_1^2 Dt}{R_p^2}\right) \quad (3.23)$$

By plotting experimental data for c/c_0 against time on a semi-logarithmic graph and then fitting a straight line to the linear long time asymptote from the slope and intercept both L, and hence K, and the diffusional time constant, D/R_p^2 , can be evaluated. The short time asymptote, which tends to be less sensitive to system interferences such as heat effects, has also been analysed (Ruthven and Brandani, 2000). In this case equation (3.20) reduces to:

$$\frac{c}{c_0} \approx 1 - 2L \sqrt{\frac{Dt}{\pi R_p^2}} \quad (3.24)$$

A plot of $\frac{(1 - c/c_0)}{\sqrt{t}}$ vs \sqrt{t} should lead to an almost linear plot, from which the diffusional

time constant can be extracted. In both these cases using the long and short time asymptotes it is assumed that $L > 5$ and the adsorption is kinetically controlled. When $L \rightarrow 0$ the limiting solution for equilibrium control is approached and equation (3.20) reduces simply to:

$$\frac{c}{c_0} = \exp\left(\frac{-Ft}{KV_s}\right) \quad (3.25)$$

In this regime where a very low flowrate is employed and $L < 0.5$, a very reliable value for KV_s can be found by plotting $\ln c/c_0$ vs t . Brandani et al (2002) were able to demonstrate the success of this technique considering CO_2 adsorption onto zeolites. In this study the model used relaxes one of the assumptions made in that the volume of gas in the cell is not considered negligible in comparison to the adsorbed phase KV_s . In the majority of vapour phase experiments the assumption holds true but not for liquid systems. However, in vapour phase experiments this volume corresponds to the dead volume in the system, and therefore in the majority of cases should be included and quantified from blank runs. The form of equation (3.20) once the gas volume has been included in the cell equations is derived by Brandani and Ruthven (1995):

$$\frac{c}{c_0} = 2L \sum_{n=1}^{\infty} \frac{\exp(-\beta_n^2 \frac{Dt}{R_p^2})}{\beta_n^2 + (L - 1 - \gamma\beta_n^2)^2 + L - 1 + \gamma\beta_n^2} \quad (3.26)$$

$$\text{with } \beta_n \cot \beta_n + L - 1 - \gamma\beta_n^2 = 0 \quad (3.27) \qquad \text{and } \gamma = \frac{V_f}{3KV_s} \quad (3.28)$$

If a slab of adsorbent is considered rather than particles then the result is of the form (Brandani et al, 2003):

$$\frac{c}{c_0} = 2L \sum_{n=1}^{\infty} \frac{\exp(-\beta_n^2 \frac{Dt}{l^2})}{L + (1+\gamma)\beta_n^2 + (L-\gamma\beta_n^2)} \quad (3.29)$$

$$\text{with } L - \gamma\beta_n^2 - \beta_n \tan \beta_n = 0 \quad (3.30)$$

$$\text{and } L = \frac{Fl^2}{V_s KD} \quad (3.31)$$

Solutions can again be found, considering either geometry, assuming L is large or small as before, and the kinetic and mass transfer parameters found from experiment.

In addition to including fluid phase hold up other researchers have considered the effect of non uniform particle size (Duncan and Moller, 2002), non isothermal systems (Brandani et al, 1998) and non linear isotherms (Brandani, 1998). In addition the approach has also been extended to measure self and counter diffusion effects (Brandani et al, 1996).

3.3 Characterisation experiments

Using the activated carbon columns available, characterisation experiments were performed using the chromatography and ZLC experiments. The ZLC study was undertaken in parallel to this study but independently by Federico Brandani. The experimental procedure is outlined briefly below but can be found in full in Brandani (2002). In addition a short comparison between the results from the two experimental approaches can be found in Brandani (2002).

3.3.1 The columns

In order to look at the effect of different cell widths and wall thicknesses two columns were characterised, the structure of the first can be seen in fig. 3.4. It consists of five 10cm long, 2.9 diameter activated carbon monoliths. Gas is allowed to pass through parallel passages created by the honeycomb structure of the columns. Each monolith is contained within an aluminium casing with rubber seals between the outer aluminium and the inner carbon columns at each end.

To connect the individual columns together the housing shown in fig 3.4 was designed. Looking at the top and bottom plates, both made of brass, the pipework that allows gas to flow from one column to the next can be seen. In the arrangement shown the gas to be separated enters at position 1 into column 1. It then passes through all the columns in turn, finally passing through column 5 and out through the centre. One of the features of this system is the variation that can be made to overall column length by turning the top plate. For example, if position 1 is placed over column 2 then the gas can only pass through 3 columns rather than 5.

To help to distribute the gas fig.3.4 shows the graduated holes made in the underside and topside of the top and bottom plates respectively. The whole assembly is designed to stand upright on five stainless steel feet and is held together with five stainless steel screws that run vertically between the plates, secured at the top with wing nuts. Fig.3.5 shows the details of the individual monolith.

The second column, shown in fig.3.6, comprised an aluminium casing 45cm long, 3cm in diameter. At each end was a brass fitting screwed on to seal the ends but allowing pipework to be fitted to allow gas into the unit. Within the casing were housed 45 1cm long activated carbon monolith sections of 1.56cm diameter. In this case the sections were originally cut from rectangular pieces, which were 6x4.7x1cm prior to being packed into the tubular housing. Figs.3.7 and 3.8 shows magnified cross sections of the columns while table 3.1 gives the dimensions associated with each column. Both monoliths were made by extrusion using a mixture of 40% activated carbon and 60% of a ceramic material, added for strength, by the Mead-Westvaco Corporation.

3.3.2 Chromatography Experimental Procedure

The purpose of the experiments was to obtain breakthrough curves for both columns using feed streams containing a small concentration of CO₂ in a carrier of either He or N₂. The

experimental procedure was repeated at various flowrates so that the first and second moment data could be obtained, using the method outlined in section 3.2.2.2.

In addition experiments were also carried out using N₂ in a helium carrier in order to try and determine the first and second moment values.

Fig. 3.9 shows the experimental set up used. For each run the system was initially purged with the carrier gas, He or N₂. To do this the three way valves were turned such that the gas passed from the cylinder (labelled “CARRIER”) to one side of the TCD. The carrier then passed through the column, and left the system after flowing through the other side of the TCD. By ensuring the flowrate remained steady during this time and recording the voltage a steady baseline could be obtained. During this period the flow through both sides of the TCD was identical and hence the voltage obtained corresponded to an effective zero for the breakthrough experiments. The voltage signal of the TCD was recorded using a computer running the real-time control and monitoring package, VISSIM.

Once purging was complete the feed concentration required was decided and the expected response of the TCD could be checked. By turning all the three way valves such that the column was bypassed the gas stream flowed only around the TCD loop. Since the analysis of the breakthrough curves was only valid in the Henry’s Law region, it was necessary to make the concentration of the adsorbate as small as possible while still ensuring a good clear response from the TCD. Therefore this initial test was able to show the sensitivity of the TCD to various CO₂ concentrations, and demonstrated that a concentration of 1% would be adequate, provided subsequent breakthrough curves demonstrated linearity.

Since the analysis was carried out on a dimensionless basis and the relationship between the voltage and concentration is linear for the range considered, no calibration of the TCD was required. Once the adsorption was complete, desorption could be carried out. This involved

turning the three way valves such that only the carrier gas passed to the column. Obtaining the desorption curve is useful as a test for linearity since if the adsorption and desorption curves are mirror images then the system can be said to be linear and be operating in the Henry's law region as desired. The same procedure was carried out for both columns and at a variety of flowrates. The details of each experiment completed is given in table 3.9.

3.3.3 ZLC Experimental procedure

The basic experimental set up for gaseous systems is shown in fig. 3.10. The zero length column itself consists of a very small amount of adsorbent material held in place between two porous sinter discs. The intention is to have a monolayer of adsorbent distributed evenly across the sinter disc area. If contact with the purge gas stream is good then external resistance to heat and mass transfer is minimised. The experimental procedure begins with introducing a low uniform concentration of sorbate into the test cell. A concentration that ensures that the experiment occurs within the Henry's law region is ideal. Once at equilibrium desorption is begun by purging the cell with inert carrier gas at a high enough flowrate to ensure the assumption of zero sorbate concentration at the external surface of the adsorbent remains valid. Measuring the sorbate concentration in the effluent gas allows determination of the rate of desorption. The method by which this is achieved depends on the system of interest. A flame ionisation detector may be used for organic sorbates. It has the advantage of being both able to detect the very low concentrations present and is also not sensitive to water. Another method makes use of an ultraviolet absorption detector to detect aromatics in a purge stream of saturated hydrocarbons.

Detection itself is not a challenge but ensuring the correct results are obtained is. Blank runs made with the adsorbent absent ensures that any extraneous adsorption is accounted for and also allows the dead volume of system, likely to be large when compared with the cell volume, to be calculated. Also desorption curves obtained using different carrier gases such as He and Ar can be useful in considering the effect of extracrystalline resistances. If the

resistances are significant then there will be an effect on the molecular diffusivity and hence the shape of the curve would change. For very sensitive detection a quadropole spectrometer can be used, as was used by Brandani et al (2002).

3.4 Results from Characterisation Experiments

The results obtained from the chromatography experiments are discussed in detail. The values found for the adsorption equilibrium constants and effective diffusivities are compared to those found from a published ZLC study.

3.4.1 Graphical Results from Chromatography Experiments

3.4.1.1 Confirmation of linear adsorption behaviour

The first breakthrough curves obtained were those to confirm the concentration that could be used to ensure that the adsorption equilibrium was linear. Figs.3.11 and 3.12 show the adsorption and desorption curves obtained when using 15% and 1% of CO₂ in the He carrier respectively. In order to check for linearity the adsorption (i.e. c/c_o)and inverted desorption (i.e. 1-c/c_o) curves can be plotted together. If they are coincident then linearity is confirmed. These alternative plots are shown in figs.3.13 & 3.14. When the concentration is 15% then the system is very clearly non linear, however the match between the two curves when the concentration is 1% is much closer. Even so the desorption curve is still not as sharp as that obtained when adsorbing suggesting that even at this low concentration level the equilibrium isotherm is slightly favourable rather than linear. Reducing the concentration level further was explored but the TCD sensitivity and the accuracy obtainable from the flowmeters made 1% the lowest possible concentration. To obtain a more linear curve an average of the adsorbed and inverted desorption curves could be used. This curve is shown in figs.3.13 & 3.14.

3.4.1.2 Analysis of chromatography curves

Examples of the adsorption, “inverted” desorption and averaged curves obtained for both large and small columns and for CO₂ in both carriers are shown in figs. 3.15-3.36. The adsorption curves for N₂ in He for the large column are shown in figs. 3.37-3.39. In order to extract the kinetic and mass transfer parameters the moments approach was used to analyse the curves. To obtain the first and second moments numerical integration of the averaged adsorption curves was performed using (Ruthven and Karger, 1992):

$$1^{\text{st}} \text{ moment: } \mu = \int_0^\infty (1 - \frac{c}{c_0}) dt \quad (3.32)$$

$$2^{\text{nd}} \text{ moment: } \sigma^2 = 2 \int_0^\infty (1 - \frac{c}{c_0}) t dt - \mu^2 \quad (3.33)$$

To find first the equilibrium constant the first moment was evaluated at the various flowrates and a plot of the values vs 1/F drawn. The plots obtained for both columns using CO₂ in each of the carrier gases are shown in figs. 3.40 and 3.41. Fig. 3.42 shows the plot for N₂ in helium for the large column. In each figure the linear regression slope fitted to the experimental data makes it possible to find the K value from the slope of the line, using equation (3.7), where L/v=V/F. The values of K calculated are shown in table 3.3. To find the diffusional time constants the calculated values for the second moments for CO₂ in both carriers were expressed as HETP values using equation (3.13) and plotted against F. For these experiments since the flowrate used was high the first term of the HETP expression derived from Spangler’s expression for a rectangular column could be neglected. By plotting HETP vs F then fitting a straight line to the data and finding the slope of the line the diffusional time constant could be evaluated. Again employing L/v=V/F the slope of the line was equal to:

$$\text{Gradient} \approx \frac{L}{V_c} \left(\frac{70r^2}{48D_m} + \frac{Wr}{3KD_e} \right) \quad (3.34)$$

So using the K values found from the first moment finding D_e/R² was straightforward. Figs. 3.43-3.44 show the HETP plots obtained using the two columns and two carriers available. The values found for the diffusional time constants are given in table 3.3. Since it was only

possible to obtain reliable data at low flowrates for N₂ in helium then the HETP analysis could not be carried out.

3.4.2 Comparing Chromatography and ZLC results

3.4.2.1 Equilibrium adsorption coefficients for CO₂

Looking at the K values obtained from analysis of the first moment data from the chromatography experiments the first thing to note is that the values found are different. It would be normal to expect that the values are not the same for both carriers, since while He has an extremely low affinity for activated carbon the nitrogen is likely to compete slightly with CO₂, although only to a small extent despite its relatively high partial pressure. Since both columns are manufactured from the same materials it would have been reasonable however to expect the results for both columns using the same carrier to be in agreement. For the N₂ carrier the results are reasonably close (within around 15%) but for the He carrier the K value for the smaller monolith is around 30% larger than that for the larger monolith. Considering the results obtained from the ZLC study reported by Brandani et al (2003) and reproduced in table 3.3, the K values for both carriers are both smaller than those obtained from the breakthrough curves. However an exact match between the two experimental studies is unlikely since the ZLC measurements were carried out at 30degC whereas the chromatography runs were undertaken at a room temperature of around 23degC. Making the correction for the temperature difference using the isoteric heat of adsorption, found to be around 23kJ/mol, and giving a correction ratio of 1.24, the K values could be more confidently compared. In this case the corrected ZLC K value with the N₂ carrier at 23degC was found to be 39.2, which agreed well with the results from the breakthrough experiment using the larger monolith of 39.7. Agreement is not as good when considering the smaller monolith, however this can be explained in part by variations in the room temperature while carrying out the breakthrough experiments. Other sources of explanation include the errors encountered in determining the first moment values using numerical integration as well as any uncertainty in the weight of the material packed in the ZLC column (1-2 mg).

Correcting the ZLC results for temperature differences when the He carrier was used leads to a result of 52.2. This is within 5% of the results found using the large column but within 13% of that found using the small column.

Comparing the 3 sets of K values obtained then the difference between the values obtained using the two different carriers is around 20-25%. This is consistent with the difference that may be encountered when allowing for competitive adsorption, experienced when using N₂ the agreement between the results is good.

3.4.2.2 Equilibrium adsorption coefficients for N₂

The K value found from the chromatography experiment is given in table 3.3. Again the temperature at which the experiment was carried out must be taken into account. Using the isosteric heat of adsorption for nitrogen which is 14kJ/mol, and adjusting as before then the equilibrium adsorption coefficient for nitrogen is found to be around 1.3. Preliminary ZLC experiments, undertaken using the small column material, suggest that this value is reasonable. Difficulties in analysing the ZLC results for these experiments made the values unreliable but it was estimated that a K value of less than 10 was likely.

3.4.2.3 Diffusional time constants

When considering the results found for the effective diffusivity values the agreement between the two experimental approaches is not good. For both the small column ZLC and breakthrough results obtained using the large column the diffusivity values obtained using the He carrier is larger than that found using N₂ by a factor of 2. This would be the case if transport within the pores is controlled mainly by Knudsen diffusion with a little contribution from molecular diffusion and suggests that one of the values found using the smaller monolith is anomalous. The reasonable agreement between the value found from the ZLC results and chromatography results when the N₂ carrier was used (~factor of 2) suggests that the result found using the He carrier is incorrect. Using the second moment to derive diffusivity values

often leads to errors. In order to get accurate results a very sensitive detector must be used but any noise or atmospheric interference must be eliminated. In characterising the small column using the He carrier a great deal of noise was encountered due to the “oversensitivity” of the TCD and hence the results were adversely affected. In addition the technique whereby axial diffusion and Golay dispersion terms are neglected from the HETP expression can also lead to some error. Comparing the D_e values obtained from the smaller and larger monolith chromatography experiments when the N₂ carrier was used, the values differ by a factor of around 2.5, suggesting that diffusion in the larger column is slower. Without ZLC data, however, this conclusion cannot be supported.

3.5 Concluding Remarks

Two methods have been used to characterise the two available adsorption columns. Breakthrough curves from chromatography experiments undertaken using both columns were analysed using first and second moments and the adsorption equilibrium constant, K, and effective diffusivity, D_e , calculated. Similarly ZLC experiments using just the smaller column were performed and the desorption curves analysed. When comparing the K values obtained those found when the carrier gas was helium were always larger than those found when the carrier gas was nitrogen. This is because when nitrogen is present there is a small amount of competitive adsorption occurring. The equilibrium constants found compare well between the columns, especially when the ZLC results are corrected for the slightly higher experimental temperature used.

The effective diffusivity values obtained do not compare as well. While, from both the small column ZLC results and large column chromatography results, the values found from for the two different carriers differ by a factor of 2, this is not the case for the small column chromatography results. The fairly good agreement between the effective diffusivity from the ZLC and chromatography results for the nitrogen carrier suggests that the value found when

using helium is anomalous. Since when analysing chromatography results the second moment technique is often prone to errors, due to curve averaging and noisy detector signals , the ZLC method tends to more reliable for extracting diffusional time constants.

The values found can now be used within the mathematical model of the dual piston driven PSA, described in Chapter 5, so that the experimental behaviour of the rig can be predicted.

Chapter 3: Figures



Fig.3.1 Honeycomb adsorber structure (Silica gel on ceramic fibre) (Ruthven, 2001)

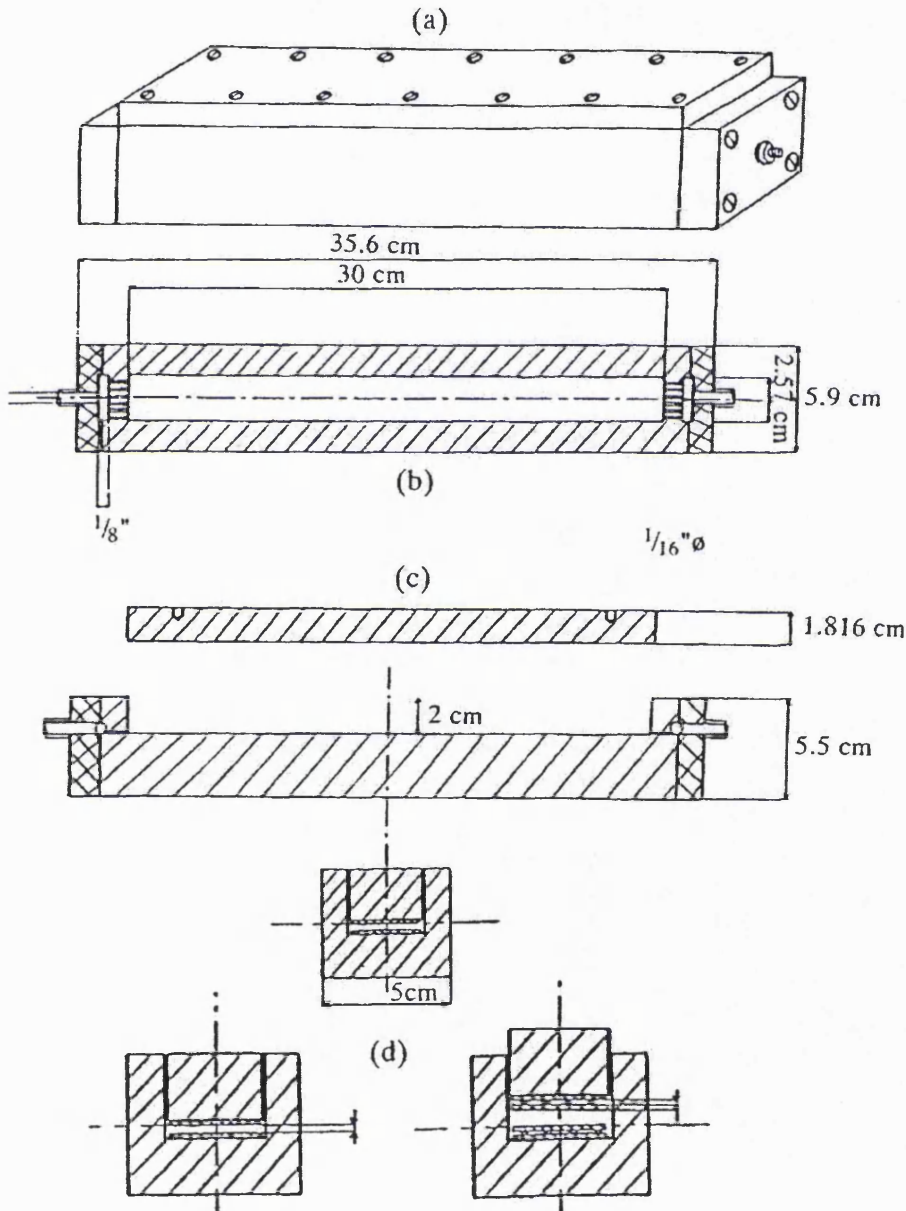


Fig.3.2 Details of the parallel passage adsorber (a) Outside view of the cell (b) Top view of the open cell (c) Side view of the open cell (d) Cross section view of the parallel sided duct coated with two or more layers of activated carbon fiber (reproduced from Ruthven and Thaeron, 1996)

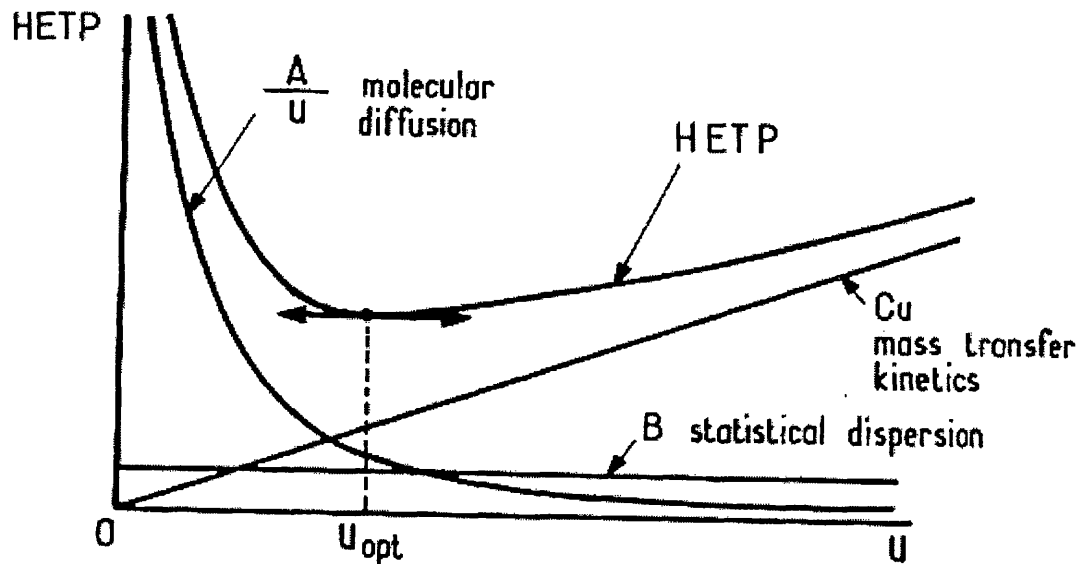


Fig.3.3 The contributions to HETP (HETP vs superficial velocity, u) (Yang, 1987)

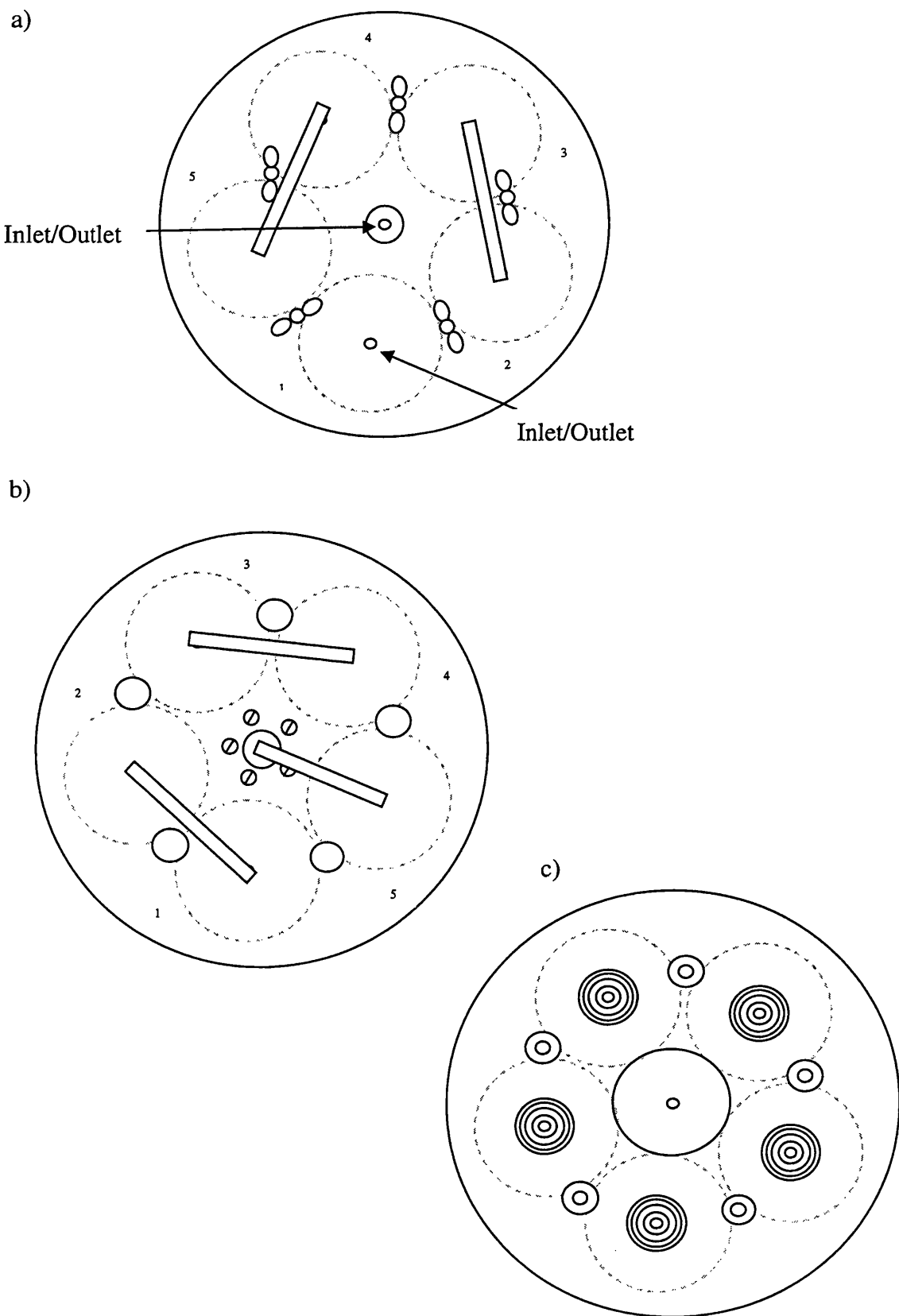


Fig.3.4 Top and bottom view of larger column assembly a) Top viewed from above b) bottom viewed from below c) bottom viewed from above (no columns in place)

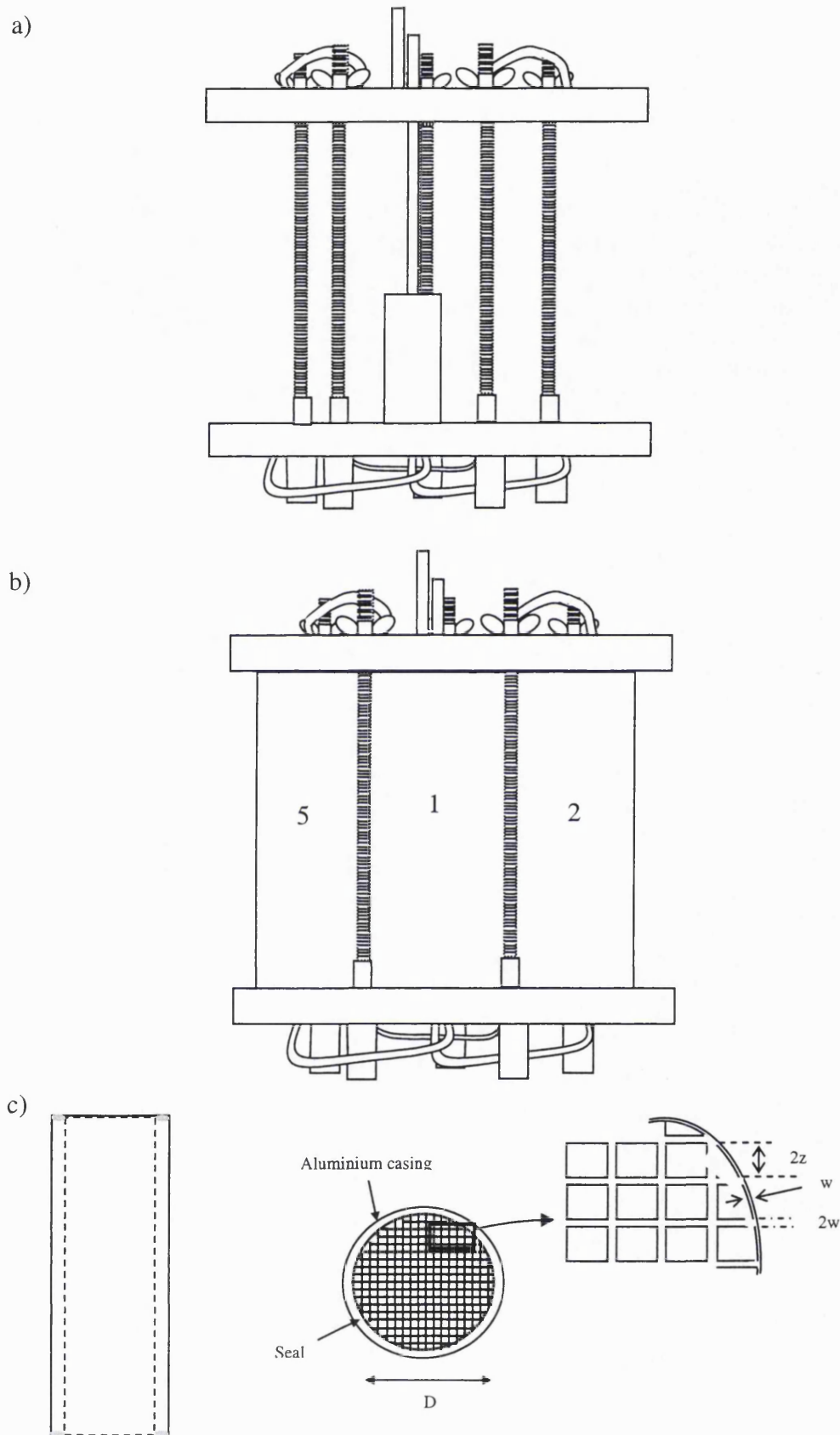


Fig.3.5 Side and cross sectional views of the larger column structure and monolith a) Side view without columns b) Side view with columns c) Individual column from side and cross section view

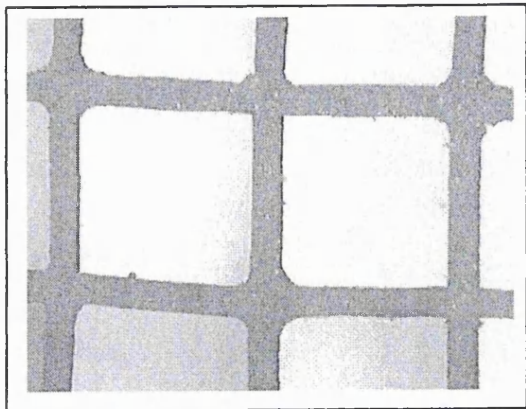


Fig.3.7 Small Monolith Cross Section (x24)

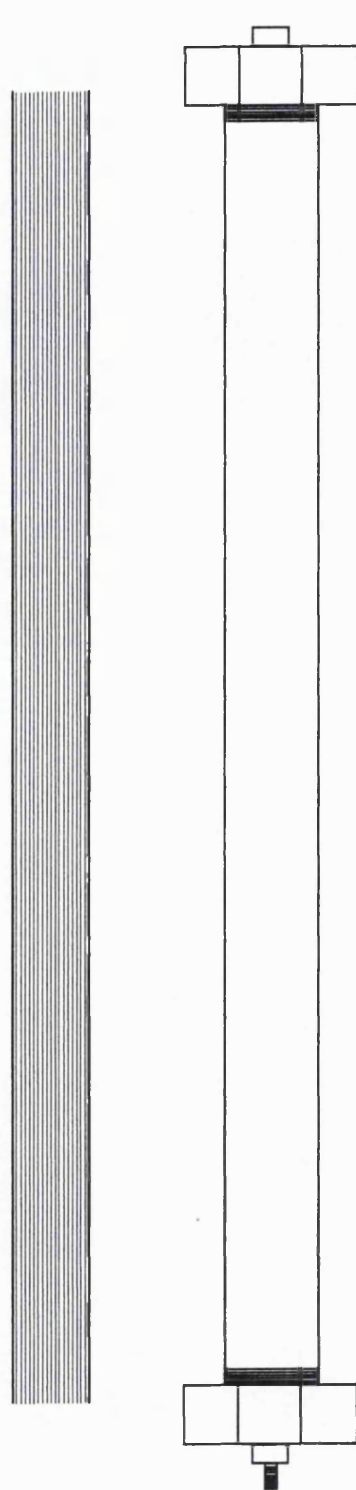


Fig.3.8 Large Monolith Cross Section (x 2)

Fig.3.6 Smaller column structure

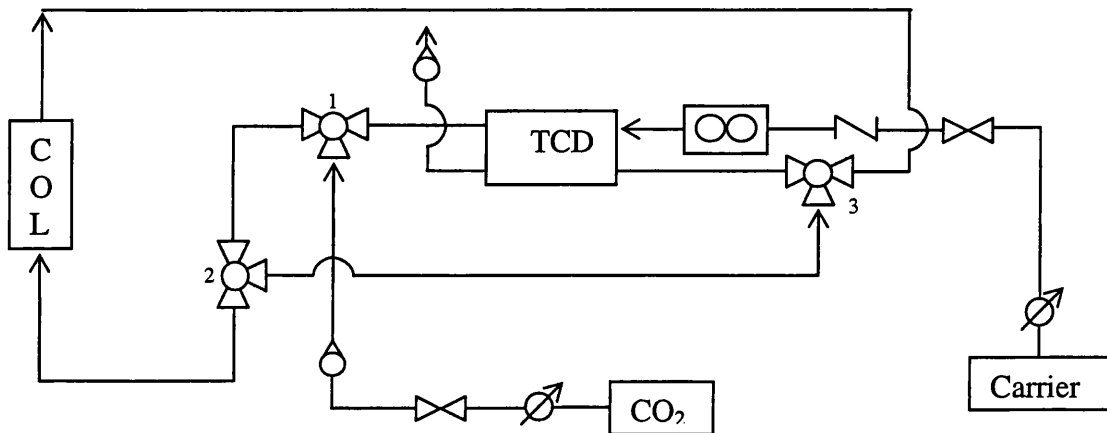


Fig.3.9 Chromatography Experimental Set Up

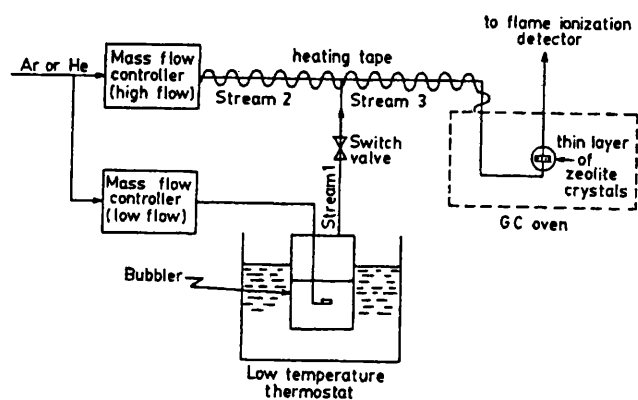


Fig.3.10 ZLC experimental set up (From Eic and Ruthven, 1988)

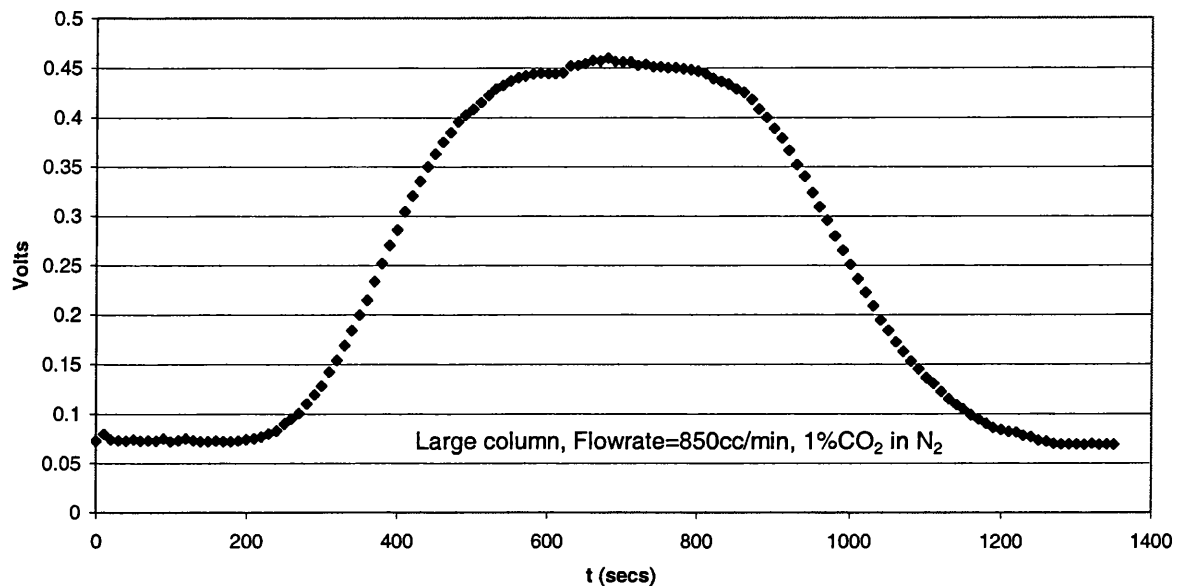


Fig.3.11 Adsorption And Desorption Plots for 1% CO₂ in N₂

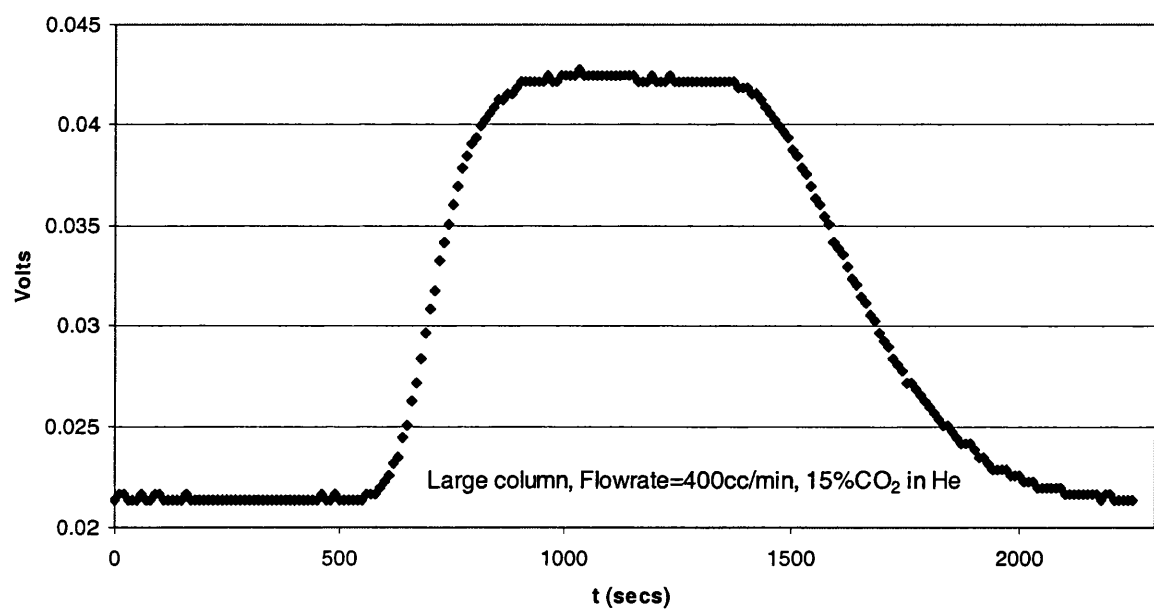


Fig.3.12 Adsorption And Desorption Plots For 15% CO₂ in He

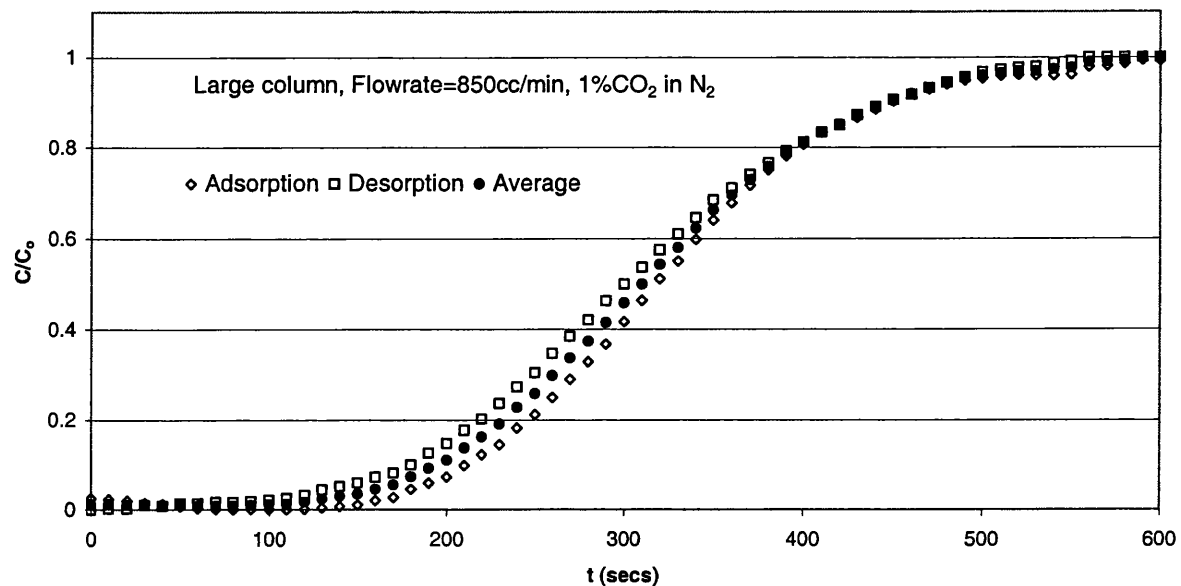


Fig.3.13 Alternative adsorption, desorption and average plots for 1% CO₂ in N₂

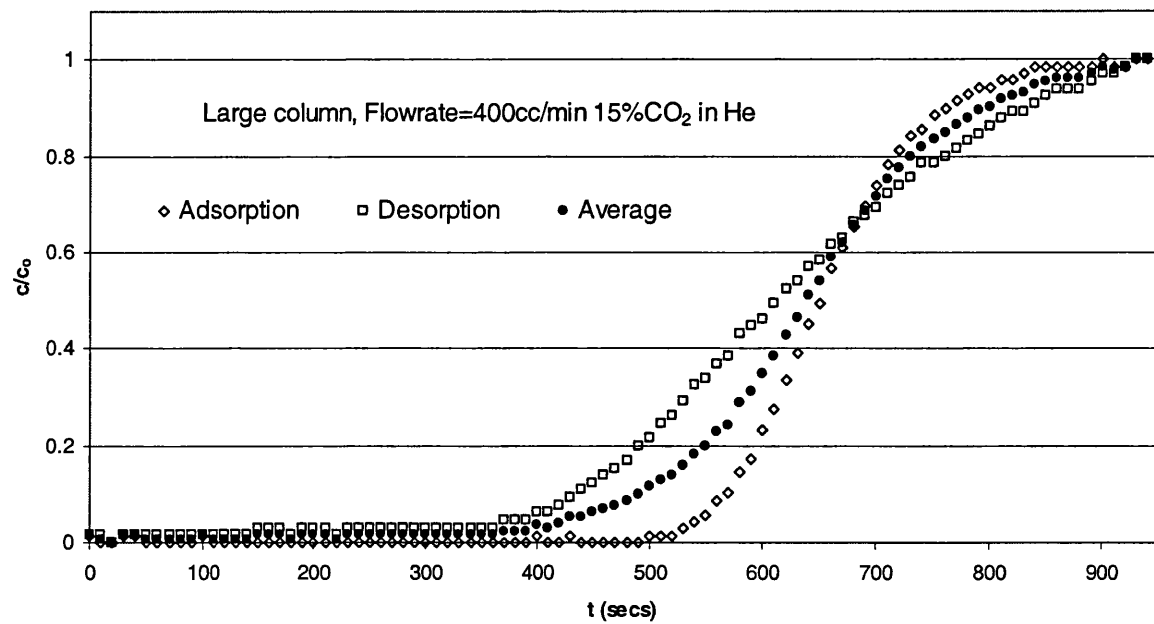


Fig.3.14 Alternative adsorption, desorption and average plots for 15% CO₂ in He

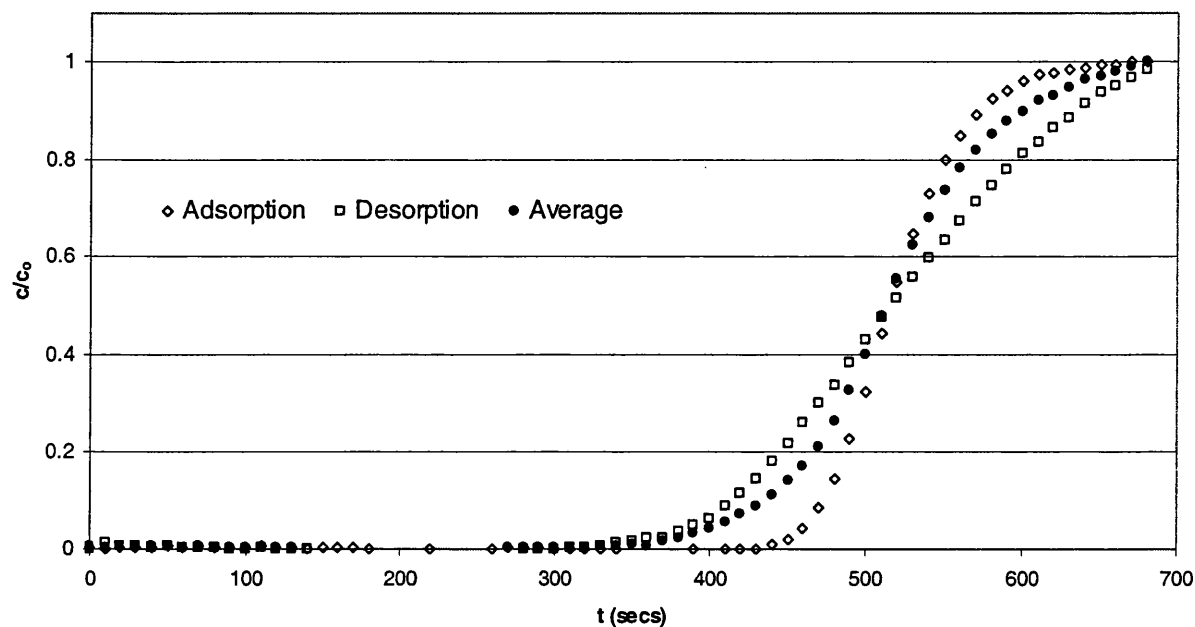


Fig.3.15 Adsorption/Desorption/Average Plot Conditions: Small column,
Flowrate=190cc/min, 1%CO₂ in He

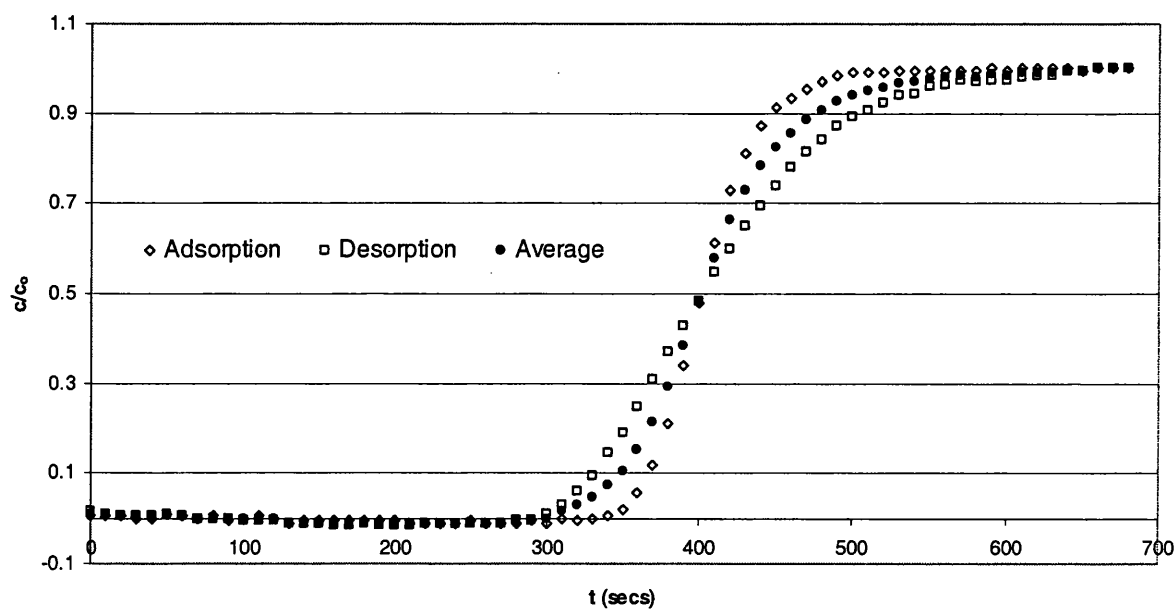


Fig.3.16 Adsorption/Desorption/Average Plot Conditions: Small column,
Flowrate=242cc/min, 1%CO₂ in He

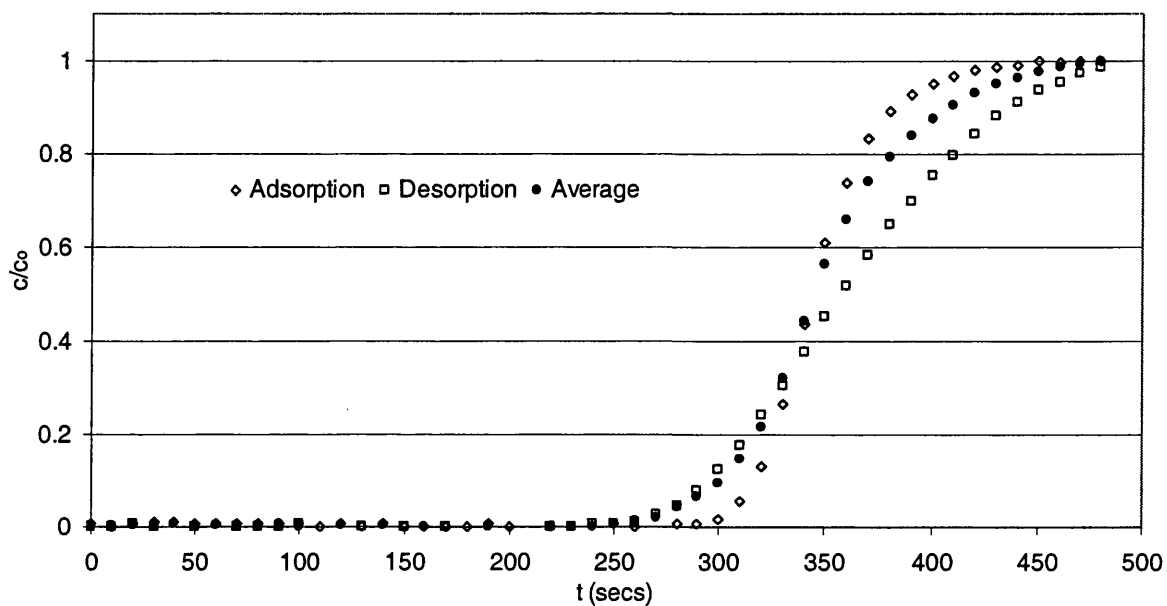


Fig.3.17 Adsorption/Desorption/Average Plot Conditions: Small column,
Flowrate=294cc/min, 1%CO₂ in He

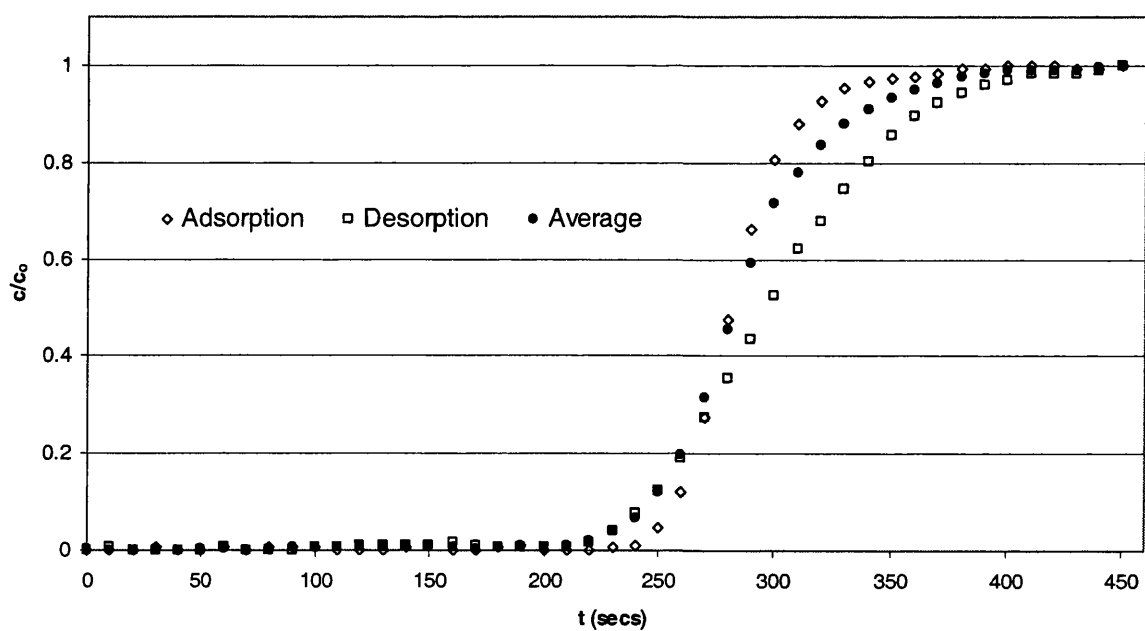


Fig.3.18 Adsorption/Desorption/Average Plot Conditions: Small column,
Flowrate=346cc/min, 1%CO₂ in He

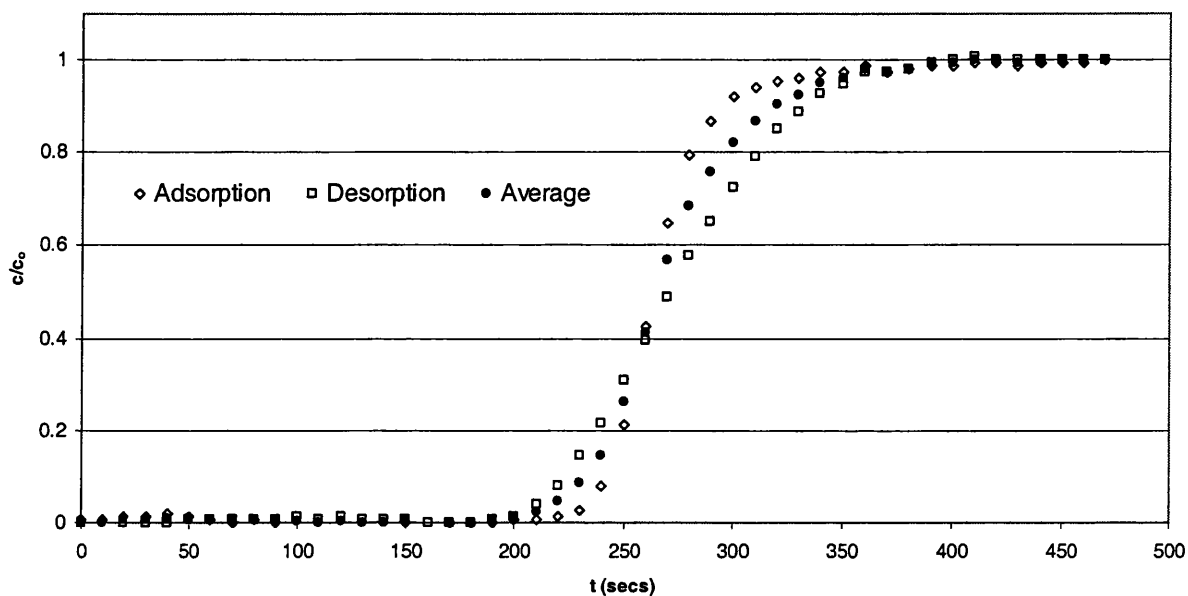


Fig.3.19 Adsorption/Desorption/Average Plot Conditions: Small column,
Flowrate=398cc/min, 1%CO₂ in He

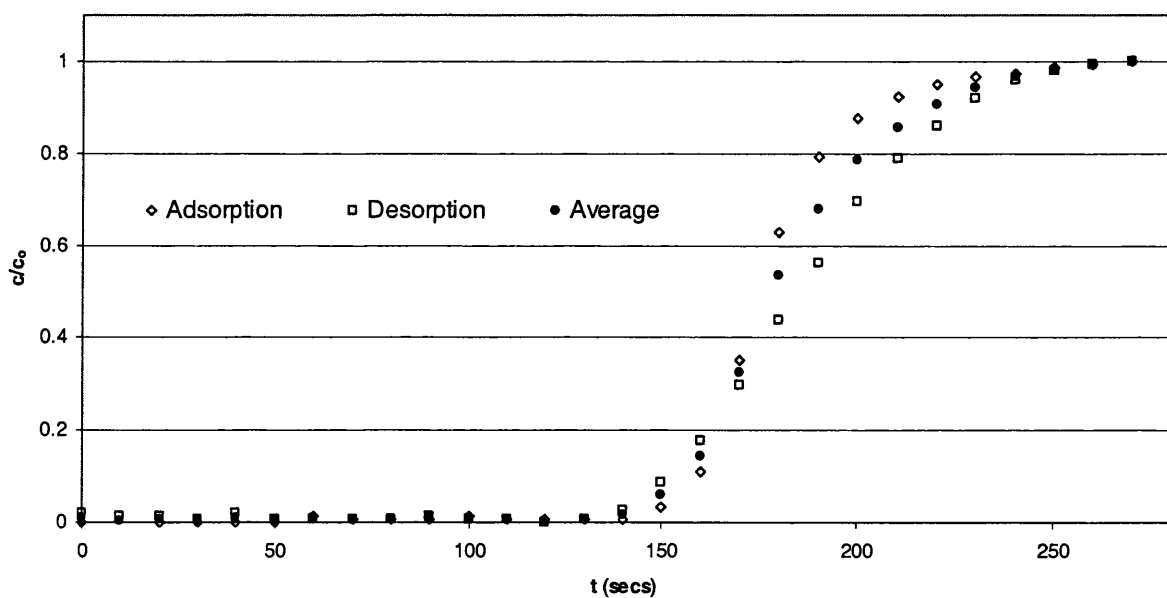


Fig.3.20 Adsorption/Desorption/Average Plot Conditions: Small column,
Flowrate=350cc/min, 1%CO₂ in N₂

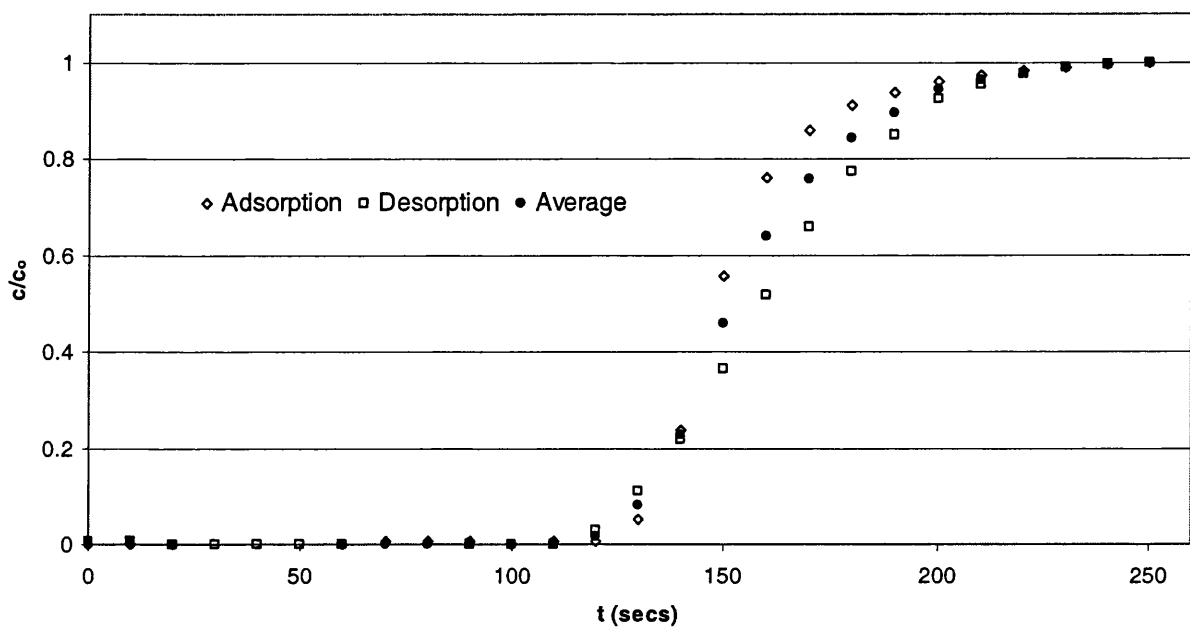


Fig.3.21 Adsorption/Desorption/Average Plot Conditions: Small column,
Flowrate=410cc/min, 1%CO₂ in N₂

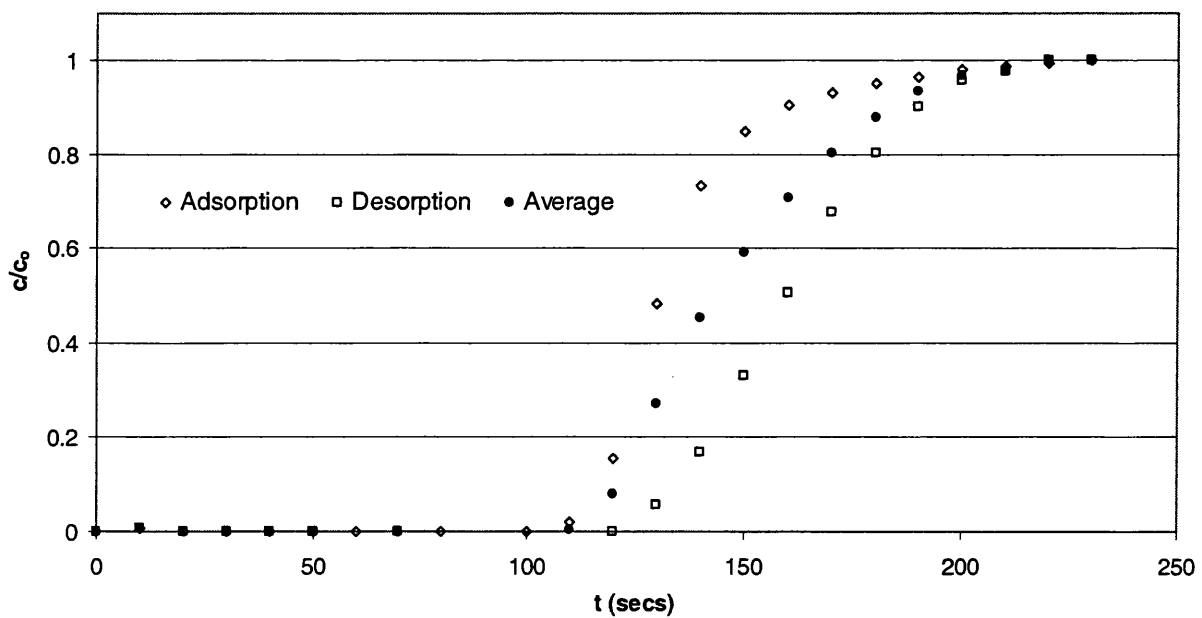


Fig.3.22 Adsorption/Desorption/Average Plot Conditions: Small column,
Flowrate=470cc/min, 1%CO₂ in N₂

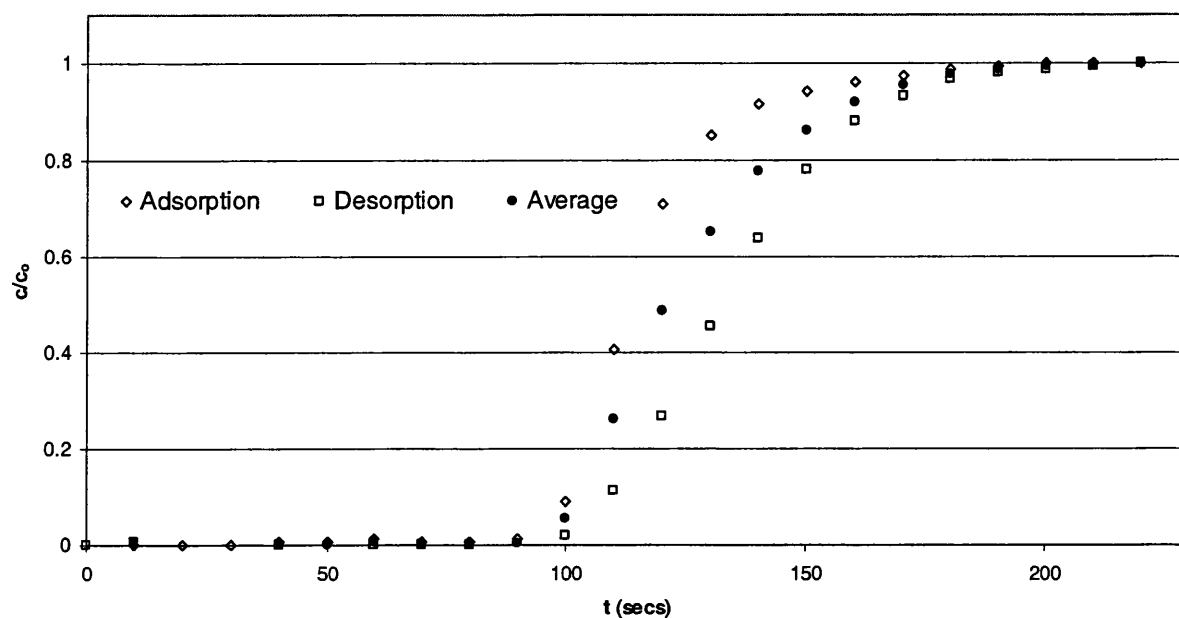


Fig.3.23 Adsorption/Desorption/Average Plot Conditions: Small column,
Flowrate=530cc/min, 1%CO₂ in N₂

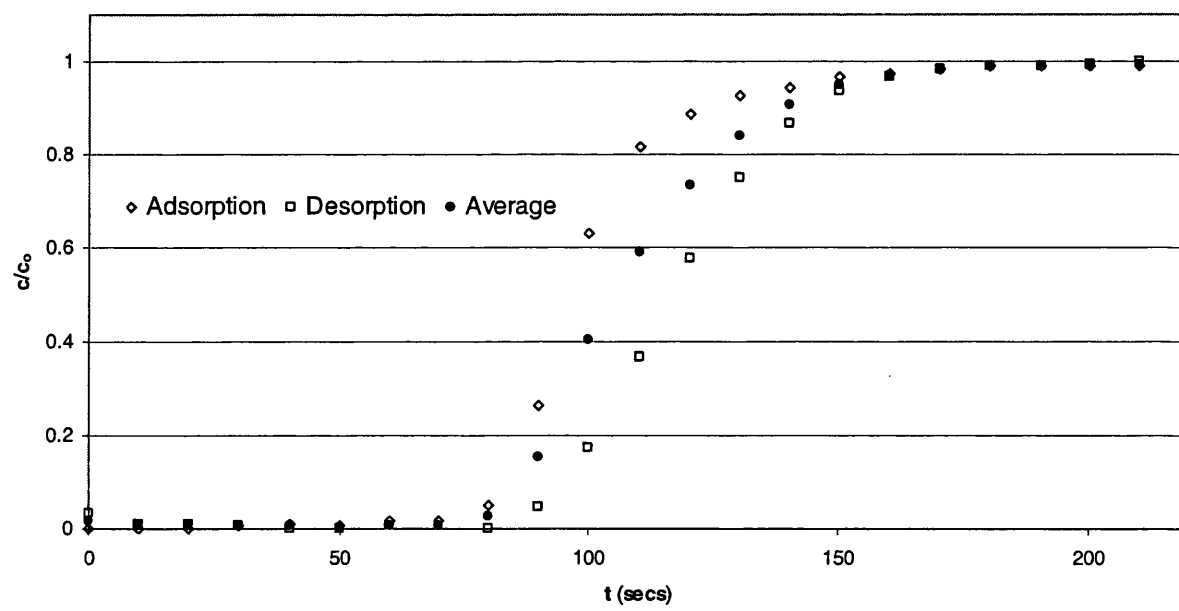


Fig.3.24 Adsorption/Desorption/Average Plot Conditions: Small column,
Flowrate=590cc/min, 1%CO₂ in N₂

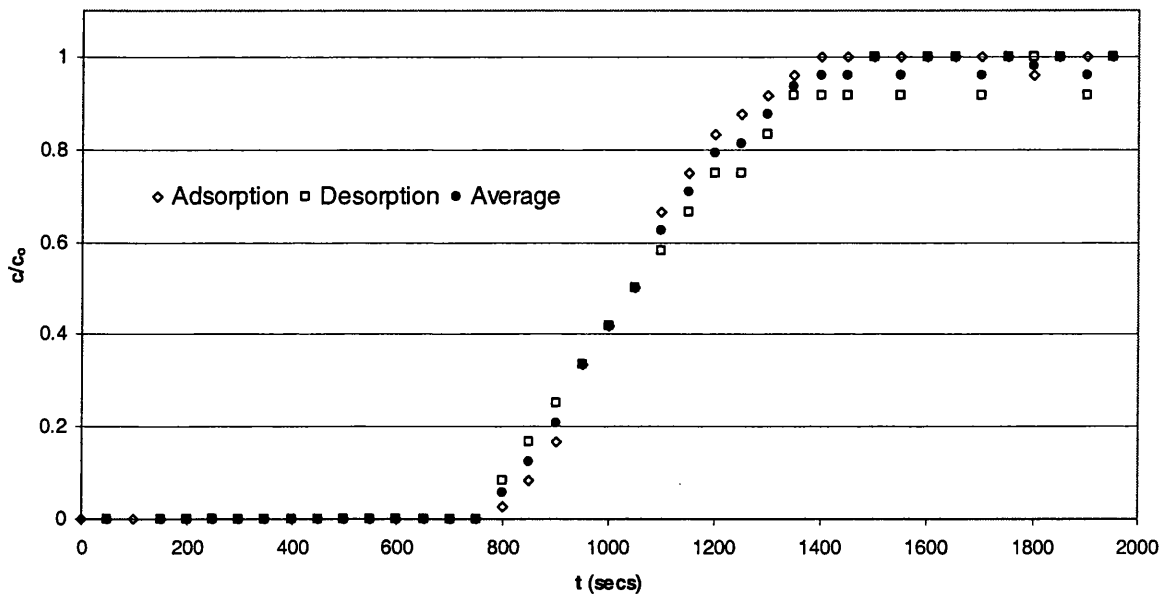


Fig.3.25 Adsorption/Desorption/Average Plot Conditions: Large column,
Flowrate=300cc/min, 1%CO₂ in He

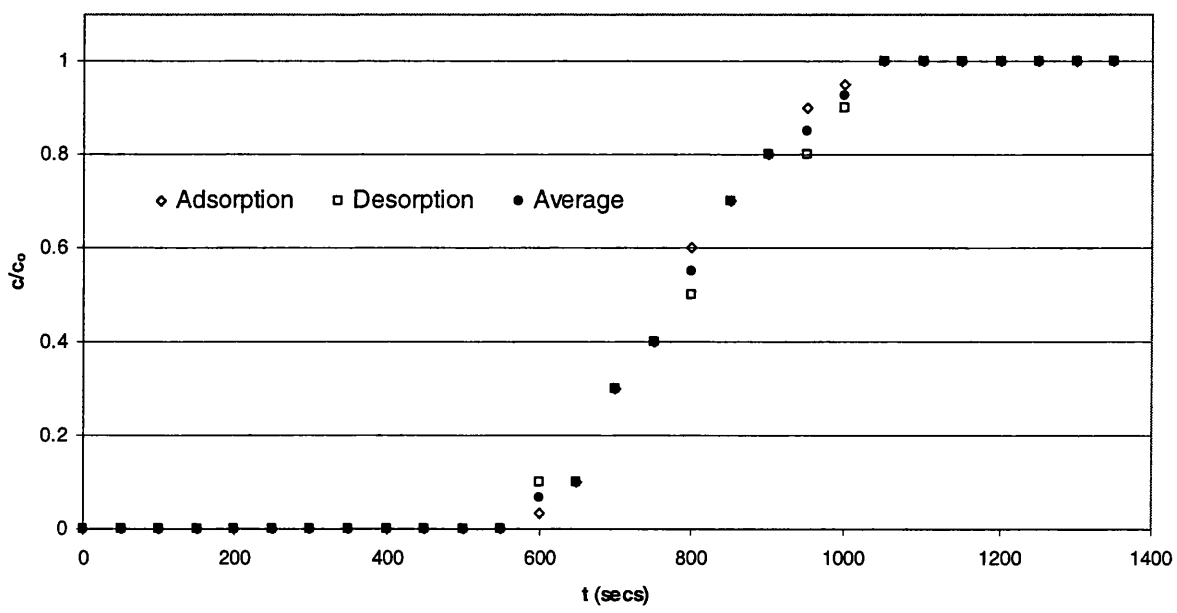


Fig.3.26 Adsorption/Desorption/Average Plot Conditions: Large column,
Flowrate=400cc/min, 1%CO₂ in He

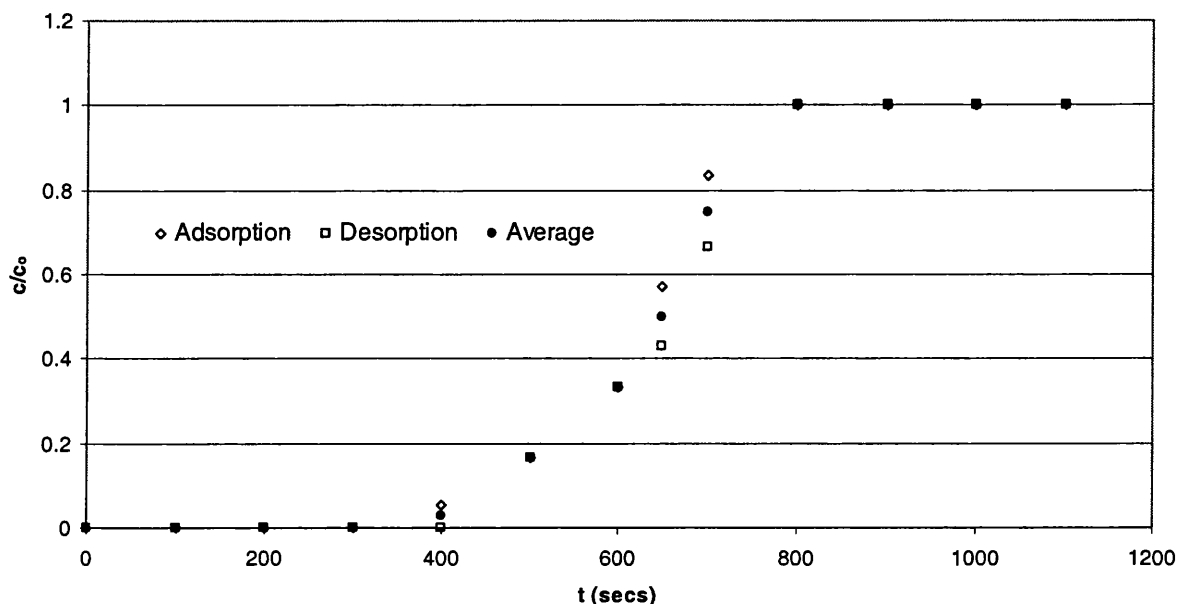


Fig.3.27 Adsorption/Desorption/Average Plot Conditions: Large column,
Flowrate=500cc/min, 1%CO₂ in He

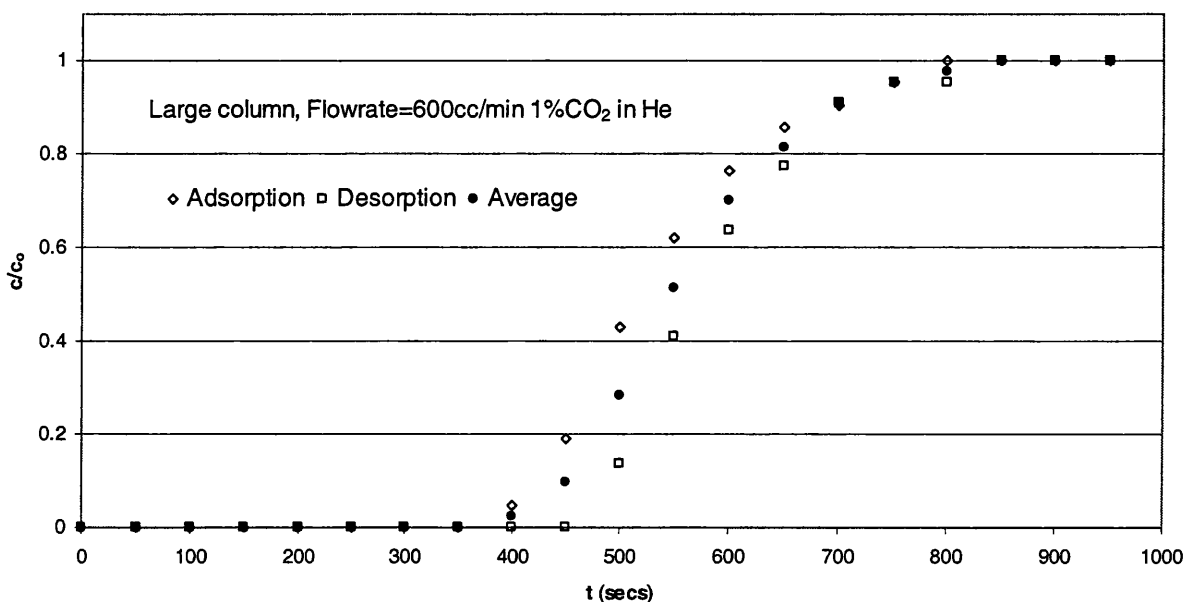


Fig.3.28 Adsorption/Desorption/Average Plot Conditions: Large column,
Flowrate=600cc/min, 1%CO₂ in He

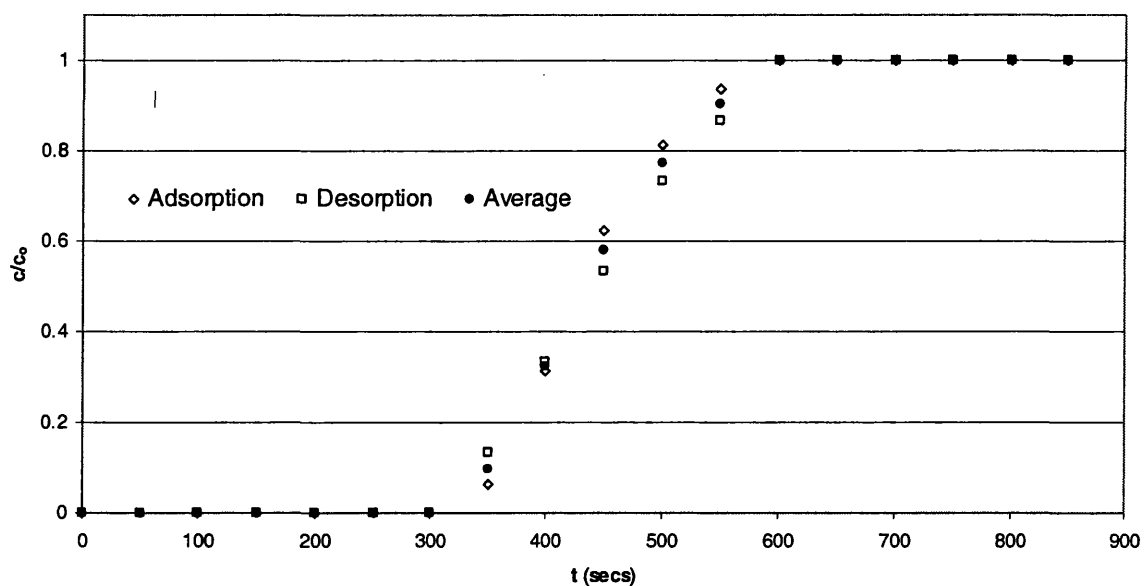


Fig.3.29 Adsorption/Desorption/Average Plot Conditions: Large column,
Flowrate=700cc/min, 1%CO₂ in He

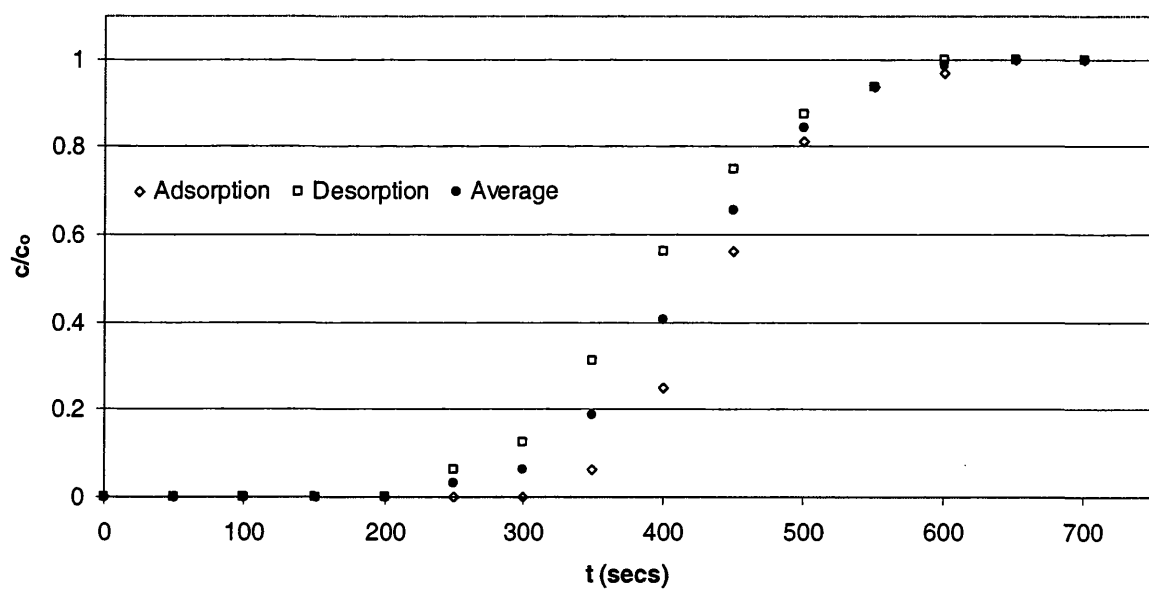


Fig.3.30 Adsorption/Desorption/Average Plot Conditions: Large column,
Flowrate=800cc/min, 1%CO₂ in He

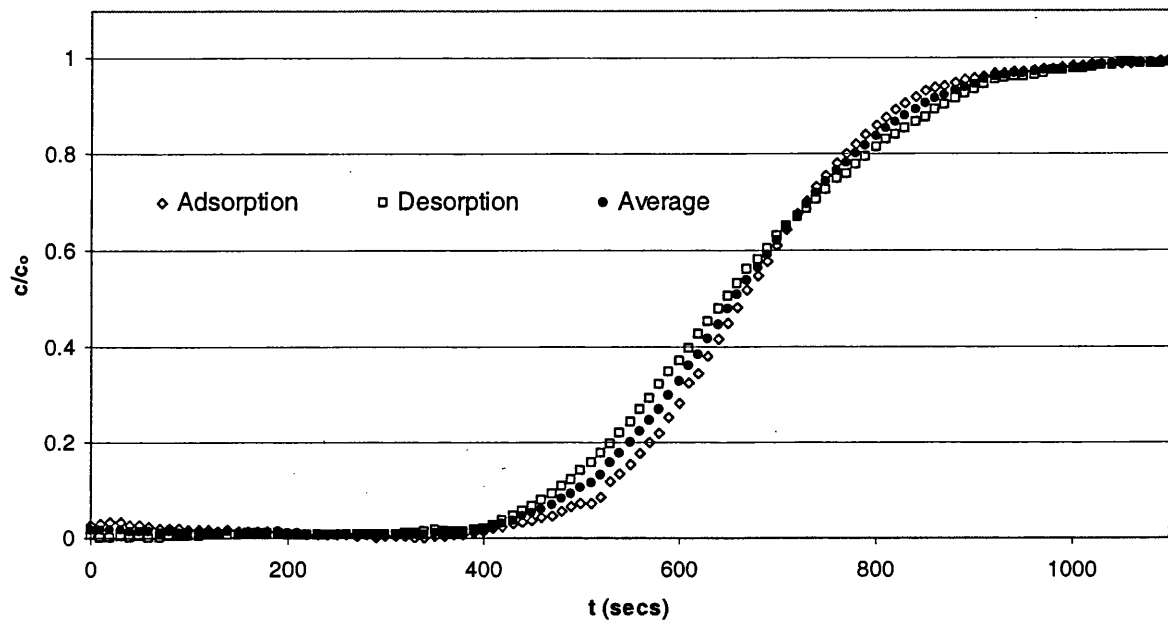


Fig.3.31 Adsorption/Desorption/Average Plot Conditions: Large column,
Flowrate=400cc/min, 1%CO₂ in He

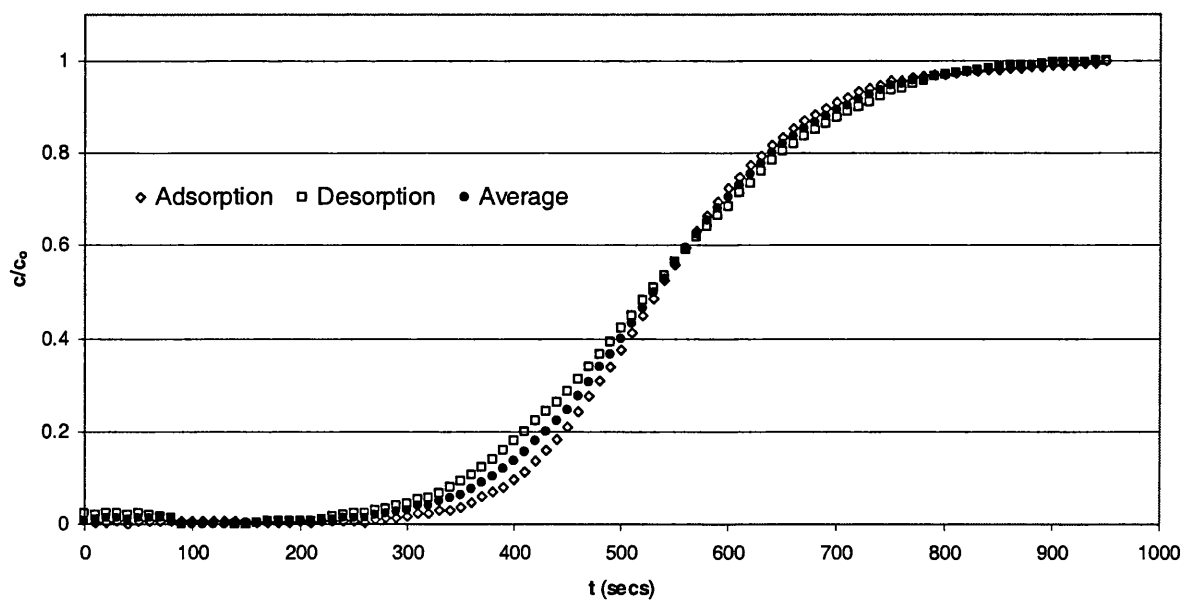


Fig.3.32 Adsorption/Desorption/Average Plot Conditions: Large column,
Flowrate=500cc/min, 1%CO₂ in He

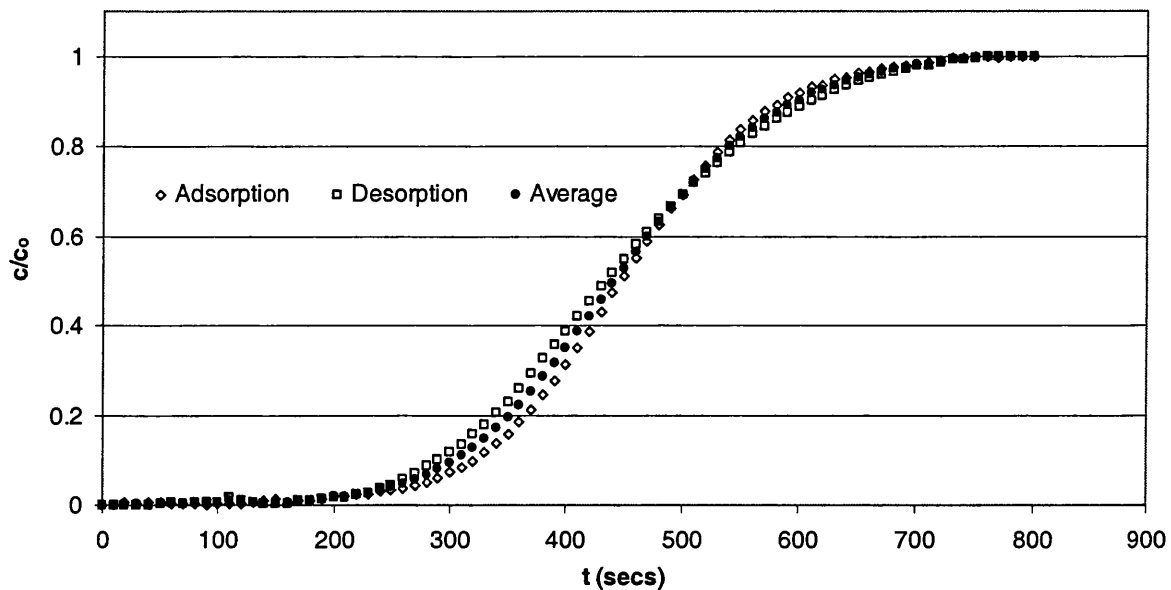


Fig.3.33 Adsorption/Desorption/Average Plot Conditions: Large column,
Flowrate=600cc/min, 1%CO₂ in He

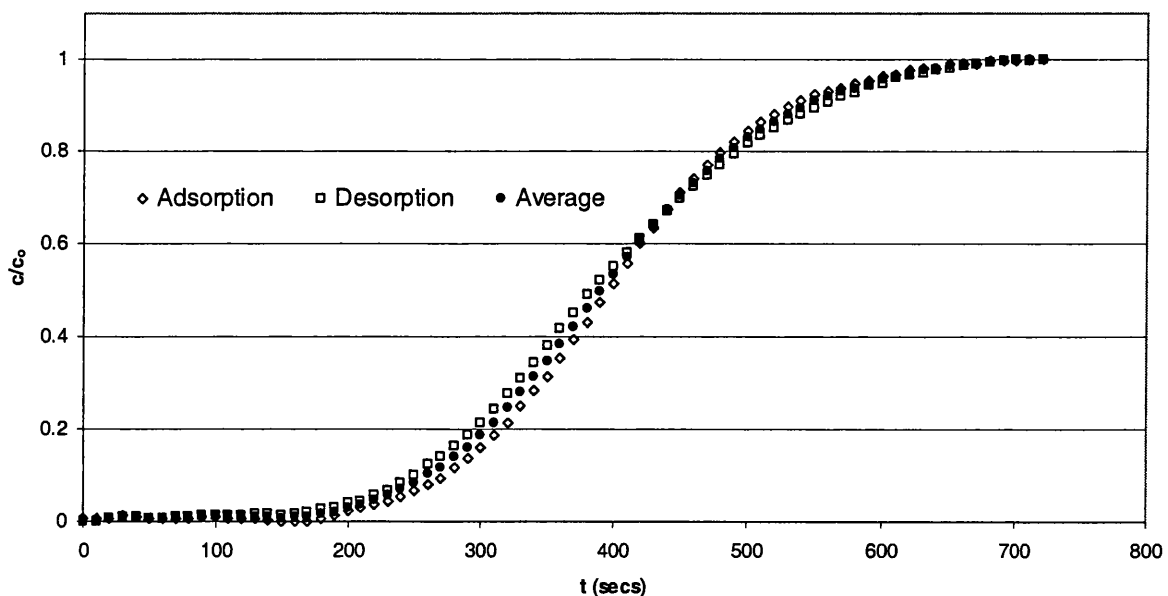


Fig.3.34 Adsorption/Desorption/Average Plot Conditions: Large column,
Flowrate=650cc/min, 1%CO₂ in He

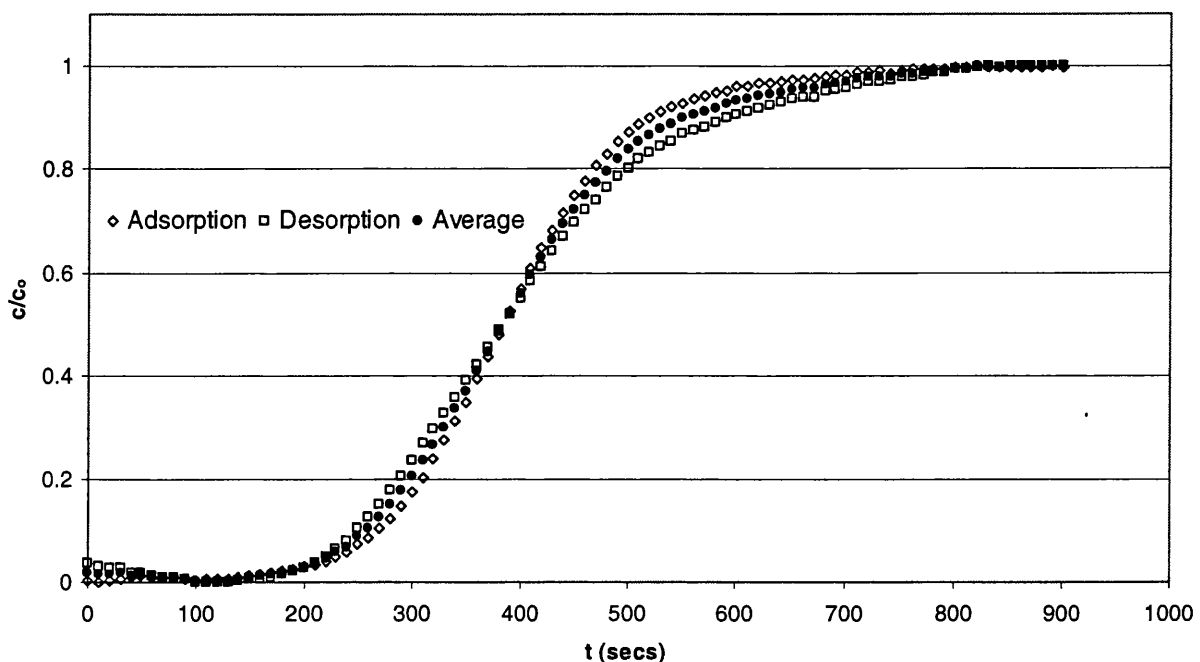


Fig.3.35 Adsorption/Desorption/Average Plot . Conditions: Large column,
Flowrate=700cc/min, 1%CO₂ in He

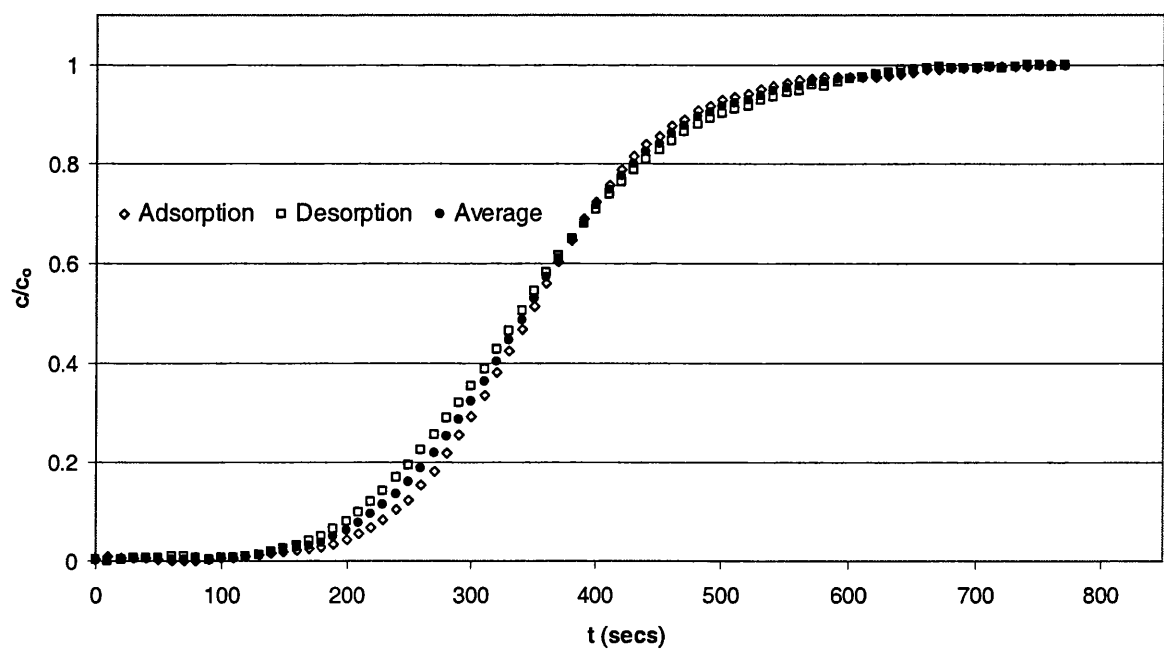


Fig.3.36 Adsorption/Desorption/Average Plot Conditions: Large column,
Flowrate=750cc/min, 1%CO₂ in He

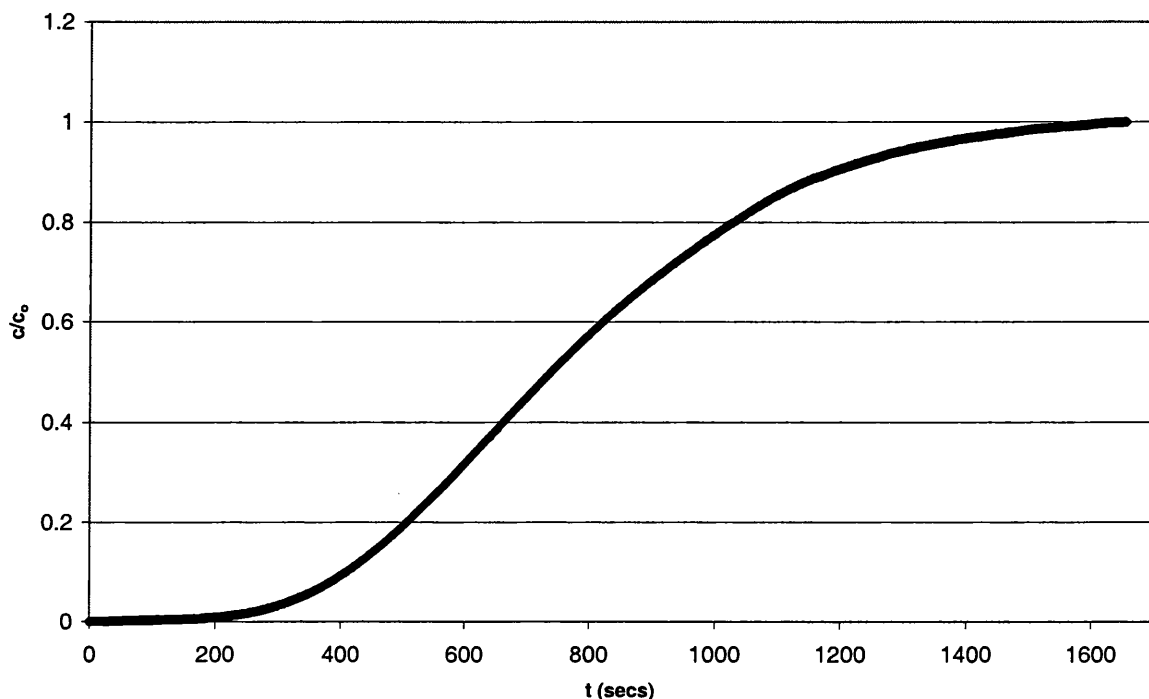


Fig.3.37 Adsorption/Desorption/Average Plot Conditions: Large column,
Flowrate=25cc/min, 1%N₂ in He

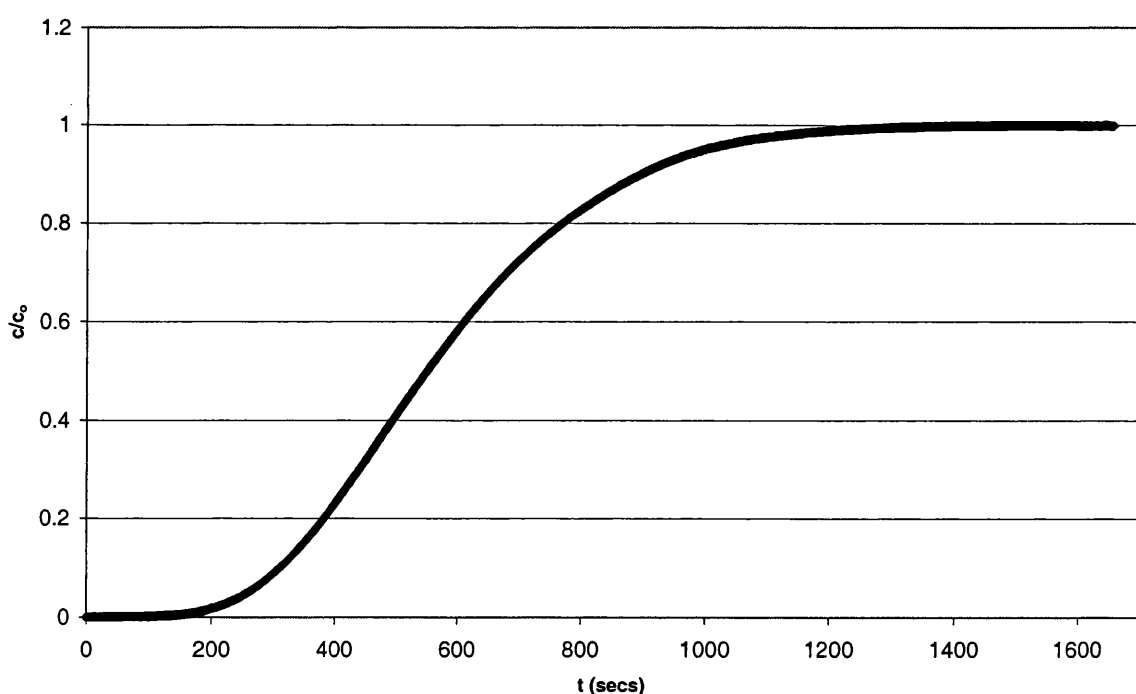


Fig.3.38 Adsorption/Desorption/Average Plot Conditions: Large column,
Flowrate=30cc/min, 1%N₂ in He

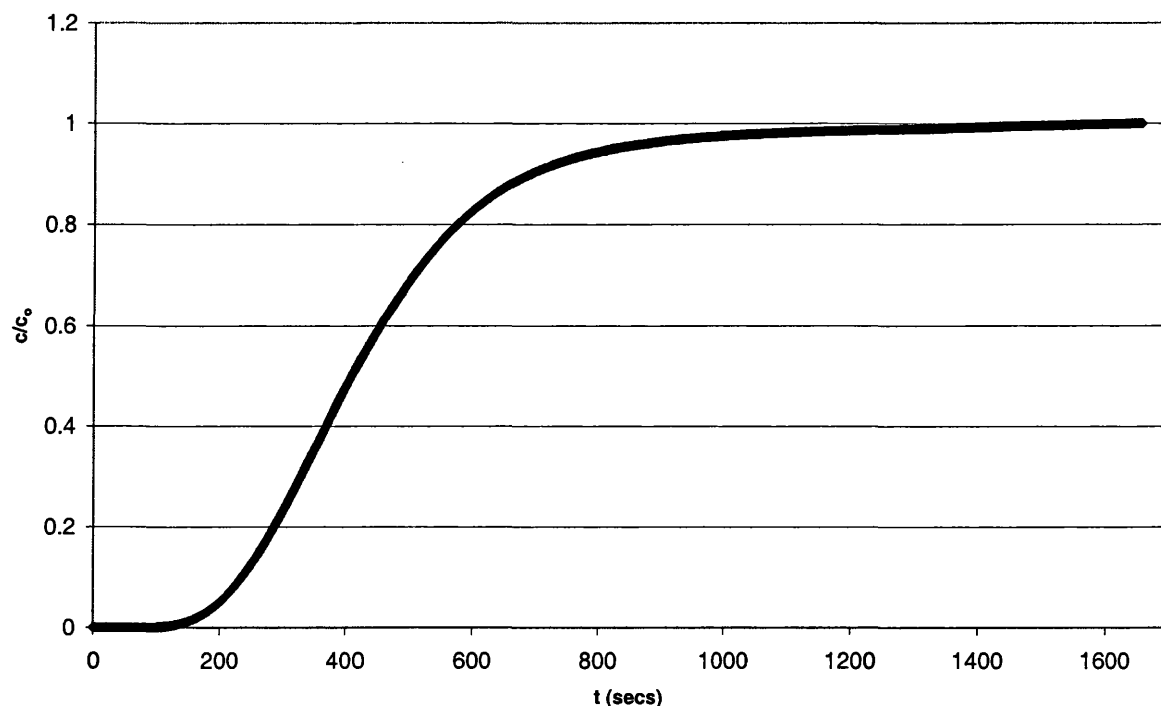


Fig.3.39 Adsorption/Desorption/Average Plot Conditions: Large column,
Flowrate=37cc/min, 1%N₂ in He

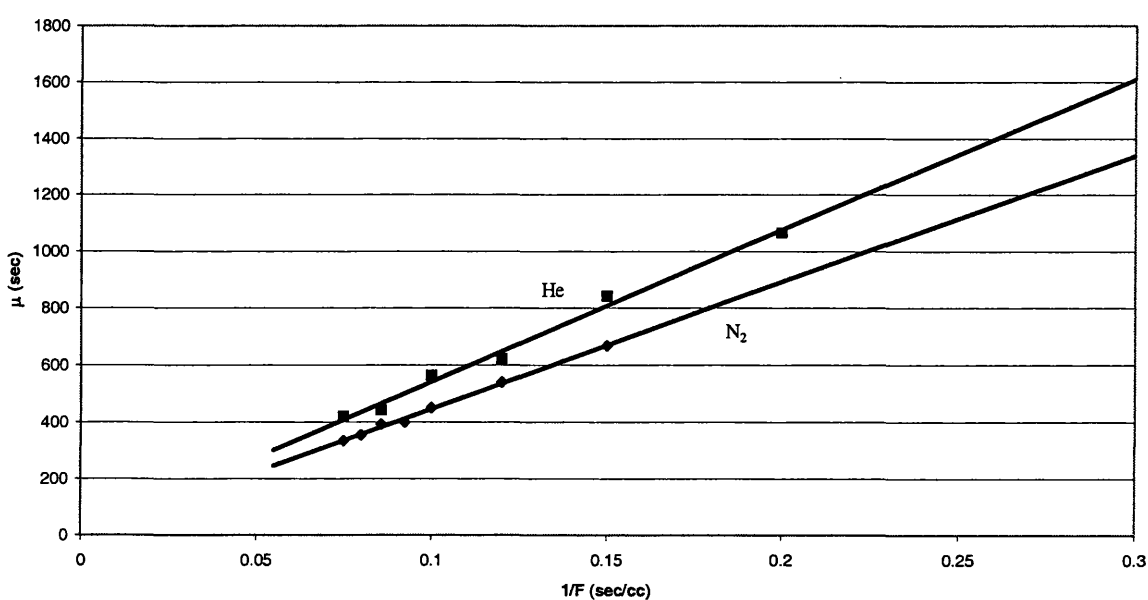


Fig.3.40 1st moment plots for the larger column using 1% CO₂ in both He and N₂ carriers

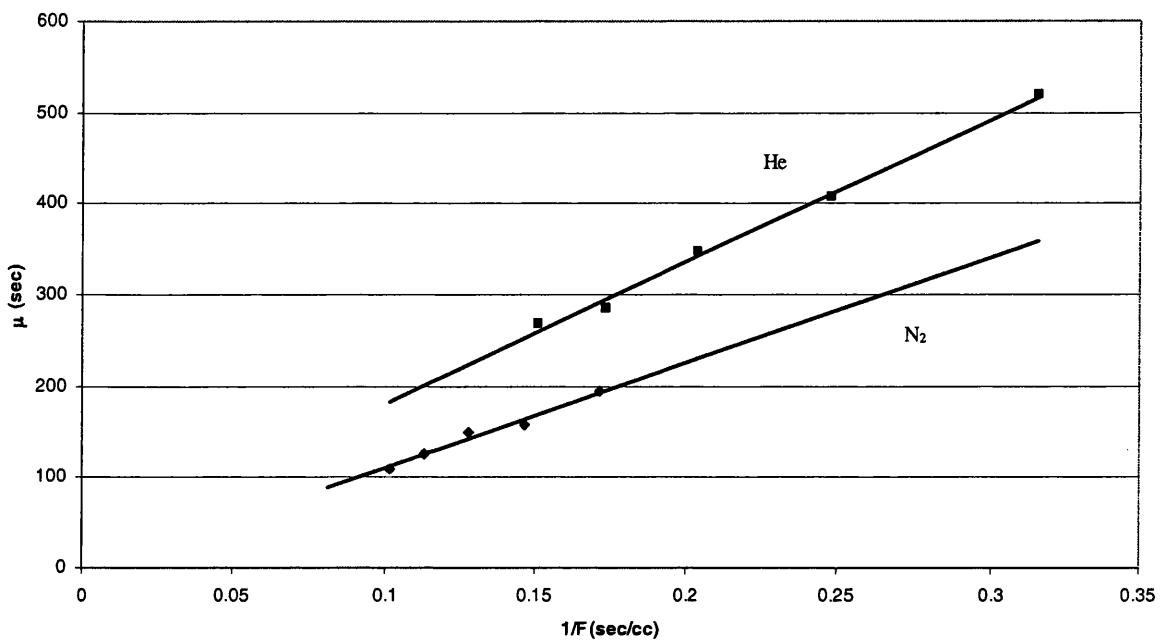


Fig.3.41 1st moment plots for the smaller column using 1% CO₂ in both He and N₂ carriers

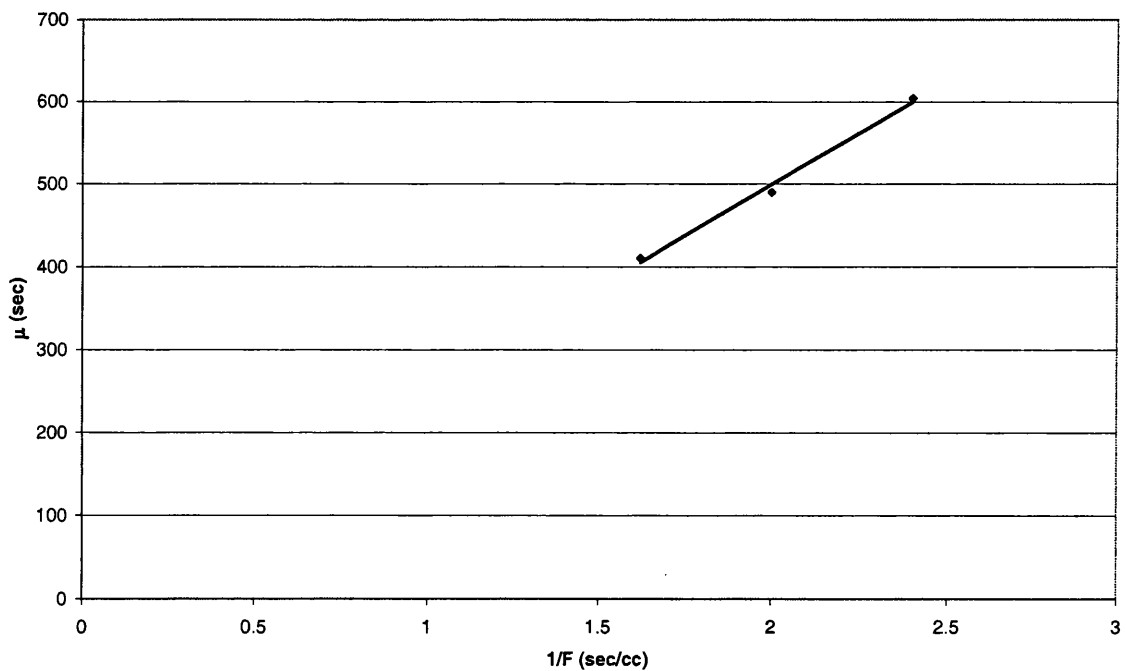


Fig.3.42 1st moment plots for the larger column using 1% N₂ in He carrier

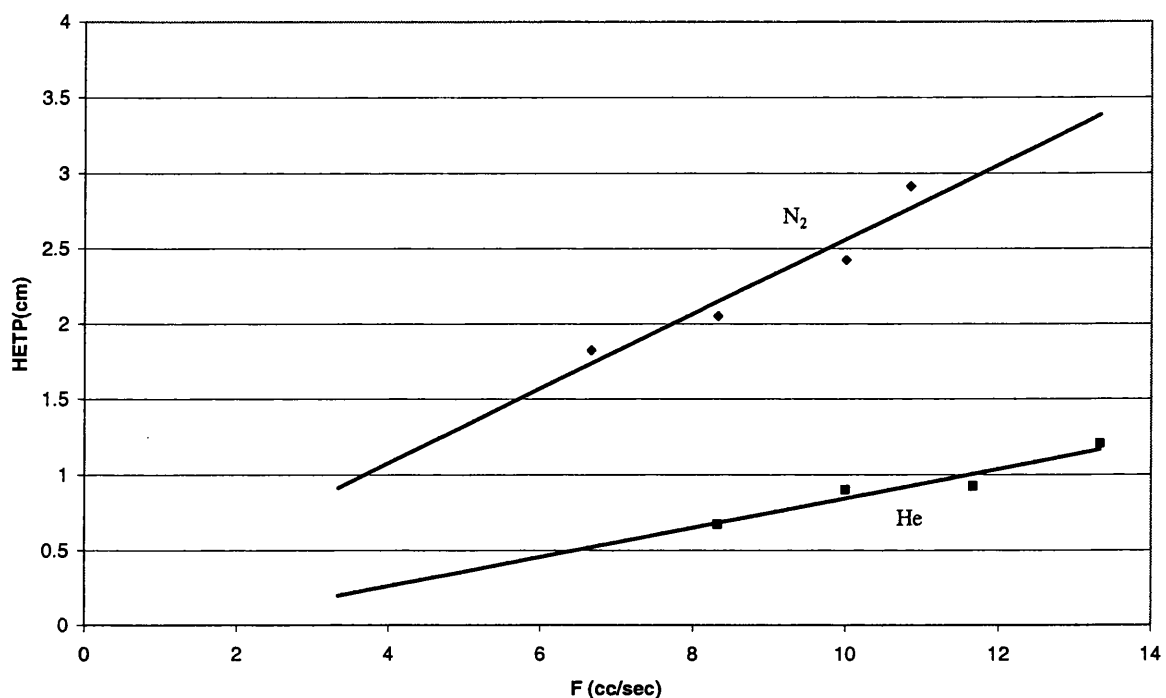


Fig.3.43 HETP plots for the larger column using 1% CO₂ in both He and N₂ carriers

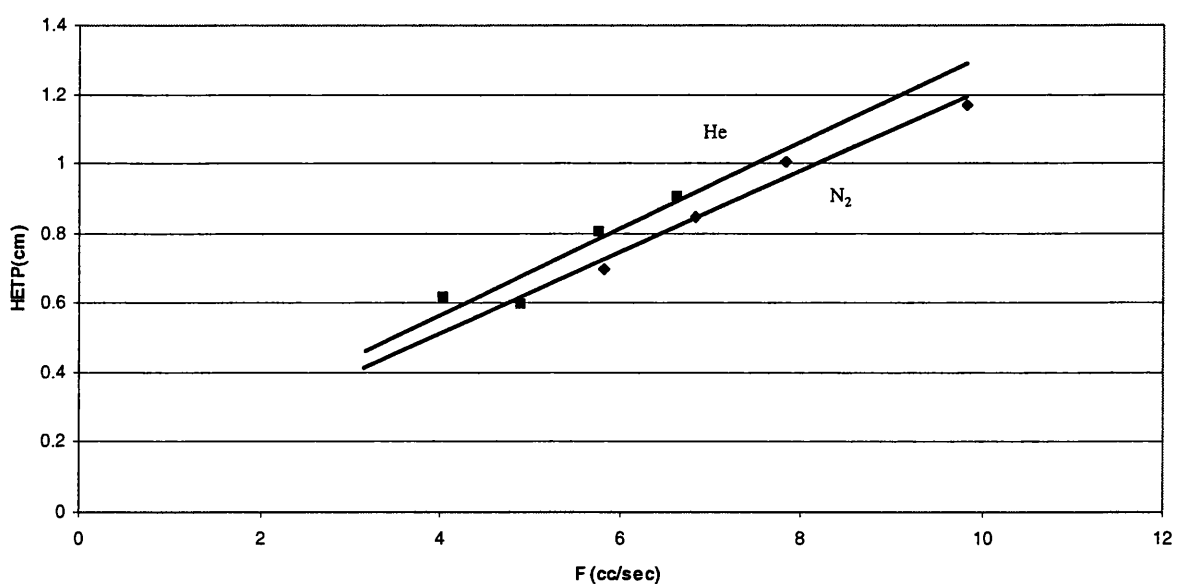


Fig.3.44 HETP plots for the smaller column using 1% CO₂ in both He and N₂ carriers

Chapter 3: Tables

Monolith: LARGE		SMALL	
Diameter, D	2.9cm	Diameter, D	1.56cm
Internal Cell width, 2z	0.136cm	Internal Cell width, 2z	0.09cm
Wall thickness, 2w	0.028cm	Wall thickness, 2w	0.0165cm
Voidage, ϵ	0.69	Voidage, ϵ	0.71
Length, L	50cm	Length, L	45cm

Table 3.1 Column Dimensions

Run	Column	Carrier	Adsorbate & % conc	Flowrate (cc/min)
1	Large	He	15% CO ₂	450
2	Large	He	1% CO ₂	300
3	Large	He	1% CO ₂	400
4	Large	He	1% CO ₂	500
5	Large	He	1% CO ₂	600
6	Large	He	1% CO ₂	700
7	Large	He	1% CO ₂	800
8	Large	N ₂	1% CO ₂	400
9	Large	N ₂	1% CO ₂	500
10	Large	N ₂	1% CO ₂	600
11	Large	N ₂	1% CO ₂	650
12	Large	N ₂	1% CO ₂	700
13	Large	N ₂	1% CO ₂	750
14	Large	N ₂	1% CO ₂	800
15	Small	He	1% CO ₂	190
16	Small	He	1% CO ₂	242
17	Small	He	1% CO ₂	294
18	Small	He	1% CO ₂	346
19	Small	He	1% CO ₂	398
20	Small	N ₂	1% CO ₂	350
21	Small	N ₂	1% CO ₂	410
22	Small	N ₂	1% CO ₂	470
23	Small	N ₂	1% CO ₂	530
24	Small	N ₂	1% CO ₂	590
25	Large	He	1% N ₂	25
26	Large	He	1% N ₂	30
27	Large	He	1% N ₂	37

Table 3.2 Experimental Chromatography Runs

Column	Small column		Large column		
Carrier	He	N ₂	He		N ₂
Adsorbate	CO ₂	CO ₂	CO ₂	N ₂	CO ₂
ZLC					
Temperature (K)	303	303			
Dead Volume V _g (ml)	0.14	0.14			
Sample weight (mg)	7.6	7.6			
Density (g/ml)	1.33	1.33			
V _s (ml)	5.7x10 ⁻³	5.7x10 ⁻³			
KV _s + V _g (ml)	0.38	0.32			
l (cm)	0.0083	0.0083			
K	42.1	31.6			
D _e /l ² (1/s)	0.92	0.48			
D _e (cm ² /s)	6.3x10 ⁻⁵	3.3x10 ⁻⁵			
Chromatography					
Temperature (K)	296	296	296	327	296
Slope of μ vs 1/F (ml)	1515	1153	5333	258	4319
Slope of HETP vs F (s/cm ²)	0.124	0.12	0.095	-	0.247
K	59.1	44.4	49.5	0.22	39.7
D _e /l ² (1/s)	0.187	0.281	0.181	-	0.038
D _e (cm ² /s)	1.27x10 ⁻⁵	1.93x10 ⁻⁵	1.51x10 ⁻⁵	-	7.4x10 ⁻⁶

Table 3.3 Summary of parameters derived from Chromatography and ZLC experiments for the larger and smaller monoliths

Chapter 4

An Experimental Study of a Dual Piston Driven PSA Rig

4.1 Introduction

The motivation behind finding effective and economically viable methods of separating and capturing CO₂ from stack gas emissions has never been greater (US DoE, 1999). All current commercial CO₂ separations are performed using an expensive chemical absorption process with a MEA solvent (Herzog, 1999). However there are other alternatives available and of these options this work centres on Pressure Swing Adsorption (PSA). To enhance performance of the technology two improvements can be made. Firstly a dual piston driven configuration can be used which helps reduce compression and expansion costs, and, secondly, structured adsorbent beds can be used to reduce pressure drop. While Chapter 3 details the suitability, manufacture and characterisation of such columns, this chapter, along with chapters 5 and 6, considers the dual piston driven PSA system. Our overall aim is to look at the performance of such a unit for separating CO₂ and N₂ where the adsorbent beds consist of two differently sized activated carbon monoliths. By comparing experimental data, gained from trials undertaken using a test rig, to results obtained from a theoretical model then the system can be fully scrutinised and its economic viability assessed.

In this chapter a literature survey charting the steps leading to the dual piston driven system development is presented. A detailed description of the experimental set up and the modes of operation then follows along with some results that demonstrate the general behaviour of the rig given certain experimental conditions. The observations made during the experimental study are of great importance as they may have an effect on the mathematical modelling work as proves to be the case here.

4.2 Literature review of Pressure Swing Adsorption related technologies

Beginning with the original PSA concept, developed in the 1950s, the various approaches taken to develop and improve the technology, including Rapid PSA and Single Piston Driven PSA, are discussed below. The invention and initial studies of the Dual Piston system are reviewed as are further experimental studies undertaken subsequently. Discussion of the mathematical modelling approaches taken is limited to Chapter 5.

4.2.1 Pressure Swing Adsorption

Pressure Swing Adsorption (PSA) technology is commonly thought to have been introduced by Skarstrom (1958) with a patent by Montgareuil and Domine (1957) appearing in the same year. However some similar processes are outlined in the patents of Hashe and Dargan (1931), Perley (1933) and Finlayson and Sharp (1930) as far back as 1930 although they have largely been unrecognised. The basic two-bed Skarstrom cycle consists of four steps. These are:

- 1) Pressurisation,
- 2) Adsorption,
- 3) Countercurrent blowdown and
- 4) Countercurrent purge.

The sequencing of the steps, shown in fig. 4.1, is operated in such a way as to give a continuous product stream.

In step 1 bed 1 is brought to pressure using feed, while bed 2 is blown down. In step 2 feed at pressure is fed to bed 2 in which the more strongly adsorbed component stays with the adsorbent and the less strongly adsorbed leaves, some as product and some as purge stream for bed 1. Steps 3 and 4 are the same but the beds are interchanged. During the adsorption step a concentration front moves from the feed to product end of bed 2, the velocity of which

is determined by the equilibrium constants. The step is completed when the front breaks through at a certain preallowed limit. Bed 1 is purged simultaneously to flush out the more strongly adsorbed component; the reason being that it ensures the column end where the product leaves is “clean”. At steady state the front is pushed back in the purge and blowdown steps by exactly the same distance as it progressed in the adsorption and pressurisation steps.

Pressure swing adsorption technology has been used commercially from the 1960s onwards, the first three major applications being air separation, air drying and hydrogen purification (Sircar, 1996). Since PSA is capable of producing a high purity product stream, albeit with the penalty of a low recovery, then the latter two processes are especially suited since product purities of greater than 99.9%, as desired, can be easily obtained and both feed streams are inexpensive, meaning that low recovery is not a deciding factor. The largest scale units are those in the petrochemical industry where product flowrates such as 100tonnes/day are common. There is also a market for small-scale units, performing O₂ and N₂ separations to provide, for example, portable oxygen units for asthmatics and aircraft breathing supplies.

Development in the PSA field has focused both on developing new and improved adsorbents with higher capacity and selectivity, and on making improvements in terms of increasing productivity and reducing operating costs. It has been noted (Ruthven et al, 1994) that the energy requirement contributes greatly to costs and the introduction of pressure equalisation steps has gone some way to improving energy efficiency. However, the increased process complexity has meant that capital costs have risen. “Next generation” adsorbents with improved selectivity and capacity have helped to reduce adsorbent inventory, offsetting some of the cost, and incorporating steps at vacuum have removed the need for additional energy recovery steps previously used. The majority of industrial processes use multibed systems since this increases productivity, the number being restricted by the capital costs entailed. However another less commercialised approach to increase productivity has been to use a single bed, operating at reduced cycle times. This has the effect of increasing throughput but

keeping capital costs low. Clearly this technology must rely on a system in which pressure changes can be rapidly effected. “Parametric pumping”, developed by Wilhelm (1966), in which an adsorbent bed is subjected to a cyclic flow while at the same time an intensive variable such as temperature or pressure is periodically changed, is an important development which shows how this can be achieved.

4.2.2 Parametric pumping

Initially Skarstrom’s PSA process was thought of as a parametric pump but, as Ruthven et al (1994) point out this is not so since independent control of pressure and flow is not possible in standard PSA whereas this is key to parametric pumping.

Fig. 4.2 shows the first process considered by Wilhelm (1966), which demonstrates the basic concept of the technology. Flow is cyclically moved through an adsorbent bed using a piston arrangement. Each cycle is composed of two distinct steps. When the fluid flow is upwards the cooler removes heat. This has the effect of causing the sorbate to transfer to the sorbent. When the flow is reversed and the fluid is heated the sorbate desorbs. The cyclic change in temperature induces an overall mass flux, which results in separation at both ends of the adsorbent column. However this simple system was not greatly successful since the separation factors (defined as the ratio of the solute concentrations in the reservoirs) were only of the order of 1.5. Later Sweed and Rigaudeau (1975) were able to optimise the process a little by increasing the volume displacement by around 4 times the column volume which gave separation factors of up to 1000. However in 1968 Wilhelm et al (1968) altered the process further, allowing flow and temperature variations to be imposed independently as shown in fig. 4.3. This gave a great improvement, and separation factors in excess of 100,000 were achieved. To verify the process further experimental and simulated results were matched with a great degree of success.

Pigford et al. (1969) show the simple mathematical concept behind the technique by demonstrating how the concentration front moved over the cycles. Assuming that the wave velocity can be described by:

$$v_w = \left(\frac{\partial z}{\partial t} \right)_w = \frac{v}{1 + \frac{1-\epsilon}{\epsilon} \frac{dq^*}{dc}} \quad (4.1)$$

and that for any isotherm

$$\frac{dq^*}{dc}(cold) > \frac{dq^*}{dc}(hot) \quad (4.2)$$

then $v_w(hot) > v_w(cold)$ and hence the concentration front moves faster when the bed is hot than when it is cold. This gives rise to the behaviour seen in fig. 4.4, where the slope of each line is equal to the wave velocity and the net movement of the more adsorbed component upwards can be observed. As yet, there are no commercial scale applications but the technology has served to inspire others looking into other related and unrelated cyclic processes.

4.2.3 Rapid PSA

In the cyclic adsorption field, a major breakthrough was made Kadlec et al. the early 1970s (Turner and Kadlec, 1971, Kowler and Kadlec, 1972) in pioneering rapid PSA (RPSA). In all PSA systems the cycle time, i.e. the time taken to complete one adsorption and desorption step, determines the productivity of the system; shorter cycle times lead to increased productivity. The main advantage of the RPSA system was that cycle times were of the order 3-10secs (Ruthven et al, 1994), much faster than that possible with a traditional PSA system. The process, shown in fig. 4.5a, utilises a single column packed with small adsorbent particles (100-500μm) and relies on the high pressure drop incurred (1-2atm). Originally it consisted of just two equal steps;

- 1) simultaneous pressurisation and product withdrawal and
- 2) exhaust.

The pressure gradient experienced between the feed and product column end is required both to maintain the purity of the raffinate product and to allow it to be continuously removed, even during regeneration, which occurs during countercurrent depressurisation. The movement of the concentration front through the bed is very similar to that seen in the parametric pump. During the first step the more strongly adsorbed component moves through the column more slowly than the less adsorbed component, which can be removed at the product end as pure product. During the second step this product continues to be removed while the flow is reversed, and at the feed end the more strongly adsorbed component, which is now desorbing, is removed as a waste stream. Again the wave velocity for the less strongly adsorbed species is higher than for the other and hence there is a net forward movement over the cycles. Fig.4.5b shows the typical axial pressure profiles in a two bed system at cyclic steady state. Unfortunately the performance when compared with the energy cost meant that the system was not economic (Alpay et al, 1994). However improvements in the 1980s by Keller et al (Jones, Keller and Wells, 1980; Jones and Keller, 1980; Keller and Jones, 1980), where a delay step prior to blowdown and a shorter pressurisation step was introduced, made the system more attractive. When compared to a traditional PSA system producing O₂ from air the modified system undertaking the same separation had not only the advantages of a short cycle time (~18.5 secs) and a continuous product stream but it also gave a productivity of 2.3 gO₂/gadsorbent, nearly four times greater than that found using traditional PSA for the same product purity.

Subsequent studies, concentrating mainly on air separation, have focused on the timings of the three key steps and the use of additional delay steps as well as feed gas pressure and product delivery rate. A study by Alpay, Kenney and Scott (1994), considering air separation using RPSA, examines the importance of adsorbent particle size. Using the basic two step process experimental work was undertaken using 5A zeolite of 5 different sizes between 150 and 710µm. For any combination of operating conditions experimental observations showed that an optimum particle size could be identified with respect to product (O₂) purity. If, for a

chosen set of conditions, the particle size was increased then the O₂ recovery decreased. Using a theoretical model separation performance was shown to be limited by both ineffective pressure swing and axial dispersion for small particles, and by intraparticle diffusional resistance for large particles. When small particles were used the ineffective pressure swing at the product end of the bed led to inefficient use of the adsorbent. When observing that, in the majority of cases, the smaller particles led to higher product purity then this underutilisation is clearly a problem that must be addressed.

Because of the high energy requirement, created by the large pressure drop incurred, RPSA technology is only economically viable for small to medium scale operations (Ruthven et al, 1994). Commercial units for the small scale production of O₂ (e.g. for medical applications, wastewater treatment) began to appear in the 1980s (Yang, 1987). In terms of the separation under consideration in this present study; the removal of CO₂ from flue gas, clearly a very low added value large scale process, it is obviously not suitable. However, the move to faster cycle times, and increased throughput, was a desirable process feature and something that Keller and his co-workers chose to exploit further in subsequent studies.

4.2.4 The origins of Dual Piston Driven PSA

The idea behind piston driven PSA originated with Eriksson (1979). In his patent Eriksson describes a single piston system, shown and annotated in fig. 4.6, that was used to separate oxygen from air. In this unit feed gas enters the piston chamber (17) and is compressed by the piston. The gas passes through the adsorbent bed (21), where the more strongly adsorbed component (here, nitrogen) adsorbs, and exits (26). On expansion the bed is flushed with the non adsorbing gas and desorption occurs, with the flushed gas leaving via a different port (38). The claim of the patent is that the gas product collected on the compression stroke is purer than that previously possible because part of the cycle operates at partial vacuum. This is not however supported with any performance information.

The dual piston-driven PSA (DP-D PSA) concept was introduced through a patent by Keller and Kuo (1982), in which they christen the system, shown in fig. 4.7, “The Molecular Gate”. The patent demonstrates how rapid cycling could be achieved by employing coupled pistons, of unequal volume (i.e. different stroke length), at each end of a single adsorption column to affect pressure changes. Clearly such a system could lead to significant improvements in power consumption, expansion in one piston helping to drive compression in the other, and separation capabilities, the extent of which could be linked to various critical parameters. These are identified as cycle speed, piston stroke lengths and phase angle, the latter being the difference between the piston positions within their casings.

One separation studied by Keller and Kuo (1982) was air separation employing a 13X molecular sieve as the adsorbent bed. The feed was injected half way through the bed and control valves (labelled “V” in fig. 4.7) were used to control the product flowrates at each piston. Key system parameters are shown in table 1.1. Their intention was to consider how maximum productivity could be achieved and they found that a smaller piston lead of 45deg (i.e. 1/8 cycle ahead of the larger piston) and a stroke length ratio of 3, roughly equal to the ratio of the equilibrium constants of nitrogen and oxygen, gave the best results. It was also discovered that when feed is introduced midway through the column, as it was in their studies, then two pure products from the stripping and rectifying sections could be recovered. As an example, for one run, in which an equimolar feed of H₂ and CH₄ were introduced to a bed of bead activated carbon, the product streams contained 100% CH₄ and 99% H₂. This process therefore, when compared to conventional PSA, has the advantage of energy savings created by the coupled pistons, improved productivity and two pure product streams. However when considering large scale applications the size of the pistons required to contain all the desorbed gas may become a barrier and commercial applications may be limited to small-medium scale processes. Additionally it is usual practice to use an adsorbent bed packed with small particles, in the Keller and Kuo patent the particles were 40-80mesh, however this can lead to substantial pressure drops which, unlike the RPSA process, are a

hindrance and require extra power to overcome. Without development in this area then column design could be another barrier to scale up.

4.2.5 More recent experimental Piston Driven PSA studies

Since the initial work by Keller and Kuo (1982) there has been some interest in the DP-D PSA concept, and subsequent studies have been focused on both experimental and mathematical modelling of the system. Interest in exploring the numerous key parameters of the system has been pursued by undertaking representative experimental studies using a test rig followed by simulations, verified using experimental observations, that allow full exploitation of the system.

One of the first of these studies was undertaken by Suzuki, Sakoda, Suzuki and Izumi (1997), who considered separation of CO₂ from flue gas assuming a single piston driven PSA system. Much of the study focused on the adsorbent bed itself. To investigate the effect of moisture on the bed they used a hydrophobic and hydrophilic adsorbent. Since the former was unaffected by moisture whereas the latter led to poor separation performance they were able to recommend that hydrophobic adsorbent should be used. They also demonstrated using calculations that the mass transfer for CO₂ was fast and not all the bed was being utilised. Finally they reported a phase lag and amplitude difference between the ends of the bed, clearly created by the frictional pressure drop due to the small adsorbent particles. To tackle the problems of pressure drop and under utilisation of the bed partly caused by poor flow distribution, use of a structured adsorbent in the shape of a honeycomb was suggested.

In the study of Farooq et al (1998) a structured adsorbent column, the parallel passage contactor, discussed in Chapter 3 section 3.2.1.2 and shown diagrammatically in fig. 3.2 , was used within a dual piston driven system. In this case the separation was again CO₂-N₂ and the experimental study was undertaken using the rig of the design shown in fig 4.7. Runs were carried out initially at total reflux, allowing no feed and product into or out of the system, and

using an inert system. Pressure profiles obtained from these runs showed how increased asymmetry developed as cycle speeds became higher and was attributed to rapid compression and expansion and frictional heat effects due to fast piston movement. Profiles for a number of phase angle differences for both the inert and adsorbing cases showed that, as expected, the maximum pressure difference over a cycle was observed when the starting system volume was at a maximum. It was clear that, when adsorbing, the pressure difference observed was smaller than for the inert case. This can be explained by recognising that some of the gas is adsorbed onto the adsorbent and therefore there is less gas volume in the bulk. A limited parametric study considering the effect of cycle time on adsorbing pressure profiles shows that as the speed exceeds 20rpm then a phase lag begins to develop. Therefore, as concluded, mass transfer kinetics clearly become more important as cycle time increases. Despite these important observations regarding the pressure profiles there is no discussion of the effectiveness of the separation and runs involving feed and product streams are only discussed briefly with reference to the mathematical modelling.

In a further study by Arvind et al (2002) the same experimental rig was used but in this case a packed adsorbent column of 13X zeolite was used and an air separation considered. The experimental study consisted of four types of run; empty column runs, packed column non adsorbing runs, air separation at total reflux and air separation with feed and product streams. From the empty column runs the pressure profiles recorded clearly showed phase and amplitude differences from the two sides of the system at a cycling frequency above 21rpm. This was attributed to resistance in the pipework of the unit. Non adsorbing runs using a packed columns were able to show that at 10rpm there was no pressure drop incurred across the column, however, when total reflux adsorbing runs were carried out a pressure drop was encountered. This was explained by reasoning that when adsorbing there was increased flow in the connecting tubes in which the pressure was measured and hence phase and amplitude differences developed. A parametric study looking at particle size, phase angle and stroke length was carried out and showed that:

- A ratio between the stroke lengths close to that between the equilibrium coefficients of the components gave the best separation performance.
- To obtain maximum separation the smaller piston should lag the larger by 135deg. This will not necessarily lead to maximum productivity.
- Reducing adsorbent particle size enhances the separation but leads to increased pressure drop.

From the feed and product experiments results show that faster cycling did increase productivity but resulted in a lower purity product. Unlike the study of Keller and Kuo (1982) the unit was only able to produce one pure product but this was because the feed was placed at a column end rather than in the middle therefore one product was always being contaminated with feed. Even so the best system set up was able to give a product purity of 90% and a productivity of 2.0gO₂/gday, which is comparable to that found from RPSA, and presumably for a lower energy cost

Experimental work is clearly highly important for highlighting various system idiosyncrasies that mathematical modelling alone would not reflect.

4.3 The Description of the Experimental Rig

The emphasis, in this study, is on finding the optimal system set up to get the best possible separation of CO₂ from N₂ for a given mixture. Modelling of the system has been undertaken (Chapter 5) but to get an idea of the real behaviour experimentation is invaluable. One of the features of the dual piston system is the numerous physical parameters that can be varied to change the performance of the rig. The focus of the experimental work has been to look at some of the key variables to try and determine how performance is affected. This section describes the experimental set up and procedures used.

4.3.1 The rig

The Dual Piston PSA Rig was designed at Highquest Engineering Co. and constructed at J.King Engineering in Vancouver. The system uses out of phase, coupled pistons at each end of a single column to affect pressure changes.

Fig. 4.7 shows the main parts of the system. The Eurodrive Varimot motor (1) has a variable speed control and is connected to a reduction gear box (3) by means of a V-belt (2). The motor drives the two pistons. Two flywheels (4) mounted on each side of the gear box are used to adjust the phase angle between the two pistons. The stroke length of each piston can be adjusted using a pillow block arrangement (see figs. 4.8 & 4.9) that effectively changes the length of the connecting arms (5 and 5') between the flywheels and the piston rods. The piston rods (6 and 6') connect to the piston heads (7 and 7'), housed in stainless steel casings. As these move the gas to be separated is moved through the adsorbent bed (8). The feed stream (9) enters through a flowmeter (10) and product is withdrawn from both ends, again metered using flowmeters (11 and 11').

In addition the instrumentation used to control and monitor performance of the rig is shown in fig. 4.10. Cylinders of N₂ and CO₂ were connected to the feed tank metered by flowmeters (F4) & (F2). The feed solenoid (SF) was controlled using the feed-product relay system. When the valve opened, gas entered piston 1 passing through a non-return valve. Non return valves were also employed on the product withdrawal lines to prevent back flow. The TCD sample loop was used to sample at points TR1 and P1. Pressure transducers and thermocouples were present on each piston to monitor pressure and temperature variations.

4.3.2 The columns

Two columns, both of which were characterised in Chapter 3, sections 3.3 and 3.4, were used during the experiments. The first column, named the large column and shown diagrammatically in Chapter 3 figs. 3.4 and 3.5, was composed of an assembly of five

smaller columns joined together with pipework. Each section contained an activated carbon monolith of 10cm height and 2.9cm diameter. The dimensions of the column can be seen in Chapter 3 table 3.1. The second column, shown in Chapter 3, fig. 3.6, consisted of smaller carbon monoliths of 1cm height and 1.56cm diameter stacked together in an aluminium casing of 45cm long and 3cm outer diameter. This column, named the small column, was always placed in an upright position within the rig.

4.3.3 The pistons

In order to act as both lubricant and sealant silicone grease was applied to the sides of piston heads. This was done at regular intervals and frequent leak checks were undertaken to ensure the seal was complete.

Because of the design of the pistons there was some dead volume created when the pistons were fully closed. Despite efforts to reduce the piping to the least necessary, dead volume, due to piping, was also experienced. To assess the total dead volume in the pistons and piping a simple total reflux run was undertaken with no column present. Raising the pressure to 10psig using helium and then executing some cycles at a known cycle time gave some experimental pressure profiles. Calculating the difference between these and calculated profiles, found using the swept volumes of the pistons, led to finding the dead volume.

4.3.4 Phase angle adjustments

In order to set both the starting volume of the system and the volume variations thereafter the starting position of each piston in its' casing must be set. This was achieved by adjusting the relative phase angles. For each piston a connecting arm runs from the piston to a hub on the side of the reduction gearbox. Each hub has 8 points 45degrees apart to which the arm can be connected. This is demonstrated clearly in fig. 4.11. To set the starting position the hub was positioned such that axis 1 was perpendicular to the ground and the rod was fixed to the appropriate position.

4.3.5 Stroke length arrangement

The effect of varying the piston stroke lengths is to change the ratio of volume variation within the system. Four different lengths were available on the rig (4.34cm, 6.7cm, 10.2cm 15.24cm), using a pillow block arrangement as shown in fig. 4.8. Each of the connecting arms passed from their respective hubs on the side of the gearbox, where they were fixed, through the pillow block to the piston rod, where the other end was fixed. This resulted in the pillow blocks acting as pivots thereby giving rise to shorter stroke lengths the closer they were placed to the pistons.

4.3.6 Feed-product relay system

To introduce feed and withdraw product a system was devised consisting of a switch, relay circuit and solenoid valve. From fig. 4.11 a tab can be seen mounted on each of the flywheels. Each tab is moveable and could be placed at a variety of positions around the flywheels. Spring activated switches connected to rollers which contacted with the wheels were used to activate the solenoid valves. When the roller passed over the tab the relay caused the valve to open. The presence of two tabs was to allow feed and product control from either piston. The software used for control allowed the timing of the valves to be controlled automatically.

4.3.7 TCD sampling loop

There were several sampling techniques available to analysis for concentration. In a previous study (Arvind et al, 2002) samples were taken using syringes inserted via injection ports and then analysed using a thermoconductivity detector (TCD) within a gas chromatograph. In this study we have chosen to use a TCD directly. The TCD consists of two hot wire anemometers and a Wheatstone bridge. When the gas passing through the two sides of the TCD over the hot wires is steady and balanced then zero voltage is returned to the null detector. When the concentration on one side differs the change in thermal conductivity of the gas causes the wire

to cool at a different rate and hence the voltage returned is no longer zero. Obviously differing flowrates on either side of the TCD would create a similar effect.

A variety of different sampling loop structures were trialled before the final approach was decided upon. Initially it was hoped that the TCD could be used to give “on-line” measurements. However the pressure variations experienced by the system meant that delivering a steady and representative sample flow to the sample side of the unit was not possible. Therefore an off line method was developed.

4.3.7.1 TCD calibration

Prior to use accurate calibration of the TCD was required. This was done with care as the chosen set up was not conventional for a TCD. Initially a flow of nitrogen of 50cc/min was passed to both sides of the unit and a baseline value established. Then a small flow of 10cc/min of nitrogen was introduced to the sample side. This created an imbalance, causing the differential voltage to be recorded. The sample stream was then stopped and the baseline value returned to. When steady the sample stream, in this case containing a known CO₂ concentration was introduced. The voltage, adjusted for the imbalance recorded previously, therefore corresponded to the concentration introduced. This was repeated with several concentrations until a calibration curve could be constructed. Again care was required as over an entire range of concentrations, TCDs are notoriously non linear, but, for our range of interest, the calibration curve tended towards linearity. The curve obtained is shown in fig.

4.12.

4.3.7.2 Sampling technique

When sampling from the system the TCD loop relied on the pressure and volume of the gas immediately upstream. A pressure greater than atmospheric was required to drive the gas through the sample flowmeter and there had to be sufficient volume upstream to allow the TCD to become steady. The response time was around 5 minutes. The loop could only be

operated when the pistons were not moving and hence sampling was carried out at the end of each run when the required number of cycles were complete. The operating procedure of section 4.4 shows more clearly when and how sampling took place.

4.3.8 Data acquisition

To control and monitor the PSA rig VISSIM software was used. This is a Windows based simulation package which was run on an Intel Pentium II 64 RAM 150MHz computer. The various monitoring and controlling devices are listed in table 4.2.

4.4 Experimental procedure

There were two main types of experiment performed using the experimental design detailed in fig. 4.10. Firstly total reflux runs were used to see how the columns and pistons behaved as an isolated system both when in non adsorbing and adsorbing mode. Secondly feed-product adsorbing runs were undertaken. In this case the solenoid valve openings, allowing flow in and out, were set automatically using the VISSIM control panel. In all cases all the physical parameters of the rig were first set:

Phase angle: In all cases piston 1 acted as the reference piston and the desired phase angle difference was obtained by altering the connection of the piston arm 2 to the hub as described in section 4.3.4.

Stroke length : Again since it is the stroke length ratio that is of importance then piston 2 remains in position whereas the pillow block arrangement is altered for piston 1, as described in section 4.3.5, to give the correct stroke length ratio.

Cycle speed: Changes in cycle speed were made simply using minor adjustments to the varispeed motor. To ensure an accurate cycle time the motor was first run with the system empty and a stopwatch used to visually check the cycle time.

Choice of column: Runs used the large, small or no column.

For the base case the phase angle difference was $\pi/2$, S1 was set at 15.24cm and S2 set at 4.34cm and the cycle speed was set at 10rpm.

4.4.1 Non adsorbing total reflux runs

In these runs helium gas was used to study the system both with and without the adsorption columns. Since helium has an extremely low affinity for activated carbon then, when the columns were present, effectively the system was operating with the absence of adsorption. At the start of each run the key parameters were set as described and then the helium was fed, ensuring that product (SP1 and SP2 in fig. 4.10) and sampling (V5) valves were closed. Once the desired system pressure was attained, as recorded by the pressure sensors, the feed valve (SF) was closed. Before cycling began the pressure was observed for up to 20 minutes to confirm no leakage in the system. Once confirmed the motor was begun as was the collection of pressure and temperature data. Cycling was stopped when the predecided number of cycles was complete.

4.4.2 Adsorbing total reflux runs

After setting the key parameters the next step, when undertaking adsorbing runs, was to purge the entire rig and regenerate the adsorbent from the previous run. This was achieved by passing nitrogen at high flowrate through the system for around 2 hours. Once purged with nitrogen, the 10%CO₂, 90%N₂ mixture, of a flowrate set using the inlet flowmeters (F4 & F2), was passed through the section between the product solenoid valves, the “TR system” and allowed to leave via the sampling loop. The gas mixture was allowed to pass through the TR section using a little back pressure until it was reasonable to assume that the purging nitrogen gas had been completely displaced. This lasted for around 20-30minutes as dictated by the gas flowrate and system volume. The system was then brought up to pressure and allowed to come to equilibrium. Initial tests showed that this took around 1 hour. After this time cycling could begin. For the total reflux runs this simply involved starting the motor which drives the

pistons. When the required number of runs was reached then the motor was stopped. Simultaneously the two sides of the system were isolated using the valve (V4) immediately downstream from the column. Since temperature has an effect on the TCD, sampling was begun as described only when temperature had returned to the value at the start of the run thus ensuring the temperature on both sides of the TCD was the same.

4.4.3 Adsorbing feed-product runs

The initial rig set up for these runs included not only setting the phase angle, stroke length, cycle speed and making a column choice but also required valve decisions. Firstly the time in the cycle where each valve was to open was adjusted using the tab system (as described in section 4.3.6). The length of time each remained open for was then set using the computer software. As with the total reflux runs purging and regeneration with nitrogen could then be started, in this case this involved the entire system including the product tanks and took 2-3 hours. Once complete the product valves (SP1 & SP2) were closed and the mixture of 10%CO₂ and 90%N₂ introduced to flood the TR system and then bring it to pressure as in the total reflux case. Once equilibrium was attained cycling could begin while simultaneously the feed and product flowmeters were switched to their setpoints. When the run was complete isolation of side 1 of the TR system was again achieved by closing valve V4 while at the same time all the solenoid valves were closed. The sampling loop could then be used to analyse first the isolated section and then product 1 gas. Making a small adjustment to the system meant that the contents of the feed tank could also be analysed.

The experimental procedures used are summarised in table 4.3 and a list of all the experiments undertaken are shown in table 4.4.

4.5 Experimental Results

The purpose of all the experiments carried out is to provide information about the rig that can be used to construct and verify the mathematical model, indicating what assumptions may sensibly be made and how the potential differences between the results obtained may be explained.

4.5.1 Results for total reflux non adsorbing helium runs

The purpose of these experiments is to obtain the pressure and temperature profiles generated by the system in the absence of adsorption.

4.5.1.1 *Empty system runs*

Considering first the system when no column is present fig 4.13 shows the dimensionless pressure profiles obtained at 10rpm and 20rpm. It can clearly be seen that there is no lag between the pressures recorded at each piston. This would be as hoped since, by design, there is little resistance created by pipework and fittings. Since all peaks are identical it is clear that there are no leaks in the system. Fig. 4.14 shows the corresponding temperature profiles obtained for 10 and 20rpm. An interesting point to notice is that the maximum temperature recorded at piston 1 is higher than that at piston 2 for both cycle speeds. This can be explained by noting that piston 1 has the longer stroke and hence the higher compression ratio encountered leads to a greater temperature rise. The temperature profile at piston 1 is also interesting. While at piston 2 the profile over 1 cycle is fairly symmetrical this is not true for piston 1. Since the shape is not reflected in the pressure profiles the asymmetry is not due to the uneven movement of the piston but more likely to be due to the response of the temperature sensor. As with the pressure profiles the temperature rises are slightly higher for the faster cycle time which suggests a small heat effect due to frictional resistance in the pistons. This is further supported by fig.4.15, which shows the average temperatures recorded for 10 and 20rpm over 160 cycles. Clearly as cycling begins there is a large temperature rise

due to compression and expansion. The subsequent small rise observed over the next 100 cycles can be attributed to the friction created by the piston movements. The figure shows how a steady temperature is reached after about 140 cycles at 20rpm.

When cycling at slower speed (10rpm), with little temperature variation encountered, the dead volume of the system can be calculated. In a non adsorbing total reflux run the system pressure can be found analytically using:

$$\frac{P}{P_0} = \frac{V_{P1} + V_{P2} + V_D}{V_{P1}|_0 + V_{P2}|_0 + V_D}, \quad (4.3)$$

derived simply from the ideal gas law. The experimental curves can then be matched to those calculated by adjusting the dead volume accordingly. From experiments a value of around 120cm³ was found.

4.5.1.2 Helium runs including columns

The purpose of these runs is to look at the effect including a column in the system has on temperature and pressure profiles. Fig. 4.16 shows the dimensionless pressure profiles when the large and small columns were placed in the set up. Clearly whichever column was used the overall volume was larger than for the “empty” system so the difference between the maximum and minimum pressures are smaller. The temperature and pressure profiles, assuming the ideal gas law, should be directly proportional yet comparing fig.4.17, showing the temperature profiles obtained for the two columns at 10rpm, to fig. 4.14 then this is not the case. Therefore it is possible to surmise that the columns attenuate the temperature. The porous carbon acts as a heat sink removing some of the heat produced by the piston movements. Again, as in the empty column, the shape of the temperature profiles are of interest. In this case the asymmetry is observed in piston 2 whereas the same shape was observed previously for piston 1. For these experiments the two temperature probes were

switched and the observed behaviour therefore supports the suggestion that the behaviour is due to the response of one of the probes.

Fig. 4.16 also demonstrates how the different columns affect the pressure variations in the system. When the larger column is used there is a noticeable lag between the two sides of the system. Since this is not observed when the smaller column or no column is present then this can be attributed to the small piping sections used to join the five individual columns in the large column assembly. The effect is to create a pressure drop across the column as a whole, a pressure drop not associated with the monolithic adsorbent columns but the chosen assembly. This is an important observation since there are clearly implications for the large column mathematical model where these pressure drops must be included.

4.5.2 Results for total reflux adsorbing runs

Although total reflux runs have no practical use they can be used to look at a variety of operating parameters prior to feed and product runs being carried out.

4.5.2.1 Temperature, pressure and concentration profiles

Comparing the helium and adsorbing runs shows the effect adsorption has on the system. Figs. 4.18 & 4.19 show the pressure and temperature profiles for the adsorbing runs for both columns at 10rpm. As expected when adsorption is taking place the peaks of the pressure profiles are smaller than for the helium runs; the volume of gas present is less since some of the gas is being adsorbed.

The lag and amplitude differences are seen for the large column as before, again, as shown in fig. 4.20 where the dimensionless pressure profiles at 10 and 20rpm are given, the effect is worse as the cycle speed increases. However the difference is similar to that found when analysing the helium runs and therefore this supports the explanation that the effect is caused by piping restrictions.

The temperature profiles of fig. 4.19 show that the rise observed at 10rpm is slightly higher for the large column than that seen when there was no adsorption. This small difference can be attributed to the temperature rise due to the heat of adsorption. However the cyclic temperature changes seen are clearly still dominated by the compression/expansion and frictional effects as in the non adsorbing case. The assymmetry seen at piston 2 is the same as that seen for the non adsorbing case.

Total reflux runs were undertaken with both the large and small columns for a variety of cycle times and over a variety of time periods. By sampling the concentration at piston 1, the larger stroke length piston, when the run was completed concentration profiles could be built up until steady state was reached. The profiles obtained are shown in fig 4.21. The column characterisation experiments of Chapter 3 suggested that with comparative equilibrium constants for CO₂ and N₂ but with a smaller diffusional time constant using the column with the smaller passages and thinner walls would lead to better separation. This assumption is shown to be true in fig. 4.21 where the gas at the N₂ rich piston (piston 1) is shown contain the least concentration of CO₂ at steady state when the smaller column was used. The figure also shows that, in general, steady state is reached more quickly (after around 200 cycles) when the smaller column is used. For both columns at 20rpm the separation is markedly worse than at 10rpm, however there is little difference between the results obtained at 5 and 10rpm. Therefore this would suggest that the optimum cycle time is located in this region. One would have hoped that this optimum would have been somewhat higher, allowing cycle times of a few seconds but the adsorbent is less effective as might have been expected due to the large amount of binder and supporting material (60%) mixed with the activated carbon (40%). “Purer” adsorbent material would lead to better separation performance however this would be at the cost of poorer mechanical strength. Since mechanical strength is more important for some applications than for others (e.g. particles subject to high flows which cause high attrition rates), then the compromise between the two properties would obviously

be decided based on the technology choice. When using a fixed, structured adsorbent bed mechanical strength is of less importance and suggests that maybe less binder may be used.

4.5.2.2 *The effect of parametric variation*

While considering total reflux adsorbing runs key system parameters were varied. These included the stroke length ratio, the phase angle and the effect of using ice. Fig. 4.22, showing the variation in steady state mole % of CO₂ at piston 1 with phase angle difference, demonstrates two of these effects. Changing the phase angle between the two pistons clearly has an effect on the steady state concentration and the profiles obtained show that both with and without an ice bath an optimum phase angle difference exists (around $\phi_1 - \phi_2$ 90 deg) at which the separation is greatest. When using an ice bath the results are similar to those obtained when it is not employed but the separation is greatly improved. The ice bath has the effect of increasing the equilibrium constants therefore this is as would be predicted. Fig. 4.23 shows the consequence of changing the stroke length ratio on the mole % of CO₂ at piston 1. As expected the best separation is observed when the stroke length ratio ,S1/S2, is highest. It has been suggested (Keller and Kuo, 1982; Arvind et al, 2002) that the optimum ratio is that nearest to the ratio between the equilibrium constants of the two gases present. Since the equilibrium constant for N₂ (~1.3 for the large column) is much smaller than that for CO₂ (~49.5 for the small column) then the highest S1/S2 ratio would be best for the separation.

4.5.3 Feed-product runs

In the case of the feed-product runs the setup, which included the small column only, now incorporated continuous feed and product flows to and from the tanks, metered by feed and product flowmeters. The flows to the product tanks and from the feed tanks however were discontinuous. This made the overall system pressure hard to balance. Therefore care had to be taken to ensure that this was achieved as well as bringing the system to cyclic steady state.

In addition to the parameters identified in the total reflux experiments additional parameters exist for these experiments namely:

- The point in the cycle at which each solenoid valve opens
- The length of time the valve is open for

The variation for the first of these parameters was partially set by the dynamics of the system. Clearly since the CO₂ adsorbs more strongly as the pressure increases then the N₂ rich stream must be removed as the pressure reaches its maximum. Furthermore the feed must obviously be introduced as compression is occurring in order that feed CO₂ is adsorbed. The CO₂ rich stream must be removed as expansion is occurring and the CO₂ desorbing. Therefore the feed valve must be open between 0-0.5 t_{cyc}, where t_{cyc} is the length of one cycle, the product 1 valve (N₂ rich stream) must open at 0.5t_{cyc} and the product 2 valve (CO₂ rich stream) must open between 0.5t_{cyc}-t_{cyc}.

Fig. 4.24 shows a sample dimensionless pressure profile for a feed-product adsorbing run from start up. In this case the feed, product 1 and product 2 valves open at 0.25t_{cyc}, 0.5t_{cyc} and 0.75t_{cyc} respectively, each for 0.05 secs. The feed flowrate is 120cc/min and the product 1 and 2 flowrates were 100cc/min and 20cc/min respectively. The moments in the cycle where the feed and product valves open can clearly be seen and the system adjustment to reach steady state is evident. In this case careful selection of feed and product flowrates and valve timings led to a stable cyclic steady state behaviour whereas when the selections are made incorrectly fig. 4.25 depicts the effect on the pressure profiles. The profile is erratic throughout, the pressure drop during start up is drastic and steady state is never achieved.

As previously separation performance was again measured using the sampling loop, but in this case, the concentration of CO₂ in the TR section and in two of the buffer tanks; feed and product 1 was established. This was done to look at how the entire system adjusts to cyclic steady state. Results confirmed that the concentration in the feed tank remained steady

throughout the run at around 10-10.5%CO₂. Fig. 4.26 shows the concentration profiles for CO₂ found in the TR section and in product tank 1. While the TR profile reflects a gradual approach to steady state the profile obtained for the product tank reflects the fact that the tank initially contains only N₂. The concentration in the tank only begins to approach the steady state concentration observed in the TR section once the entire tank is purged of N₂ and filled with product produced at steady state. Calculating the volume of the product tanks to be around 3500cm³ then at 350 cycles and at a cycle speed 6 secs one entire tank volume has passed through the product 1 flowmeter. By 1050 cycles where fig. 4.26 shows that the concentrations are beginning to agree more closely 3 tank volumes have been removed as product and most of the original N₂ has been removed. By 3000 cycles the two measured concentrations are in good agreement. As expected when no longer operating at total reflux the separation performance is not as good. In addition the feed is fed at end 1 of the column which leads to contamination of the product stream. The ideal parameters found from experiment for the feed and product experiments are given in full in table 4.5.

4.6 Concluding Remarks

In this chapter a detailed description of the test rig set up, its' operation and the experimental results obtained has been discussed. Within the rig two differently size activated carbon monoliths have been trialled to assess their performance capabilities. When undertaking the simplest experimental trial, where helium, a non adsorbing case, is used to pressurise the system so that its' behaviour can be observed, it was revealed that the larger column suffered from a pressure drop. This was attributed to the piping, which joined each of the monolithic section together. This is of consequence for the modelling approach.

Separation performance was first analysed using total reflux runs, where no feed and product were allowed into or out of the rig, for both columns, and it was found that the smaller column gave better performance. A parametric study whereby cycle time, phase angle

difference, stroke length and column temperature was performed. The results, shown in table 3.3, demonstrated that an ideal set up existed for the separation. To find an optimum set up when feed and product streams were allowed to enter involved establishing the point in the cycle when each solenoid values controlling the flows were allowed to enter and for how long. Again optimal conditions were established and are presented in table 3.3 Temperature profiles obtained over all runs showed that temperature rise did occur over the cycling period, due mainly to rapid compression and friction. The average rise, however, for the cycle speeds analysed was small.

The observations from the experimental study can be carried forward to the mathematical modelling, where the aim is to achieve a match between the experimental and simulated results thus verifying the model, so that the system can be further explored without further experimental work.

Chapter 4: Figures

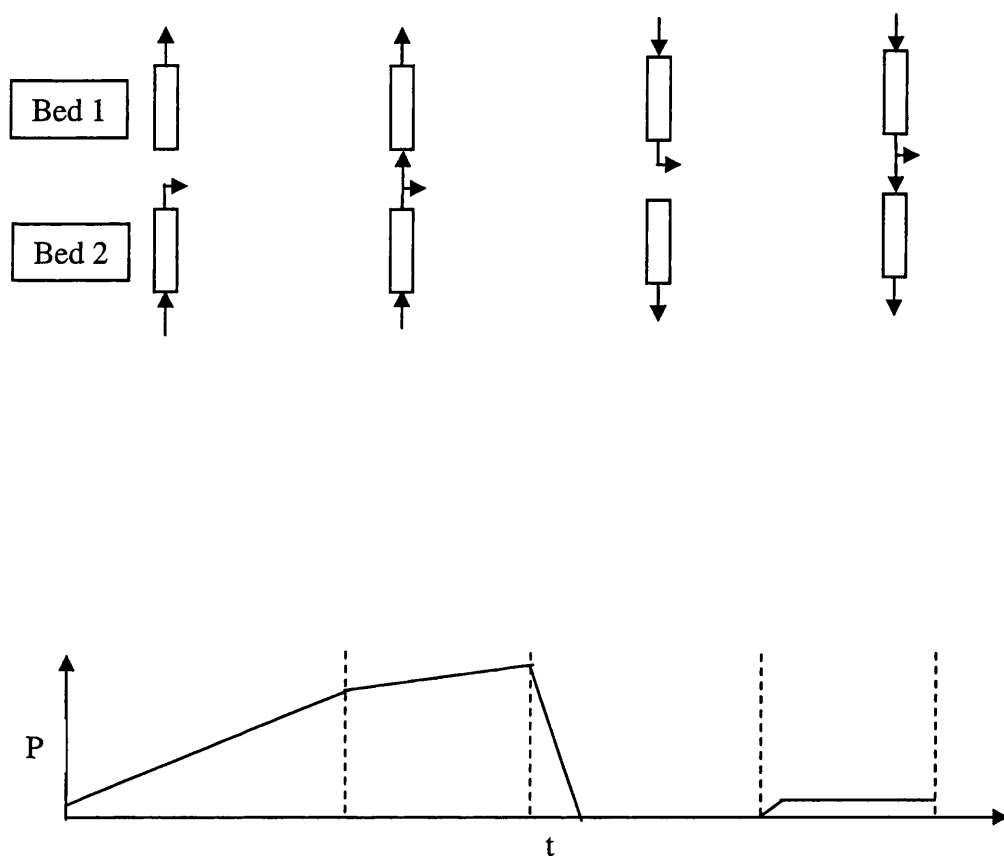


Fig.4.1 Steps of a typical Skarstrom cycle (Ruthven et al, 1994)

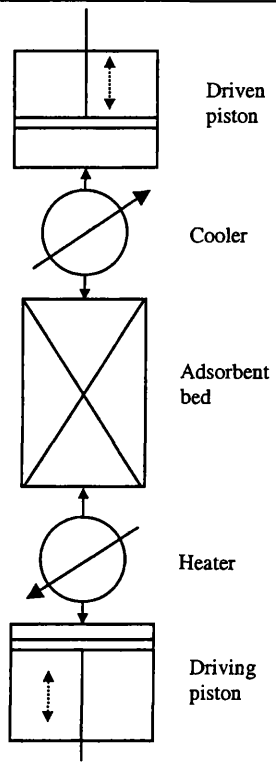


Fig.4.2 Batch-recuperative thermal mode of parametric pumping (reproduced from Sweed, 1988)

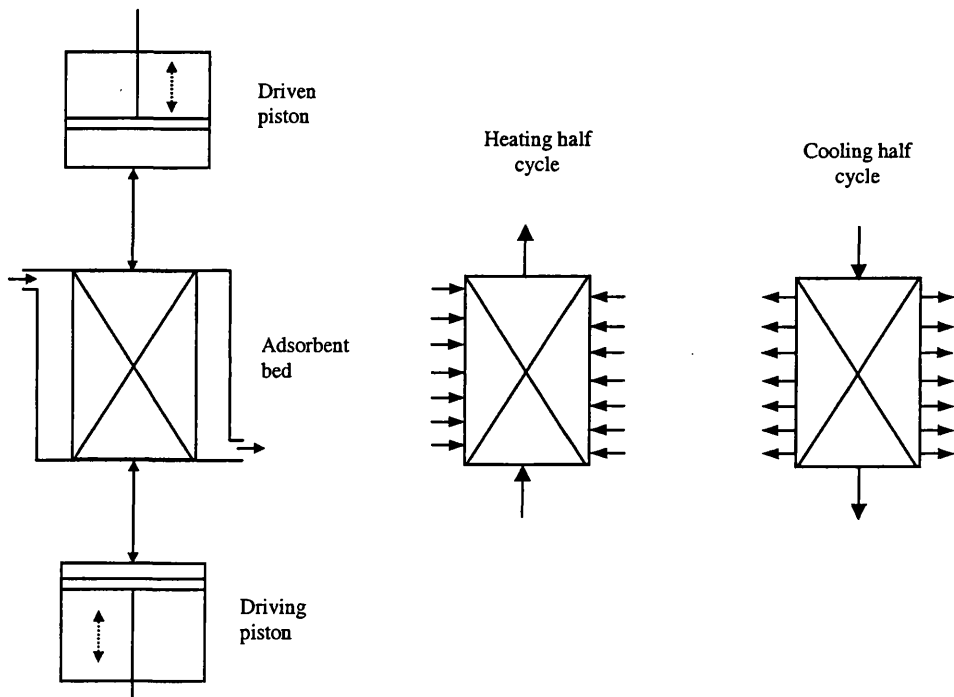


Fig.4.3 Direct mode of parametric pumping (reproduced from Sweed, 1988)

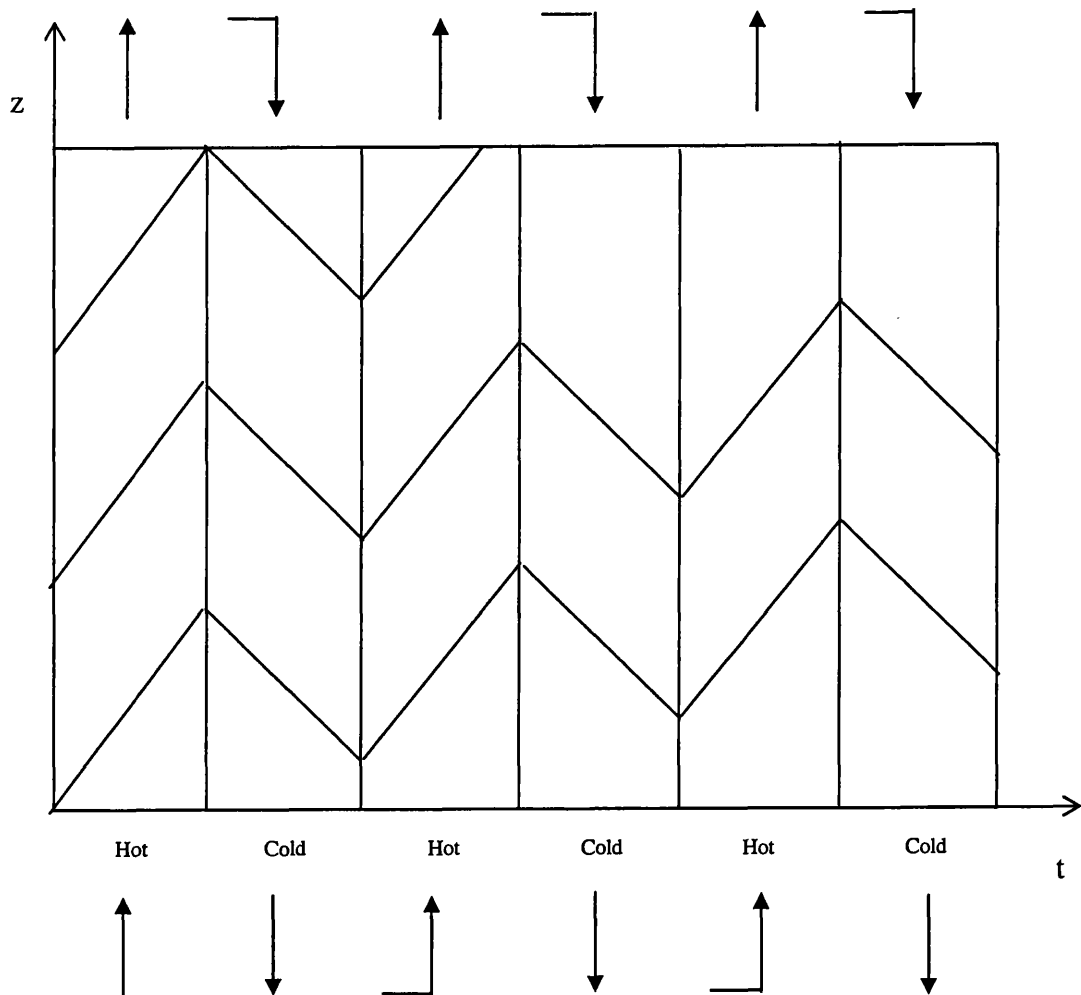


Fig.4.4 Movement of a chosen variable in a batch mode parametric pump, where upflow and heating are in phase (Pigford et al, 1969)

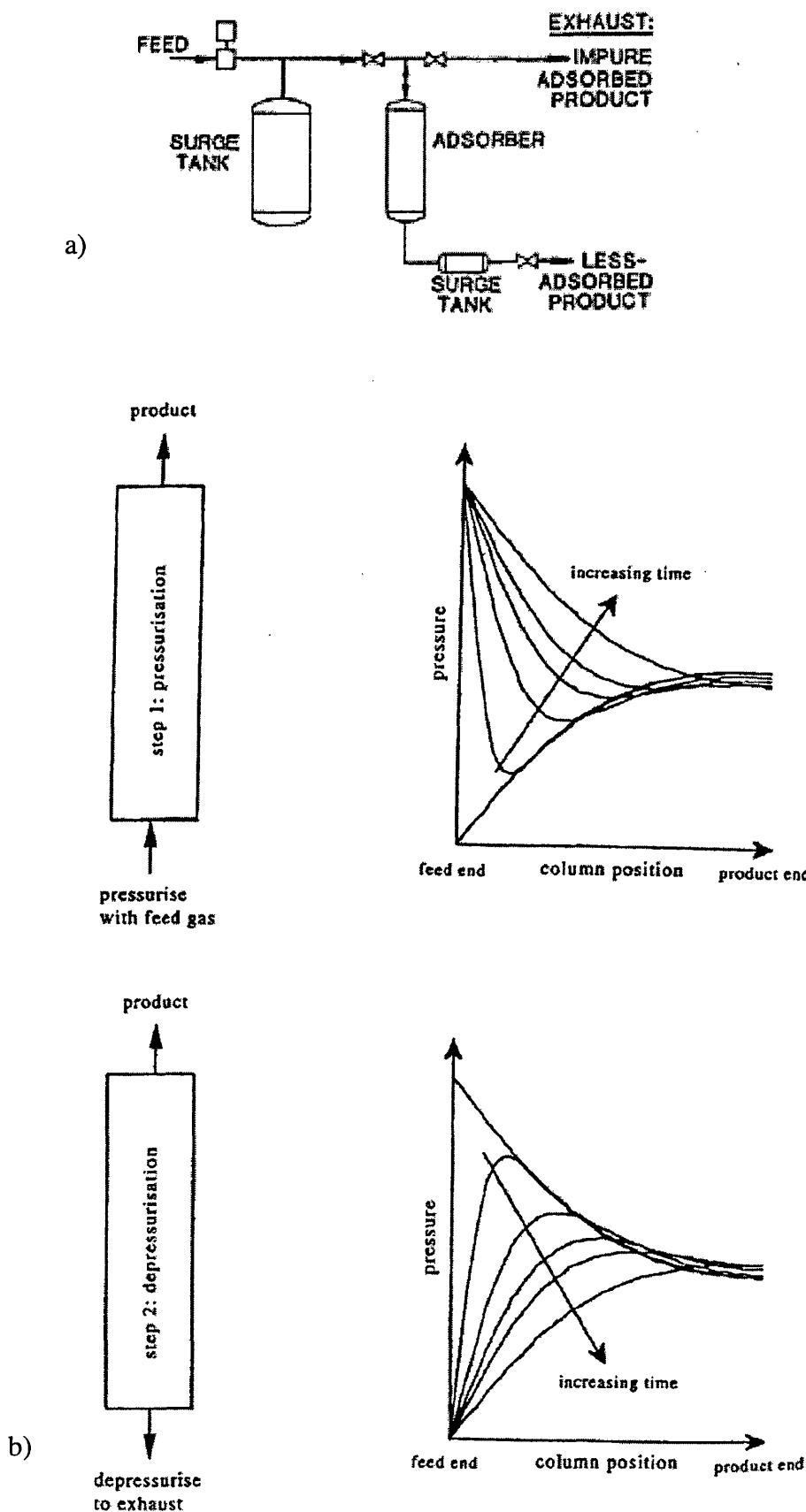


Fig.4.5 Rapid RPSA a) One-bed “PSA-parametric pumping” system (Keller, 1983)
 b) Typical axial pressure profiles at cyclic steady state during steps 1 and 2 (Alpay et al, 1994)

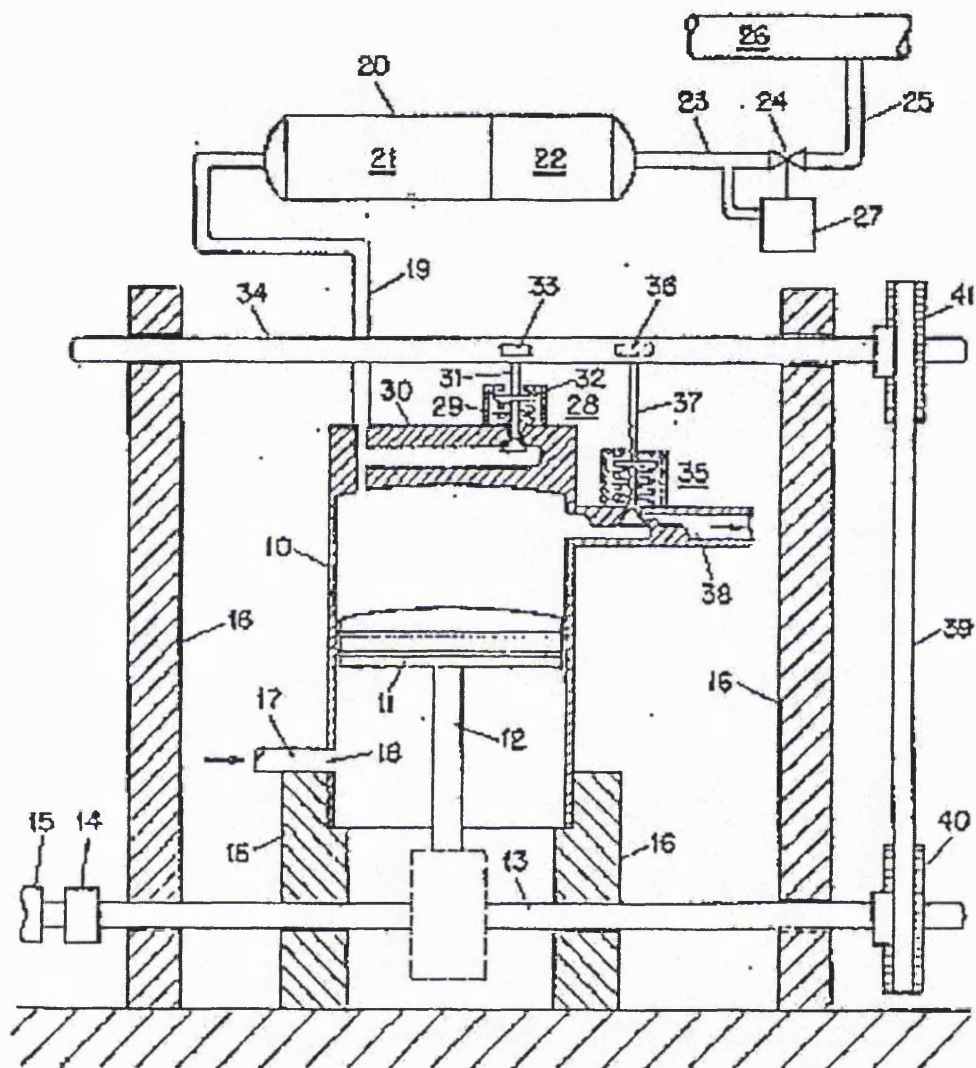


Fig.4.6 Single piston PSA apparatus of Ericksson (1979)

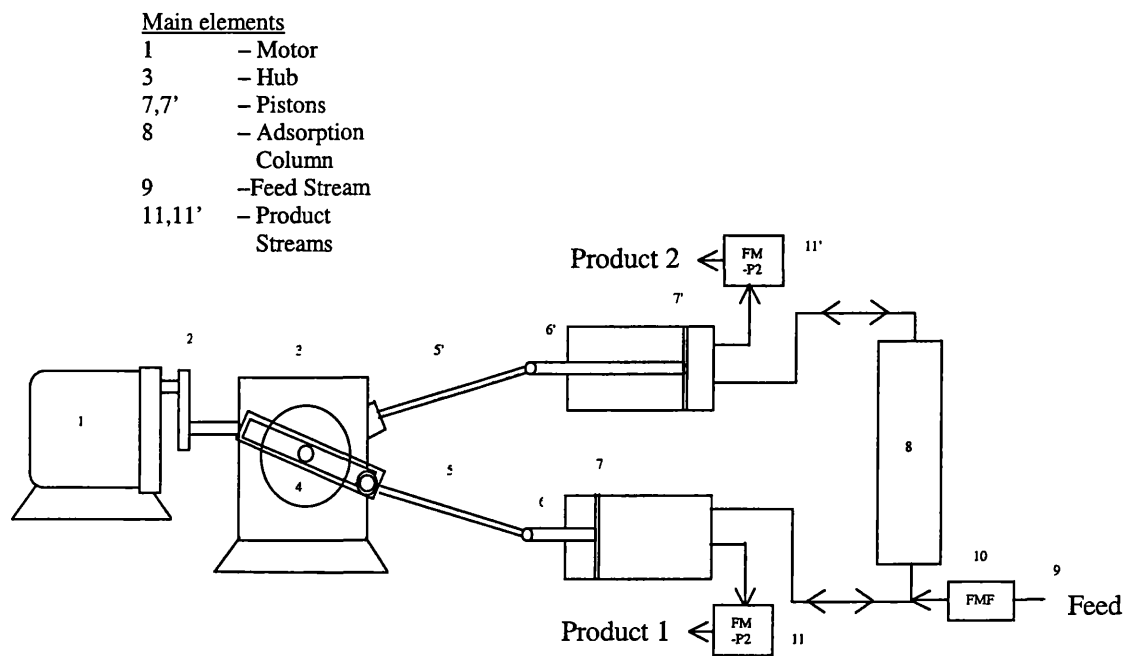


Fig.4.7 Dual-Piston Driven PSA unit (adapted from Keller and Kuo, 1982)

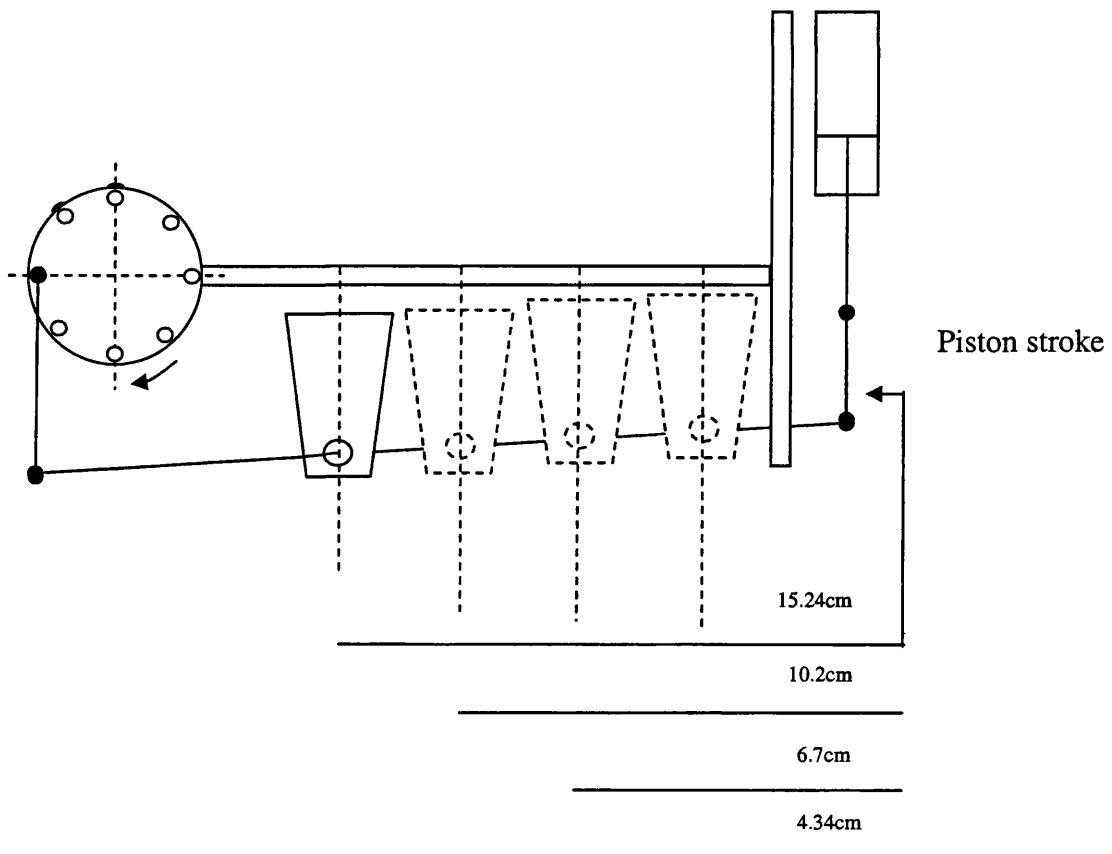


Fig.4.8 Pillow block arrangement from side

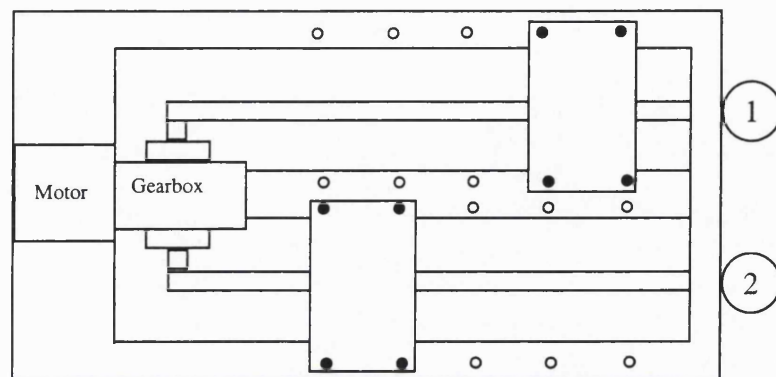


Fig.4.9 View of dual piston driven rig from above showing pillow block arrangement

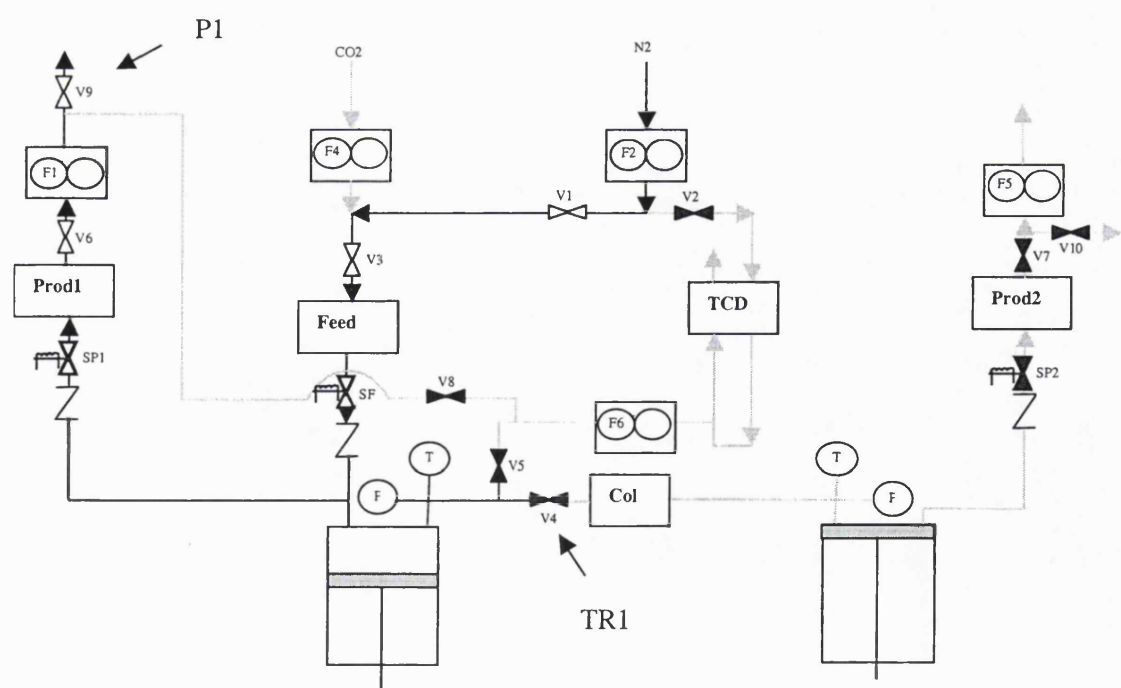


Fig.4.10 Dual Piston Driven PSA test rig instrumentation

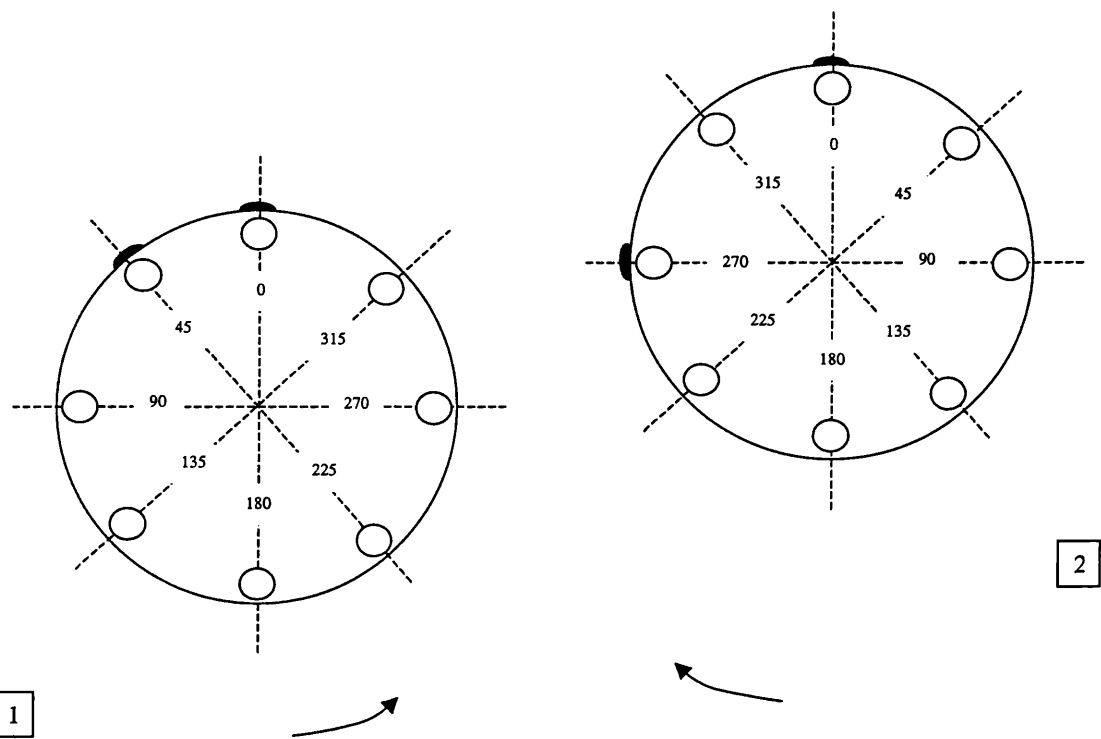


Fig. 4.11 Phase angle arrangement for hubs 1 and 2.

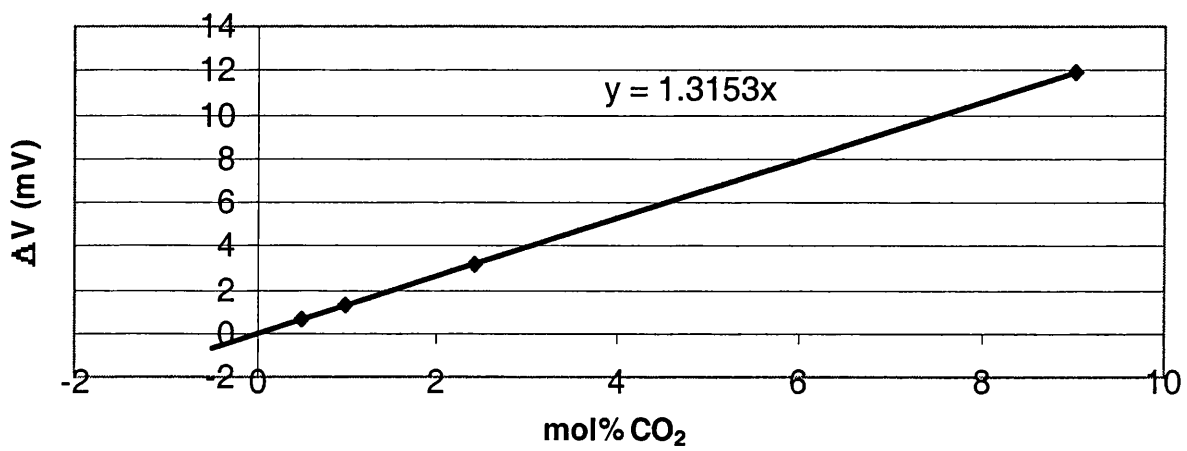


Fig. 4.12 TCD calibration curve

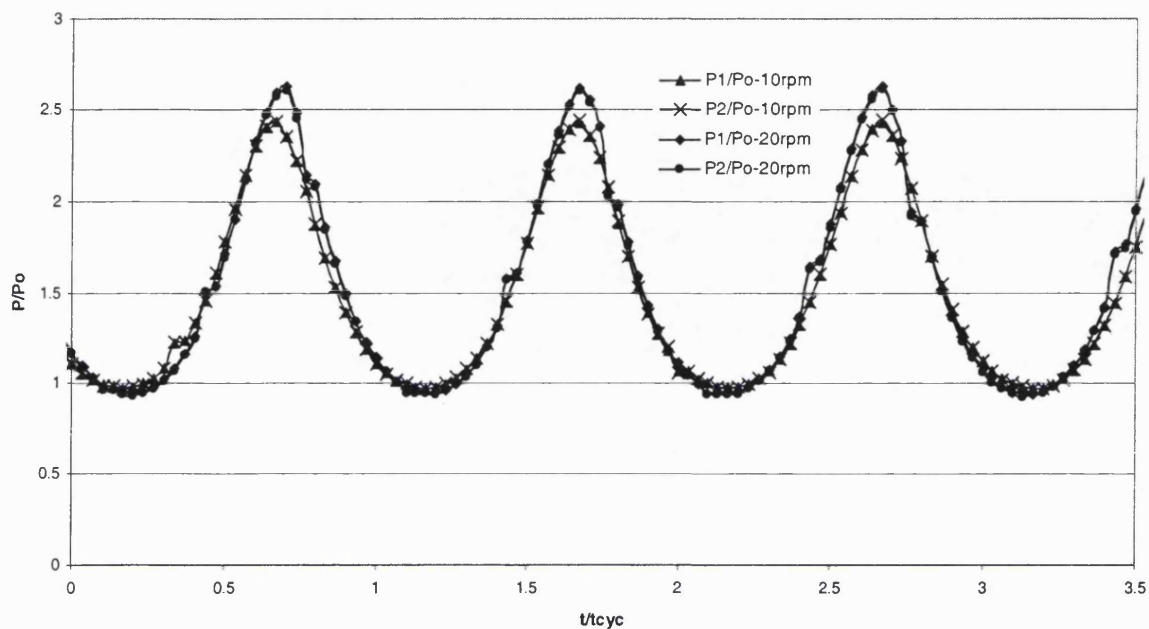


Fig.4.13 Dimensionless pressure profiles when no column is present (Helium total reflux runs at 10rpm and 20rpm $\phi_1=0$ $\phi_2=\pi/2$ $S1=15.24\text{cm}$ $S2=4.34\text{cm}$)

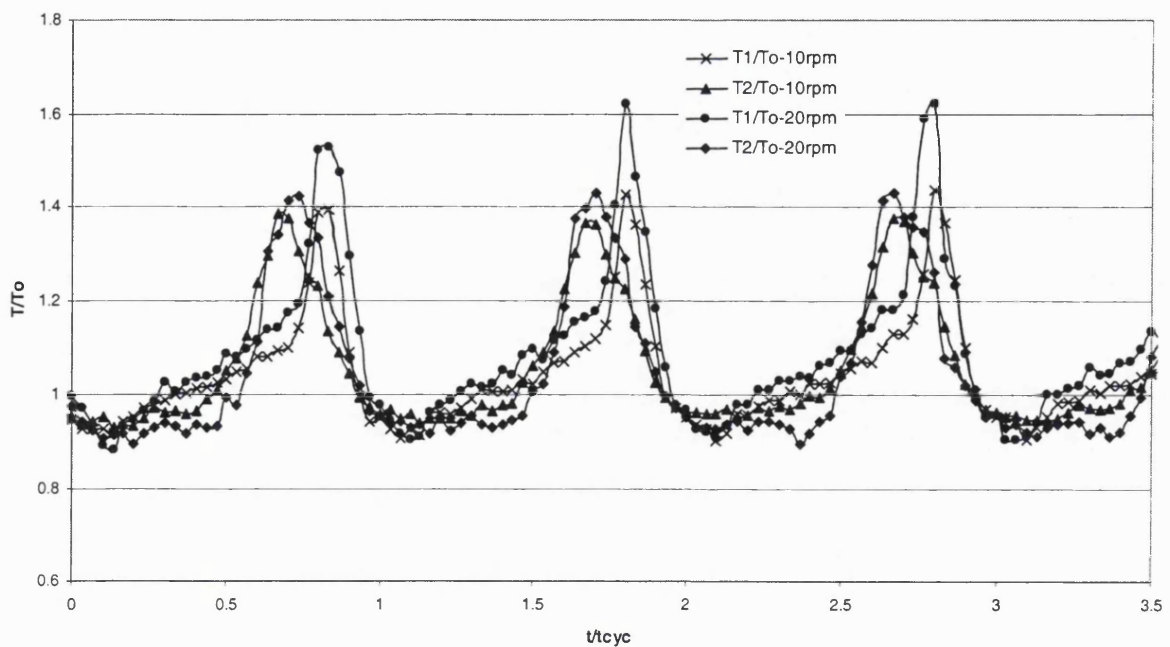


Fig.4.14 Dimensionless temperature profiles when no column is present (Helium total reflux runs at 10rpm and 20rpm $\phi_1=0$ $\phi_2=\pi/2$ $S1=15.24\text{cm}$ $S2=4.34\text{cm}$)

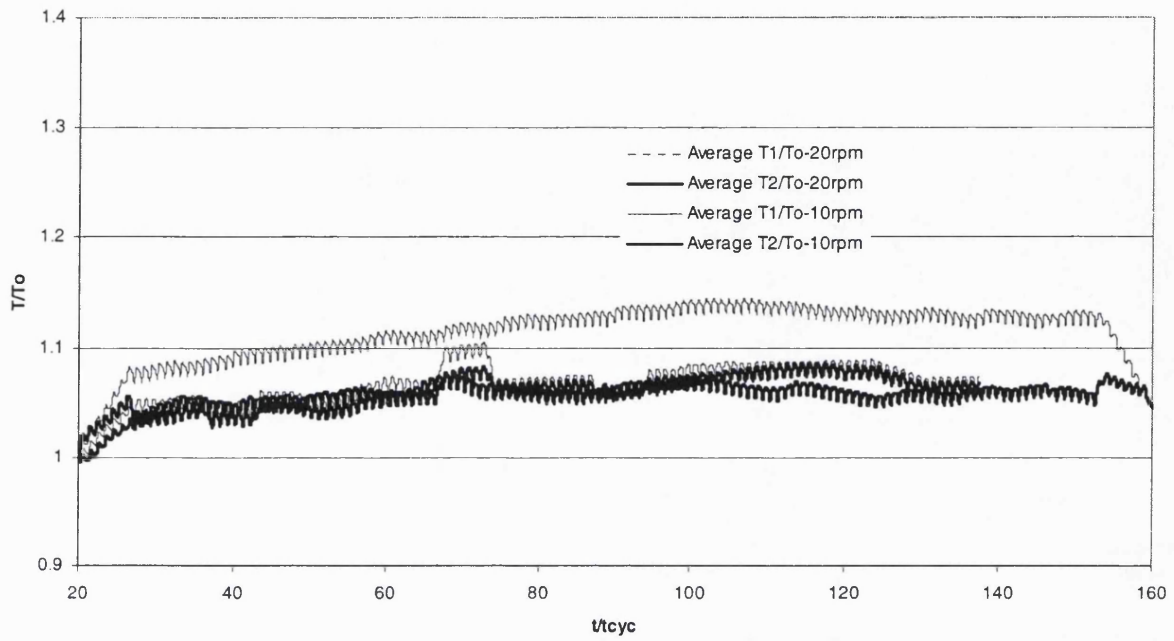


Fig.4.15 Dimensionless average temperature profiles when no column is present (Helium total reflux runs at 20rpm $\phi_1=0$ $\phi_2=\pi/2$ S1=15.24cm S2=4.34cm)

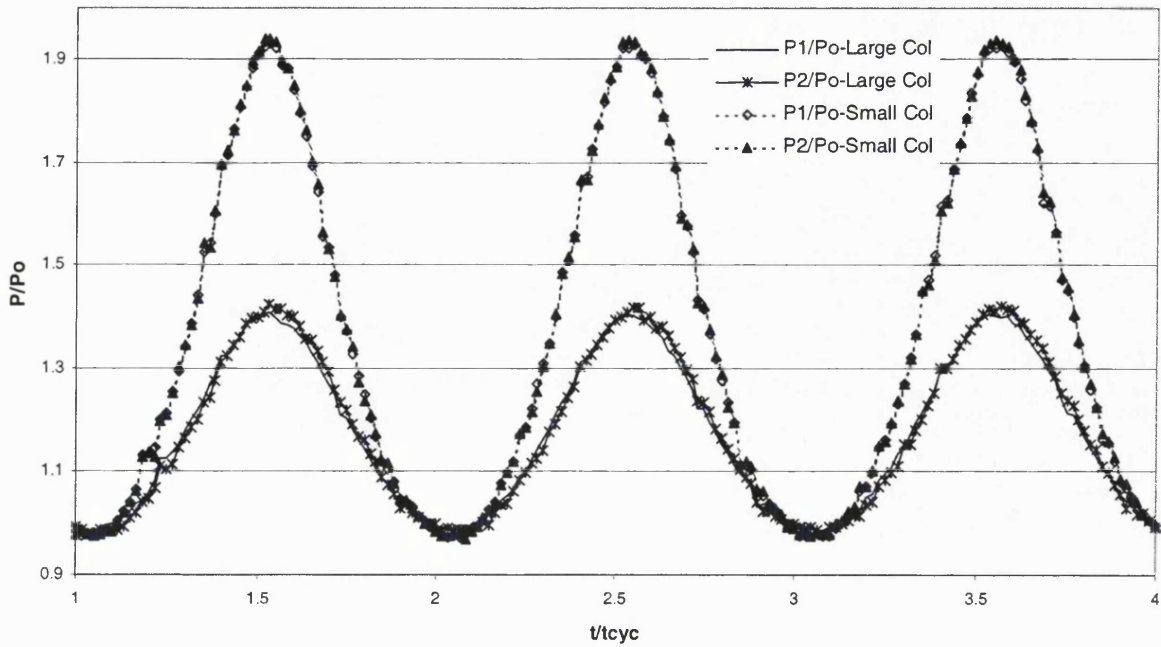


Fig.4.16 Dimensionless pressure profiles when large and small columns are present (Helium total reflux runs at 10rpm $\phi_1=0$ $\phi_2=\pi/2$ S1=15.24cm S2=4.34cm)

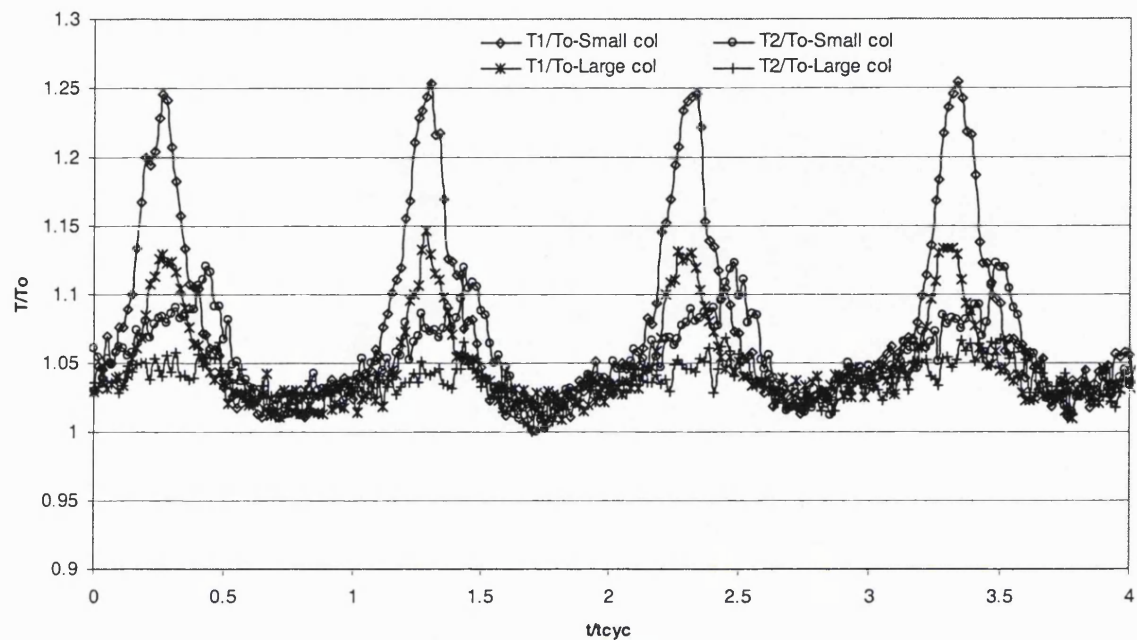


Fig.4.17 Dimensionless temperature profiles when large and small columns are present
(Helium total reflux runs at 10rpm $\phi_1=0$ $\phi_2=\pi/2$ S1=15.24cm S2=4.34cm)

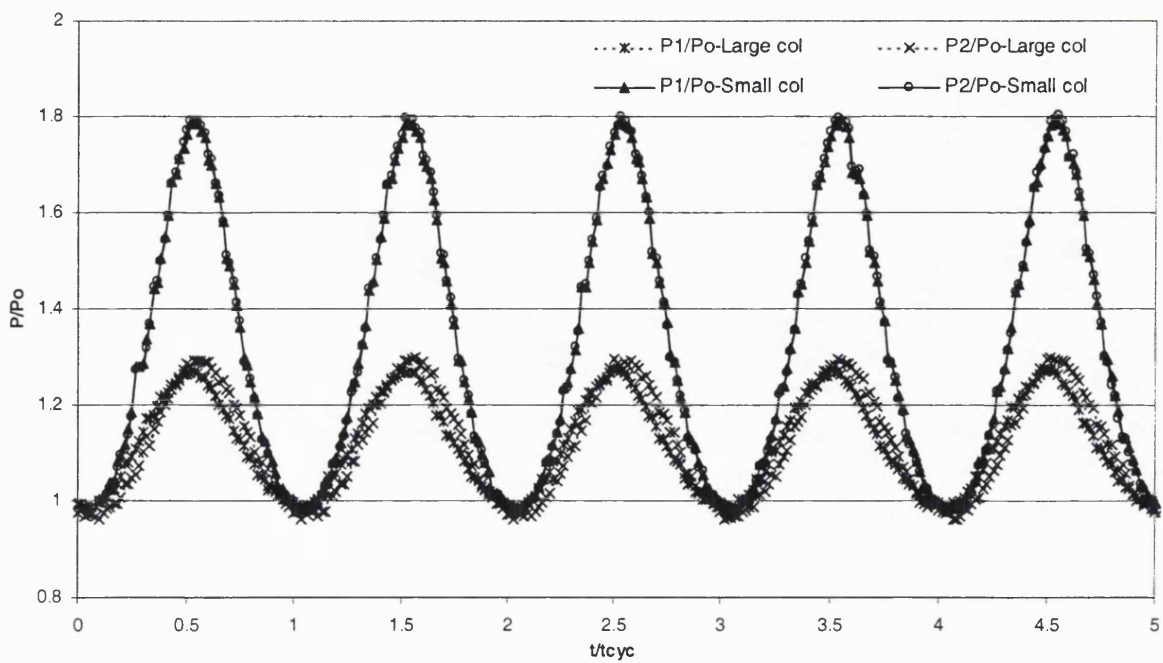


Fig.4.18 Dimensionless pressure profiles when large and small columns are present (Total reflux runs 10%CO₂/90%N₂ 10rpm $\phi_1=0$ $\phi_2=\pi/2$ S1=15.24cm S2=4.34cm)

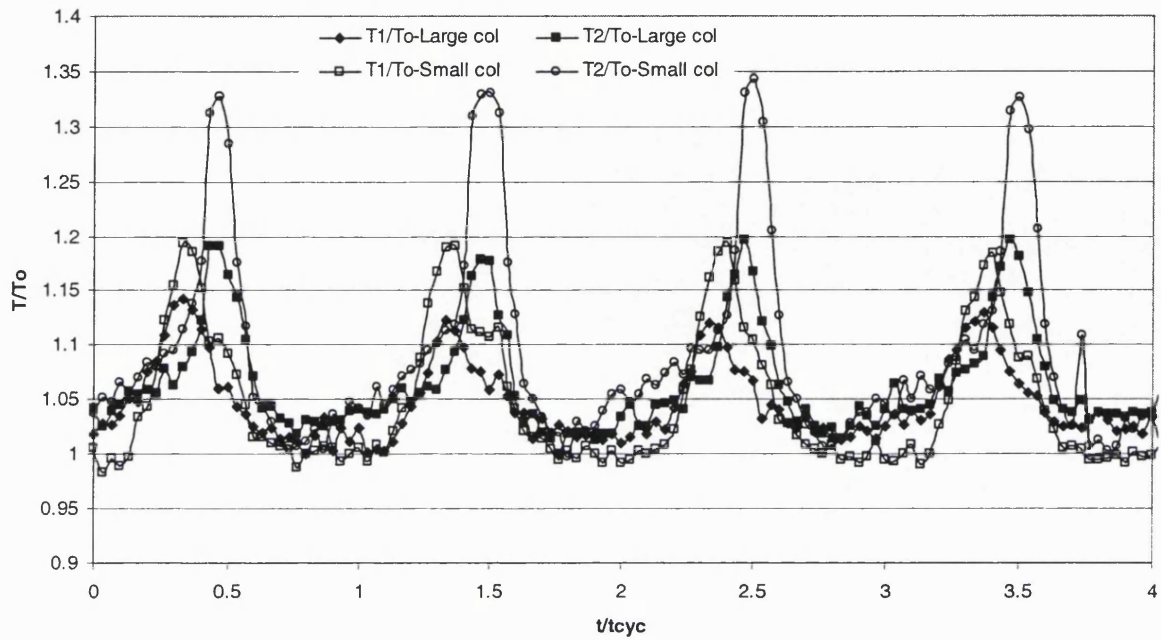


Fig.4.19 Dimensionless temperature profiles when large and small columns are present (Total reflux runs 10%CO₂/90%10rpm N₂ $\phi_1=0$ $\phi_2=\pi/2$ S1=15.24cm S2=4.34cm)

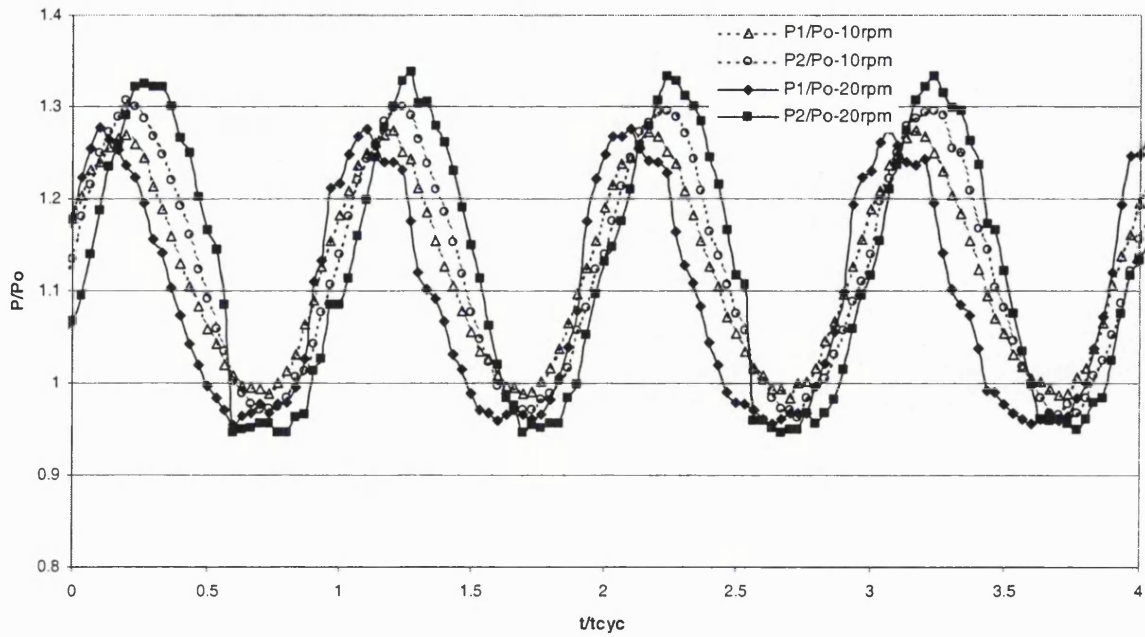


Fig.4.20 Dimensionless pressure profiles when large column is present (Total reflux runs 10%CO₂/90%N₂ 10rpm and 20rpm $\phi_1=0$ $\phi_2=\pi/2$ S1=15.24cm S2=4.34cm)

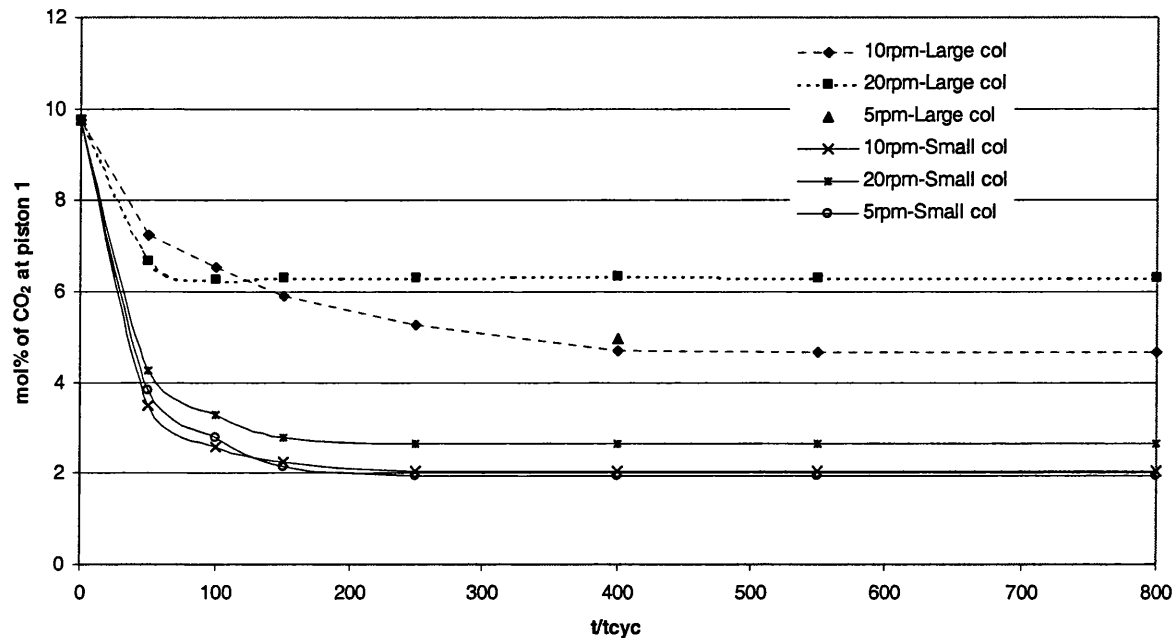


Fig.4.21 Mole % of CO₂ measured at piston 1 as steady state is approached using both large and small columns (Total reflux runs 10%CO₂/90%N₂ 5,10 and 20rpm $\phi_1=0$ $\phi_2=\pi/2$ S1=15.24cm S2=4.34cm)

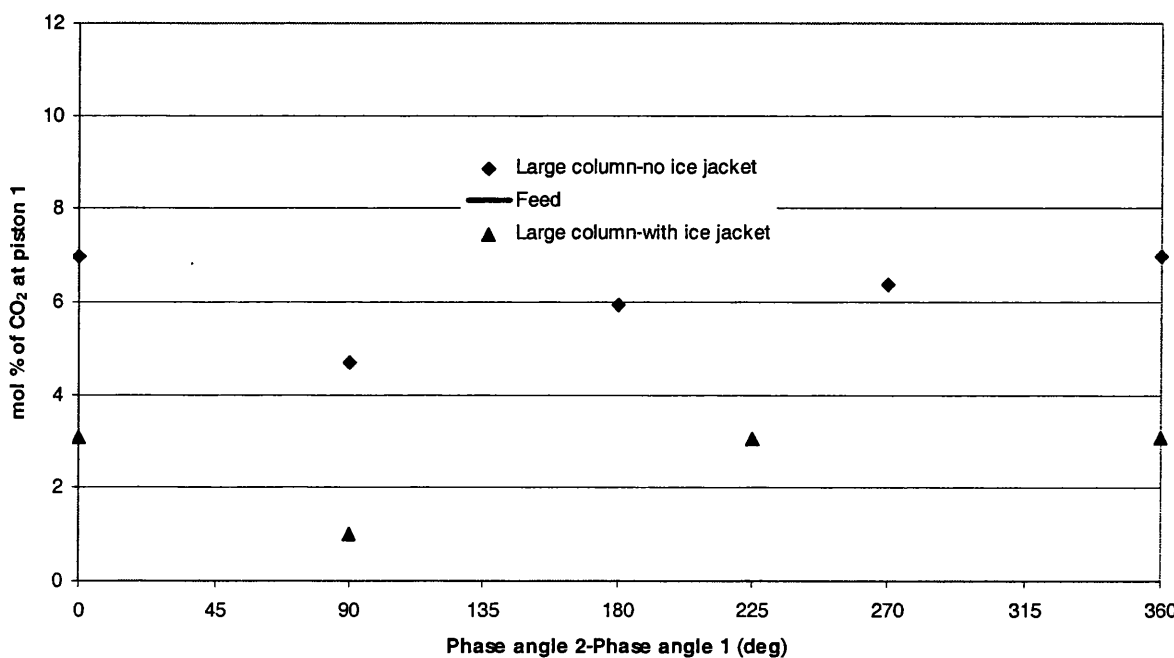


Fig.4.22 Variation in the mole % of CO₂ at piston 1 at steady state with changes in phase angle 2 (Total reflux runs 10%CO₂/90%N₂ $\phi_1=0$ S1=15.24cm S2=4.34cm)

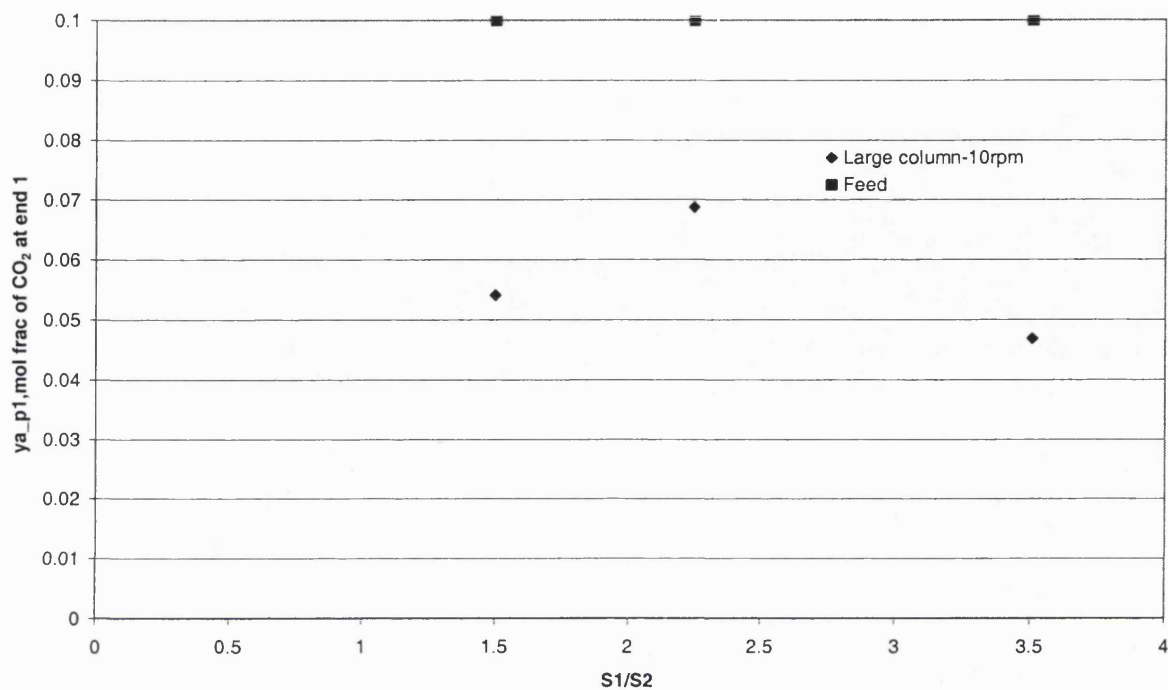


Fig.4.23 Variation in the mole % of CO₂ at piston 1 at steady state with changes in stroke length ratio (Total reflux runs 10%CO₂/90%N₂ $\phi_1=0$ $\phi_2=\pi/2$ S1=15.24cm)

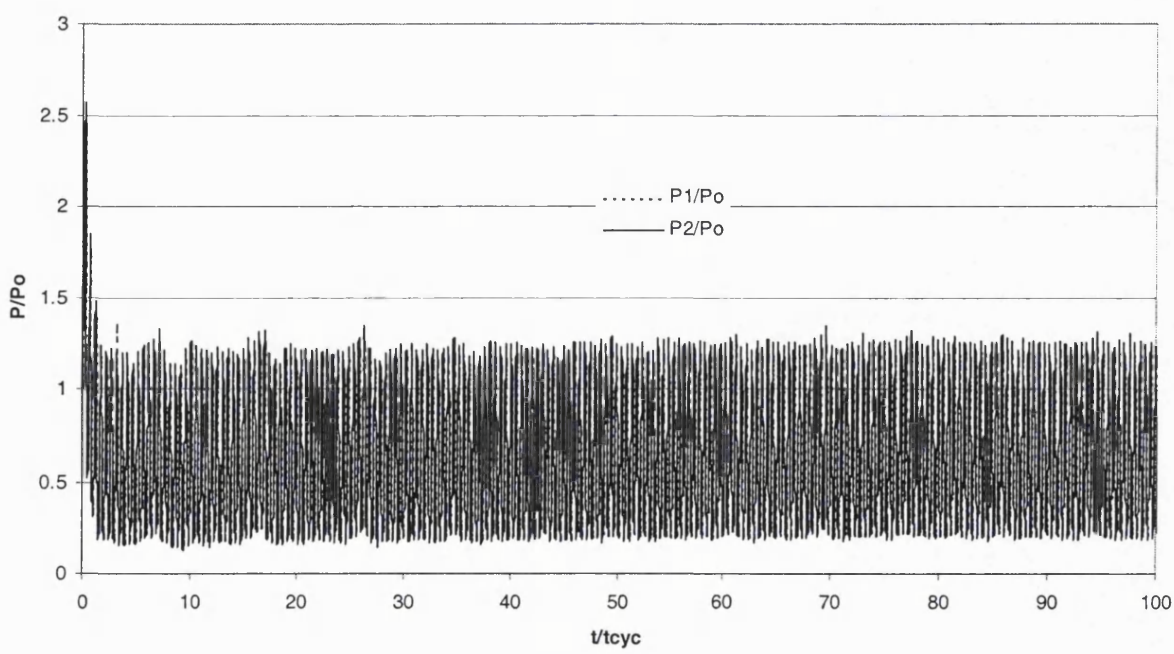


Fig.4.24 Dimensionless pressure profiles when small column is present (Feed-Product runs 10%CO₂/90%N₂ 10rpm $\phi_1=0$ $\phi_2=\pi/2$ S1=15.24cm S2=4.34cm $\phi_F=\pi/2$, $\phi_{P1}=\pi$, $\phi_{P2}=3\pi/2$ $t_{valve}=0.05$ secs for all)

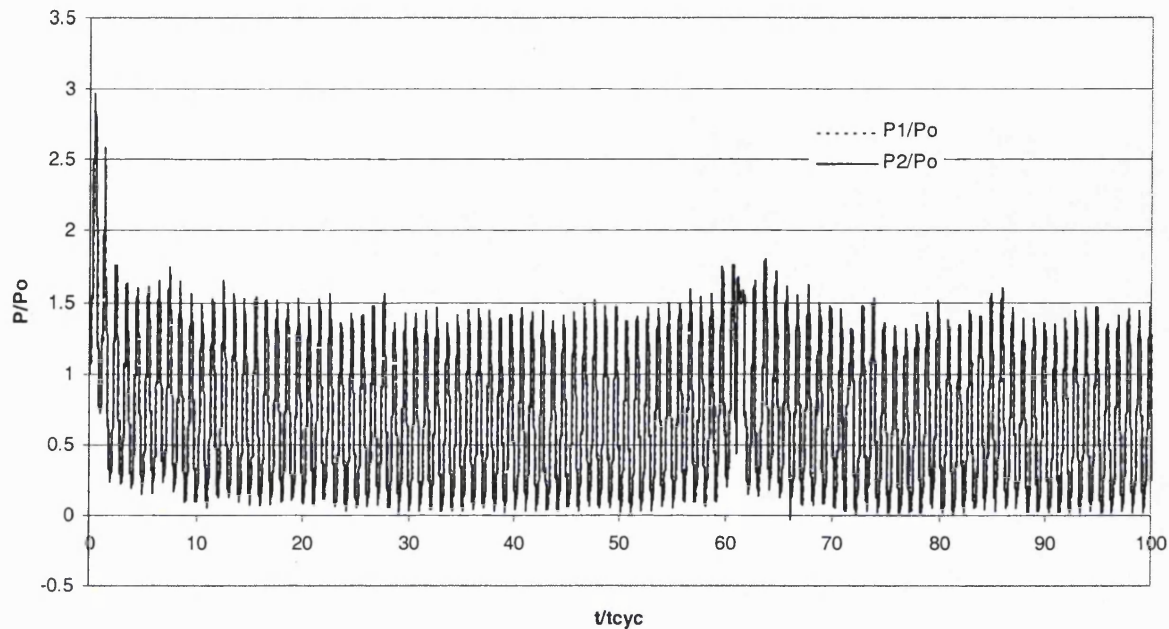


Fig.4.25 Dimensionless pressure profiles when small column is present (Feed-Product runs 10%CO₂/90%N₂ 10rpm $\phi_1=0$ $\phi_2=\pi/2$ S1=15.24cm S2=4.34cm $\phi_F=0$, $\phi_{P1}=\pi$, $\phi_{P2}=3\pi/2$ $t_{valve}(\text{feed and product } 2)=0.1\text{secs}$, $t_{valve}(\text{product } 1)=0.05\text{secs}$)

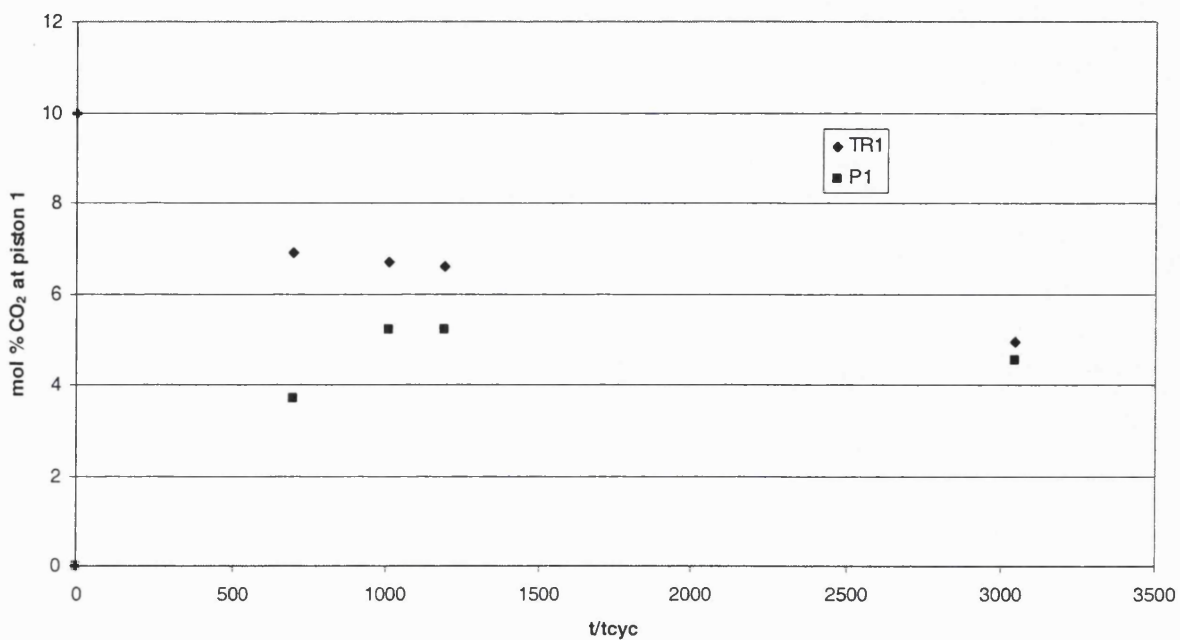


Fig.4.26 Mole % of CO₂ measured at piston 1 tank as steady state is approached using small column (Feed-Product runs 10%CO₂/90%N₂ 10rpm $\phi_1=0$ $\phi_2=\pi/2$ S1=15.24cm S2=4.34cm $\phi_F=\pi/2$, $\phi_{P1}=\pi$, $\phi_{P2}=3\pi/2$ $t_{valve}=0.05\text{secs}$ for all)

Chapter 2: Tables

System parameters	
Piston diameter(cm)	4.45
Column diameter (cm)	2.66
Column length*	22.48
Stroke length 2' (cm)	7.62
Stroke length 2 (cm)	2.54
Phase angle 2'	0
Phase angle 2	$\pi/4$
Cycle time (secs)	2

Table 4.1 System parameters for dual piston driven PSA experiments (*column length=17.78cm for H₂/CH₄ separation) (Keller and Kuo, 1982)

<i>Item</i>	<i>Catalogue information</i>
Pressure transducers	Motorola differential pressure transducers MPX5700 DF
Thermocouples	Omega KMQSS K-type thermocouples with sheath diameter 0.01"
Thermocouple transducer	Designed in house
Data acquisition board	Computer Boards Inc DAS 801/802
Solenoid valves	ASCOlectric Ltd. Normally closed. 8262G232
Flowmeters	F2, F4 – Matheson 8102 F1 – Matheson 8141 F5, F6 – Brooks 5850TR
TCD	Gow-Mac Instrument Co.

Table 4.2 Monitoring and controlling devices for dual piston driven PSA rig

<i>Total reflux helium runs</i>	<i>Total reflux adsorbing runs</i>	<i>Feed-product adsorbing runs</i>
a) Key parameters set	a) Key parameters set	a) Key parameters set
b) Helium fed until correct pressure reached.	b) System purged and adsorbent regenerated using N ₂ (~2 hours).	b) Valve parameters set
c) Cycling begun	c) CO ₂ /N ₂ mixture fed until correct pressure reached.	c) System purged and adsorbent regenerated using N ₂ (~2-3 hours).
d) Motor stopped when required of cycles reached	d) System left to come to equilibrium (~1 hour).	d) CO ₂ /N ₂ mixture fed until correct pressure reached.
	e) Cycling begun.	e) System left to come to equilibrium (~1 hour).
	f) Motor stopped when required of cycles reached and sampling loop activated	f) Cycling begun while feed and product flowmeters set to setpoint.
		g) Motor stopped when required of cycles reached and sampling loop activated

Table 4.3 Summary of experimental procedures

Run	Cycle speed (rpm)	He/CO ₂ & N ₂	ϕ_1 (deg)	ϕ_2 (deg)	S1 (cm)	S2 (cm)	Run type	Sample point	Column	No. of cycles
1	10	He	0	90	15.24	4.34	TR	-	None	500
2	20	He	0	90	15.24	4.34	TR	-	None	500
3	30	He	0	90	15.24	4.34	TR	-	None	500
4	10	He	0	90	15.24	4.34	TR	-	Large	500
5	20	He	0	90	15.24	4.34	TR	-	Large	500
6	30	He	0	90	15.24	4.34	TR	-	Large	500
7	10	He	0	90	15.24	4.34	TR	-	Small	500
8	20	He	0	90	15.24	4.34	TR	-	Small	500
9	30	He	0	90	15.24	4.34	TR	-	Small	500
10	10	CO ₂ /N ₂	0	90	15.24	4.34	TR	TR	Large	50
11	10	CO ₂ /N ₂	0	90	15.24	4.34	TR	TR	Large	100
12	10	CO ₂ /N ₂	0	90	15.24	4.34	TR	TR	Large	150
13	10	CO ₂ /N ₂	0	90	15.24	4.34	TR	TR	Large	200
14	10	CO ₂ /N ₂	0	90	15.24	4.34	TR	TR	Large	250
15	10	CO ₂ /N ₂	0	90	15.24	4.34	TR	TR	Large	400
16	10	CO ₂ /N ₂	0	90	15.24	4.34	TR	TR	Large	550
17	10	CO ₂ /N ₂	0	90	15.24	4.34	TR	TR	Large	800
18	5	CO ₂ /N ₂	0	90	15.24	4.34	TR	TR	Large	400
19	20	CO ₂ /N ₂	0	90	15.24	4.34	TR	TR	Large	50
20	20	CO ₂ /N ₂	0	90	15.24	4.34	TR	TR	Large	200
21	20	CO ₂ /N ₂	0	90	15.24	4.34	TR	TR	Large	400
22	10	CO ₂ /N ₂	0	180	15.24	4.34	TR	TR	Large	400
23	10	CO ₂ /N ₂	0	270	15.24	4.34	TR	TR	Large	400
24	10	CO ₂ /N ₂	0	0	15.24	4.34	TR	TR	Large	400
25	10	CO ₂ /N ₂	0	90	15.24	6.78	TR	TR	Large	400
26	10	CO ₂ /N ₂	0	90	15.24	10.16	TR	TR	Large	400
27	10	CO ₂ /N ₂	0	90	15.24	4.34	TR	TR	Small	50
28	10	CO ₂ /N ₂	0	90	15.24	4.34	TR	TR	Small	150
29	10	CO ₂ /N ₂	0	90	15.24	4.34	TR	TR	Small	250
30	5	CO ₂ /N ₂	0	90	15.24	4.34	TR	TR	Small	50
31	5	CO ₂ /N ₂	0	90	15.24	4.34	TR	TR	Small	150
32	5	CO ₂ /N ₂	0	90	15.24	4.34	TR	TR	Small	250
33	20	CO ₂ /N ₂	0	90	15.24	4.34	TR	TR	Small	50
34	20	CO ₂ /N ₂	0	90	15.24	4.34	TR	TR	Small	150
35	20	CO ₂ /N ₂	0	90	15.24	4.34	TR	TR	Small	250
36	10	CO ₂ /N ₂	0	0	15.24	4.34	TR	TR	Small ice	500
37	10	CO ₂ /N ₂	0	270	15.24	4.34	TR	TR	Small ice	500
38	10	CO ₂ /N ₂	0	180	15.24	4.34	TR	TR	Small ice	500
39	10	CO ₂ /N ₂	0	225	15.24	4.34	TR	TR	Large ice	500
40	10	CO ₂ /N ₂	0	315	15.24	4.34	TR	TR	Large ice	500
41	10	CO ₂ /N ₂	0	135	15.24	4.34	TR	TR	Large ice	500
42	10	CO ₂ /N ₂	0	0	15.24	4.34	TR	TR	Large ice	500

a)

Run	Cycle speed (rpm)	He/CO ₂ & N ₂	ϕ_1 (deg)	ϕ_2 (deg)	S1 (cm)	S2 (cm)	Run type	Sample point	Column	No. of cycles	Valve opening angle, ϕ (deg)			Length of time valve is open(secs)		
											Feed	Prod 1	Prod 2	Feed	Prod 1	Prod 2
43	10	CO ₂ /N ₂	0	90	15.24	4.34	FP	TR,P1,P2	Small ice	500	0	180	270	0.1	0.2	0.1
44	10	CO ₂ /N ₂	0	90	15.24	4.34	FP	TR,P1,P2	Small ice	500	0	180	270	0.1	0.05	0.1
45	10	CO ₂ /N ₂	0	90	15.24	4.34	FP	TR,P1,P2	Small ice	700	0	180	0	0.05	0.05	0.05
46	10	CO ₂ /N ₂	0	90	15.24	4.34	FP	TR,P1,P2	Small ice	700	270	180	0	0.05	0.05	0.05
47	10	CO ₂ /N ₂	0	90	15.24	4.34	FP	TR,P1,P2	Small ice	840	90	180	270	0.05	0.05	0.05
48	10	CO ₂ /N ₂	0	90	15.24	4.34	FP	TR,P1,P2	Small ice	1340	90	180	270	0.05	0.05	0.05
49	10	CO ₂ /N ₂	0	90	15.24	4.34	FP	TR,P1,P2	Small ice	1690	90	180	270	0.05	0.05	0.05
50	10	CO ₂ /N ₂	0	90	15.24	4.34	FP	TR,P1,P2	Small ice	1010	90	180	0	0.05	0.05	0.05
51	10	CO ₂ /N ₂	0	90	15.24	4.34	FP	TR,P1,P2	Small ice	1190	90	180	0	0.05	0.05	0.05
52	10	CO ₂ /N ₂	0	90	15.24	4.34	FP	TR,P1,P2	Small ice	3040	90	180	0	0.05	0.05	0.05

b)

Table 4.4 List of experimental runs a) Helium and total reflux experiments b) Feed-product experiments

Stroke Length ratio (S1/S2)	3	Choice of column	Small (in ice bath)
Cycle speed	10rpm	Phase angles	$\phi_1=0, \phi_2=\pi/2$
	When Open:		Time (secs):
Feed valve	$0.25t_{cyc}$		0.05
Product 1 valve	$0.5t_{cyc}$		0.05
Product 2 valve	$0.75t_{cyc}$		0.05

Table 4.5. Best System set up (NB 1700 cycles for entire system (inc. tanks) to reach s.s, feed pressure maintained at 15psig)

Chapter 5

A Mathematical Model of a Dual Piston Driven PSA System

5.1 Introduction

The purpose of undertaking mathematical modelling of a chosen technology is to allow the system to be examined and explored without having to undertake a long, time consuming experimental study. A fully representative and verified simulation can offer an efficient means of establishing whether a particular process is viable, both realistically and economically. However there are clearly two areas in which the model must excel. Firstly to be efficient, computing time must be at a minimum. As computing power has increased dramatically over the last 20 years then fast simulations are certainly more achievable. However speed and accuracy can only be assured when the correct choice of computing method is chosen. The problem is more fundamental than just selecting a powerful computer. In addition the simulation is of no use unless it is representative of the real system. It is common practice to make relevant assumptions to reduce the number and complexity of equations needed to solve a mathematical equation set. This may make the problem simpler to solve but the model is only valid if the solutions found agree with experimental observations. Therefore it is crucial to compare experimental and simulated results.

In this chapter we look at the development of mathematical models to represent the Dual Piston Driven PSA system described in Chapter 4. The chapter begins with a short review of mathematical approaches to cyclic adsorption processes followed by consideration of the various modelling approaches taken to Pressure Swing Adsorption processes. A general mathematical representation of the Dual Piston Driven PSA system is then presented along with the simplifying assumptions made. Finally the necessary adaptations made, as dictated from preliminary experimental results, are demonstrated and discussed.

5.2 Literature review of mathematical techniques and mathematical modelling of PSA processes

The common techniques used to solve complex equation sets are discussed below followed by short discussion of the various approaches taken to modelling PSA processes, both traditional PSA as well as Rapid PSA and Dual Piston Driven PSA.

5.2.1 Mathematical approaches to cyclic adsorption processes

Traditional, rapid and piston driven PSA can all be classed as cyclic adsorption processes. Mathematically such systems all consist of parameters that vary both with space and time. Therefore representative models consist of both partial differential equations (PDEs), relating to these parameters, and algebraic equations (AEs), which equate the parameters to each other. The resultant equation set can only be solved using numerical methods, whereby the Partial Differential Algebraic Equations (PDAEs) are reduced to Differential Algebraic Equations (DAEs). Several methods in which this can be achieved by discretising the spatial and/or the temporal domains. These include finite difference methods, orthogonal collocation, orthogonal collocation on finite elements and cells in series.

5.2.1.1 *Finite difference methods*

Finite difference methods, which have been widely used, involve dividing up the domain of interest using a grid. At each equally spaced node on the grid the dependant variable has a discrete value. Fig. 5.1 demonstrates how the domain z is discretised. Approximating the values to the nodes can be achieved by using either a series such as Taylor's, a polynomial or by using a control volume approach. Using Taylor's series, for example, solution of the problem can be achieved by evaluating the discrete node values by moving across the grid. With boundary conditions at each extreme the solution at every point can be found, leading to a solution for the entire domain. The work of Nilchan (1997) discusses the various techniques that are used to do this in more detail.

5.2.1.2 Orthogonal Collocation

The method of orthogonal collocation (OC) differs from finite difference methods in so much as the grid imposed over the domain of interest no longer consists of equally spaced nodes. The positions of the nodes are determined by the roots of an appropriate polynomial. Again fig. 5.2 demonstrates how the nodes would be distributed over the z domain. In order that sufficient points are present across the domain to ensure an accurate solution the polynomial must necessarily be high order. As noted by Alpay et al (1993) this often leads to numerical instability and slow computing times. The work of Nilchan (1997) gives more details about OC methods.

5.2.1.3 Orthogonal Collocation on Finite Elements

For this method the domain is first divided into equally sized elements. Across each of these elements orthogonal collocation is applied, giving rise to a few additional unevenly spaced points across each element. This is demonstrated in fig. 5.3. The smaller number of collocation points means that a low order polynomial may be used. The total number of nodes distributed across the entire domain, both on the grid and from the collocation, is now large, and gives a stable solution, as demonstrated by Alpay et al (1993) and Nilchan (1997) for example.

5.2.1.4 Cells in Series

The spatial domain, in this case, is split into a number of cells. In each well mixed cell variables are dependant only on time. Boundary conditions at the edges of each cell however are written such that a gradient exists between cells. The problem therefore becomes iterative as a solution is evaluated. This method is discussed in more detail in Alpay et al. (1993).

Each of the methods discussed has its own merits and the choice of which to use is generally dependant on the problem to be solved.

5.2.2 Development of PSA modelling

Mathematical modelling of PSA processes began in earnest 20 years after the technology was invented. Shendalman and Mitchell (1972) began the effort by developing the basic equilibrium theory model for a system containing a trace absorbable component in an inert carrier (CO_2 in He). They made the simplifying assumptions of plug flow and linear equilibrium but found that the agreement between simulation and experiment was poor. The approach taken was extended in their second study (Mitchell and Shendalman, 1973) where a dynamic model that included finite mass transfer resistance was adopted. Two extreme cases were considered. In the first the gas and solid were assumed to be at equilibrium at the end of the pressurisation steps, and in the second, the pressure changes made were assumed to be so rapid that there was no exchange between solid and gas. Therefore at the end of the pressurisation steps the solid concentration was assumed to be frozen and to remain so throughout the purging and blowdown steps. Simulating these two cases and evaluating the concentration profiles showed that, while the simulated results bracketed those found from experiment, the first case results agreed better to those found from the experiment. To carry out the simulation the equations were transformed using the method of characteristics and then the concentration profiles obtained using a Fortran program. The efficiency of the simulation is not discussed. Although there was some quantitative agreement between experimental and simulated results, the model could not accurately predict the system behaviour. A similar approach was taken by Chihara and Suzuki (1983) except that heat effects were included. Here the frozen assumption was again employed and a parametric study of air drying using an activated alumina PSA system was presented. While specific comparison to experiment is not discussed the study does consider the effect of, for example, bed length, purge-to-feed ratio and cycle time, on the system performance. In this study the numerical calculation was undertaken by first converting the equation set to a non dimensional form. The Crank-Nicholson implicit method was then used to simulate the transient period to steady state. In general cyclic steady state was reached after 40 cycles and each simulation took 15 hours.

The study of Raghavan, Ruthven and Hassan (1985) identifies two important elements associated with PSA modelling. Firstly they focus on the importance of finite mass transfer resistance and axial dispersion in real adsorption systems, especially the latter which had not, to date, been included in PSA modelling. Secondly the efficiency of numerical methods was discussed. Building on the work done using single adsorption columns the suitability of the finite difference methods previously adopted was explored along with the newer collocation methods, shown to be more efficient for single columns. The mathematical model that was subsequently developed, which included the axial dispersion term in the column, was solved using both methods and two case studies examined. In the first, parameters are taken from the study of Chiara and Suzuki (1983). Considering the method of simulation, results showed that the collocation method allowed the simulation to be performed 3 times faster than when finite difference methods are used. In addition, by varying the Peclet number and noting the large variation in results obtained, the importance of including the axial dispersion term was confirmed. The second case study, the same as that examined by Mitchell and Shendallmann (1973), is used to verify the model against experimental results. The profiles obtained showed that, with the correct choice of mass transfer and dispersion coefficients, the experimental runs could be well matched. By allowing the mass transfer coefficient to vary inversely with pressure, consistent with a system in which adsorption is controlled by film or macropore diffusional resistance, the agreement was much closer than found previously.

As computational power has increased the number of assumptions that can be scrutinised has increased. In another PSA study by Raghavan, Ruthven and Hassan (1986) it is the linear driving force (LDF) assumption, associated with mass transfer, that is examined. The assumption allows the concentration profile across the adsorbent to be averaged, meaning that modelling of the adsorbent itself can be neglected. This greatly reduces the complexity of the modelling problem. For a more detailed description of the LDF model see Chapter 2 where equivalence between the LDF and diffusion models is discussed at length. In the PSA study attention was paid to the nature of the mass transfer resistance and the previous blanket

application of the LDF model questioned. Since the resistance for a porous adsorbent is mainly intraparticle rather than external a diffusional representation would be more accurate. By modelling the PSA system assuming both diffusion and LDF models for mass transfer resistance this hypothesis was tested. The models themselves can be seen replicated in Chapter 2 section 2.3.4 where similar simulations were undertaken. The conclusion of the study was that the simplifying LDF model could be used but the associated coefficient employed would need to be carefully chosen in accordance with the cycle time of the system in order that the model would replicate experimental performance. Again simulations were undertaken using orthogonal collocation and cyclic steady state was found at 35 cycles. Assuming 9 internal interval points each simulation took 28 minutes.

All the simulations discussed above, all for the Skarstrom cycle, show how the different assumptions have been made regarding fluid flow pattern, the equilibrium relationships, kinetic rate expressions, inclusion of heat effects and numerical solution techniques and are summarised in table 5.1. A full review of the great many dynamic modelling studies for pressure swing adsorption can be found in Pressure Swing Adsorption p.167-171 (Ruthven et al, 1994), which includes investigations into more complex operating cycles, the effect that assuming the velocity is constant or varied across the adsorbent bed has and how the choice of an equilibrium or kinetically controlled separation affects the modelling approach.

The advances made in traditional PSA modelling have also led to improvements in the related fields in both rapid and piston driven modelling.

5.2.3 Mathematical modelling of Rapid PSA

The main difference between modelling traditional PSA systems and Rapid PSA is the assumption of negligible pressure drop. Since pressure drop is key to Rapid PSA systems then clearly allowance for this must be made in the model. Generally this has involved the inclusion of either Darcy's or Ergun's law. As with traditional PSA major developments in

modelling have been related to the modelling method and its efficiency. Studies have, in general, built on the lessons learnt from PSA with regard to relevant assumptions and modelling has allowed the exploitation of various key parameters. The development of theoretical studies of RPSA have followed from the work of Jones and Keller (1981) with a great many advances made in the 1980s and 1990s. For example, the work of Doong and Yang (1988), in which the air separation system of Jones and Keller (1981) was considered, showed that by using an LDF representation matching between experiment and simulation could be achieved. The importance of mass transfer resistance was also highlighted. Parametric investigations into the effect of feed, delay and exhaust times on the purity or recovery of O₂ were also undertaken. In the study of Alpay, Kenney and Scott (1994) a mathematical model was used to investigate, amongst other issues, the effect of particle size. Experimental results obtained by the researchers allowed validation of the model while the simulation meant that a wealth of information about performance could be gained. This included looking at the single and combined effects of not just particle size but also feed pressure, cycle time, feed to cycle time ratio and product delivery rate. The study demonstrates just how powerful a robust and accurate model can be, but also shows how important the mathematical approach is. The paper builds on a previous related study, considering combining RPSA and reaction (Alpay, Kenney and Scott, 1993), in which a great deal of attention is paid to simulation techniques. A variety of discretisation methods were utilised and the results obtained compared. The techniques included spatial discretisation using polynomial approximations, low order polynomial approximations on finite elements and cells in series. A global method, based on low-order polynomial approximations for derivatives in space and time was also used. Solutions were rated both for accuracy and speed and the most suitable method was found to be orthogonal collocation on finite elements. It was this method that could then be used in the subsequent study (Alpay et al, 1994) with confidence.

5.2.4 Mathematical modelling of Piston Driven PSA

Although experimental studies into piston driven PSA began to be published in the 1980s mathematical representations used to exploit the technology only began in the 1990s. One of the first of these being that undertaken by Sakoda et al.(1992). The study considered a single piston process similar to that proposed by Ericksson (1979). In this case the process was oxygen enrichment and the bed characteristics were studied by using three different sized 5A zeolite particles; 48-80mesh, 80-150mesh and 200-325mesh. From their simulations it was found that the oxygen purity was strongly dependant on the particle size, being highest when the medium sized particles were used, and on the difference between the maximum and minimum pressure of the cycle. They also found that the pressure difference increased with cycling speed and reasoned that this was because at higher speeds the rate of adsorption was slower than the cycle speed, and hence product purity was reduced once a certain speed was reached. In addition they were able to demonstrate that productivity was greatly improved over that possible with conventional PSA.

This work was continued and another experimental and computational study, considering the separation of CO₂ from flue gas, was presented assuming a single piston driven PSA system (Suzuki, 1997). The mathematical model assumed that the LDF equation with an appropriate coefficient based on cycle time could represent mass transfer, that the adsorption kinetics were macroporous diffusion controlled, pressure drop could be represented by the Ergun equation and that the system was isothermal. The cells in series mathematical approach was used to evaluate solutions, as developed in a previous work (Suzuki, 1996). While the experimental work considered the effect of moisture on hydrophilic and hydrophobic adsorbents, the modelling work considered only the hydrophobic adsorbent. The experimental trends relating to CO₂ recovery for this adsorbent compared well with those calculated, except at low production capacity where it was suggested experimental error may have been to blame. The simulated pressure profiles at each end of the adsorption bed also agreed well with experimental profiles, predicting the observed phase and amplitude

differences which arose due to the pressure gradient across the bed. Calculations performed using the model results showed that the adsorption capacity of the bed was not fully utilised. The causes suggested included unoptimised valve sequencing and needlessly high pressure drop across the adsorbent bed.

The first model that considers Dual Piston Driven PSA is presented by Singh and Jones (1997), who assumed a non isothermal representation. The approach they used, adapted from Stirling engine literature (Finkelstein, 1964), involved dividing the adsorbent bed into a number of control volumes, each one being well mixed and having uniform temperature, pressure and composition. To solve the model a pressure was assumed at one piston, the flows into and out of the piston calculated and then, in turn, the variable values of each control cell found until the end of the bed was reached and the volume for the other piston could be calculated. If this volume compared well, within a given tolerance, to the known actual volume then the solution was complete, if not, iteration continued with further guesses for the initial pressure at the start piston. This method showed some success but exhibited two major problems. Firstly, the iterations meant that often the simulation was lengthy, and secondly it was found that the number of cells had to be carefully chosen to avoid “false dispersion”, a problem that arose from assuming each of the cells was well mixed. To verify the model standard breakthrough experiments were used to set the correct number of cells. From experiment it was clear that, even at slower cycle speeds of 10rpm, there was a pressure drop across the adsorbent bed, which became even more noticeable at faster speeds. Despite making the incorrect assumption of constant pressure across the bed simulated profiles agreed reasonably well with those observed. Other results presented show how the energy requirement can be up to half that for a comparative traditional PSA unit. A short adiabacity study, carried out by varying the heat transfer coefficient for the column, showed that best performance was achieved under isothermal conditions.

The dual piston driven study by Farooq et al. (1998) in which a parallel passage contactor is employed, a system of PDEs was used to describe the isothermal total reflux system. Transposing into dimensionless form, the equations were discretised in space using a collocation method and solved simultaneously using Gear's variable step method with Jacobian analysis. In order to speed computation the velocity profile through the column was assumed to be linear and therefore linearly interpolated values could be calculated from the velocities at each end of the column. Results shows that for total reflux runs, both with and without adsorption, the experimental and calculated pressure profiles agreed well, with slight discrepancies being attributed to heat effects. A total of 9 internal collocation points was found adequate to give accurate solutions. Although there are no comments on the length of time the simulation took the paper states that the modelling approach was a definite improvement on previous attempts. However the exclusion of feed and product stream expressions suggested further work was required.

In the most recent study undertaken this has been tackled. In 2002 a study by Arvind et al. (2002) looked at the simulation of an isothermal dual piston driven PSA model for air separation assuming a packed bed of 13X zeolite. Expanding the previous work, the model includes not only verification of the model for both total reflux and feed and product cases but also includes a detailed parametric study. In addition the model also makes allowance for observed resistance encountered in pipework. Equations are again made dimensionless, discretised using orthogonal collocation and solved using Gear's method. Pressure and concentration profiles obtained from simulation and experiment are well matched for total reflux runs and there is good qualitative agreement when feed and product streams are included; imperfect matching was attributed to the difficulty in predicting the feed and product flowrates when the model was in transient mode. However trends associated with parametric variations are well captured. While the speed of calculation is not reported it is clear that the model is verified for total reflux cases. The discontinuous feed and product functions that change in the transient period seem to create the main problem when trying to

model the feed and product experiments. The parametric study, however, was able to highlight the importance of a representative model for identifying an optimum operating configuration.

A summary of published work concerned with piston driven PSA is given in table 5.1.

5.3 Model Development

The model of the dual piston driven PSA system, similar to that derived by Farooq et al (1998) and Arvind et al (2002), was formulated using the conventions shown in fig 5.4.

5.3.1 Model assumptions

The following simplifying assumptions were made:

- 1) The ideal gas law is valid
- 2) Frictional pressure drop is assumed to be negligible
- 3) Axial dispersion in the adsorption column is accounted for
- 4) There is no concentration gradient in the radial direction in the column
- 5) The mass transfer rate is described by a linear driving force model dependant on cycle time
- 6) The piston chambers are well mixed
- 7) The system is isothermal with thermal equilibrium between gas and solid phases
- 8) The adsorption isotherm is linear

When considering that the temperature and pressure changes encountered are modest (temperature and pressure never exceed 40degC and 3 atm respectively) and the gas travels through the structured adsorption column in uniform channels then assumptions 1-4 are valid. The investigations undertaken into the validity of the LDF model presented in Chapter 2 showed that so long as the newly developed 2 parameter approach is used then the LDF model can be used with confidence for any cycle time. The rapid movement of the pistons

would suggest that good mixing in the chambers would be achieved and hence assumption 6 is likely to be valid. While there are temperature changes encountered during operation of the system, and a non isothermal model would be more representative of the true behaviour, the changes observed are small and inclusion of heat effects would greatly complicate the model. Only the results will show whether neglecting heat effects still allow a representative model to be formed. The same is true for the final assumption of linear equilibrium.

5.3.2 Modelling of the adsorption column

5.3.2.1 Mass Balances

The conventions shown in fig. 5.4 state that the velocity moving from end 1 to end 2 is positive, where end 1 is the longer piston end (on the left side). With these conventions in mind the overall mass balance over the column can be written as:

$$-D_L \frac{\partial^2 C_T}{\partial z^2} + \frac{\partial(C_T v)}{\partial z} + \frac{\partial C_T}{\partial t} + \frac{(1-\varepsilon)}{\varepsilon} \sum_i \frac{\partial q_i}{\partial t} = 0 \quad (5.1)$$

and for each component i the component mass balance is expressed as:

$$-D_L \frac{\partial^2 c_i}{\partial z^2} + \frac{\partial(c_i v)}{\partial z} + \frac{\partial c_i}{\partial t} + \frac{(1-\varepsilon)}{\varepsilon} \frac{\partial q_i}{\partial t} = 0 \quad (5.2)$$

From the ideal gas law:

$$\frac{P}{RT} = \sum_i c_i = C_T \quad (5.3)$$

$$\text{and } \frac{Py_i}{RT} = c_i \quad (5.4)$$

which implies the overall mass balance (5.1) can be simplified to give:

$$\frac{\partial v}{\partial z} = -\frac{1}{P} \frac{dP}{dt} - \frac{(1-\varepsilon)}{\varepsilon} \frac{RT}{P} \sum_i \frac{dq_i}{dt} \quad (5.5)$$

where all pressure gradient terms are neglected in line with the assumption (2) above.

Using (5.4) and substituting for the velocity gradient using (5.5) the component mass balance (5.2) is rewritten as:

$$D_L \frac{\partial^2 y_i}{\partial z^2} - \nu \frac{\partial y_i}{\partial z} + \frac{(1-\varepsilon)}{\varepsilon} \frac{RT}{P} \left[(y_i - 1) \frac{dq_i}{dt} + y_i \frac{dq_j}{dt} \right] = \frac{\partial y_i}{\partial t} \quad (5.6)$$

5.3.2.2 Equilibrium isotherm

The adsorption equilibrium between the gas and the adsorbed phase is assumed to be linear.

The solid phase concentration of component i in equilibrium with the gas phase is expressed as:

$$q_i^{eq} = K_i \frac{y_i P}{RT} \quad (5.7)$$

5.3.2.3 Mass transfer resistance

In its simplest form the linear driving force model can be written as:

$$\frac{dq_i}{dt} = k'_i (q_i^{eq} - q_i) \quad (5.8)$$

While for a noncyclic adsorption process Glueckhuaf showed that the mass transfer coefficient could be given simply by:

$$k'_i = \frac{15 D_p}{R_p^2} \quad (5.9)$$

More recent studies (Glueckauf (1955), Ragahavan et al. (1986) and Alpay et al. (1992)) have showed that for a cyclic process this parameter is cycle time dependant. In Chapter 2 of this study further analysis has showed that as cycle times increase a second parameter must be introduced to allow for the reduced adsorbent penetration. Investigations have shown that the introduction of this additional parameter is necessary when the dimensionless half cycle time, a , exceeds 1, where a is defined, for a flat plate, by:

$$a = \frac{D_e t_c}{l^2} \quad (5.10)$$

From the characterisation experiment results reported in table 3.3, the values for D_e/l^2 do not merit the introduction of the additional parameter at the cycle times under consideration (10-20rpm). This would not be the case if shorter cycle times (greater than 30rpm) were considered.

5.3.2.4 Boundary conditions

The boundary conditions for the component mass balances are dependent on the direction of gas flow at the column ends. In previous studies (Farooq et al, 1998; Arvind et al, 2002) this has given rise to six possible sets of the standard Danckwerts' boundary conditions. Here computational efficiency is enhanced by combining all the cases and writing these as:

$$D_L \frac{dy_i}{dz} \Big|_{z=0} = -\frac{(v_1 + |v_1|)}{2} (y_i - p_1 - y_i(0)) \quad (5.11)$$

and

$$D_L \frac{dy_i}{dz} \Big|_{z=L} = -\frac{(v_2 - |v_2|)}{2} (y_i - p_2 - y_i(L)) \quad (5.12)$$

An additional boundary condition is given as:

$$v(0) = v_1 \quad (5.13)$$

5.3.3 Modelling of the pistons

The velocities and concentrations at either end of the adsorbent column can be calculated using the overall and component mass balances

5.3.3.1 Overall mass balances for the pistons

By considering the material entering the piston as feed, leaving the piston as product and the material exchanged with the adsorption column the overall mass balance for piston 1 can be written:

$$\frac{dn_{p1}}{dt} = \frac{1}{RT} \frac{d(V_{p1}P)}{dt} = f_{f1}(t) - f_{p1}(t) - \frac{v_1 PA_c \epsilon}{RT} \quad (5.14)$$

where f_{f1} and f_{p1} are discontinuous functions representing the feed and product flows to and from the pistons. Rearranging (5.14) leads to:

$$v_1 = \frac{(f_{f1}(t) - f_{p1}(t))RT}{PA_c \epsilon} - \frac{V_{p1}}{PA_c \epsilon} \frac{dP}{dt} - \frac{1}{A_c \epsilon} \frac{dV_{p1}}{dt} \quad (5.15)$$

A similar expression for the velocity of the gas at end 2 can also be derived:

$$v_2 = -\frac{(f_{f2}(t) - f_{p2}(t))RT}{PA_c \epsilon} + \frac{V_{p2}}{PA_c \epsilon} \frac{dP}{dt} + \frac{1}{A_c \epsilon} \frac{dV_{p2}}{dt} \quad (5.16)$$

5.3.3.2 Component mass balances for the pistons

Since the assumption is made that each of the pistons is well mixed then the concentration in the pistons change only as a function of time, due to material entering and leaving. The component mass balances can therefore be written, for piston 1, as:

$$\frac{dn_{i,p1}}{dt} = \frac{1}{RT} \frac{d(V_{p1} P y_{i-p1})}{dt} = y_{i-f1} f_{f1}(t) - y_{i-p1} f_{p1}(t) - \frac{v_1 PA_c \epsilon y'_{ii}}{RT} \quad (5.17)$$

where

$$y'_{ii} = \begin{cases} y_{i-p1} & \text{if } v_i \geq 0 \\ y_i(0) & \text{if } v_i < 0 \end{cases} \quad (5.18)$$

This can be rewritten more compactly as:

$$\frac{d(y_{i-p1})}{dt} = \frac{(v_1 - |v_1|)A_c \epsilon}{2V_{p1}} (y_{i-p1} - y_i(0)) + \frac{f_{f1}(t)RT}{PV_{p1}} (y_{i-f1} - y_{i-p1}) \quad (5.19)$$

Similarly for piston 2 the component mass balance can be expressed as:

$$\frac{d(y_{i-p2})}{dt} = \frac{(v_2 + |v_2|)A_c \epsilon}{2V_{p2}} (y_i(L) - y_{i-p2}) + \frac{f_{f2}(t)RT}{PV_{p2}} (y_{i-f2} - y_{i-p2}) \quad (5.20)$$

5.3.3.3 Piston volume changes

To describe the displacements of the pistons the following expressions can be written, for piston 1;

$$D_{p1} = S_1 \left\{ 1 - \frac{1}{2} (1 - \cos(\omega t + \phi_1)) \right\} \quad (5.21)$$

and, for piston 2:

$$D_{p2} = \frac{S_2}{2} (1 - \cos(\omega t + \phi_2)) \quad (5.22)$$

where ω , the cycling frequency, = $2\pi/t_{cyc}$.

Therefore the cyclic volume displacements can be written as:

$$V_{p1} = A_p \left\{ S_1 - \frac{S_1}{2} (1 - \cos(\omega t + \phi_1)) \right\} + \frac{V_d}{2} \quad (5.23)$$

and

$$V_{p2} = A_p \left\{ \frac{S_2}{2} (1 - \cos(\omega t + \phi_2)) \right\} + \frac{V_d}{2} \quad (5.24)$$

where V_d represents the dead volume of the system, divided equally between the pistons.

5.3.4 Overall Mass Balance

The overall mass balance for the entire system can be written as:

$$MB = \frac{P}{P_0} - \frac{V_{p1}|_0 + V_{p2}|_0 + V_c + \frac{RT}{P_0} V_{ads} \sum_i \frac{\int q_{0i} - q_i dz}{L}}{V_{p1} + V_{p2} + V_c} \quad (5.25)$$

This offers an additional check that the equation set is consistent since, when in total reflux mode, then MB should equal zero.

5.3.5 Initial conditions

Where a time derivative exists, the parameter concerned must be initialised. Assuming that the system starts at equilibrium, initial conditions for the relevant parameters were defined as:

$$\begin{aligned} P(0) &= P_o & y_i(z,0) &= y_{io} \\ y_i - p_1(0) &= y_{io} & q_i(z,0) &= q_i^{eq} \\ y_i - p_2(0) &= y_{io} \end{aligned} \quad (5.26)$$

The entire mathematical model was then transferred to dimensionless form and the resulting equation set is shown in table 5.3

5.3.6 Direct steady state model

When cyclic steady state has been reached in a dynamic process it is true, by definition, that all variables have the same value at the start and end of the cycle. Utilising this a model was developed whereby all previous equations were discretised over a temporal domain, the total length of which being equal to the cycle time. The same technique was also used in Chapter 2 when considering both CSTR and PSA models, details can be found in sections 2.4.1.2 and 2.4.4.2. In the previous cases, fully discretising the model across the new temporal domain and replacing what were, in the standard dynamic model, initial conditions with periodicity conditions of the form:

$$x(z,0) = x(z,t_{cyc}) \quad \text{or} \quad x(0) = x(t_{cyc}) \quad (5.27)$$

led to correct representation of a steady state cycle. In the case of the Dual Piston Driven PSA at total reflux the periodicity conditions consisted a mixture of conditions such as (5.27) and overall and component balances. The balances are of the general form,

$$\begin{aligned} \text{Moles in gas}(t=0) + \text{Moles adsorbed}(t=0) &= \text{Moles in gas}(t'=0) + \text{Moles adsorbed}(t'=0) = \\ \text{Moles in gas}(t'=t_{cyc}) + \text{Moles adsorbed}(t'=t_{cyc}) \end{aligned} \quad (5.28)$$

where t is the standard time domain and t' the imposed domain. The number of moles in the system could therefore be defined using the original initial conditions of the standard model. The first of these conditions was obtained using (5.25). Rearranging the dimensionless form given in table 5.3 gives:

$$\Pi(t_{cyc}) = \frac{\text{Volp } 1(t=0) + \text{Volp } 2(t=0) + 1 + \text{psi} \sum_i \text{Intega}(t'=0) + \text{Integb}(t'=0) \left(\frac{q_{bo}}{q_{ao}} \right)}{\text{Volp } 1(t'=0) + \text{Volp } 2(t'=0) + 1} \quad (5.29)$$

In a similar manner the overall component mass balances can be determined. For component a , this implies:

$$\begin{aligned}
 & y_a - p_1(t'=0) \frac{V_{p1}(t'=0)P(t'=0)}{RT} + y_a - p_2(t'=0) \frac{V_{p2}(t'=0)P(t'=0)}{RT} + \\
 & \frac{V_c P(t'=0)}{RT} \int_0^L y_a(t'=0) \frac{dz}{L} + \frac{V_{ads} P(t'=0)}{RT} \int_0^L q_a(t'=0) \frac{dz}{L} = \\
 & y_{ao} \frac{V_{p1}(t=0)P_o}{RT} + y_{ao} \frac{V_{p2}(t=0)P_o}{RT} + y_{ao} \frac{V_c P_o}{RT} + \frac{V_{ads} P_o}{RT} \int_0^L q_{ao} \frac{dz}{L}
 \end{aligned} \tag{5.30}$$

and for component b:

$$\begin{aligned}
 & y_b - p_1(t'=0) \frac{V_{p1}(t'=0)P(t'=0)}{RT} + y_b - p_2(t'=0) \frac{V_{p2}(t'=0)P(t'=0)}{RT} + \\
 & \frac{V_c P(t'=0)}{RT} \int_0^L y_b(t'=0) \frac{dz}{L} + \frac{V_{ads} P(t'=0)}{RT} \int_0^L q_b(t'=0) \frac{dz}{L} = \\
 & y_{bo} \frac{V_{p1}(t=0)P_o}{RT} + y_{bo} \frac{V_{p2}(t=0)P_o}{RT} + y_{bo} \frac{V_c P_o}{RT} + \frac{V_{ads} P_o}{RT} \int_0^L q_{bo} \frac{dz}{L}
 \end{aligned} \tag{5.31}$$

Converting to dimensionless form, using the parameters and groups defined in table 5.3, gives:

$$\begin{aligned}
 & y_a - p_1(t'=0) \bar{V}_{p1}(t'=0) \Pi(t'=0) + y_a - p_2(t'=0) \bar{V}_{p2}(t'=0) \Pi(t'=0) + \\
 & \Pi(t'=0) \int_0^1 y_a(t'=0) dZ + \Pi(t'=0) psi \int_0^L Q_a(t'=0) dZ = \\
 & y_{ao} (\bar{V}_{p1}(t=0) + \bar{V}_{p2}(t=0) + 1) + psi
 \end{aligned} \tag{5.32}$$

and

$$\begin{aligned}
 & y_b - p_1(t'=0) \bar{V}_{p1}(t'=0) \Pi(t'=0) + y_b - p_2(t'=0) \bar{V}_{p2}(t'=0) \Pi(t'=0) + \\
 & \Pi(t'=0) \int_0^1 y_b(t'=0) dZ + \Pi(t'=0) psiqboqao \int_0^L Q_b(t'=0) dZ = \\
 & y_{bo} (\bar{V}_{p1}(t=0) + \bar{V}_{p2}(t=0) + 1) + psiqboqao
 \end{aligned} \tag{5.33}$$

To complete the fully discretised model the following periodicity conditions, defined using the dimensionless parameters, were required:

$$Q_i(z,0) = Q_i(z, t_{cyc}), \quad y_i(z,0) = y_i(z, t_{cyc}), \tag{5.34}$$

$$y_a - p_2(0) = y_a - p_2(t_{cyc}), \quad y_b - p_2(0) = y_b - p_2(t_{cyc})$$

5.3.7 Initial experimental observations and model refinement

Throughout the mathematical modelling it was assumed that the pressure was the same throughout, in both the pistons and the column. Since the experimental study that the model

was designed to simulate incorporated a structured adsorbent column then this assumption was thought to be justified. Experiments were carried out using two differently sized activated carbon monoliths, details of which can be found in Chapter 3 section . Figs. 3.5 and 3.6, demonstrating how the monoliths were assembled, show that while the smaller column consisted of many monolith sections in series, the large column assembly included five 10cm long monoliths joined together with small lengths of 1/8" piping. The full experimental study undertaken using the Dual Piston Driven PSA rig is detailed in Chapter 4. Initial runs undertaken using helium were first used to consider the behaviour of the rig in non adsorbing mode. Dimensionless pressure profiles obtained from pressure transducers positioned at each piston on either of the end of the column are shown in Chapter 4 fig. 4.16 for these runs. The figure demonstrates that when the large column was placed in the system there was a small but noticeable amplitude and lag difference between the two pressures recorded. Since this was not the case for the smaller column then it was reasoned that resistance in the pipework joining the individual monoliths was to blame. A similar observation was made by Arvind et al (2002), although in their study the resistance was thought to be the result of restrictions in the piping between the pistons and the columns. Using the resistance model that was developed, the model described in section 5.3 above can be adapted to make it more appropriate for simulating runs involving the large column. Rather than writing one model for the entire system, the model was rewritten expressing each piston, monolith and piping section as individual units. The correct number of units necessary to describe the whole system were then joined together. Figure 5.5 shows diagrammatically how this is achieved. The mathematical model for each piston and monolith section remains as before, except that the pressure is obtained from the previous and/or subsequent piping sections. The piping sections is made up of two simple equations:

$$\frac{\nu P_c A c \epsilon}{RT} = f(P_p - P_c) \quad (5.35)$$

$$\text{and } \frac{\nu P_c}{RT} = \frac{\nu_p P_p}{RT} \quad (5.36)$$

where v = velocity of gas entering pipe section, v_p = velocity of gas leaving pipe section, P_c = pressure before the pressure drop, P_p = pressure after the drop and f = a friction factor to be determined by comparison between experimental and simulated results.

Once the equations were converted to dimensionless form and the connections made between the unit models then the large column model was complete. Due to the nature of the unit based software used for modelling then this was a straightforward alteration to make.

5.3.8 Equilibrium, kinetic and system parameters

All the parameters required for the simulations are detailed in table 5.4, where the base case values for the rig specific parameters, such as stroke length, are given. All equilibrium and kinetic values are taken from the results of the characterisation experiments described in Chapter 3.

5.3.9 Numerical Simulation

With all the equations for the standard model, direct steady state model and adapted large column model in dimensionless form the next step was to ascertain the most suitable numerical integration method. The work of Alpay et al (1993), looking at a Rapid PSA system, showed that, for a cyclic adsorption process involving flow reversal, orthogonal collocation on finite elements was the most appropriate spatial discretisation technique. To decide what order of polynomial would be required for the collocation method and how many finite elements would be suitable a series of simulations runs were carried out. The order of the polynomial was kept at 3 while the number of elements were increased until no discernable difference could be seen in the results obtained. Eight elements were found to be sufficient. When simulating the large column, in order to maintain the same level of accuracy, the elements were distributed across each of the column sections. When considering the direct steady state model discretisation is required in both the spatial and temporal domains. While the same method could be used for the spatial domain a 2nd order

backward finite difference method with 30 elements was found to be most suitable for the time domain. In order to check this, results were compared to those obtained using the standard dynamic model and found to agree. Simulations were undertaken using gPROMS, an extremely user friendly modelling package in to which the equation set can be written directly. On choosing the discretisation technique the software converts the PDAEs into DAEs and solutions can be generated.

Unlike in previous studies, where the average velocity profile in the column has been calculated, gPROMS made it possible to solve for the true velocity profile. Although Arvind et al. (2002) suggest that using the averaged profile and interpolating the velocity values is a reasonable assumption, this is only an approximation and the mass balance breaks down as the number of simulated cycles increases, especially for the total reflux mode. Therefore the fact that the explicit velocity profile can be included in the present model without complication is an important development.

5.4 Concluding Remarks

Three mathematical models have been developed to represent the experimental Dual Piston Driven PSA system. The first is relevant to the small column, and can be easily adapted to simulate non adsorbing, total reflux and feed-product runs. Secondly an adaptation to this model was made, using a complete discretisation approach, so that a direct steady state solution could be obtained.

In the third large column model allowance has been made for true configuration of the column and small pressure drops that occur in the small pipe work sections are included. By breaking the column into units resistance terms could be introduced over the piping sections, the scale of the resistance to be determined by matching the experimental non-adsorbing runs.

Simulations can now take place, using the adsorption parameters derived from the characterisation experiments of Chapter 3, to establish the validity of models.

Chapter 5: Figures

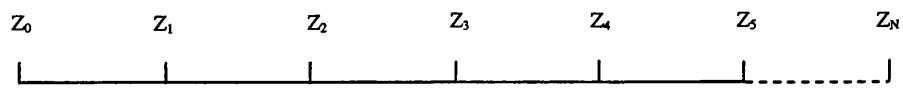


Fig.5.1 Finite element grid for z domain

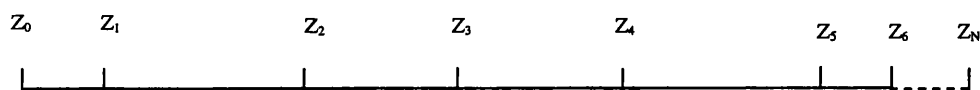


Fig.5.2 Orthogonal collocation grid for z domain

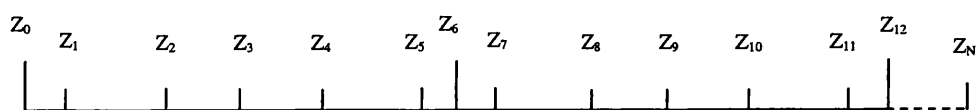


Fig.5.3 Orthogonal collocation on finite elements grid for z domain

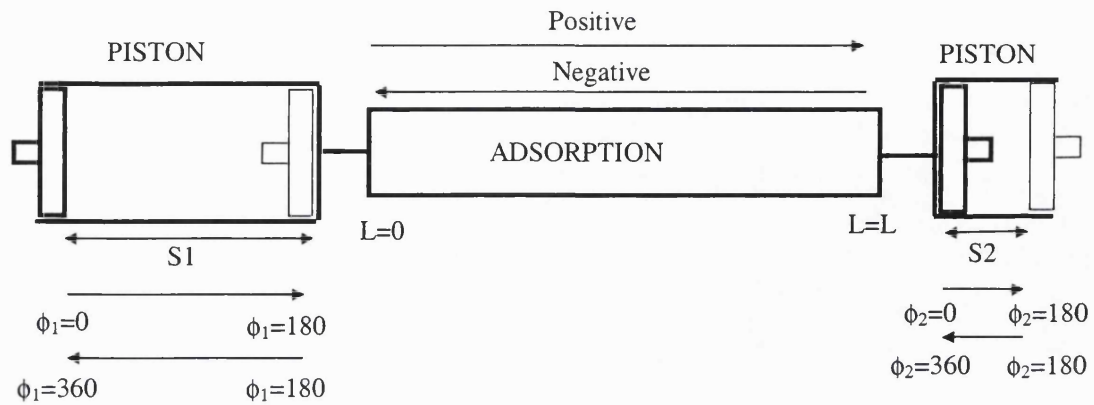


Fig. 5.4 Conventions used for Dual Piston Driven PSA Modelling

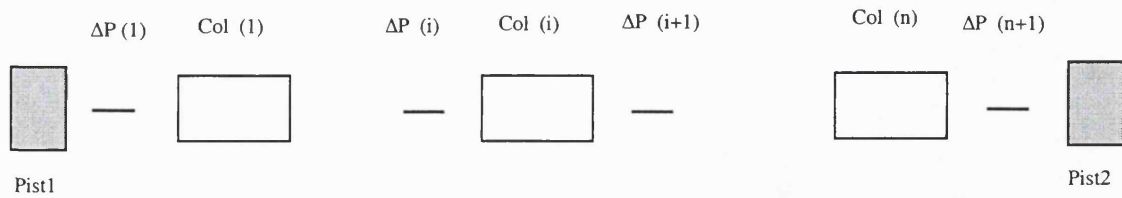


Fig. 5.5 Representation of Large Column Model

Chapter 5: Tables

Study	System of interest	Absorbable component in inert carrier?	Flow assumption?	Linear equilibrium?	Linear driving force model?	Isothermal?	Pressure drop allowed for?	Modelling method
Mitchell and Shendalman (1972)	CO ₂ /He Silica gel 6-16 mesh	Yes	Plug Flow	Yes	Yes	Yes	No	Method of characteristics
Chihara and Suzuki (1983)	Air drying Activated alumina	Yes	Plug Flow	Yes	Yes	No	No	Crank-Nicolson implicit method
Ragahan, Hassan and Ruthven (1985)	CO ₂ /He Silica gel 6-16 mesh	Yes	Axially dispersed plug flow	Yes	Yes	Yes	No	Finite difference/ Orthogonal collocation
Ragahan, Hassan and Ruthven (1986)	Air drying Activated alumina	Yes	Axially dispersed plug flow	No, Langmuir	No, full diffusion model	Yes	No	Orthogonal collocation

Table 5.1 Modelling assumptions for a selection of Pressure Swing Adsorption studies

Study	System description	Experimental work?	Adsorbent bed	Pressure drop	Mathematical Model?	Solution method	Type of isotherm	Heat considerations	Mass transfer assumption
Ericksson , 1979 (Patent)	Single piston PSA, O ₂ from air separation	Yes (no performance data given)	"crystallised, zeolitic molecular sieve"	-	No	-	-	-	-
Keller and Kuo, 1982 (Patent)	Dual piston PSA – The Molecular Gate, a) air b) H ₂ /CH ₄ separation	Yes	a) 40/80mesh 13X molecular sieve b) 40/80mesh bead activated carbon	-	No	-	-	-	-
Sakoda et al (1992)	Single piston PSA, Oxygen enrichment	Yes	40-80, 80-150 & 200-325 mesh 5A zeolite particles	Yes	Yes	Not disclosed	Not disclosed	Not disclosed	Not disclosed
Suzuki et al. (1996)	Single piston PSA, CO ₂ removal from stack gas	Yes	80-150mesh 5A zeolite and modified Y zeolite	Yes, Ergun equation used	Yes	Stop and go method	Linear/ Langmuir	Isothermal	LDF (using Nakao and Suzuki (1982)
Singh and Jones (1997)	Dual piston PSA,	Yes	40-60 mesh10X zeolite and VSA II	Yes	Yes	Control volume approach	Langmuir	Non isothermal	LDF
Farooq et. al, (1998)	Dual piston PSA, CO ₂ /N ₂ separation	Yes	Parallel passage contactor, activated carbon fiber sheets	No	Yes	Orthogonal collocation and Gear's method	Linear/Langmuir	Isothermal	LDF (using Nakao and Suzuki (1982)
Arvind et al. (2002)	Dual piston PSA, Air separation	Yes	8-12 mesh 13X zeolite particles	Yes*	Yes		Langmuir	Isothermal	LDF

Table 5.2 Key features and assumptions of published piston driven PSA work

Dimensionless parameters:	Dimensionless groups:
$\Pi = \frac{P}{P_0}$, $V = \frac{v}{v_o}$, $Volp1 = \frac{V_{p1}}{V_c}$, $Volp2 = \frac{V_{p2}}{V_c}$, $Q_i = \frac{q_i}{q_{io}}$, $Q_i^{eq} = \frac{q_i^{eq}}{q_{io}}$, $\tau = \frac{t}{t_c}$, $Z = \frac{z}{L}$, $Velo1 = \frac{v_i}{v_o}$, $Velo2 = \frac{v_2}{v_o}$, $F_{f1} = f_{f1}\left(\frac{RTt_c}{V_c P_0}\right)$, $F_{f2} = f_{f2}\left(\frac{RTt_c}{V_c P_0}\right)$, $F_{p1} = f_{p1}\left(\frac{RTt_c}{V_c P_0}\right)$, $F_{p2} = f_{p2}\left(\frac{RTt_c}{V_c P_0}\right)$	$aps1 = \frac{A_p S_1}{V_c}$, $aps2 = \frac{A_p S_2}{V_c}$, $t_c = \frac{L}{v_o}$, $Pe = \frac{v_o L}{D_L}$, $\bar{\omega} = \omega t_c = 2\pi$, $VD = \frac{V_d}{V_c}$, $mtc_i = \frac{k_i L}{v_o}$, $psi = \frac{(1-\epsilon) RT}{P_o} q_{ao} = \frac{(1-\epsilon)}{\epsilon} K_a y_{ao}$ for initial eqm.
COLUMN equations	
Overall mass balance:	
$\frac{\partial V}{\partial Z} = -\frac{1}{\Pi} \frac{d\Pi}{d\tau} - \frac{psi}{\Pi} \sum_i \frac{dQ_i}{d\tau}$	Mass transfer
Component mass balances:	
$\frac{1}{Pe} \frac{\partial^2 y_a}{\partial Z^2} - V \frac{\partial y_a}{\partial Z} + \frac{psi}{\Pi} \left[(y_a - 1) \frac{dQ_a}{d\tau} + y_a \frac{dQ_b}{d\tau} \frac{q_{b0}}{q_{ao}} \right] = \frac{\partial y_a}{\partial \tau}$	$\frac{dQ_i}{d\tau} = mtc_i (Q_i^{eq} - Q_i)$
$\frac{1}{Pe} \frac{\partial^2 y_b}{\partial Z^2} - V \frac{\partial y_b}{\partial Z} + \frac{psi}{\Pi} \left[(y_b - 1) \frac{dQ_b}{d\tau} \frac{q_{b0}}{q_{ao}} + y_b \frac{dQ_a}{d\tau} \right] = \frac{\partial y_b}{\partial \tau}$	$Q_i^{eq} = \frac{y_i \Pi}{y_{io}}$
Boundary conditions	
$\frac{dy_i}{dZ} \Big _{z=0} = -\frac{(Velo1 + Velo1)}{2} Pe (y_i - p_i - y_i(0))$	
$\frac{dy_i}{dZ} \Big _{z=L} = -\frac{(Velo2 - Velo2)}{2} Pe (y_i - p_2 - y_i(L))$	
$V(0) = Velo1$	
PISTON 1 equations	
Piston volume	
$Volp1 = aps1 \left\{ 1 - \frac{1}{2} (1 - \cos(\bar{\omega} \tau + \phi_1)) \right\} + \frac{VD}{2}$	PISTON 2 equations
Overall mass balance on piston	
$Velo1 = \frac{(F_{f1} - F_{p1})}{\Pi} - Volp1 \frac{1}{\Pi} \frac{d\Pi}{d\tau} - \frac{dVolp1}{d\tau}$	Piston volume
Component mass balance in piston	
$Volp1 \frac{d(y_i - p_1)}{d\tau} = \frac{F_{f1}}{\Pi} (y_i - f_1 - y_i - p_1) + \frac{(Velo1 - Velo1)}{2} (y_i - p_1 - y_i(0))$	$Volp2 = aps2 \left\{ 1 - \frac{1}{2} (1 - \cos(\bar{\omega} \tau + \phi_2)) \right\} + \frac{VD}{2}$
Overall mass balance on piston	
$Volp2 = -\frac{(F_{f2} - F_{p2})}{\Pi} + Volp2 \frac{1}{\Pi} \frac{d\Pi}{d\tau} + \frac{dVolp2}{d\tau}$	
Component mass balance in piston	
$Volp2 \frac{d(y_i - p_2)}{d\tau} = \frac{F_{f2}}{\Pi} (y_i - f_2 - y_i - p_2) + \frac{(Velo2 + Velo2)}{2} (y_i(L) - y_i - p_2)$	
Overall Mass Balance:	
$\Pi - \frac{Volp1 _0 + Volp2 _0 + 1 + psi \sum_i Intega + Integb (\frac{q_{b0}}{q_{ao}})}{Volp1 + Volp2 + 1} = MB$	
With $Intega = \int_0^L (1 - Q_a) dZ$ and $Integb = \int_0^L (1 - Q_b) dZ$	

Table 5.3 Dimensionless DP- PSA models

Parameter	Value used in simulation
<i>Large column:</i>	
Length (cm)	50
Diameter (cm)	2.9
Bed voidage	0.69
Adsorption equilibrium constant, CO ₂	45
Adsorption equilibrium constant, N ₂	1.1
LDF Mass transfer coefficient, CO ₂	1.32
LDF Mass transfer coefficient, N ₂	13.2
<i>Small column:</i>	
Length (cm)	45
Diameter (cm)	1.56
Bed voidage	0.71
Adsorption equilibrium constant, CO ₂	50
Adsorption equilibrium constant, N ₂	1.3
LDF Mass transfer coefficient, CO ₂	2.76
LDF Mass transfer coefficient, N ₂	27.6
<i>Rig parameters</i>	
Piston diameter (cm)	3.94
Stroke length of piston 1 (cm)	15.24
Stroke length of piston 2 (cm)	4.34
Phase angle of piston 1 (deg)	0
Phase angle of piston 2 (deg)	90

Table 5.4 Parameters used for simulations

Chapter 6

A Comparison Between the Mathematical and Experimental Studies of the Dual Piston Driven PSA

6.1 Introduction

When considering the potential of a new or adapted technology for a particular process the emphasis is on exploring its capabilities as fully as possible. To do this a representative mathematical model of the system and an experimental study can be used. Comparing the simulated results obtained to those found experimentally allows refinement of the mathematical model and leads to a more representative simulation. The model can then be used to consider the feasibility of the process of choice. It is important, however, not only to consider the performance of the system under idealised experimental conditions but also to make consideration of the additional “real life” issues. A true decision about the practical and economic potential of the system can then be made.

In the previous two chapters an experimental study and mathematical description of a dual piston driven PSA system for the separation of CO₂ from N₂ are presented. In this chapter the results obtained from both studies, for all classes of experiment performed, are compared. Initially the agreement between profiles obtained when non adsorbing runs were undertaken is considered, and the relevance of the derived models examined. Comparison between adsorbing total reflux runs then shows how the models behave under these conditions. Finally agreement between profiles from the feed and product runs is evaluated. To conclude the feasibility of the system for the removal of CO₂ from flue gas is questioned, considering both the idealised performance from the experimental study and the problems that might be encountered in an industrial context.

6.2 Comparison of results

In order to verify the Dual Piston Driven Pressure Swing Adsorption models, derived in Chapter 5, the profiles from the experimental study of Chapter 4 are used. Validation of the models occur in steps so that any differences can be looked at in detail and the reasons for the discrepancies suggested. Comparisons are made for both of the columns used in the experimental study, for non adsorbing, total reflux adsorbing and feed and product adsorbing runs. The system behaviour in the total reflux mode when key parameters are varied is also investigated. For reference a diagram of the test rig may be found in Chapter 4 fig. 4.7.

6.2.1 Total Reflux Helium Runs

The first analysis was undertaken looking at the rig characteristics in the absence of adsorption and feed and product streams. To perform the simulations the rig specific parameters remained at their default values, as shown in table 5.4, while the dimensionless parameters associated with adsorption were adapted.

6.2.1.1 *Empty system runs*

Under empty system conditions the rig was operated with the absence of an adsorption column and hence, in the simulation, V_c was set to zero. As stated in Chapter 4 section 4.5.1.1, under these conditions the pressure profiles could be evaluated numerically and the dead volume of the rig calculated from equation (4.3). This also allows the first validation step for the modelling technique. Since there is no resistance encountered then the small column model of section 5.3 could be used, with parameters altered accordingly. Fig. 6.1 shows the dimensionless pressure profiles obtained from experiment, calculation and simulation for 10 rpm. As would be expected there is no difference between the calculated and simulated profiles; they are exactly coincident. This shows that the model equations and modelling method employed are correct under these conditions. Fig. 6.2 shows the same profiles for 20 rpm. The calculated and simulated profiles agree well both at 10 and 20 rpm

with those from experiment suggesting that the model is representative for the system without the column.

6.2.1.2 Small column non adsorbing runs

Again the small column model of section 5.3 was employed for these simulations. Validation of the modelling approach could again be achieved by adapting equation (4.3) to include the column volume such that:

$$\frac{P}{P_0} = \frac{V_{P1} + V_{P2} + V_D + V_C}{V_{P1}|_0 + V_{P2}|_0 + V_D + V_C} \quad (6.1)$$

Comparing the calculated, simulated and experimental dimensionless pressure profiles, as shown in fig. 6.3, again shows that the calculated and simulated profiles are coincident. The good agreement between these profiles and that obtained from experiment demonstrates how well the model predicts the non adsorbing small column behaviour. There is a slight discrepancy between the results but only because the simulation gives very smooth profiles while the profiles from the rig are less so. Even when well lubricated it seems the piston movement is not totally unhindered. In addition the pressure transducers are extremely sensitive so any external interferences such as the rig moving slightly due to cycling can have an effect.

6.2.1.3 Large column non adsorbing runs

As discussed in section 4.5.1.2 initial observations of the experimental results using the large column indicated that the modelling would need to reflect the pipework resistance encountered when using this column. Across each of the small sections joining each of the individual columns, shown in fig. 3.5, a small pressure drop due to friction was assumed. The challenge therefore was in finding the associated friction factor for each section. Since the sections are of equal length then the friction is assumed to be equal in each. Taking just one of the column sections then the model is the same as if the small column were used. As this has been shown to be valid then it would suggest that on obtaining the friction factors for the

piping sections the large column model could be verified. In order to find the factors a trial and error method was used. Matching the simulated pressure profiles with guessed “f” values to the experimental profiles repeatedly until they agreed gave the final correct “f” values. The skill in obtaining the match is in ensuring that the maximum and minimum pressures at each piston are reached at the same point in the cycle for both the experimental and simulated profiles, i.e. that the lag incurred was the same. In addition the difference between the two simulated maximums and minimums must agree with that observed experimentally i.e the amplitude differences agreed. Fig. 6.4 shows the experimental and simulated pressure profiles, with a value of 0.1 used for the dimensionless “f” values, as well as the result that would have been obtained if equation (6.1) or the small column model (with large column parameters) would have been used. Clearly while a good estimate is obtained by doing the latter, it is the large column simulation including the resistance terms that gave profiles closest to those found experimentally. Again there are slight differences between the experimental and simulated profiles but these, as before, are likely to be due to comparing the slightly uneven experimental data with the smooth simulation results. The large column model can therefore be seen to be verified.

6.2.2 Total Reflux Adsorbing Runs

Although total reflux runs have no practical use they can be used, first to further verify the mathematical model, and also to look at key operating parameters prior to feed and product runs being carried out. For these runs the behaviour of the mathematical model is compared to that of the experimental rig. The separation performance as well as the pressure profiles can be examined. In all cases discussed the base case values, as presented in table 5.4, were used in the simulations.

6.2.2.1 Small Column Total Reflux Adsorbing runs

Considering first the dimensionless pressure profiles obtained from experiment and simulation, fig. 6.5 shows how the results compare for cycle speed of 10rpm. Again, as for

the non adsorbing case, agreement is good and there is little difference between the two lines. Fig. 6.6 shows the mole fraction % profiles for CO₂ at end 1 of the piston, closest to the piston with the larger stroke length, from both experiment and simulation for 10rpm. While the model does not accurately predict the transient behaviour it can predict the profile at steady state well. This is further supported by the result from the direct steady state simulation, described in section 5.3.6, for 10rpm, also shown on the figure. The disagreement between the results during the transient stage may be linked to the temperature gradient incurred over the entire run. Although slight, the rise in temperature due to the piston movement could cause the approach to steady state to differ to that encountered when the system is assumed to be isothermal. Additionally there is some uncertainty in the experimentally obtained kinetic and mass transfer parameters, especially those found for nitrogen, and also some uncertainty in the axial Peclet number used within the mathematical model. Because of the complex gas flow within the column estimating the Peclet number is difficult and an adjustable parameter had to be employed. With these potential sources of error in mind the match between experiment and simulation is very good and hence the model for the small column when adsorbing is verified.

6.2.2.2 Large Column Total Reflux Adsorbing runs

Dimensionless pressure profiles, from a simulation of the large column model and an experimental run for 10rpm, are shown in fig. 6.7. There is some small disagreement between the dimensionless pressure profiles obtained but this is in line with that observed in the non adsorbing case. Another cause for the disagreement could be the “f” values used. These were estimated from the non adsorbing case where the gas used was helium. Clearly for the adsorbing runs the gas was a N₂/CO₂ mixture, with a different viscosity to helium, therefore there is some uncertainty involved in using these factors.

Profiles of the mole % of CO₂ at end 1 for the same simulated and experimental runs are given in fig. 6.8. and show that, again, agreement between the results is good, especially at

steady state. Again both temperature effects and the possible errors in the equilibrium and kinetic parameters derived in Chapter 3 could have led to the lack of matching the transient section. The large column parameters are at most risk of being incorrect since only the chromatographic method was used to establish the values. While analysis of the first moment, as described in section 3.4.1, tends to allow good estimation of the adsorption equilibrium constant K, the second moment, calculated in order to determine the diffusional time constant, is more prone to error. This is especially the case if there are any disturbances affecting the experimental data.

6.2.3 Small Column Total Reflux Parametric Study

In order to evaluate the best system set up, in terms of separation capability, for the rig the key parameter values must be explored. This was achieved during the experimental study the results of which are shown in section 4.5.2.2. As well as trialling two different columns, the parameters considered were phase angle difference, stroke lengths of the pistons, cycle time and the temperature of the column.

6.2.3.1 Effect of column choice

As found from the experimental study, and confirmed in figs. 6.6 and 6.8 discussed above, the composition profiles have shown that using the small column led to better separation performance. For the large column the mole fraction of CO₂ in the N₂ rich stream at steady state was 0.052 while for the small column it was 0.022. Since the feed contains a mole fraction of 0.1 CO₂ then, when using the large column, only 50% of the CO₂ is removed while, when using the small column, nearly 80% of the CO₂ is removed. Since the results, found from experiment, are confirmed using simulations then the behaviour must be due to the adsorption specific parameters. By considering the results from the chromatography and ZLC experiments, as can be seen in table 3.3, better kinetic and mass transfer characteristics were demonstrated for the small column, which has smaller passage widths and thinner cell walls and hence its separation capability is better.

6.2.3.2 *Effect of cycle time*

Considering the effect of cycle time fig. 6.9 shows the composition profiles at piston 1 obtained for the small column at 5, 10 and 20 rpm, both from experiment and simulation. Again agreement between the two sets of data is very good. In both cases at 20 rpm the separation is markedly worse than at 10 rpm, however there is little difference between the results obtained at 5 and 10 rpm. Mass transfer limitations therefore suggest that cycling should not exceed 10 rpm, which is lower than was hoped. Arvind et al (2002) chose to run their air separation using the DP-D PSA at 30 rpm but did note that decreasing the cycle time, hence increasing productivity, did lower purity. It was suggested smaller adsorbent particles could be used but obviously this would lead to a higher pressure drop which may compromise the efficiency of the unit in terms of power requirement. Experimental results show that, although there is a pressure drop across the large column due to piping resistance, there is no pressure drop across the monolithic columns since the passages are wide enough not to restrict the gas flow. This feature does, however, seem to compromise separation. It would be ideal to engineer an optimised monolith such that the passages were small enough and walls thin enough to allow unhindered gas flow but optimum kinetic and mass transfer characteristics can be achieved, at an increased cycle time. It should also be remembered, of course, that the columns contain 60% binder and other materials and 40% activated carbon. The added supporting materials are required to help give the monoliths structure and strength, however separation capabilities could be greatly improved if the amount of activated carbon present were increased.

6.2.3.3 *Effect of Stroke length*

Fig. 6.10 shows the simulated and experimental steady state compositions of CO₂ at piston 1 as a function of stroke length ratio. Experimental points are shown for 3 different ratios for the large column and for just 1 ratio for the small column. Simulated results for the small column are also presented and show how the separation improves as the stroke length ratio increases; 20% more CO₂ is removed at S1/S2 = 3.5 as compared to that removed when

$S1/S2=1$. It has been suggested (Thaeron, 1996) that the optimum stroke length ratio ($S1/S2$) is that nearest to the ratio between the equilibrium constants of the two gases present. Since the equilibrium constant for N_2 is much smaller than that for CO_2 then this would correspond to the largest difference between stroke lengths, $S1$ and $S2$ used. It would also suggest that separation should improve as the stroke length increases and therefore the experimental point at $S1/S2 = 1.5$ is clearly anomalous.

6.2.3.4 Effect of phase angle difference and column temperature

Fig. 6.11 shows the simulated and experimental steady state compositions of CO_2 at piston 1 as a function of phase angle difference. The experimental results obtained when using the large column at room temperature, and also when the column temperature was lowered to around zero, are shown. A single point is shown for the small column at the phase angle difference of 90 deg which was shown from large column experiments to be the optimum. Simulated results for the small column across phase angle differences of 0-180 deg are also presented, along with a single simulated point for the large column at 90 deg.

Clearly considering the large column results when the ice bath was used the separation improved markedly. This is due to the fact that as the temperature lowers the equilibrium constants increase as discussed in Chapter 3 section 3.4.2. Using the heat of adsorption the value of K at a room temperature of 23 °C for CO_2 in N_2 may be 40, whereas at 0 °C this quadruples to around 160 °C. Modelling the cooled system would therefore require adjustment to the equilibrium constants. In a practical, industrial sense it would be unlikely that the column would be cooled in this way. Sensibly it would only be at all likely if redesigning the column, as described in section 6.2.3.2 above, did not improve the properties of the column enough for it to be useful.

The simulated points for the small column are of interest as the profile obtained clearly shows that a minimum exists corresponding to maximum separation. Looking closer at the region

between 90deg and 135deg an optimum phase angle difference was identified at 104 deg. Determining the optimum in this way is an example of how the results of the model and experiment can be used together to determine an optimum system set up for a particular application.

6.2.4 Small column Feed-Product runs

Experimental and simulated runs including feed and product streams were undertaken using both the small and large columns, retaining the same parameter values, such as cycle time, stroke length ratio and phase angle difference, used in the total reflux cases. However since the total reflux results indicated that using the small column led to better separation performance analysis was focused on this column. The ideal parameters identified in the total reflux study, listed in table 4.5, were used throughout the feed and product experiments. The optimum steady state flowrates in and out of the system were determined experimentally as 120cc/min, 100cc/min and 20cc/min for the feed flowrate and product flowrates, Ff1 and Ff2, respectively.

The approach to cyclic steady state observed experimentally is shown below in figs. 6.12 and 6.13 in terms of the dimensionless pressure and end 1 CO₂ composition profiles. The first approach taken to include the feed and product streams in the simulation involved simply expressing the discontinuous stream flowrates as continuous functions at their steady state values. This was the technique used by Arvind et al (2002).

Clearly, as found by Arvind et al (2002) using this approach led to very poor agreement between the experimental and simulated pressure profiles. Once capturing of the transient period has failed then the steady state period can also not be accurately modelled. The agreement between the experimental and simulated profiles for the mole fraction of CO₂ at end 1, demonstrated in fig. 6.13, however is reasonably good.

In the real system the flowrates are variable and, to reflect this, a second technique was employed, which involved recognising that, during the transient period, flowrates into and out of the test rig were different for each cycle. Until cyclic steady state was reached the number of moles into and out of the system did not balance. In order to simulate this behaviour the experimental profiles were examined. By estimating the flowrates into and out of the system for each cycle the simulated profiles could be matched, by trial and error, to those obtained experimentally. Once cyclic steady state was considered to have been reached the steady state values calculated from the test runs could be used in the model.

This method is shown to provide a pressure profile, shown in fig. 6.12, which is very close to that observed experimentally, as would be expected from the matching process. The important issue, however, is how the composition profiles compare.

Clearly from fig. 6.12 the overall pressure is seen to drop and once cyclic steady state is reached the average operating pressure is less than 1. Since the operating pressure affects the adsorption and desorption capability of the system then the composition profiles should intuitively be different for the two modelling approaches. While this is the case it seems that as steady state is approached the first of the two techniques used, in which steady state flowrate values are assumed throughout, gives a composition profile which agrees better with the experimental results. Even so it can be seen that neither approach captures the observed profiles especially well, and even less so in the transient period. This is due in part to the extreme difficulty in adjusting flowrates at start up to ensure optimal steady state operation of the rig, but also to the modelling technique adopted. Clearly expressing the feed and product streams as the continuous functions is an inaccurate approximation and a model in which the streams are discontinuous, where models of the valves and buffer tanks could be included, could better capture the process. From a model such as this, incorporating the real flows into and out of the system, there would be the potential for full optimisation of the unit's operation.

One area that was not investigated was where in the column the feed should be fed. As Arvind et al (2002) highlight by feeding at one end one product is always being contaminated with the feed stream. Extensive concentration analysis was not carried out at piston 2 of the rig either experimentally or through simulations. The limited samples taken showed that the CO₂ in this stream never exceeded 35%. While, when using the small column, a relatively large 60% of the CO₂ had been removed from the N₂ rich stream the concentration of CO₂ in the other product stream was disappointing. Using the same principles behind distillation technology it would be ideal to feed in the middle of the column thus creating stripping and enriching sections. Keller and Kuo (1982) when considering air separation using Dual Piston Driven PSA did undertake experiments where the feed was introduced in the middle of the column. The result was that two high purity product streams were produced, containing 100% CH₄ in one and 99% H₂ in the other. Using an arrangement much like the large column this possibility could be investigated experimentally, and, making a simple alteration to a large column type model, a mathematical model could also be developed.

6.2.5 Modelling efficiency

The efficiency of the modelling package and techniques used to solve the mathematical model can be examined by considering the length of time required to perform the simulations. Table 6.1 shows the length of time to complete each of the different classes of run using a Intel Pentium 4 1700MHz computer. As the model becomes more complex the time taken for execution is longer, hence the non adsorbing cases are completed fastest with the large column adsorbing model being the slowest. Even so the longest time taken is still only 20 minutes. Comparing the time taken for the direct steady state solution of the small column adsorbing total reflux model to be found with time required for the traditional model to reach steady state the direct method is faster as expected.

6.3 Practical considerations

With reasonable agreement established between the experimental and modelling studies the feasibility of using a Dual Piston Driven PSA unit for removing CO₂ from stack gas emissions must now be addressed. In order to achieve this some comparison must be made with existing CO₂ removal technologies, the most common of these being absorption using MEA. When considering a process on an industrial scale the challenges faced are of a different nature to those encountered on a pilot scale. Some of these are discussed qualitatively below.

6.3.1 Flue gas pre-treatment.

Within the study the gas supplied for treatment has simply contained 10%CO₂ and 90%N₂. However, in reality, the flue gas is likely to contain around 3-10%CO₂, 70-75%N₂, 1-14%O₂ and 7-17% steam as well as up 300 ppmv NO_x and 280 ppmv SO_x. Within an MEA process, such as that described by Simmonds et al (2002) in which a proprietary amine system of Fluor's named the Econamine FGSM process is discussed, chemical inhibitors must be introduced. These counter the effects of corrosion and degradation of the MEA caused by oxygen in the flue gas. Looking at the dual piston system while corrosion of equipment could still be a problem activated carbon is unaffected by oxygen.

Since activated carbon is hydrophobic then moisture has little detrimental effect, in fact, a study by Suzuki et al (1997), in which the effect of moisture on hydrophilic and hydrophobic adsorbents was examined, showed that the separation was completely unaffected when the hydrophobic adsorbent was used in a moist atmosphere.

For any amine system the amount of SO_x and NO_x introduced is extremely important. Both of these components react to produce salts which degrade the solvent. For the Econamine FGSM process pre-treatment is required to reduce the levels to 10ppmv for SO_x and 20ppmv for

NO_x. Both processes are extremely costly making up 15% of the entire plant cost. SO_x and NO_x at the concentrations present in flue gas, however, would not pose a significant problem for a physical adsorbent such as activated carbon.

6.3.2 Power

Fig. 6.14 shows the generalised units required to remove CO₂ from flue gas once pre-treatment has been achieved. One of the first requirements is that the temperature of the gas be reduced. One of the most effective and more economic ways of doing this is by using a direct contact cooler. The main advantage this offers is that steam generation can be achieved and hence some energy can be recovered to be used elsewhere. When considering the abatement technologies for the MEA the main energy requirement is in providing the heat to strip to solvent after absorption. For the dual piston process the highest energy demand is that required to move the pistons. However since they are out of phase there are points within the cycle where, with careful design, expansion in one piston can help to drive compression in the other. This would not be trivial to design but may offer an opportunity to recover some energy.

6.3.3 Design and manufacture

One of the most important barriers to commercialising the dual piston process is that it is a novel technology. The out of phase pistons, although in many ways similar to traditional compressors, may be prone to manufacturing problems. It is the pistons and how large and/or how many it is reasonable to manufacture that limits the scaled up size of the technology.

6.3.4 Use and storage of CO₂

While the experiments and simulations undertaken have shown that, for the cases analysed, only a fairly pure nitrogen product stream can be achieved it is envisaged that by altering the column so that feeding occurs in the middle the CO₂ stream can be enriched. The question, however, is what can be done with this separated CO₂. In the plant design in the MEA study

(Simmonds et al, 2002) it was anticipated that the CO₂ rich stream could be used for enhanced oil recovery (EOR). In order that the stream can be used the purity must be in excess of 90%. Other industries that use CO₂ include drinks and chemicals manufacturers. The demand on purity in these cases is very high, greater than 99%. In addition CO₂ can simply be stored. Studies are considering placing CO₂ in the ocean in saline aquifers and in unmineable coal seams, where it can aid the production of methane by displacing it. In both these cases the purity demand is less stringent than for manufacturing purposes and is closer to that required for EOR. It remains to be seen whether the dual piston driven system can achieve this.

6.4 Concluding Remarks

Analysis of a dual piston driven PSA system for the separation of CO₂ has been undertaken. An experimental study using a test rig was carried out, whereby various key parameters could be examined, including consideration of two adsorption columns available. These columns consisted of activated carbon monoliths, designed to give uniform, narrow passages for gas to pass along. A general, isothermal mathematical model was derived, but proved, after initial investigations, to be suitable for only one of the columns. Therefore an alternative model was proposed which was able to take account of piping resistances created by the column structure of the large column. In addition, a model was also developed to give direct steady state solutions, therefore saving computation time. Results from simulated and experimental total reflux runs showed that experimental pressure and concentration profiles for the small column could be well predicted from both the dynamic and cyclic steady state models; the slight disagreement was attributed to possible heat effects and poor estimation of kinetic and mass transfer parameters. Runs assuming feed and product streams flowing into and out of the system were undertaken using the small column. Analysis showed that the model assumption of continuous flowrates for the streams led to incorrect predictions, especially for the simulated pressure profiles.

The emphasis throughout has been to verify that the mathematical models correctly describe the system behaviour and, with this confirmed, these models can now be hopefully be further developed to represent an optimised CO₂ separation using DP-D PSA on a larger scale. Significance will obviously need to be placed on separation performance, in terms of achievable productivity and purity, as well as minimising power efficiency, in order to make DP-D PSA an attractive option for CO₂ separation in the future.

Chapter 6: Figures

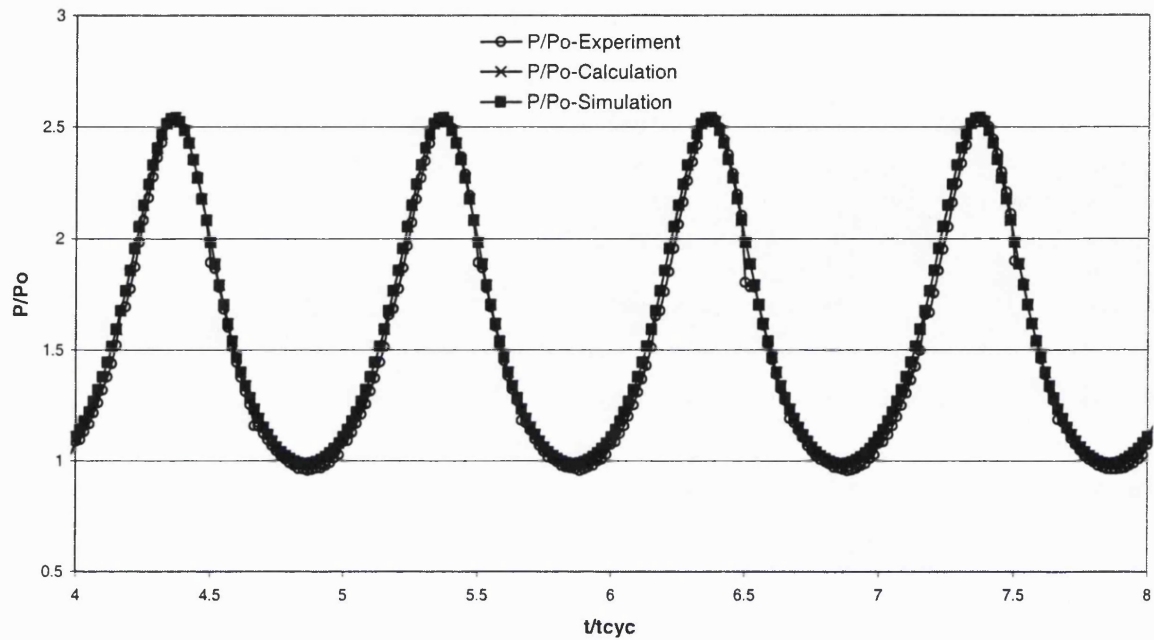


Fig.6.1 Comparison between experimental observations, calculated and simulated dimensionless pressure profiles for the empty system (Helium total reflux run at 10rpm $\phi_1=0$ $\phi_2=\pi/2$ S1=15.24cm S2=4.34cm)

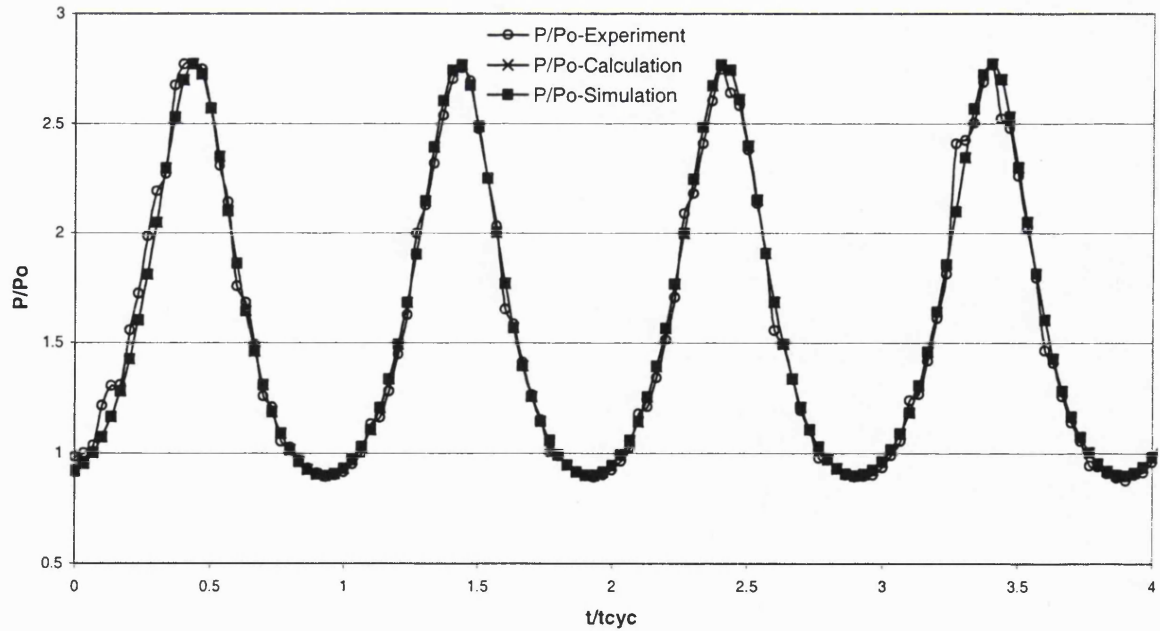


Fig.6.2 Comparison between experimental observations, calculated and simulated dimensionless pressure profiles for the empty system (Helium total reflux run at 20rpm $\phi_1=0$ $\phi_2=\pi/2$ S1=15.24cm S2=4.34cm)

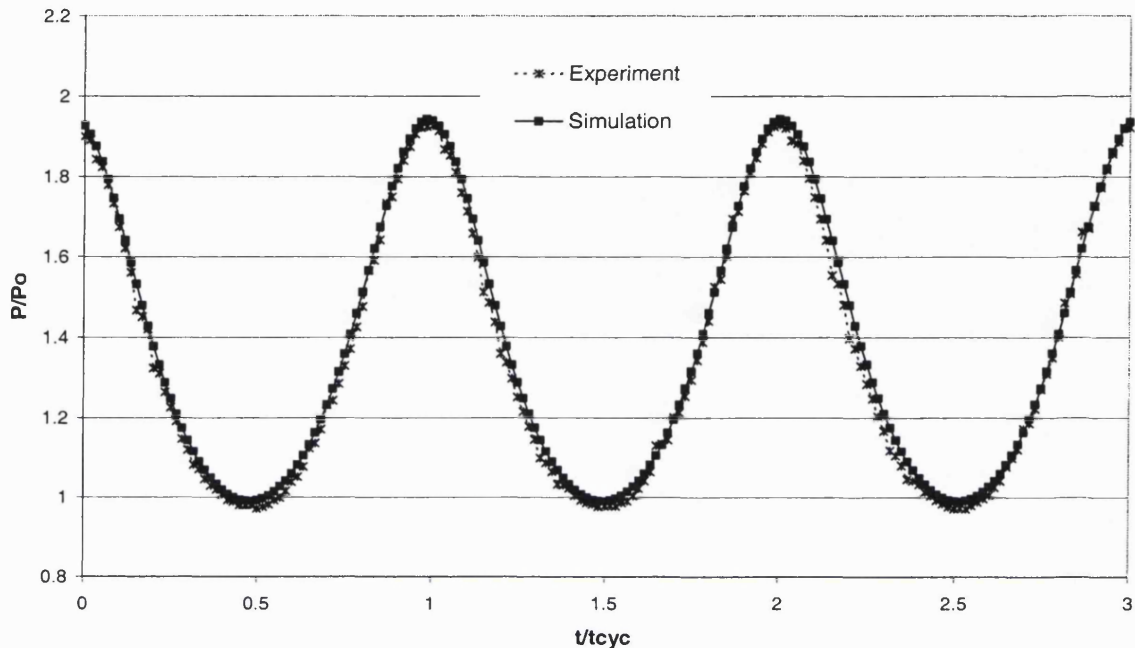


Fig.6.3 Comparison between experimental observations and simulated dimensionless pressure profiles for the small column (Helium total reflux run at 10rpm $\phi_1=0$ $\phi_2=\pi/2$ S1=15.24cm S2=4.34cm)

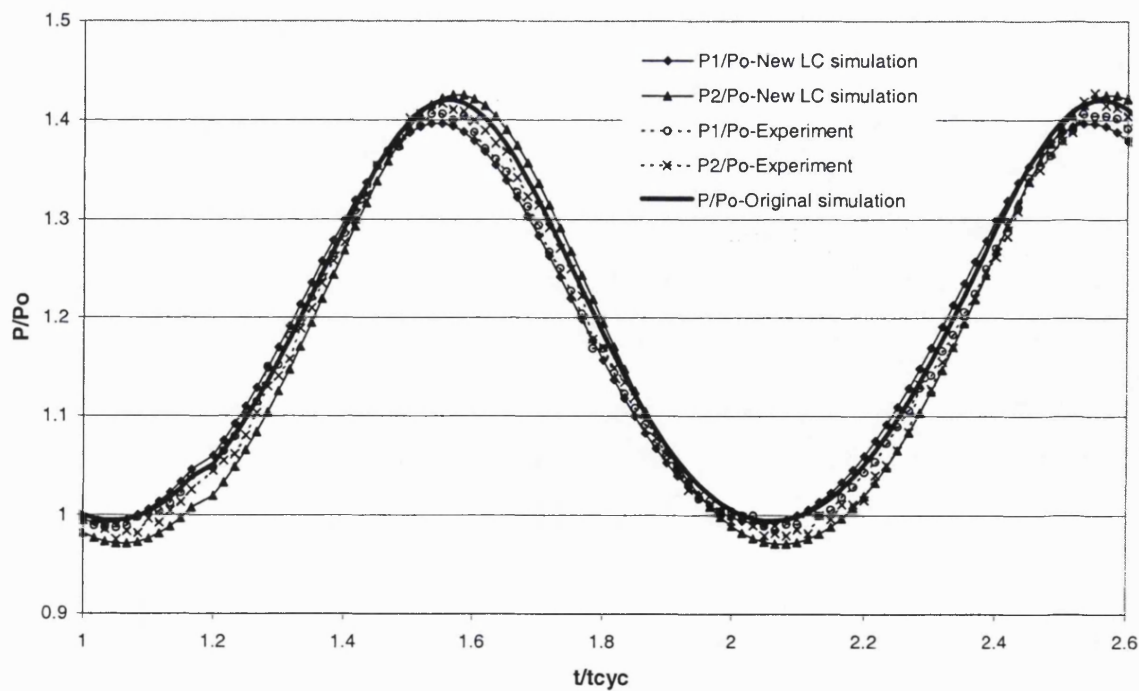


Fig.6.4 Dimensionless pressure profiles comparing experimental and simulated dimensionless pressure profiles using the original and new model approaches for the large column (Helium total reflux run at 10rpm, $\phi_1=0$ $\phi_2=\pi/2$ S1=15.24cm S2=4.34cm)

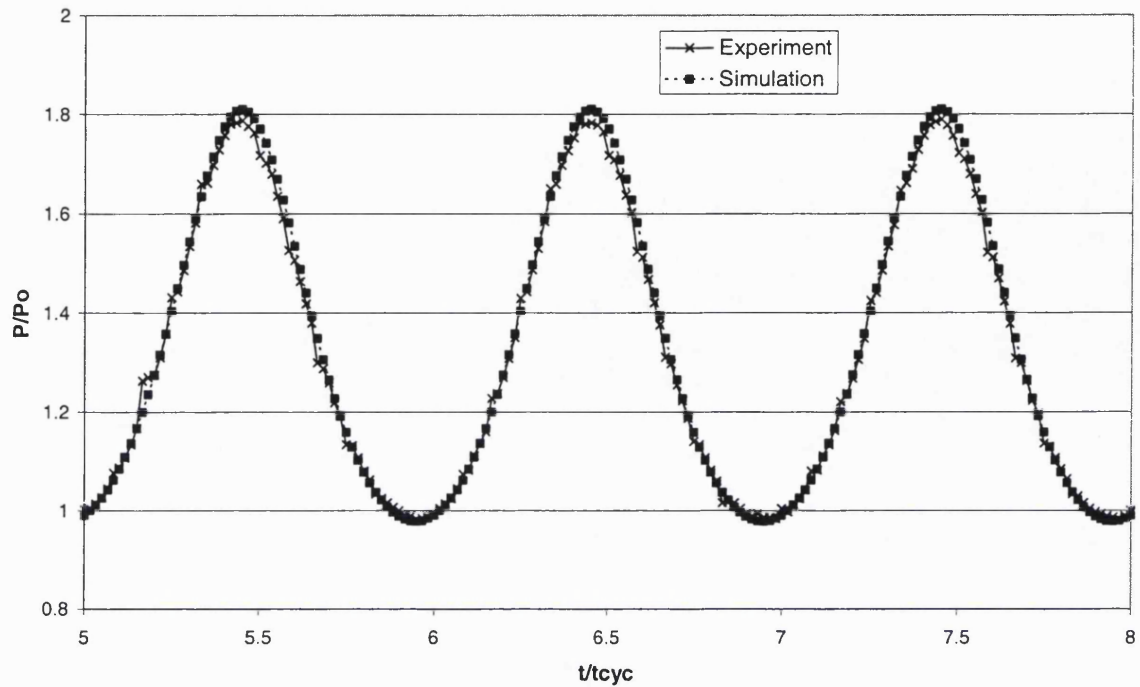


Fig.6.5 Comparison between experimental and simulated dimensionless pressure profiles when adsorbing (Small column, CO_2/N_2 total reflux runs at 10rpm $\phi_1=0$ $\phi_2=\pi/2$ $S1=15.24\text{cm}$ $S2=4.34\text{cm}$)

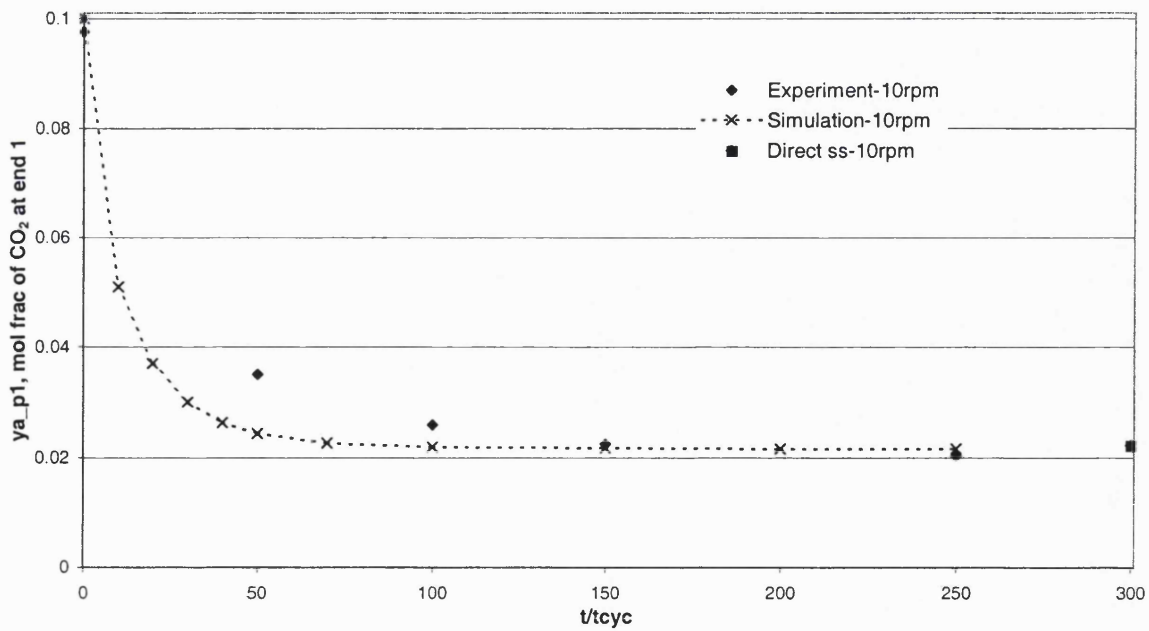


Fig.6.6 Experimental and simulated composition profiles for CO_2 at end 1 for the small column (CO_2/N_2 total reflux runs $\phi_1=0$ $\phi_2=\pi/2$ $S1=15.24\text{cm}$ $S2=4.34\text{cm}$)

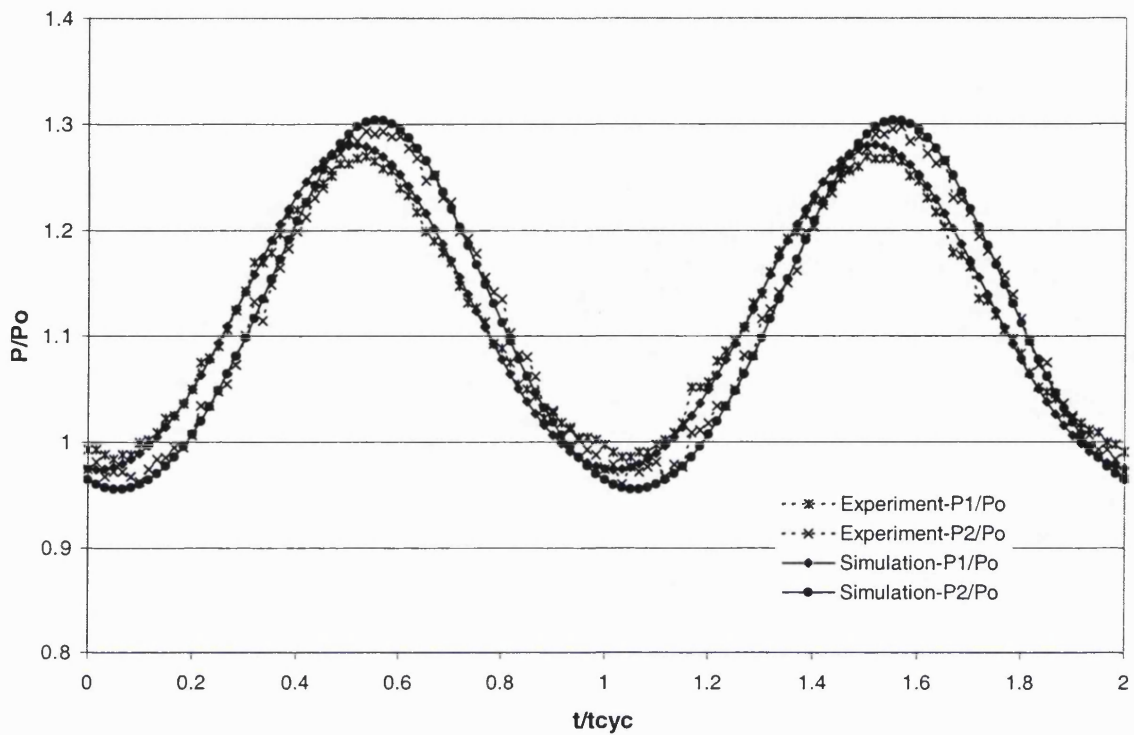


Fig.6.7 Experimental and simulated dimensionless pressure profiles for the large column when adsorbing (CO_2/N_2 total reflux runs $\phi_1=0$ $\phi_2=\pi/2$ $S1=15.24\text{cm}$ $S2=4.34\text{cm}$)

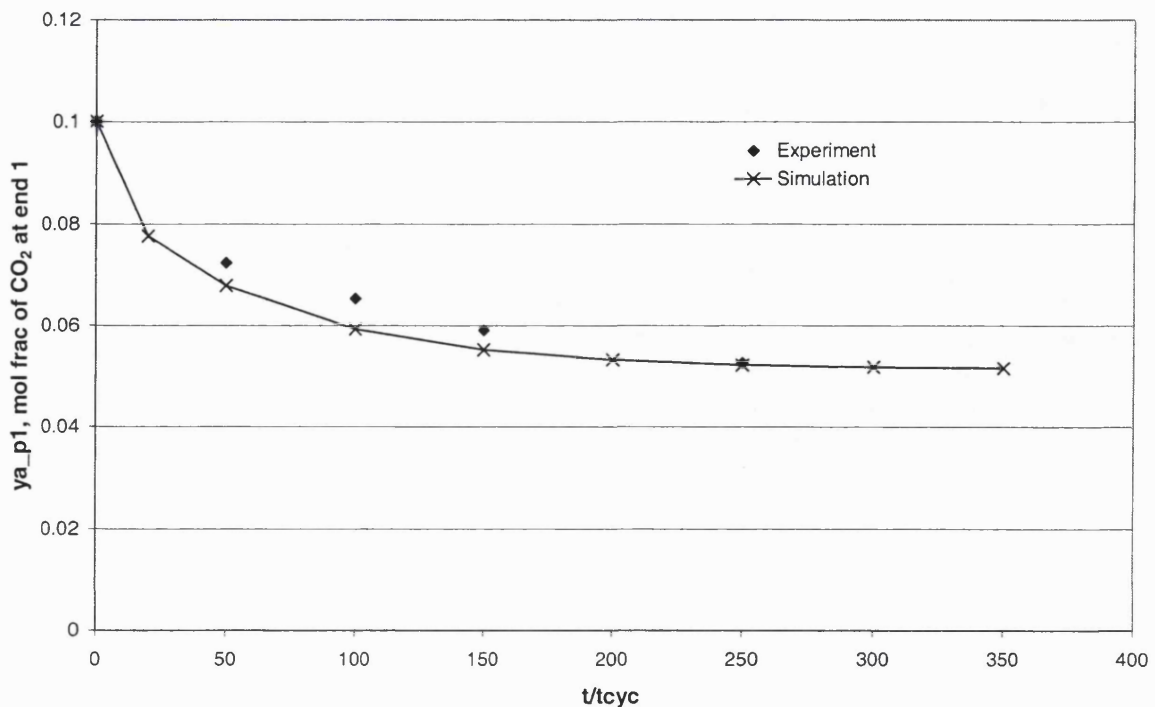


Fig.6.8 Experimental and simulated composition profiles for CO_2 at end 1 for the large column (CO_2/N_2 total reflux runs $\phi_1=0$ $\phi_2=\pi/2$ $S1=15.24\text{cm}$ $S2=4.34\text{cm}$)

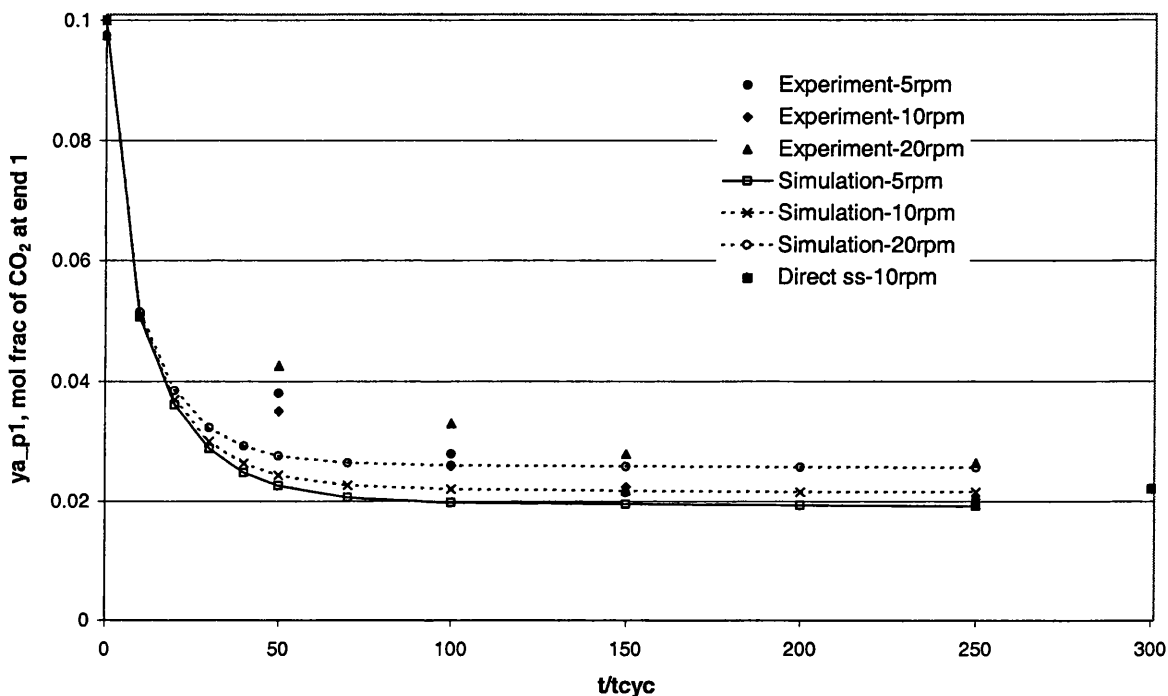


Fig.6.9 Comparison between experimental and simulated concentration profiles for CO_2 at end 1 for runs undertaken at 5, 10 and 20 rpm (Small column CO_2/N_2 total reflux runs $\phi_1=0$ $\phi_2=\pi/2$ $S1=15.24\text{cm}$ $S2=4.34\text{cm}$)

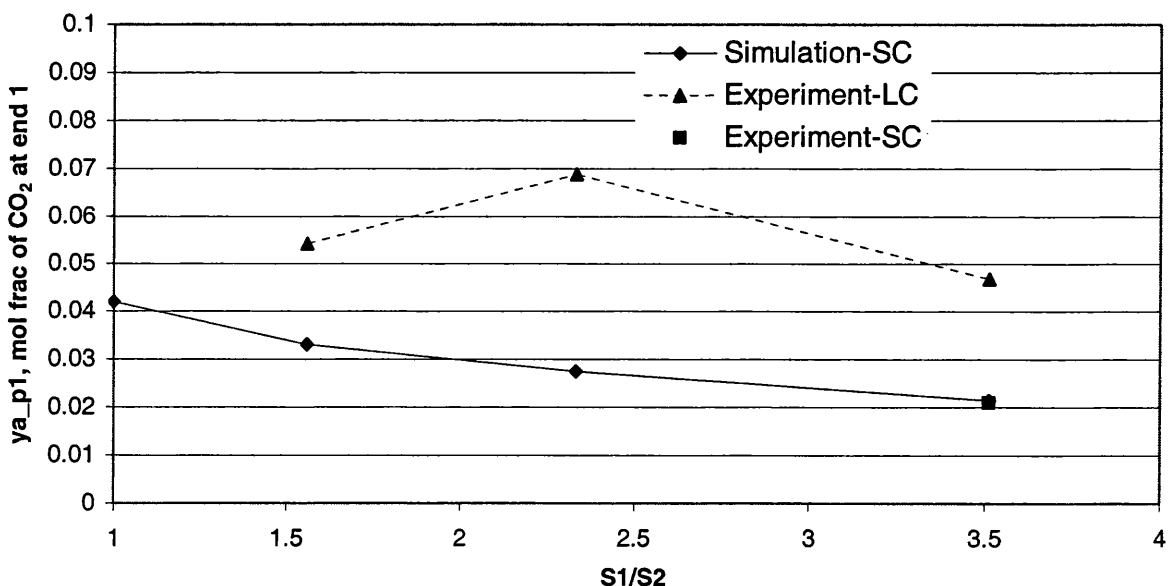


Fig.6.10 Effect of changing stroke length ratio on the concentration of CO_2 at end 1, shown experimentally for the large column. Simulated results for the small column, along with one experimental result, is shown. (CO_2/N_2 total reflux runs $\phi_1=0$ $\phi_2=\pi/2$ $S2=4.34\text{cm}$)

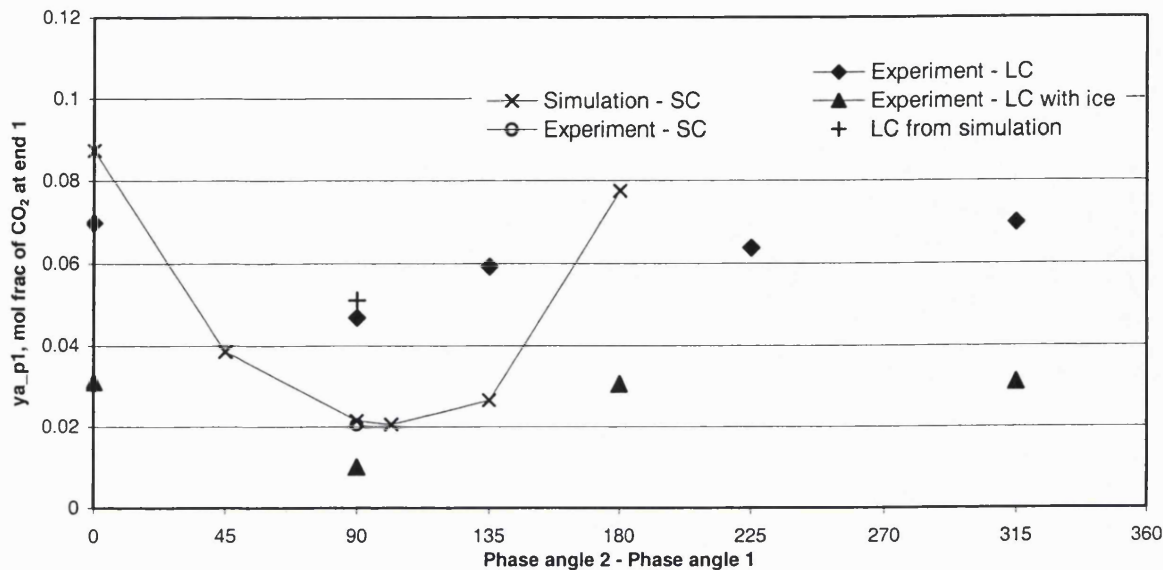


Fig.6.11 Effect of changing ϕ_2 on the concentration of CO₂ at end 1, shown experimentally for the large column and the large column in an ice bath. Simulated results for the small column along with one experimental result are shown. A simulated large column point is also shown (CO₂/N₂ total reflux runs $\phi_1=0$ S1=15.24cm S2=4.34cm)

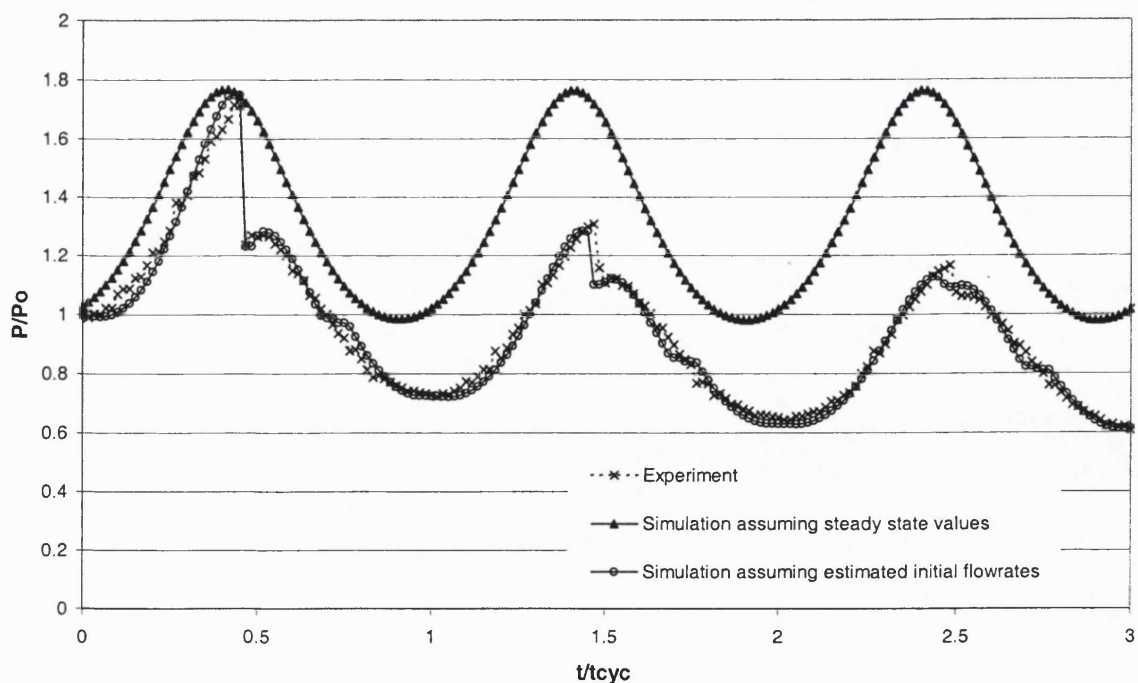


Fig.6.12 Comparison between experimental and simulated dimensionless pressure profiles for the small column (Ideal feed-product operating procedure used CO₂/N₂ feed-product runs $\phi_1=0$ $\phi_2=\pi/2$ S1=15.24cm S2=4.34cm)

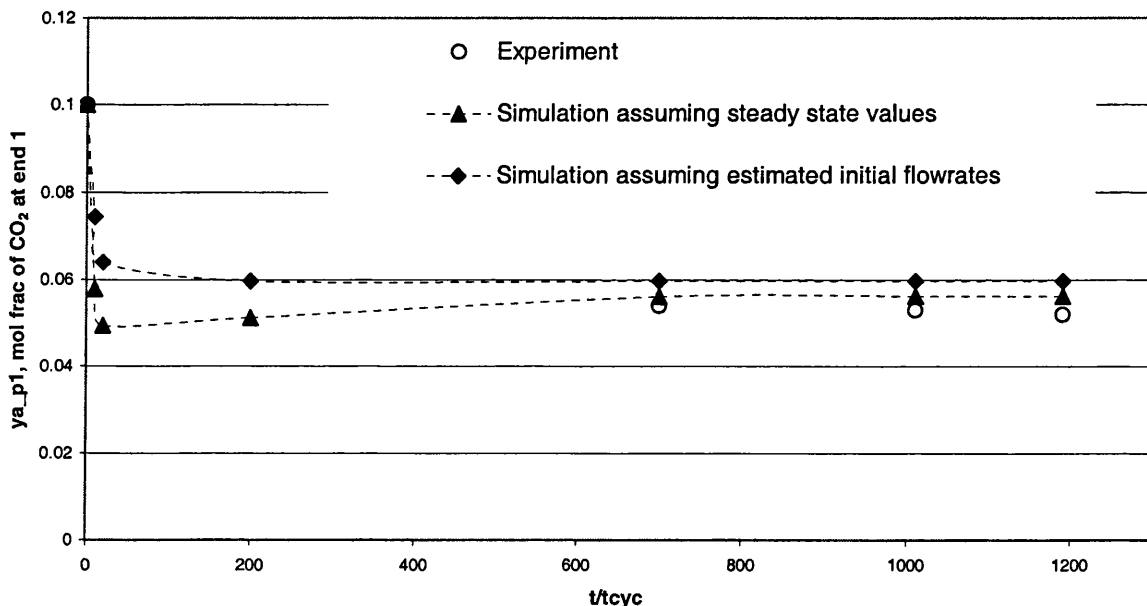


Fig.6.13 Comparison between experimental and simulated concentration profiles for CO₂ at end 1 for the small column (Ideal feed-product operating procedure used CO₂/N₂ feed-product runs $\phi_1=0$ $\phi_2=\pi/2$ S1=15.24 S2=4.34cm)

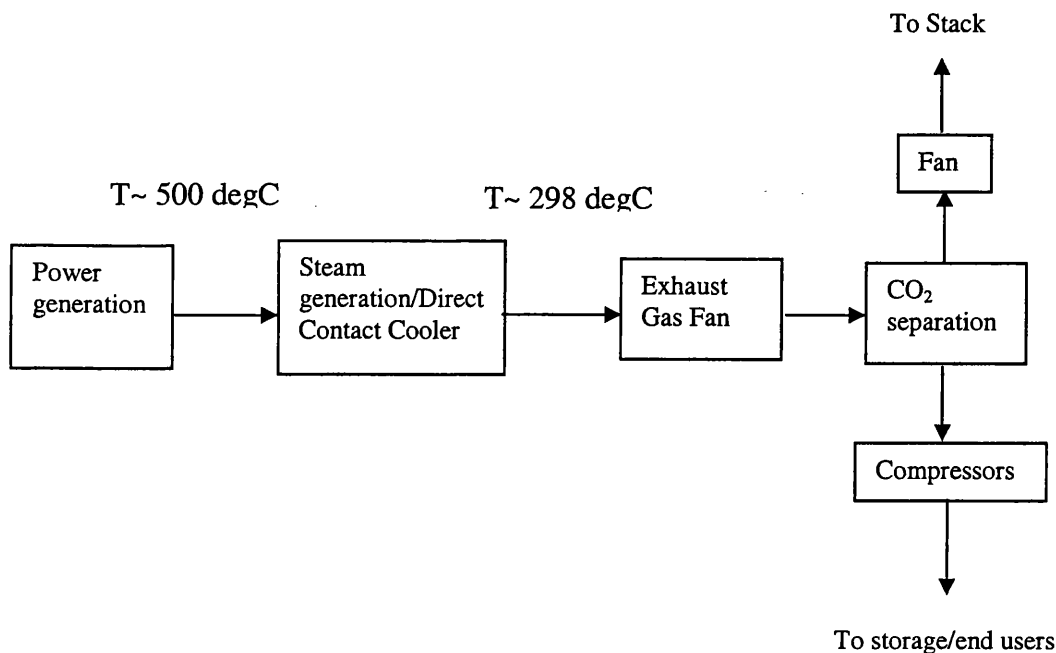


Fig. 6.14 General layout of CO₂ separation system

Chapter 6: Tables

Model	Simulation time (minutes)
Empty system	1
Non adsorbing Small column	1
Non adsorbing Large column	1.5
Adsorbing Total Reflux Small column	12
Adsorbing Total Reflux Small column (Direct Steady State solution)	7
Adsorbing Total Reflux Large column	20
Adsorbing Feed-Product Small column	14

Table 6.1 Comparison between computing times for all simulations

Chapter 7

Conclusions and Recommendations for Further Work

7.1 Conclusions and contributions of the thesis

The overall aim on this thesis was to obtain a verified mathematical model that could be used to exploit the dual piston driven PSA system for CO₂ separation. To achieve this aim the thesis has comprised:-

- A theoretical evaluation of the LDF equation for cyclic adsorption processes
- Experimental studies of
 - Two activated carbon monolithic adsorption columns and,
 - A dual piston driven PSA test system
- Mathematical modelling of the dual piston driven PSA system
- Comparison and analysis of the experimental and mathematical DP-D PSA studies

The conclusions and contributions from each element are discussed below.

7.1.1 LDF approximation for cyclic adsorption processes

In past studies the LDF approximation, used to represent mass transfer in adsorption processes, was shown to require some refinement when utilised for fast cycle adsorption systems. While it offers considerable benefits in terms of reducing simulation effort over the diffusion model this benefit is lost if it is inaccurate. Attempts to make the model more widely applicable for cyclic processes had focused on introducing a cycle time dependant parameter, which is used to modify the standard equation. This was originally introduced by Glueckhauf (1955) with a slightly different approach being taken by Alpay and Scott (1992), who derived their adjustment by using penetration theory.

Through the work detailed in Chapter 2, this thesis has shown that using a single parameter correction term means that only one of the adsorbed or bulk concentration profiles can be simulated correctly. As such the work of Chapter 2 is the first such study to identify the

requirement for two parameters, which ensure that both concentration profiles can be accurately simulated. These parameters were derived from an analytical phase lag and amplitude difference study, suggested by control theory. The use of phase lag and amplitude difference was also exploited by Rodrigues and Dias (1998), who chose to represent their findings using Bode diagrams.

The first of these parameters is similar to that developed by Nakao and Suzuki (1983), simply correcting for cycle time, whereas the second relates to the degree of penetration of the adsorbent. The newly developed model was shown to be highly successful and widely applicable. It was verified using both simple and more complex cyclic adsorption case studies, which included PSA system simulations, and was shown to be universally applicable to cyclic adsorption systems, so long as geometry and different diffusion mechanisms were taken into consideration. The second parameter also proved to be useful for calculating the penetration depth, which could be of importance when the adsorbent is being designed. The model was also shown to dramatically improve the computation speed and gave results of a high accuracy.

7.1.2 Adsorbent characteristics

The adsorption columns, analysed in Chapter 3, were selected for their potential efficiency and effectiveness in performing the CO₂ separation within the Dual Piston Driven systems. While there have been studies considering monolithic columns for PSA applications (notably Li et al, 1998), previous Dual Piston Studies have used either packed columns (Raghavan et al, 1986, Arvind et al, 2002) or a parallel passage contactor (Ruthven and Thaeron, 1996). The monolithic columns, constructed from a mixture of approximately 40% activated carbon and 60% binder, were characterised using chromatography and ZLC techniques. Analysis of the chromatography results was undertaken using first and second moment techniques, where diffusional time constants were derived from the second moment using an approach by

Spangler (2001). This approach was adapted from a study considering miniature rectangular chromatography columns and has not previously been explored in this way.

Results obtained from the adsorption equilibrium constants from the two experimental methods compared well, especially when corrected for the slight experimental temperature difference between the methods. The effective diffusivities obtained did not however agree as closely. Since the analysis of chromatography results using the second moment technique is often prone to errors then the result from the ZLC experiments are more reliable.

7.1.3 Experimental study of a Dual Piston Driven PSA system

Chapter 4 detailed the set up, operation and obtained profiles from the Dual Piston Driven PSA test rig. In terms of the set up, taking into account the observations from previous studies (specifically Arvind, 2002), pipework was kept to a minimum to avoid undesirable pressure drops in the system.

Initial non adsorbing experimental runs were undertaken employing the two characterised monolithic columns described in Chapter 3. These experiments showed that due to small pipework sections joining the composite sections of one of the columns there was a pressure drop incurred across this column as a whole. This was particularly undesirable since the choice of monolithic columns was made to reduce the pressure drop, and hence the energy requirement, on the system to a minimum. There was also a consequence for the mathematical modelling.

Separation performance was analysed using both of the columns where a gas mixture of 10% CO₂ and 90% N₂ was introduced to the Dual Piston Driven PSA system. Initially total reflux experiments were undertaken. These had the advantage of helping to identify an optimal system set up, when the system was operating at its' most efficient in total reflux mode, with disturbances from feed and product streams eliminated. A parametric study showed that the

column with the smaller monolith dimensions led to better separation but at cycle times lower than was hoped (5-10rpm). This disappointing performance was considered to be due to the high amount of binder in the columns.

Feed and product runs were undertaken using the more effective of the two columns and these experiments were also able to provide some ideal operating conditions.

The main aim of the experiments was to provide some data that would help to verify a mathematical model of the system, and as such the experimental study achieved its' objective.

7.1.4 Mathematical modelling

Mathematical modelling of cyclic adsorption processes has become ever more prevalent with increasing computational power. Previous simulations have been undertaken using a variety of computer packages and languages, whereas this study is the first to consider the modelling of DP-D PSA system using the gPROMS package. Whilst the mathematical model used was similar to that derived both by Ruthven and Thaeron (1996)and more recently Arvind et al (2002), the gPROMS model allowed both the direct velocity profiles within the system to be calculated and allowed, by manipulating the code, six boundary conditions to be compressed into just two. This removes a degree of complexity from the model which helps to increase computing time. A similar technique was employed for the piston component mass balances.

A further reduction in computing time was achieved exploiting the work of Nilchan and Pantelides (1998), who suggested a framework for calculating a single steady state profile. While this involves some complication of the model a significant time saving can be made when simulating. Since it is steady state behaviour that is of greatest interest then this was a useful finding.

The adaptability of the modelling package was also valuable when incorporating the pressure drops incurred for the runs when the larger of the two columns was to be simulated. By introducing a pressure drop “unit” into the model to allow for each of the pipework sections the column could be more realistically represented.

7.1.5 Validating the model using the experimental results

Chapter 6 of this thesis reconciles the experimental results and those obtained from simulating the dual piston driven system under various conditions. The results showed that for non adsorbing conditions both the pressure profiles obtained from the smaller column model and those from the more complex larger column model (which included the pipework pressure drops) matched the experimental results with a high degree of accuracy.

Under adsorbing total reflux conditions the agreement between the pressure profiles remained good while agreement between the concentration profiles was good at cyclic steady state but less so in the transient period. This was possibly due to heat effects or poor estimation of the diffusional time constants from the characterisation experiments.

Achieving agreement for the feed-product experiments was not greatly successful since the model did not accurately capture the discontinuous nature of the inlet and outlet streams. In addition the data from the experimental runs was also not greatly reliable due to the difficulty in ensuring that the experiments reached steady state. However the experiments and simulations did show that, with the smaller of the two columns, a product stream containing 50% less CO₂ could be produced by the unoptimised rig and unoptimised adsorbent column.

7.2 Directions for further work

With the overall objective of this study in mind further work should focus on improvement in both experimental and simulation design.

With regard first to the adsorbent columns, the columns supplied by WestVaco were of a fairly high mechanical strength, where the binder constituted 60% of the composite material. As a consequence the performance of the column is not as high as could be hoped. It would therefore be interesting to investigate, with particular relevance to the Dual Piston Driven PSA system, how much the binder can be reduced to allow improved performance without comprising the structure of the column.

With regard to column design it is suggested that a future area for investigation could focus on the effect of different monolith channel widths and wall thicknesses on the separation capability of the column. The HETP analysis suggests that the thinner the walls and the narrower the passages the more effective the column becomes. However there are clearly engineering limits as to what can be realistically manufactured. Use of current research in this field would be highly applicable and could lead to development of a column design that may help to make the Dual Piston system more attractive, although it would be important to keep costs as low as possible. Future column designs should also allow for feeding in the middle, since observations by past researchers including Keller and Kuo (1982) suggested that this could greatly improve the separation efficiency of the column.

In terms of methods used for characterisation it is suggested that three independent methods be used in future studies, since it would allow the results to be compared more effectively and conclusively and would allow any anomalies to be better identified. Alternatively if this is not possible then set of experiments could be carried out at different temperatures. In addition improved detector sensitivities especially for low concentrations would help give better results from the chromatography runs since experiments could be carried out in the Henry's Law region with confidence.

In terms of the experimental study, improvements in concentration analysis suitable for this application must be made. It was originally hoped that the TCD sampling employed in this

study could be used to make on line measurements. However, in reality, the pressure variations meant that this was not possible. The technique that was used provided to be time consuming and its' accuracy was dependant on the degree of mixing in the system and the calibration of the TCD. Previous sampling to determine concentrations was undertaken using withdrawal from injection ports followed by analysis. This technique is both less time consuming and allows a sample to be taken at a very specific time within a cycle. It would be ideal to obtain on line measurements but pressure and temperature variations make this difficult to achieve. If runs are undertaken using different concentrations of CO₂ in the feed, reflecting those encountered in industrial stack gases, then the analysis technique must also be flexible and able to measure a range of concentrations. In addition the sampling technique should also allow piston or product concentrations on each side of the test rig to be determined.

In terms of further experimental work using the Dual Piston Driven PSA Rig, the major difficulty encountered in this study was in the control of the feed and product experiments. Any improvements in this area would greatly improve the accuracy and reliability of the results obtained. It would be, in terms of this specific point and in general, a great advantage if the mathematical modelling and experimentation could be carried out simultaneously. Using an iterative comparison process would help to reduce and focus the number of experiments required to capture the rig's behaviour and performance, and would ensure that the models correctly represent the real system behaviour. In addition this should also lead to more scope for optimisation. Such an optimised system could be used to determine the true economic potential of the technology and would also allow more direct comparison with existing CO₂ separation technologies.

In terms of modelling improvements further work within the Dual Piston Driven PSA field should include extending the models developed to incorporate all elements of the entire

system, which would allow correct representation of the discontinuous feed and product streams.

This thesis has shown that the Dual Piston Driven PSA system has some potential as a CO₂ separation technology. Should the further work suggested be implemented in a future study it is hoped that the technology would prove to be a highly competitive industrial alternative for the removal of CO₂ from stack gases.

References

- Alpay E & Scott D.M. The linear driving force model for fast-cycle adsorption and desorption in a spherical particle. *Chem. Eng. Sci.* **47**, 499-502, 1992.
- Alpay E, Kenney C.N, & Scott D.M, Simulation of rapid pressure swing adsorption and reaction proceses. *Chem. Eng. Sci.* **48**, 3173-3186, 1993.
- Alpay E, Kenney C.N, & Scott D.M, Adsorbent particle-size effects in the separation of air by rapid pressure swing adsorption *Chem. Eng. Sci.* **49**, 3059-3075, 1994.
- Aris R, Proc R Soc A, 235, 67, 1956
- Arvind R, MSc Thesis, National University of Singapore, 2000.
- Arvind R, Farooq, S & Ruthven D.M, *Analysis of a piston PSA process for air separation.* *Chem. Eng. Sci.* **57**, 419-433, 2002.
- Bardhan P, Ceramic honeycomb filters and catalysts, Current opinion in Solid State and Materials Science 2 (5) 577-583, 1997
- Brandani F, PhD Thesis, University of Maine, USA, 2002
- Brandani F, Brandani S, Coe C & Ruthven D.M. Measurement of Henry constants and equilibrium isotherms by the ZLC Technique in Fundamentals of Adsorption 7, K.Kaneko, H.Kanoh & Y.Hanzawa eds. P.21-28, International Adsorption Society, I.K. International, Chiba, Japan, 2002.
- Brandani F, Rouse A.J, Brandani S and Ruthven D.M, Adsorption, 2003, *in press.*
- Brandani S & Ruthven D.M, Analysis of ZLC desorption curves for Gaseous Systems, Adsorption 2, 133-143, 1996
- Brandani S & Ruthven D.M, Analysis of ZLC desorption curves for Liquid Systems, Chem. Eng. Sci, 50, 2055-2059, 1995
- Brandani S, Effects of Non Linear equilibrium on ZLC experiments, Chem. Eng. Sci, 53, 2791-2798, 1998
- Brandani S, Cavalcante C, Guimares A & Ruthven D.M Heat Effects in ZLC experiments, Adsorption 4, 275-285, 1998
- Brandani S, Hufton J, Ruthven D.M, Self Diffusion of Propane and Propylene studied by the Tracer ZLC method, Zeolites 15, 624-631, 1995
- Buzanowski M.A. & Yang R.T, Approximations for intraparticle diffusion rates in cyclic adsorption and desorption. *Chem. Eng. Sci.* **46**, 2589-2598, 1991.
- Carta, G. The linear driving force approximation for cyclic mass transfer in spherical particles. *Chem. Eng. Sci.* **48**, 622-625, 1993.
- Chihara, K. & Suzuki, M., Simulation of non-isothermal pressure swing adsorption. *J. Chem. Engng. Jap.* **16**, 53, 1983.

David, J. Economic Evaluation of Leading Technology Options for Sequestration of Carbon Dioxide, Masters Thesis, Massachusetts Institute of Technology, 2000.

Defra , Climate Change: Action to tackle Global Warming,
<http://www.defra.gov.uk/environment/climatechange/01.htm>, 31 December, 2002

Doong S.J & Yang R.T, *AICHE Symposium Series* 84(264), 145, 1988.

Dti, Energy White Paper – Our Energy Future – Creating A Low Carbon Economy (Cm 5761), HMSO, February 2003.

Duncan W.L. & Moller K.P. The effect of a crystal size distribution on ZLC experiments, *Chem. Eng. Sci.* 57 (14): 2641-2652, 2002

Eic & Ruthven, A new experimental technique for measurement of intracrystalline diffusivity, *Zeolites*, 8, 40-45, 1988

Eriksson, R. US Patent 4,169,715, assigned to AGA Aktiebolag, Lidingo, 1979.

Farooq, S., Thaeron, C. & Ruthven, D.M. Numerical simulation of a parallel passage piston-driven PSA unit. *Separation and Purification Technology*, 13, 181-193, 1998.

Finkelstein, T. Analysis of practical reversible thermodynamic cycles. ASME Paper No. 64-HT-37, 1964.

Finlayson D & Sharp A.J. UK Patent 365,092 assigned to British Celanese Corp., 1930.

Gadkaree K.P. Carbon Honeycomb Structures for Adsorption Applications, *Carbon*, 36 (7-8), 981-989, 1998

Giddings J.C, Chang J.P, Myers M.N, Davis J.M. & Caldwell K.D Capillary Liquid-Chromatography In Field Flow Fractionation-Type Channels *Journal of Chromatography*, 255, 359-379, 1983

Glueckauf, E. & Coates, J.I.E. Theory of chromatography, Part 4. The influence of incomplete equilibrium on the front boundary of chromatogram and on the effectiveness of separation. *J. Chem. Soc.* 1315-1321, 1947.

Glueckauf, E. Theory of chromatography, Part 10. Formula for diffusion into spheres and their application to chromatography. *Trans. Faraday Soc.* 51, 1540-1511, 1955.

Golay, M.J.E Theory of Chromatography in Open and Coated Tubular Columns with Round and Rectangular Columns in Gas Chromatography, Ed D.H. Desty, Butterworths, London (1958)

Green Chemistry Lab, Division of Environment and Process Technology, KIST, Korea, CH₄ / CO₂ Separation, http://greenchem.kist.re.kr/research%20interest/CH4_CO2.htm, 2002

Guerin de Montgareuil P & Domine D French Patent 1,223,261, assigned to Air Liquide, 1957.

Hashe R.L. and Dargan W.N., US Patent 1,794,377, 1931.

Hausen, H. (1942) as cited in Schmidt, F.W & Willmott, A.J Thermal Energy Storage and Regeneration (Chapter 6), Hemisphere Publishing Corporation, New York, 1981.

Haynes H.W & Sarma P.N. A model for the application of gas chromatography to measurements of diffusion in bidisperse structured catalysts *AICHE J* 19(5),1043-1046, 1973

Herzog, H An introduction to CO₂ separation and Capture Technologies, Energy Laboratory Working Paper,1999.

Hufton J.R. & Ruthven D.M, Diffusion Of Light Alkanes In Silicalite Studied By The Zero Length Column Method, *Ind Eng Chem Res*, 32 (10): 2379-2386, 1993

IEA Greenhouse Gas R&D Programme, Carbon Dioxide Capture from Power Stations, <http://www.ieagreen.org.uk/>, 2003.

IEA Greenhouse Gas R&D Programme, Common Questions about Climate Change, <http://www.ieagreen.org.uk/>, 2003.

Irandoost S and Andersson B, *Catal Rev Sci Eng.* 30, 341-392, 1988

Jones R.L & Keller II G.E, *J. Separ. Proc. Tech.*, 2(3), 17, 1981.

Jones, R.L, Keller II G.E., & Wells, R.C US Patent 4,194,892, assigned to Union Carbide Corporation, 1980.

Keller G.E. & Kuo C-H.A, Enhanced air separation by selective adsorption. US Patent 4,354,859, assigned to Union Carbide Corporation, 1982.

Keller II G.E. & Jones R.L , *ACS Symp.Ser.*, 135, 275, 1980.

Kim, D.H. Linear driving force formulas for diffusion and reaction in porous catalysts. *A.I.C.H.E. J.* 35, 343-346, 1989.

Kim, D.H. A new linear formula for cyclic adsorption in a particle. *Chem. Eng. Sci.* 51, (17) 4137-4144, 1996.

Kim, D.H. A new linear approximation formula for cyclic adsorption in a biporous adsorbent. *Chem. Eng. Sci.* 52, (20) 3471-3482, 1997.

Kowler, D.E. & Kadlec, R.H, *AICHE J* 18, 1207, 1972.

Lee, JT, Kim, D.H. High-order approximations for noncyclic and cyclic adsorption in a particle. *Chem. Eng. Sci.* 53, (6) 1209-1221, 1998.

LeVan, M.D., Finn, J.E., Sridhar, K.R., Separation of Carbon Monoxide and Carbon Dioxide for Mars ISRU - Concepts, Fifth Microgravity Fluid Physics and Transport Phenomena Conference, NASA Glenn Research Center, Cleveland, OH, CP-2000-210470, pp. 1204-1216, August 9, 2000.

Li Y.Y, Perera S.P & Crittenden B.D. Zeolite Monoliths for Air Separation Part1: Manufacture and Characterisation, *Trans IChemE Part A*, 76, 921-930, 1998

Li Y.Y, Perera S.P & Crittenden B.D. Zeolite Monoliths for Air Separation Part2: Oxygem Enrichment, Pressure Drop and Pressurisation, *Trans IChemE Part A*, 76, 931-941, 1998

Liaw, C.H., Wang, J.S.P., Greenkorn, R.A. & Chao, K.C. Kinetics of fixed-bed adsorption: a new solution. *AICHE J* 25, 376-381, 1979.

- Mitchell J.E. & Shendalman L.H. *AIChE Symposium Series* **69** (134), 25, 1973
- Nakao, S. & Suzuki, M. Mass transfer coefficient in cyclic adsorption and desorption. *J. Chem. Eng. Japan* **16**, 114-119, 1983.
- Nilchan S, The Optimisation of Periodic Adsorption Processes, PhD Thesis, University of London, 1997
- Nilchan S & Pantelides CC, On the optimisation of periodic adsorption processes, *Adsorption*, **4**, 113-147, 1998.
- Perley G.A. US Patent 1,896,916, 1933.
- Pigford, R.L, Baker III, B. & Blum, D.E. An Equilibrium Theory of the Parametric Pump, *Ind. Eng. Chem. Fundamentals*, **8**(1), 144-149, 1969.
- Process Systems Enterprise Ltd., gPROMS Advanced User Guide, London, 1999
- Raghavan, N.S., Hassan, M.M. & Ruthven, D.M. *AIChE J.* **31**(3), 385, 1985.
- Raghavan, N.S., Hassan, M.M. & Ruthven, D.M. Numerical Simulation of a PSA System Using a Pore Diffusion Model. *Chem. Eng. Sci.* **41**, 2787-2793, 1986.
- Robens E, Early Gravimetric Adsorption Measurements, *Colloid Surface A*, **104** (2-3), 375-376, 1995
- Rodrigues, A.E. & Dias, M.M. Linear driving force approximation in cyclic adsorption processes: Simple results from system dynamics based on frequency response analysis. *Chem. Eng. & Proc.* **37**, 489-502, 1998.
- Ruthven D.M, Principles of Adsorption and Adsorption Processes, Wiley, New York, 1984
- Ruthven D.M Special Topics in Chemical Engineering: Adsorption Separation Processes, U Maine Chem 598 course notes, Autumn 2001.
- Ruthven D.M & Brandani S Measurement of Diffusion in Porous Solids by Zero Length Column (ZLC) Methods in Recent Advances in Gas Separation by Microporous Ceramic Membranes N.K. Kanellopoulos ed, p.187-212, Elsevier, Amsterdam, 2000.
- Ruthven D.M., Farooq S., Knaebel K.S. Pressure swing adsorption. VCH, New York, 1994.
- Ruthven D.M & Karger J, Diffusion in Zeolites and other Microporous Solids, Wiley and Sons Inc. New York, 1992.
- Ruthven D.M & Stapleton P, Measurement of liquid phase counter diffusion in zeolites by the ZLC method, *Chem. Eng. Sci.*, **48**, 89-98, 1993
- Ruthven D.M. & Thaeron C. Performance of a parallel passage adsorbent contactor. *Separation and Purification Technology*, **12**, 1997, 43-60, 1996.
- Sakoda, A, Suzuki, M & Izumi, J Performance and Potential of Piston Driven Rapid Pressure Swing Adsorption. In the preprint Volume of the 1st Seapartion Division Topical Conf. Separation Technology, 2-6 Nov 1992, Miami Beach, FL, 332-336.

Schmidt, F.W & Willmott, A.J, Thermal Energy Storage and Regeneration (Chapter 6), Hemisphere Publishing Corporation, New York, 1981.

Seborg, D.E., Edgar, T.F. & Mellichamp, D.A. (1989), Process Dynamics and Control (Chap.14), Wiley, New York

Shendalman, L. H. & Mitchell, J.E., *Chem. Eng. Sci.* **27**, 1449, 1972

Sheng, P. & Costa, C.A.V., Modified linear driving force approximations for cyclic adsorption-desorption processes. *Chem. Eng. Sci.* **52**, 1493-1499, 1997.

Simmonds, M., Hurst, P., Wilkinson, M.B., Watt, C. & Roberts, C.A., Amine Based CO₂ Capture from Flue Gas, Gas Processors Association Europe Annual Meeting, September 2002.

Singh, K & Jones, J, *Numerical simulation of air separation by piston-driven pressure swing adsorption*. Chemical Engineering Science, **52**, 3133-3145, 1997.

Sircar,S, "Adsorption" in *The Engineering Handbook*, R.C. Dorf (Ed) Ch.59, pp604-617, CRC Press, Boca Raton, Florida, 1996.

Skarstrom C.W. US Patent 2,194,892, assigned to Esso Research and Engineering Company, 1958.

Spangler G.E., Height Equivalent to a Theoretical Plate Theory for Rectangular GC Columns, *Analytical Chemistry*, **70**, 4805-4816, 1998.

Spangler G.E., Relationships for Modelling the Performance of Rectangular Gas Chromatographic Columns, *Journal of Microcolumn Separations*, **13**(7), 285-292, 2001.

Suzuki, T, Sakoda, A, Suzuki, M & Izumi, J. *Piston-Driven Ultra Pressure Swing Adsorption*. Adsorption, **2**, 11-119, 1996

Suzuki, T, Sakoda, A, Suzuki, M & Izumi, J. *Recovery of carbon dioxide from stack gas by piston-driven ultra-rapid PSA*. Journal of Chemical Engineering of Japan 30 (6), 1026-1033, 1997.

Sweed N.H & Rigaudeau J Equilibrium Theory and Scale-up of Parametric Pumps in *AIChE Symp. Ser*, ed by I.Zwiebel and N.H. Sweed, **71(152)**, New York, AIChE, 1975.

Sweed N.H Parametric Pumping and Cycling Zone Adsorption – A Critical Analysis, *AIChE Symp.Ser*, ed. by M.D. LeVan, **80**, 253, AIChE, New York, 1988

Thaeron C, PhD Thesis, University of New Brunswick, Canada, ?

Turnock P.H & Kadlec, R.H, *AIChE J* **17**, 335, 1971.

US DoE, Carbon Sequestration - Research and Development Chap. 2 Separation and capture of carbon dioxide. http://www.fe.doe.gov/coal_power/sequestration/reports/rd/chap2.pdf December 1999.

US DoE Fossil Energy, Carbon Sequestration- Capture and Separation http://www.fe.doe.gov/coal_power/sequestration/sequestration_capture.shtml, 2003.

Van der Laan, E. Th. *Chem Eng Sci*, **7**, 187, 1958

Wakao N & Funazkri T, Chem. Eng. Sci, 33, 1375-1384, 1978.

Wilhelm R.H., Rice A.E. & Benedilus A.R. Parametric Pumping: A Dynamic Principle for Separating Fluid Mixtures, *Ind. Eng. Chem. Fundamentals*, 5(1), 141-144, 1966.

Wilhelm R.H., Rice A.W., Rolke R.W & Sweed N.H Parametric Pumping – A Dynamic Principle of Separating Fluid Mixtures, *Ind. Eng. Chem. Fundamentals*, 7(3), 337-349, 1968.

Yang R.T, Gas Separation by Adsorption Processes, Butterworths, Boston, MA, 1987